# Cytokine Release Syndrome: Dissecting Immune Responses and Exploring Novel Anti-cytokine Strategies in Syngeneic Mouse Models

Nouveau, Lise Gilberte Francine

**UNIVERSITÉ DE GENÈVE**

**Département de Biologie Cellulaire** **FACULTÉ DES SCIENCES**

**Professeur Jean-Claude Martinou**

**LIGHT CHAIN BIOSCIENCE – NOVIMMUNE SA**

**Département de Recherche** **Docteur Walter Ferlin**

---

# Cytokine Release Syndrome:

# Dissecting Immune Responses and Exploring Novel Anti-cytokine Strategies in Syngeneic Mouse Models

THÈSE

présentée aux Facultés de médecine et des sciences de l'Université de Genève
pour obtenir le grade de Docteur ès sciences en sciences de la vie,
mention Biosciences moléculaires

par

**Lise Nouveau**

de

Dijon (France)

Thèse N° 123

GENÈVE

2021

LIFE SCIENCES PhD SCHOOL GENEVA

DOCTORAT ÈS SCIENCES EN SCIENCES DE LA VIE DES FACULTÉS DE MÉDECINE ET DES SCIENCES

**MENTION BIOSCIENCES MOLÉCULAIRES**

## Thèse de Madame Lise Gilberte Francine NOUVEAU

intitulée :

# «Cytokine Release Syndrome: Dissecting Immune Responses and Exploring Novel Anti-cytokine Strategies in Syngeneic Mouse Models»

Les Facultés de médecine et des sciences, sur le préavis de Monsieur W. FERLIN, docteur et directeur de thèse (Chief Scientific Officer, Light Chain Bioscience, NovImmune SA Geneva, Switzerland), Monsieur J.-C. MARTINOU, professeur honoraire et codirecteur de thèse (Département de biologie moléculaire et cellulaire), Monsieur D. MERKLER, professeur ordinaire (Département de pathologie et d'immunologie, Faculté de médecine), Monsieur S. JONES, professeur (Systems Immunity Research Institute, Cardiff University, Cardiff, United Kingdom), autorisent l'impression de la présente thèse, sans exprimer d'opinion sur les propositions qui y sont énoncées.

Genève, le 16 décembre 2021

**Thèse - 123 -**

**Le Doyen**
**Faculté de médecine**

**Le Doyen**
**Faculté des sciences**

N.B. - La thèse doit porter la déclaration précédente et remplir les conditions énumérées dans les "Informations relatives aux thèses de doctorat à l'Université de Genève".

**UNIVERSITÉ DE GENÈVE**

**Département de Biologie Cellulaire** **FACULTÉ DES SCIENCES**

**Professeur Jean-Claude Martinou**

**LIGHT CHAIN BIOSCIENCE – NOVIMMUNE SA**

**Département de Recherche** **Docteur Walter Ferlin**

---

# Cytokine Release Syndrome:

# Dissecting Immune Responses and Exploring Novel Anti-cytokine Strategies in Syngeneic Mouse Models

THÈSE

présentée aux Facultés de médecine et des sciences de l'Université de Genève
pour obtenir le grade de Docteur ès sciences en sciences de la vie,
mention Biosciences moléculaires

par

**Lise Nouveau**

de

Dijon (France)

Thèse N° 123

GENÈVE

2021

« *La persévérance, c'est ce qui rend l'impossible possible, le possible probable et le probable réalisé.* »

Léon Trotsky

# CONTENTS

# ABSTRACT

The cytokine release syndrome (CRS) is described as a collection of potentially life-threatening symptoms associated with a plethora of infections, such as haemorrhagic fever and other viruses, most recently COVID-19. The 'cytokine storm', underlying CRS, has also been an unfortunate side effect of highly promising cancer therapies including T cell engagers and chimeric antigen receptor (CAR) T cells. The cytokine storm is intimately linked with an excessive, uncontrolled release of proinflammatory mediators resulting in an overwhelming systemic inflammation and multi-organ failure, often fatal if left untreated. The pro-inflammatory cytokines that are involved in the CRS have been well described and often include interferon (IFN) -γ, interleukin (IL) -6 and tumour necrosis factor (TNF) -α. Little is known, however, about the hierarchy and orchestration of the cytokine storm or, importantly, if a key cytokine controls cascade of inflammatory responses.

To advance the understanding to these unanswered questions underlying CRS, two syngeneic mouse models of CRS were developed. The first, relies on potent *in vivo* T cell activation mediated by an anti-CD3ε monoclonal antibody (mAb). In parallel, a second model was developed to investigate CAR T cell-induced CRS in mice transplanted with A20 B cell lymphoma cells. Both models reproduced clinical and laboratory manifestations seen in patients afflicted with CRS, including hepatosplenomegaly, increased vascular permeability, hemotoxicity and hyper-cytokinemia. The kinetics of cytokine release to immune stimulation in blood, spleen, lung, and liver were analysed, at protein or mRNA level, demonstrating a hierarchy of production together with an organ-dependent mobilization of immune cells.

An important aim of the project was to address whether blockade of proinflammatory cytokines impacted CRS in the above models. A cocktail of neutralizing mAbs to IFN-γ, IL-6, IL-2 and TNF-α transiently improved early clinical and laboratory features of CRS in the anti-CD3ε mouse CRS model. The mAb cocktail demonstrated a clear benefit over monotherapy mAb treatment. These studies were extended to the CAR T model, where neutralisation of IFN-γ or IL-6 was investigated. Interestingly, mice administered anti-IFN-γ or anti-IL-6R mAbs and treated with the CAR T cells therapy controlled A20 lymphoma tumour growth. Nonetheless, only anti-IL-6R treatment showed an improvement in some CRS features, although not reaching significance.

In both models, benefit of anti-cytokine therapy in disease management was demonstrated, thus offering a potential opportunity to consider additional options for patients. Moreover, these models shed new light on the mechanisms underlying CRS and must be useful as predictive tools in the context of new anti-cytokine strategies to manage human CRS.

# RÉSUMÉ

Le syndrome de libération de cytokines (SRC) est décrit comme un ensemble de symptômes potentiellement mortels associés aux fièvres hémorragiques et à d'autres virus, le plus récent étant COVID-19. La « tempête de cytokines », sous-jacente au SRC, est également un effet secondaire dramatiques de certaines thérapies anticancéreuses très prometteuses, notamment les inhibiteurs de cellules T et les cellules T à récepteur antigénique chimérique (CAR T). La tempête de cytokines est liée à une libération excessive et incontrôlée de médiateurs pro-inflammatoires entraînant une accablante inflammation systémique et une défaillance multiviscérale, souvent fatale si laissée sans traitement. Les cytokines pro-inflammatoires impliquées dans le SRC ont été bien décrites et comprennent souvent l'interféron (IFN) -γ, l'interleukine (IL) -6 et le facteur de nécrose tumorale (TNF) -α. Cependant, peu de choses sont connues concernant la hiérarchie et l'orchestration de la tempête de cytokines ou si une cytokine en particulier contrôle la cascade de réponses inflammatoires.

Pour faire progresser la compréhension de ces questions sans réponse, deux modèles murins syngéniques de SRC ont été développés. Le premier repose sur une puissante activation *in vivo* des cellules T médiée par un anticorps monoclonal (AcM) anti-CD3ε. En parallèle, un deuxième modèle a été développé pour étudier le SRC induit par les cellules CAR T dans des souris transplantées avec des cellules de lymphome B (cellules A20). Les deux modèles ont reproduit des manifestations cliniques et biologiques observées chez des patients atteints de SRC, notamment une hépatosplénomégalie, une importante perméabilité vasculaire, une hémotoxicité et une hypercytokinémie. La cinétique de la libération de cytokines dans le sang, la rate, les poumons et le foie a été analysée, au niveau des protéines ou de l'ARNm, démontrant une hiérarchie de production ainsi qu'une mobilisation des cellules immunitaires dépendante des organes.

Un objectif important du projet était de déterminer si le blocage des cytokines pro-inflammatoires avait un impact sur le SRC dans les modèles ci-dessus. Un cocktail d'AcM neutralisants l'IFN-γ, l'IL-6, l'IL-2 et le TNF-α a amélioré de manière transitoire les caractéristiques cliniques et biologiques précoces du SRC dans le modèle de SRC murin induit par l'anti-CD3ε. Le cocktail d'AcM a démontré un avantage évident par rapport au traitement d'AcM en monothérapie. Ces études ont été étendues au modèle CAR T, dans lequel la neutralisation de l'IFN-γ ou de l'IL-6 a été étudiée. De façon intéressante, les souris ayant été administrées avec l'anti-IFN-γ ou anti-IL-6R et traitées avec les cellules CAR T, ont contrôlé la croissance tumorale du lymphome A20. Néanmoins, seul le traitement avec l'anti-IL-6R a montré une amélioration de certaines caractéristiques du SRC, bien que n'étant pas statistiquement significatif.

Dans les deux modèles, le bénéfice des thérapies neutralisant des cytokines a été démontré, offrant ainsi de nouvelles options thérapeutiques pour les patients. De plus, ces modèles ont permis d'approfondir les connaissances sur les mécanismes sous-jacents au SRC et peuvent être utiles en tant qu'outils prédictifs pour étudier l'efficacité de nouvelles stratégies, tels que les anti-cytokines, pour gérer le SRC humain.

# REMERCIEMENTS

En premier lieu je souhaiterais exprimer ma profonde gratitude envers mon directeur de thèse, Dr Walter Ferlin. Walter, pour commencer, désolée de t'avoir fait subir des mois de relances, quasi hebdomadaires, pour savoir si un projet de thèse s'ouvrirait à Novimmune (devenue Light Chain Bioscience (LCB) – NovImmune SA en cours de route). Si tu as pu entrevoir ma persévérance à ce moment, tu ne t'imaginais probablement pas que cela relevait plutôt du 'tête de mule'… Alors merci de m'avoir supportée durant ces années, j'espère que tu ne le regrettes pas ! Je voudrais surtout te remercier pour ton humanisme, optimisme et positivité sans faille, à chacun de nos meetings, ainsi que pour cette passion communicative que tu as de La Science. Je te suis très reconnaissante d'avoir toujours mis un point d'honneur à privilégier l'aspect pédagogique au détriment parfois du plus pratique/rapide, ainsi que de l'énergie que tu as dépensée afin de me faire progresser en anglais… et en rédaction ! Enfin, merci de m'avoir fait confiance, encouragée et laissée cheminer librement dans cet immense projet de recherche durant ces années. Bref, merci !

Dans un second temps, je tiens à remercier les membres de mon jury de thèse pour avoir accepté et pris le temps d'évaluer ce travail : Professeur Simon Jones (Université de Cardiff), Professeur Doron Merkler (Université de Genève) et Professeur Jean-Claude Martinou (Université de Genève – également co-directeur de thèse).

J'aimerais également exprimer ma reconnaissance envers Nicolas Fischer, CEO de LCB, pour m'avoir permis de poursuivre la thèse au sein de la compagnie.

Je souhaiterais également remercier les Drs Xavier Chauchet, Vanessa Buatois et Eric Hatterer. Merci infiniment pour votre temps, conseils avisés, encouragements ainsi que pour les discussions scientifiques (parfois longues à démarrer certes, mais toujours constructives !). Plus particulièrement 'Mister Chauchette', merci pour ton optimisme et ta passion pour la recherche ; ça a toujours été (re-)motivant de discuter avec toi de mes données, que ce soient dans les moments forts, ou plus compliqués. Un immense merci à toi Vanessa, surtout pour ce dernier mois de rédaction. Merci infiniment d'avoir pris du temps pour la relecture, été franche, honnête et surtout de bons conseils.

Je voudrais également adresser un immense merci à mes premières collègues de bureau : Laura et Laurence, sans qui aucune expérimentation n'aurait vu le jour. Merci d'avoir pris le temps de me former à tout : le *vitro* et surtout le *vivo*, nouveau monde pour moi. Je n'aurais pas pu rêver meilleure école que la vôtre : rigueur, organisation, efficacité ! Merci Laulau pour tous tes 'tips' acquis grâce à ton

expérience, ton auto-dérision, ta super compagnie le midi, au labo à chanter, en vacances (merci les fourmis volantes qui piquent !) et j'en passe... Laura, merci de m'avoir montré l'exemple de ce qu'est une journée rondement menée : quelques dizaines d'i.v. et passages de cellules le matin, une séance de sport entre midi et deux, et c'est reparti pour un séjour à l'animalerie, un FACS, une analyse et à demain ! Tu auras été, restes et resteras un exemple de productivité, rigueur, et dévouement ; une machine d'efficacité. Je voudrais également remercier Emeline, notre gardienne d'animaux. Quel plaisir de discuter avec toi ; ton ouverture d'esprit, tes péripéties (surtout quand tu reviens de vacances) ont toujours égaillé les journées passées à l'animalerie. Merci également pour ton oreille attentive, tes encouragements, et ton enthousiasme envers le travail accompli ; cela a été une vraie source de motivation tout au long de la thèse.

Ce projet n'aurait pas pu avancer sans l'aide de Gérard et Giovanni, qui ont partagé une partie de leur immense connaissance en biologie moléculaire pour m'aider dans la construction et l'expression des CARs. Merci également à Bruno et Valéry de m'avoir initiée au monde de la pharmacologie, et de votre expertise en cytométrie en flux. Merci donc à vous quatre pour votre aide et conseils aux différentes étapes de ce projet. Je suis également reconnaissante envers Yves et Guillemette, qui auront essayé de me convertir à la purification dans un lointain passé (en 2017) ! Vos conseils et votre bonne humeur durant cette purification interminable du 1F7, à repasser les flow-through je ne sais plus combien de fois, ont été plus qu'utiles et agréables.

Je voudrais également avoir un petit mot pour Leticia B., pour ton oreille attentive, tes conseils culinaires non reproductibles (noisettes torréfiées) ainsi que pour ton coup de main impeccable pour sortir les plaques de la centrifugeuse et les mettre à l'incubateur alors que j'étais au sport ! Puisqu'il est question de sport, merci également à mes coachs sportifs : Seb', Nico' et Xav', pour les sorties Salève et leur initiation au trail entre midi et deux. Dans la lancée sport, merci à Tereza et Ulla, pour les sorties piscine et course à pied au bord de l'aire. Tereza, merci également pour les sorties ski de rando avant le boulot (définitivement les meilleures, encore plus quand elles rendent jaloux les collègues parce que c'est tombé dans la nuit et qu'il fait beau le matin) ; j'espère pouvoir compter sur ta compagnie en montagne pour les prochaines saisons à venir !

J'aimerais également adresser mes remerciements à mes acolytes de galères : les Elise (~~Eh ! Lise !~~). Particulièrement, Elise P., merci infiniment pour toutes nos discussions à pas d'heure, à râler sur tout, sur rien, sur la vie de thésard. Merci pour ton soutien, ta compréhension, tes coups de mains et ta serviabilité. Je te souhaite tout le meilleur pour la suite, et surtout un énorme courage pour cette

dernière ligne droite qui t'attend. Mais je te promets qu'on en voit le bout et que la lumière au bout du tunnel existe !!
D'une manière plus générale, merci à tous les collègues de LCB, pour votre aide et vos encouragements. Vous êtes tous plus bienveillants les uns que les autres, et rendez l'ambiance unique et inégalable. Merci à vous qui m'avez permis de vivre cette aventure dans une atmosphère si chaleureuse (et fêtarde !).

Je tiens également à remercier tous les copains, d'avoir animés les week-ends et vacances : les ZANUs, qui ont ponctué de mariages, naissances, baptêmes, fiestas ces années de thèse ; les copains anneciens, qui m'ont permis de garder un équilibre entre la vie de thésard, et la détente. Je n'oublie bien sûr pas mes amies d'enfance ; les copines du cheval. Presque 20 ans plus tard, quelques rides en plus, mais toujours autant de fraicheur, de folie et bonne humeur! Merci à vous tous, pour vos encouragements et votre curiosité pour mon projet et ce domaine qui est à mille lieux du votre.
Enfin, merci à ma famille proche de m'avoir donné les moyens d'arriver jusqu'ici et d'avoir toujours cru en moi. Le souhait que vous avez de nous voir réussir, Léo et moi, et la fierté que vous portez à notre égard a toujours été une immense source de motivation. Maman, merci pour ton soutien indéfectible et d'avoir toujours pris le temps de m'écouter. J'espère que les thésards et stagiaires qui te côtoient se rendent compte de la chance qu'ils ont de t'avoir à leur côté. Papa, merci aussi pour tout ; tes conseils, ton écoute, tes avertissements : ''ce n'est pas un sprint, c'est un marathon'' ! Léo, mon grand frère, merci de m'avoir toujours un peu montré l'exemple : prépa, école d'ingé, thèse… (cependant, désolée mais le postdoc aux USA, no way !). Un remerciement va également vers mes grands-parents, toujours soucieux de notre bien-être et de notre réussite. Plus particulièrement, une pensée va vers pépé ; j'aurais aimé fêter la fin de cette étape avec un bon 'pinard' et un gibier sauce bourguignonne comme toi seul savait le faire (avec mémé).
Enfin, le meilleur pour la fin, un immense merci à Antoine. Bientôt 12 ans de 'concubinage' (!!) et toujours là, malgré mon caractère… ! Car si j'ai du tempérament (soi-disant !), lui seul a subi sans filtre tous mes états, du plus positif au plus négatif. Alors Dou', merci pour tout, d'avoir cru en moi, en nous. D'avoir accepté de passer des soirées et week-end seuls, pris pour les autres, ma fatigue, mon énervement, mes déceptions. D'avoir été patient, arrangeant, bienveillant... Bref, d'avoir été là.

J'espère n'avoir oublié personne et dans le cas contraire, je leur présente ici même mes plus sincères remerciements !

# PUBLICATIONS AND COMMUNICATIONS

## Publication

Nouveau L, Buatois V, Cons L, Chatel L, Pontini G, Pleche N and Ferlin WG. Immunological analysis of the murine anti-CD3-induced cytokine release syndrome model and therapeutic efficacy of anti-cytokine antibodies. *European Journal of Immunology*. 2021 Aug;51(8):2074-2085. doi: 10.1002/eji.202149181.

## Conferences

**2021 Cytokines, 9th Annual Meeting of ICIS, Cardiff, Wales, UK**

Poster presentation "Deciphering a role for IL-6-trans-signalling in a syngeneic mouse model of cytokine release syndrome induced by CD19-CAR T cells."

**2019 Cytokines, 7th Annual Meeting of the ICIS, Vienna, Austria**

Poster presentation "The cytokine hierarchy in the anti-CD3 model of cytokine release syndrome in mice."

# CHAPTER I: INTRODUCTION

The immune system protects the body from foreign, pathogens or from host cells that have become malignant. Sometimes, however, the immune response is exaggerated and uncontrolled, leading to hyperresponsive immune cells inducing potentially fatal collateral damage. The cytokine release syndrome (CRS), underpinned by a 'Cytokine storm', is one such example. CRS is characterized by the production of excessive inflammatory cytokines, leading to multiple organ dysfunction and even death if left untreated.

The term *cytokine storm* was used for the first time in 1993 to describe graft-versus host disease[1-4]. From as early as the 1918 influenza pandemic caused by the H1N1 influenza A (Spanish flu) infecting over 500 million people, the cytokine storm phenomena is seen across multiple infectious diseases including cytomegalovirus[5], Epstein-Bar virus-associated hemophagocytic lymphohistiocytis[6], group A streptococcus[7], influenza virus[2,8,9], variola virus[10], dengue[11,12], Lassa fever[13], Ebola[14], Coronavirus and, more recently, in the recent COVID-19 outbreak[15,16]. Additionally, the toxicity driven by excess cytokine release was observed as a major hurdle to the treatment of patients with the anti-T-cell antibody (Ab) muromonab-CD3 (OKT3) (often call in this setting an infusion reaction), for solid organ transplantation[17,18]. The 2006 healthy subject trial disaster with TGN1412, an agonistic CD28 monoclonal antibody (mAb), infamously popularized the *cytokine storm* term in modern day clinical practice[19]. Indeed, CRS also is now on the warning label of multiple approved drugs, such as rituximab[20], obinutuzumab[21], alemtuzumab[22], brentuximab[23], dacetuzumab[24], and nivolumab[25]. More recently, the cytokine storm was also considered as the major side effect of the highly promising T-cell–engaging immunotherapies, including the CD19-directed CD3 bispecific blinatumomab[26,27] and CAR-T cell therapy[28-30]. In 2017, five patients, for example, succumbed to cerebral oedema brought on by CAR-T cell induced CRS[31].

# 1 CLINICAL AND LABORATORY FEATURES OF CRS

## 1.1 CLINICAL MANIFESTATIONS

CRS can vary from a febrile 'flu-like' illness to life-threatening syndrome requiring intensive supportive care settings. Onset of CRS typically occurs within the first 14 days post treatment or infection, and can last several days, depending on the severity of syndrome and the trigger[34]. CRS encompasses a collection of symptoms (Figure 1), including systemic inflammation, hemodynamic instability and multiple organ dysfunction, categorized into four grades depending on the severity (Figure 2) [3,33,34,121].

Patients with grade 1 CRS, which is the mildest non-life-threatening form, presents weakness, fever, headache, skin rash, arthralgia, and myalgia. Moderate cases of CRS (grade 2) results in hemodynamic instability, including hypotension, change in blood clotting, haemorrhages, vasodilatory shock, together with respiratory symptoms. The most severe forms of CRS, corresponding to grade 3 and 4, are characterized by a high-grade fever, vascular leakage, multiple organ dysfunction such as renal, heart and liver failure, and development of acute respiratory distress syndrome (ARDS) (Figure 1). In the settings of T cell engaging therapy, patients with severe forms of CRS can also develop immune effector cell-associated neurotoxicity syndrome (ICANS). It corresponds to severe neurotoxicities, such as aphasia, seizures, paresis, and coma, occurring several days after the onset of the cytokine storm. As it is specific to therapy-induced CRS, and occurs post-CRS, considering ICANS as a symptom of CRS or as a syndrome as such is still disputed[34].

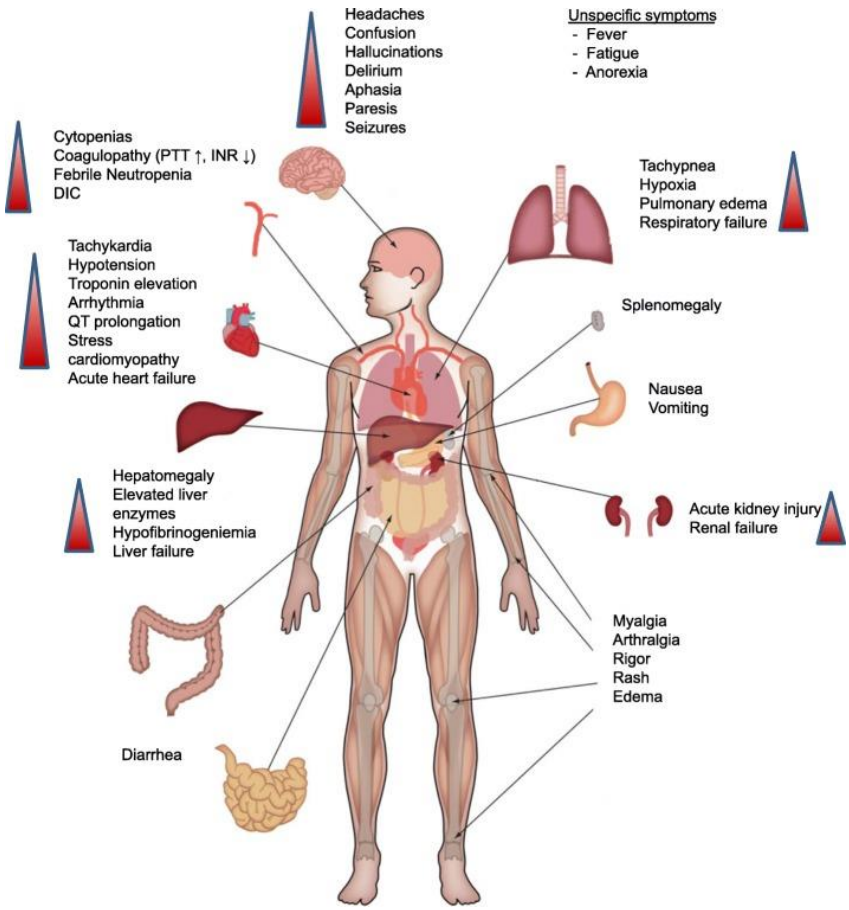


**Figure 1: Clinical presentation of CRS.** Adapted from Shimabukuro-Vornhagen *et al.*[33]

**Grade 1**

- Symptoms are not life threatening and require symptomatic treatment only
- Fever, Nausea, Fatique, Headache, Myalgia, Malaise, Organ toxicity

**Grade 2**

- Symptoms require and respond to moderate intervention
- Oxygen requirement < 40% or Hypotension responsive to fluids or low dose of one vasopressor or Grade 2 organ toxicity

**Grade 3**

- Symptoms require and respond to aggressive intervention
- Oxygen requirement < 40% or Hypotension requireing high dose or multiple vasopressors or Grade 3 organ toxicity or Grade-4 transaminits

**Grade 4**

- Life-threatening symptoms
- Requirement for ventilator support or Grade-4 organ toxicity (excluding transaminitis)

**Grade 5**

- Death

**Figure 2: CRS grading.** Adapted from Moradian *et al.*[35]

## 1.2 LABORATORY FEATURES

The severe forms of CRS are also associated with laboratory disorders (Table 1), such as increase in markers of acute inflammation, exacerbated cytokine release and cytopenia, which underly the clinical observations[33-36,40].

**Table 1: Comparison laboratory features reported in different trigger-induced CRS**. CRS was observed following viral infection, such as COVID-19, H1N1 influenza, or after treatment infusion, such as CAR T cell therapy, or in patients with hemophagocytic lymphohistiocytosis (HLH) and macrophage activation syndrome (MAS). +, ++, +++: few, moderately, strongly over-observed. Adapted from Morris *et al.*[40]

| **Abnormality** | **COVID-19** | **H1N1** | **CAR T cells CRS** | **HLH/MAS** |
|---|---|---|---|---|
| Elevated CRP | +++ | ++ | +++ | + |
| Hyperferritinemia | ++ | ++ | +++ | ++ |
| High D-Dimer levels | ++ | ++ | ++ | ++ |
| DIC | ++ | ++ | No evidence | ++ |
| Hypercoagulative state | +++ | ++ | +++ | ++ |
| High neutrophil to Lymphocyte ratio | ++ | ++ | No evidence | No evidence |
| Activated macrophages | +++ | + | +++ | +++ |
| Endotheliopathy | +++ | +++ | +++ | No evidence |
| Elevated IL-6 | +++ | ++ | +++ | ++ |
| Elevated IL-1 | +++ | ++ | ++ | ++ |
| Elevated IFN-γ | + | + | +++ | +++ |
| Elevated TNF-α | + | + | +++ | + |

### 1.2.1 Non-specific markers of inflammation

*CRP, LDH and ferritin, indicators of chronic tissues damage*

One of the most reliable markers of inflammation is C-reactive protein (CRP). This acute phase protein is produced by the liver in response to inflammation, infection, or tissue injury[38]. Lactate dehydrogenase (LDH), often associated with hepatic injury, is also representative of systemic tissue damage induced by cytokines. CRP and/or LDH is often observed in patients with CRS, including induced by infectious disease, such as Ebola[40], Dengue[42], influenza[43] and coronavirus[44,45], as well as by T-cell engaging therapies[19,27,46-49]. Moreover, in several studies, CRP and LDH was strongly correlated with disease severity and poor prognosis, especially in the context of COVID-19[44,50,51].

Ferritin is one of the main regulators of iron metabolism, sequestering it into cells. Since iron is an essential nutrient for both cells and pathogens serving as a redox catalyst, a host defence mechanism against infection consists of up-regulate cellular ferritin to limit the availability of iron to pathogens[68]. Moreover, ferritin is critical for avoiding iron overload and subsequent cellular toxicity. Indeed, in excess, iron can generate free radicals, via Fenton redox reaction, which is responsible of cellular oxidative stress and damage on DNA, lipids and proteins[68,69]. Serum ferritin is commonly recognized as an acute-phase reactant, i.e. non-specifically enhanced under systemic inflammatory conditions. Indeed, when cells are damaged, ferritin leaks into the serum and, therefore, serves as an important biomarker. In the context of CRS, hyperferritinemia was often reported in infectious- and CAR T therapy-induced CRS patients[28,45,51,53,54], and cited as one of the indicators of mortality in COVID-19 patients[50,53]. Clinical observations of hemophagocytic lymphohistiocytosis (HLH) and macrophage activation syndrome (MAS), two forms of CRS induced by genetic disorders[3], also reported elevated ferritin levels[70,71].

*D-dimer and Angiopoietin 2, markers of coagulation defects and endothelial activation*

Coagulation dysfunctions occur in almost all settings of CRS and include disseminated intravascular coagulation (DIC), which can be further exacerbated in thrombosis and haemorrhage in the severe cases of CRS[55,59,60]. D-dimer is released as a product of degeneration of cross-linked fibrin and hence, is a sensitive biomarker of coagulation dysfunctions. D-dimer was shown to be consistently elevated and predictive of mortality in patients suffering from CRS induced by COVID-19[44,45,51,60], influenza[63] or Ebola[40,57] infectious and following T cell-engagers immunotherapy[19,47,51,58].

Angiopoietin (Ang) -2, a marker of endothelial activation, is increased in patients with sepsis or ARDS[72] and is also predictive of mortality in ARDS patients[73]. Patients suffering from COVID-19-, haemorrhagic fevers- and CAR T cell- induced CRS, showed significantly elevated Ang-2 levels[56,6474].

Across CRS settings, the common observation of the increased level of D-dimers, associated with the increased Ang-2 level, suggests that endothelial dysfunction drives the coagulation dysfunction. The pathogenic role of endothelial cells in CRS induced by infections is being increasingly studied [59-64].

### 1.2.2 Serum cytokine levels

In all settings of CRS, a panel of cytokines, including interleukin (IL) -1, IL-6, tumour necrosis factor (TNF) -α and interferon (IFN) -γ, are consistently elevated in serum of patients[3,12,27,28,33,37,40,56,65]. The relationship between these key cytokines and characteristic clinical features of CRS are shown in Table 2 (non-exhaustive list). Other cytokines, including IL-2, IL-8, IL-10, monocyte chemoattractant protein-1 (MCP-1, also called CCL2), granulocyte-macrophage colony-stimulating factor (GM-CSF) and IFN-γ chemokines-induced CXCL9 and CXCL10 are also consistently elevated.

**Table 2: Relationship between key cytokines and clinical features of cytokine release syndrome**. Adapted from Yildizhan *et al.*[75] and Brisse *et al.*[191]

| Key cytokines | IFN-γ | TNF-α | IL-1β | IL-6 |
|---|---|---|---|---|
| **Clinical manifestations** | Fever<br>Decline of hematopoiesis<br>Hemophagocytosis<br>Macrophage activation<br>DIC<br>Hypoalbuminemia | Fever<br>Decline of hematopoiesis<br>Hypertriglyceridemia<br>Liver injury<br>DIC<br>Hypoalbuminemia<br>Hyperferritinemia<br>Endothelial cell activation | Fever<br>Acute phase proteins<br>Decline of hematopoiesis<br>Hyperferritinemia<br>ARDS<br>Neurotocixity<br>Endothelial cell activation | Fever<br>Acute phase proteins<br>Anaemia<br>Acute kidney Injury<br>NK cell dysfunction |

### 1.2.3 Blood cells count

Variation in blood cell count is a common abnormality observed in various setting of CRS and include leukopenia, lymphopenia, anaemia and thrombocytopenia[3,33,40]. The latter likely takes part to coagulation dysfunctions and anaemia strongly supports bleeding and/or haemolysis. Cytopenia may result from alteration of hematopoiesis and/or other hemophagocytosic mechanisms. Hemophagocytosis is the phagocytosis of red blood cells (RBC), lymphocytes or other hematopoietic precursors by histiocytes or macrophages[76]. Typically, this process is a hallmark of hemophagocytic lymphohistiocytosis (HLH) and macrophage activation syndrome (MAS), both considered as CRS[185].

Since CRS can vary from a febrile 'flu-like' illness to life-threatening syndrome, evaluating patients who may develop severe CRS is critical. Assessment of laboratory disorders, along with their clinical features, can help to determine which clinical course to take and thus prevent the severe development of CRS.

# 2 PATHOLOGY OF CRS

CRS can be induced by different triggers, including therapy (cytokine storm due to CAR T-cell therapy or T-cell engaging antibodies), pathogens (haemorrhagic fever, respiratory viruses, or parasites) or genetic disorders (hemophagocytic lymphohistiocytosis; HLH) (Table 3). In each of these states, CRS results from the uninterrupted amplification of the immune response, associated with a failure of negative feedback mechanisms, which normally prevents hyperinflammation and overproduction of inflammatory cytokines and soluble mediators.

Here, a focus on the pathophysiology associated with three different conditions leading to a CRS (CAR T-cell therapy, COVID-19, and HLH) will be done. These three entities are, so far, the best studied and/or topical.

**Table 3: Different cytokine release syndrome, its cause, and pathologic drivers**. From Fajgenbaum and June[3].

| Type of Cytokine Storm and Trigger | Cause | Pathologic Cellular or Cytokine Driver |
|---|---|---|
| **Iatrogenic** | | |
| CAR T-cell therapy | Infusion of CAR T cells | Macrophages, CAR T cells, interleukin-6, interleukin-1$\beta$ |
| Blinatumomab | Infusion of CD19- and CD3-specific T-cell receptor–engaging antibody | Activated T cells, macrophages, interleukin-6 |
| **Pathogen-induced** | | |
| Bacterial sepsis | Hematogenous bacterial infection | Heterogeneous and multifactorial drivers |
| EBV-associated HLH | EBV infection in patient with genetic susceptibility | Interferon-$\gamma$, TNF, CD8+ T cells |
| HHV-8–associated MCD | HHV-8 infection in patient with HIV coinfection, genetic susceptibility, or both | Viral interleukin-6, interleukin-6 |
| Covid-19 | SARS-CoV-2 infection, potentially in a susceptible person | Unknown driver |
| **Monogenic and autoimmune** | | |
| Primary HLH | Germline mutation in genes regulating granule-mediated cytotoxicity | CD8+ T cells, interferon-$\gamma$ |
| Secondary HLH, or MAS | Viral cause (EBV or CMV), autoimmune disorder (rheumatoid arthritis or adult-onset Still's disease), or neoplastic disorder in patient with genetic susceptibility (lymphoma) | CD8+ T cells, interferon-$\gamma$, interleukin-1$\beta$, myeloid-cell autoinflammation |
| Autoinflammatory disorders | Germline mutations in genes regulating the innate immune system and inflammasome activation | Innate cells, TNF, interleukin-1$\beta$ |
| Idiopathic MCD | Unknown cause | Interleukin-6, activated T cells, mTOR |

## 2.1 CRS INDUCED BY CAR T CELL

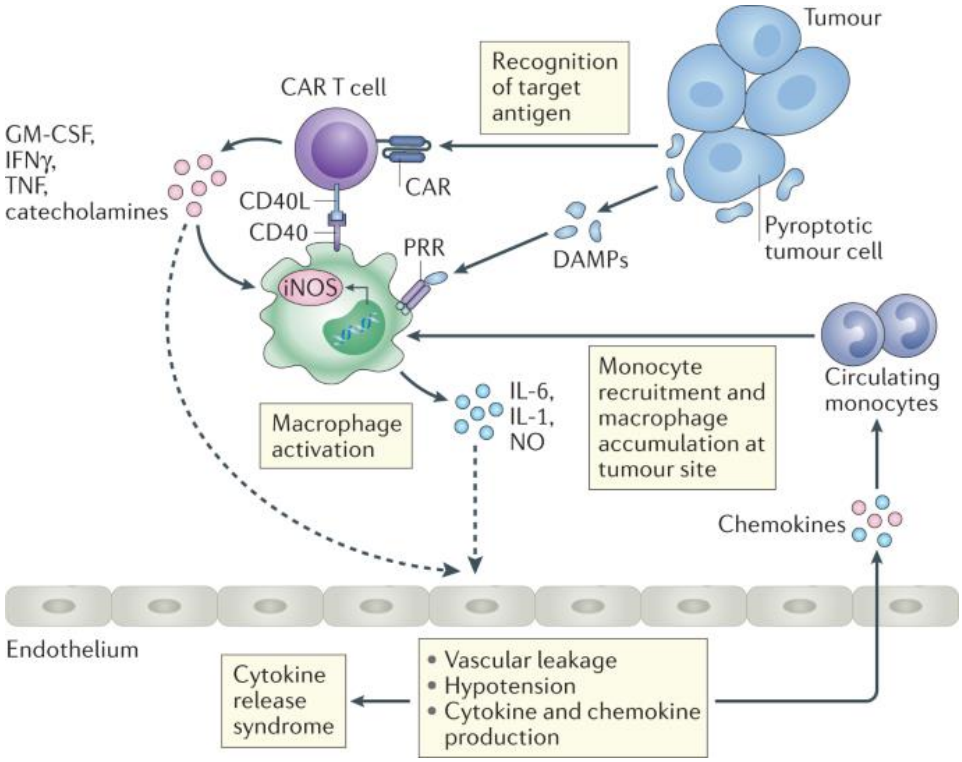


**Figure 3: Mechanisms underpinning CRS induced by CAR T cells**. CAR T cells are strongly activated via the recognition of the target antigen by the CAR, leading to a massive production of TNF-α and IFN-γ. Monocytes and macrophages are in turn activated and release a large amount of TNF-α, IL-1, IL-6 and nitric oxide (NO). These cytokines activate endothelial cells which then increase the production of IL-1, TNF-α and IL-6, amplifying the inflammatory cascade activation of the coagulation cascade. Adapted from Morris *et al.*[78]

### 2.1.1 Epidemiology and risk factors of CRS

CRS is the most common toxicity observed after CAR T cell infusion, which has been reported to occur in 54% to 100%[79] of patients, including severe CRS in 8.3% to 43%[64]. Immune effector cell-associated neurotoxicity syndrome (ICANS) is the second main toxicity arising from CAR T cells and occur in 32% to 64% of patients[80]. Importantly, CRS and neurotoxicity is not restricted to CAR T cells targeting CD19[81-84]. Both toxicities were documented with CAR T cell therapies targeting other hematological antigens, such as molecule B cell maturation antigen (BCMA)[82], CD20[83] or CD22[84].

CRS onsets often occur within hours or days following injection of the CAR T cells, and typically resolve within 7-8 days, which is correlated with the proliferation of the cellular therapy[46,85]. Neurotoxicity is often delayed and developed 5-7 days after CAR-T cell infusion, that is, near the end or just proceeding CRS onsets[104]. Generally, the severity of neurotoxicity correlates with the severity of CRS.

Several factors can increase the risk to develop severe CRS, such as elevated disease burden[46,86], type of lymphodepletion prior CAR T cells infusion[104], high number of injected CAR T cell and composition of the CAR construct[89]. Other patient-specific factors such as pre-existent state of inflammation (baseline serum ferritin) and baseline endothelial activation (thrombocytopenia) appear to be predictive of higher grade CRS[87,88].

Costimulatory signal domains (such as CD28 or 4-1BB) can significantly impact CAR-T cell proliferation and expansion[89], two characteristics that correlate with CRS and neurotoxicity severity. CARs with the CD28 costimulatory domain induce a sharp proliferative response and vigorous activation of effector functions whereas the 4-1BB costimulatory domain promotes longer persistence[90]. In two randomized trials, the incidence of CRS was reported at 93% and 57% in patients treated with a CD28-containing CAR and a 4-1BB-containing CAR T cells[91,92], respectively. Similarly in two other clinical studies, 42% of patients experienced severe neurotoxicity when treated with CD28-containing CAR[93], whereas 30% of patients treated with a 4-1BB-containing CAR T cells developed neurotoxicity[64,104]. In addition, in the two latter studies, patients treated with CD28- or 4-1BB-containing CAR that developed neurotoxicity, 72% versus 29% experienced severe neurological disorders like seizures, respectively. Conversely, in a preclinical study investigating CD44-CAR T cell for treating AML and multiple myeloma, aggravation of severe toxicities was found in case of a 4-1BB design, rather than a CD28 design[196].

### 2.1.2 Pathogenesis of CRS

*Traditional concept*

CAR T cell-induced CRS was traditionally viewed as a T cell-mediated syndrome, initiated by on target effect. Basically, injected CAR T cells migrate to the bone marrow, lymph nodes and tissues where they recognize their cognate antigen on the malignant cells and undergo a rapid activation, proliferation and expansion[94-96]. The result is a massive release of cytokines, including IFN-γ and TNF-α, which subsequently, activate bystander immune and non-immune cells, such as monocytes, macrophages, dendritic cells, and endothelial cells, that become activated and release a significant amount of cytokines (Figure 3).

*Role of monocytes/macrophages*

Recent studies suggest that activated macrophages and monocytes play a central role in CRS severity, through production of IL-6, IL-1, and nitric oxide (NO)[195,196]. In the afore mentioned studies, macrophage depletion, or selective modulation of macrophage activity with either CD40 ligand (CD40L) or inducible nitric oxide synthases (iNOS) inhibitors or anakinra, an IL-1 receptor antagonist (IL-1RA), abrogated CRS development. Consistently, in patients experiencing CRS, serum levels of cytokines characteristic of activated macrophages and monocytes, including IL-10, IL-12, TNF-α, IL-6 IFN-α, MCP-1 and MIP-1α, are often among the highest[64,98,99].

While macrophages are usually activated by T cells through CD40-CD40L binding, the requirement of the CAR T cell-macrophage contacts for their activation in CRS remains unclear. Indeed, in a humanized mouse model of CRS induced by CAR T cells, Giavridis and colleagues reported that CRS was more severe when non-obese diabetic (NOD) severe combined immunodeficiency (SCID) gamma mice (also called NSG mice) were infused with murine CD40L-expressing human CAR T cells[195], which reproduce the CD40L-CD40 interaction since hCD40L cannot directly interact with mCD40[100]. On the other hand, in the same study, the occurrence of CRS was still observed with 'classic' human CAR T cells, suggesting CAR T cells could activate myeloid cells through a variety of other pathways, likely cytokines, other cell contact–dependent pathways and Toll-like receptor stimulation[101]. For instance, CAR T-produced GM-CSF was shown to be able to stimulate and enhance the mobilization and proliferation of monocyte-macrophage lineage[102] (Figure 4). Catecholamines were also suggested as a possible macrophage activator in CRS. Consistently, an elevated concentration of catecholamine is reported during CRS in a pre-clinical study[103]. In addition, since macrophages can also secrete catecholamines, elevated catecholamines interacting with macrophages induce a self-amplification loop in macrophages[103], ultimately enhance inflammatory injury during CRS (Figure 4).

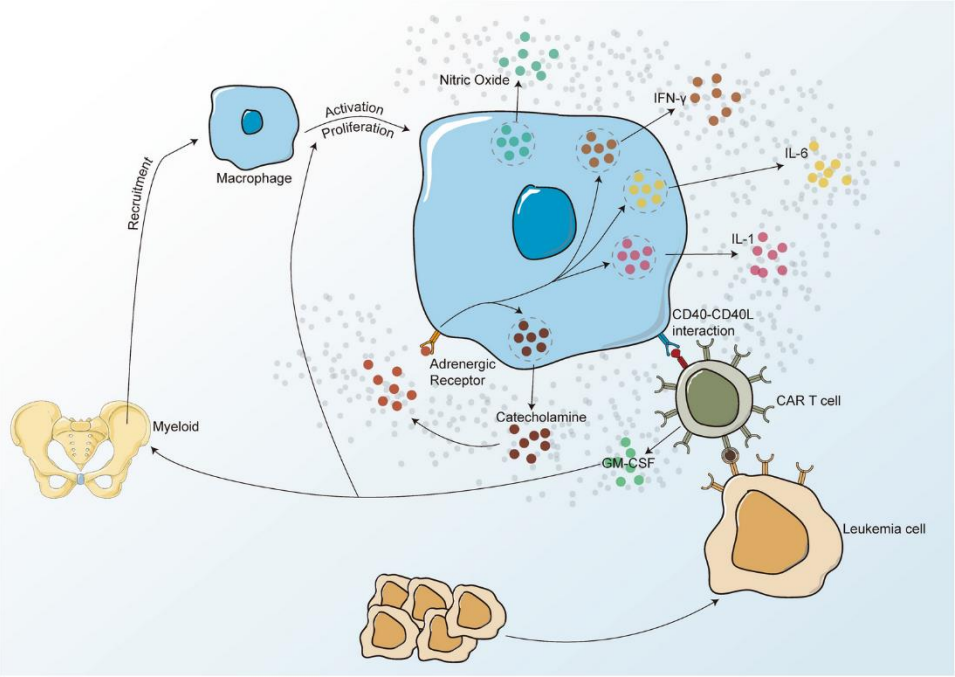


**Figure 4: The role of macrophage in CRS.** Once activated, CAR T cells produce GM-CSF to stimulate and enhance the mobilization and proliferation of monocyte-macrophage lineage. Recruited macrophages turn to activation status likely through the CD40-CD40L interaction with CAR T cells, and sensing of cytokines produced by CAR T cells. Activated macrophage release in turn proinflammatory cytokines, and ultimately participate in the CRS. Adapted from Hao *et al.*[102]

*Role of endothelial cells*

Endothelial cell (EC) activation and/or dysfunction appear to play a crucial role in the pathogenesis of CRS[64,104], which is highlighted by elevated levels of Ang-2 and von Willebrand factor in the serum of patients with CRS[64]. Ang-1 and Ang-2 regulate blood vessel remodelling through their binding on Tie2 receptor expressed on endothelial cells. Under normal conditions, the serum concentration of Ang-1 exceeds that of Ang-2 and, therefore, preferentially binds the Tie-2 receptor, which favours endothelial quiescence and vascular stability. In severe CRS, elevated amount of Ang-2 can then displace Ang-1 from the receptor, leading to endothelial activation and may explain the vascular instability, capillary leakage, and hypercoagulability[80,105]. Moreover, studies performed from one patient who succumbed to CRS revealed that endothelial cells seem to be an important source of IL-6 in severe CRS[106], suggesting that the cells play a crucial role in the maintenance and exacerbation of CRS. Moreover, the pathogenic role of endothelial cells is further evident since patients with pre-existing endothelial inflammation and/or activation showed higher risk of developing higher grade of CRS and neurotoxicity[87,88].

Activation of ECs, and the resulting vascular dysfunction, is closely correlated with the occurrence of neurological disorders[104] (Figure 5). A histological analysis documents that patient with ICANS have increased levels of protein, $CD4^+$, $CD8^+$ and CAR T cells in the cerebral spinal fluid (CSF), which indicates blood brain barrier disruption[93]. Consistently, CAR T cells and host T cells are accumulated in the CSF and brain parenchyma of rhesus macaque infused with CD20-CAR T cell and experiencing neurotoxicity[107]. Nonetheless, whether T cells are bystanders or active contributors to the development and maintenance of neurotoxicity remains an unanswered question[85]. Autopsy studies after cases of fatal neurotoxicity gave variable findings including infrequent non–CAR T cells in the brain parenchyma and CSF, macrophage infiltration, microglial[108] and endothelial activation[104].

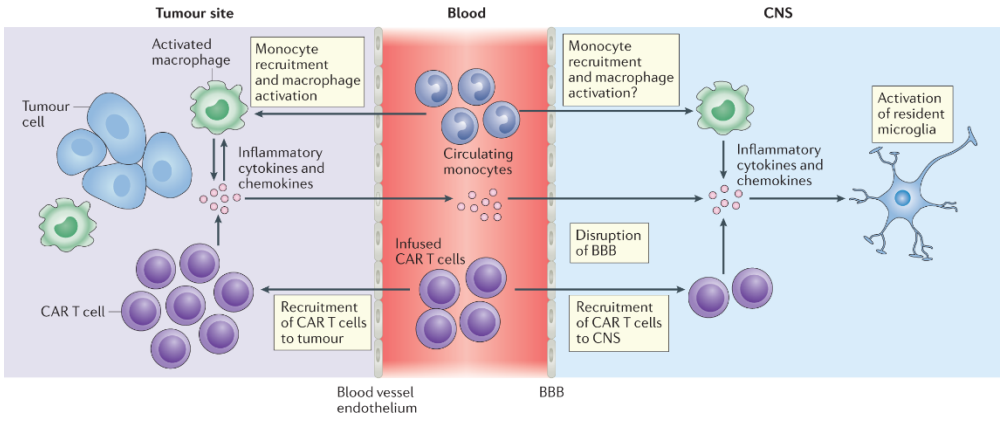


**Figure 5: Pathophysiology of immune effector cell-associated neurotoxicity syndrome (ICANS).** The activation of CAR T cells and bystander immune cells, such as macrophages, results in the production of inflammatory cytokines and chemokines, such as IL-1β, IL-6, INF-γ, TNF-α, CXCL8, CCL2, and GM-CSF. Those cytokines diffuse into the bloodstream and could favour the disruption of the blood–brain barrier, leading to an accumulation of cytokines and CAR T cells in the central nervous system and an activation of resident microglial cells. Adapted from Morris *et al.*[78]

### 2.1.3 The key role of IL-6

*Sources of IL-6*

The key role of IL-6 in CRS was rapidly suggested since its serum concentration was consistently up-regulated in patients with CRS and is often correlated with disease severity. Consistently, the US Food and Drug Administration (FDA) approved the use of tocilizumab[109], an anti-IL6R, for managing CRS induced by CD19-CAR Ts cells.

IL-6 is secreted in response to stimulation, by several types of immune cells, such as T lymphocytes, monocytes/macrophages, dendritic cells, and non-immune cells, such as endothelial cells, mesenchymal cells, and fibroblasts[110]. In the context of CRS, IL-6 appears to be predominantly produced by monocytes macrophages and endothelial cells[195,196].

*IL-6 signalling pathways*

IL-6 is a pleiotropic cytokine and exerts its biological functions via two major pathways: "classical signalling" and "*trans*-signalling" pathways (Figure 6A and B). In classical signalling, the signal transduction is mediated by binding of IL-6 to the membrane IL-6 receptor (mIL-6R) which leads to dimerization of the membrane protein gp130 (Figure 6A). In *trans*-signalling, IL-6 binds to a soluble form of the IL-6R (sIL-6R), generated by either cleavage of mIL-6R or alternative IL-6R mRNA splicing. The formed IL-6/sIL-6R soluble complex can then bind to gp130 on the cell surface[111,112] (Figure 6B). A third IL-6 signalling pathway has recently been identified, termed IL-6 *trans*-presentation. This mechanism is mediated by the binding of IL-6 to mIL-6R on a "transmitting cell," which then presents the IL-6/IL-6R complex to gp130 expressed at the membrane surface of another cells[**113**] (Figure 6C).

Under healthy conditions, serum IL-6 is almost undetectable: IL-6 binds either to mIL-6R and activates the classical signalling, or to sIL-6R and the complex is inhibited by sgp130 which hampers *trans*-signalling (Figure 6D). However, under inflammatory conditions, IL-6 concentration increases, together with the serum sIL-6R concentration, whereas sgp130 level remains comparable, leading to the activation of the IL-6 *trans*-signalling. IL-6R is expressed at the membrane surface of a restricted number of cell-subtypes, including leukocytes, epithelial cells, and hepatocytes, whereas gp130 is ubiquitously expressed. Therefore, IL-6 *trans*-signalling is potentially able to stimulate all cells of the body, including osteoclasts, synoviocytes, endothelial cells, and neural cells [110]. Concerning the IL-6 *trans*-presentation pathway, it involves specialized dendritic cells (expressing the mIL-6R), which have been shown to be required for priming of pathogenic T helper 17 (Th17) cells[113].

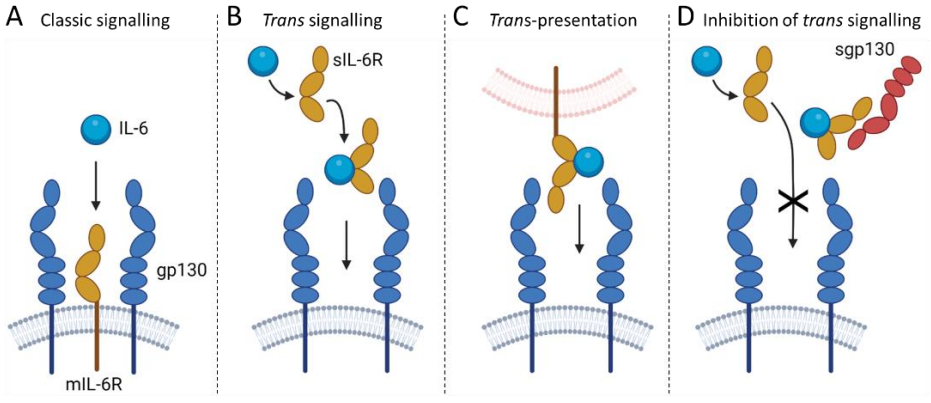


**Figure 6: IL-6 signalling pathways and constitutive inhibition**. Adapted from Kang *et al.*[113] and Lee *et al.*[114]

*IL-6 roles in the development of severe CRS features*

During CRS, IL-6 plays an important role in the development of many clinical symptoms of CRS[27]. For instance, during the acute phase of inflammation, IL-6 acts on hepatocytes in the liver, inducing the expression of acute-phase proteins, such as CRP, serum amyloid A, both hallmarks of severe CRS[115].

High IL-6 levels may also participate to the activation of endothelial cells and the coagulation cascade, which subsequently induce vascular leakage and DIC[116,117] (Figure 7), one of the severest CRS clinical symptoms. Upon exposure to IL-6, endothelial integrity can be impaired due to both VE–cadherin disassembly and increased C5a receptor expression on vascular endothelial cells (Figure 7), resulting in vascular leakage.

Activation of the coagulation cascade can be also trigger by IL-6, which induces upregulation of tissue factors from ECs[118] and on monocytes[119]. Tissue factors subsequently promote thrombin activation, involved in the terminal steps of the coagulation cascade, and fibrin clot formation, favouring thrombosis events (Figure 7). High level of D-dimer quantified in severe CRS mirrors the high amount fibrin clot. Furthermore, IL-6 induces directly (via *trans*-signalling pathway) and indirectly (via induction of tissue factors production) the production of cytokines from the immune cells and ECs, further fuelling the CRS[120,121] (Figure 7).

While the primacy role of IL-6 in CRS appears obvious, a growing amount of evidence suggests that other cytokines, such as IFN-γ, TNF-α, IL-1 and GM-CSF may also play a central role in the pathophysiology of the CRS.

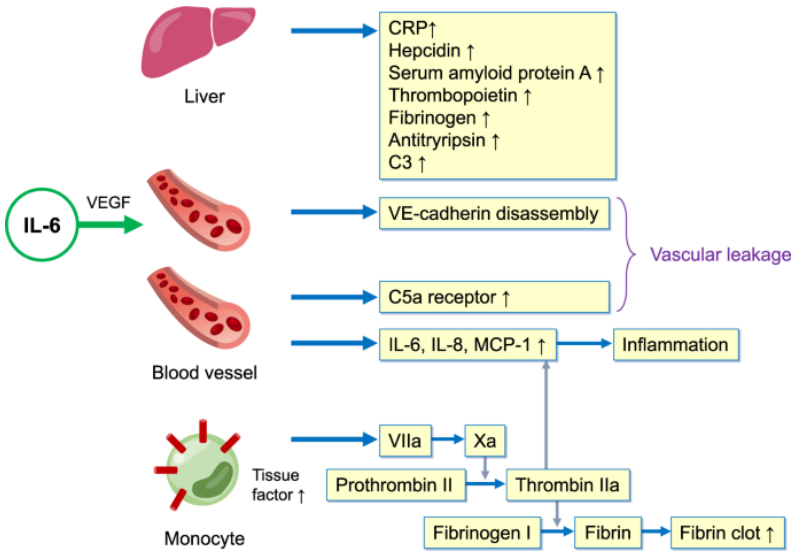


**Figure 7: IL-6 roles in the development of CRS features.** High level of IL-6 in the liver can promote the production of acute-phase proteins in the liver, such as CRP, serum amyloid A, antitrypsin, hepcidin, fibrinogen, thrombopoietin, and complement 3. IL-6 in blood circulation can also interact with endothelial cells, leading to vascular permeability and/or production of proinflammatory cytokines. IL-6 can also trigger the expression of tissue factor on circulating monocytes, resulting in an increase formation of fibrin clot. The thrombin released during this process can also induce the production of proinflammatory by vascular endothelial cells. Adapted from Kang and Kishimoto.[116]

### 2.1.4 What about the other cytokines; IFN-γ, IL-1, TNF-α and GM-CSF in the foreground

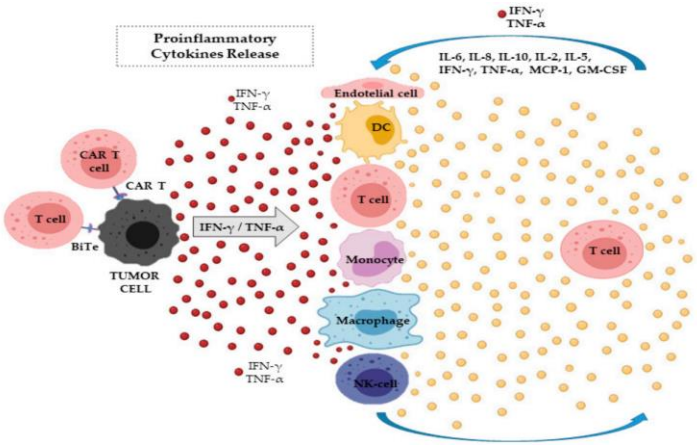


**Figure 8: Cytokines involved in the CRS.** The activation of T cells or CAR T cells induces the release of IFN-γ and TNF-α, which in turn activate other immune cells, subsequently amplifying the cytokines production. Adapted from Cosenza *et al.*[77]

In mouse models of CRS induced by another potent activation of T-cell, i.e. using anti-CD3 mAbs, a detailed description of the kinetic of cytokine production in the first hours post injection reveals that TNF-α and IFN-γ peaked within 1–2 hours and preceded the increase of IL-6[122]. In the context of CAR T

cells, the recognition of the tumours antigens by the CAR likely induces the IFN-γ and TNF-α production by CAR T cells (Figure 8). Both pro-inflammatory cytokines in turn activate other immune cells, such as macrophages[56], which produce in turn excessive quantities of cytokines[56,123], including IL-1, IL-6, TNF-α, and IL-10, further intensifying the CRS (Figure 8). Moreover, similarly to IL-6, TNF-α and IL-1, can activate endothelial cells[55,124] leading to release of procoagulant particles by ECs and production of tissue factors by ECs[118] and monocytes[125] (Figure 9). Furthermore, IL-6 and TNF-α may engage in autocrine signalling with STAT-3 and NFκB, respectively, resulting in self-amplifying and self-sustaining inflammation[121,126,127], ultimately resulting in a cytokine storm (Figure 8).

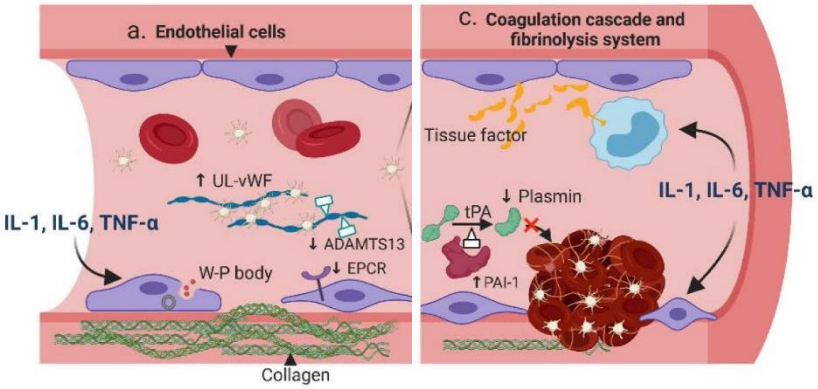


**Figure 9: Role of cytokines in endothelial cell dysfunctions and resulting disorders.** (a) Endothelial cells can be stimulated by pro-inflammatory cytokines to secrete pro-coagulant factors such as Weibel–Palade (W–P) body, reorganize its cytoskeletons to expose the highly coagulant collagen, and downregulate the expression of anticoagulant protein, such as the endothelial protein C receptors (EPCR) and ADAMTS-13. (c) Pro-inflammatory cytokines, such as IL-1, IL-6, and TNF-α can triggered the expression of tissue factor by endothelial cells and circulating monocytes. Adapted from Wang and Doran.[55]

The importance of IL-1 as a central cytokine in the CRS was recently suggested in studies recapitulating the CRS features induced by CAR T cells[195,196]. IL-1 was shown to increase earlier than IL-6 and its blockade abrogated the CRS. Most importantly, mice treated with anakinra, an IL-1RA, did not develop neurotoxicity, whereas IL-6 blockade failed to do so. Like the cellular mechanisms, the molecular mechanism underpinning the neurotoxicity is poorly understood, mainly because CRS and neurotoxicity is often present simultaneously, making it difficult to identify the neurotoxicity-specific cytokines[85]. So far, patients with severe ICANS (and also severe CRS) were found to have elevated concentrations of MCP-1, CXCL10 (an IFN-γ inducible chemokine), IL-6, IL-8, GFAP (a marker of astroglial cell injury[128]), and S100b (a marker of astrocyte activation[129]), in the CSF, suggesting CNS-specific production by activated myeloid, astrocyte, and/or endothelial cells[78,93].

Overall, other cytokines were also found to be elevated during the course of CRS, including IL-2, IL-8, IL-5, MCP-1, and GM-CSF, implicated in the disease manifestation (Figure 8).

Among the afore-mentioned cytokines, GM-CSF is a potent activator of myeloid cells promoting their maturation, which in turn produce cytokines and chemokines, such as IL-1, IL-6, TNF-α, CCL2 (MCP-1), IL-8 and CCL17[102,130]. GM-CSF can also recruit immature myeloid cells from the circulation and aid in their terminal differentiation. In addition, GM-CSF can induce dendritic cells to prime the adaptive immune response. In mouse models of CRS induced by CAR T cells, the blockade of GM-CSF resulted in a significant reduction of cytokine levels, such as IL-6, MCP-1, IL-8a IL-2, and IL-1RA, without impacting the level of key T-cell-cytokines IFN-γ and TNF-α[131,132]. Moreover, microglia, brain macrophages, and astrocytes express high levels of GM-CSF receptor[133]. Therefore, GM-CSF may be involved in the neurotoxicity associated with CAR T cell therapy, which is supported by the decreased brain inflammation, observed by brain MRIs, in xenograft mouse model of CRS induced by CAR T cells and treated with an anti-GM-CSF[131].

## 2.2 THE CYTOKINE STORM OF COVID-19

### 2.2.1 Immunopathological abnormalities

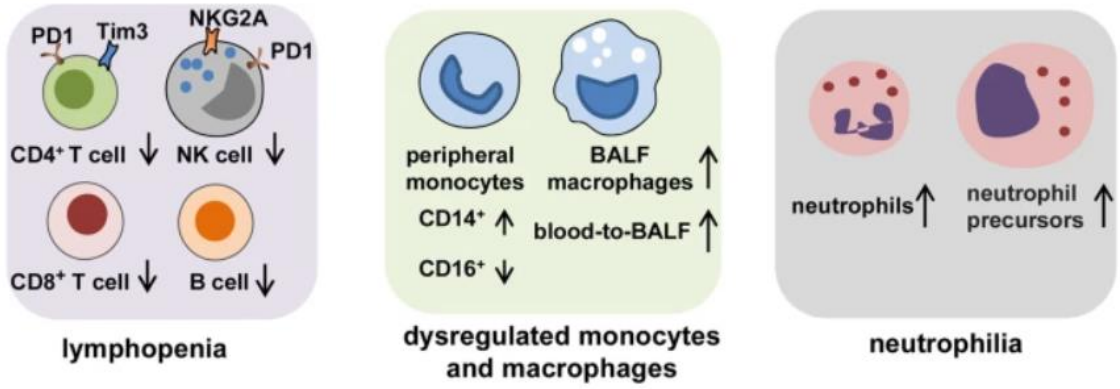


**Figure 10: Immunopathological manifestations of severe COVID-19.** Adapted from Yang *et al.*[134]

*Exaggerated cytokine levels*

While patients with COVID-19 showed elevated levels IL-1, IL-4, IL-7, IL-8, IL-9, G-CSF, MCP-1, GM-CSF, and IFN-γ in comparison to healthy controls, the particular high concentrations of sIL-2Ra, IL-6, IL-10, CXCL8 and TNF-α allowed to distinguish severe cases, that require intensive care and ventilation for oxygen support, from non-severe cases[45,135,136].

*Leukocytes trafficking to the lung*

Patients with severe COVID-19 commonly presented drastic lymphopenia, including depletion of $CD4^+$ T cells, $CD8^+$ T cells, B cells, and natural killer cells[40,134,137,138] (Figure 10). In addition, expression makers of lymphocyte exhaustion, such as programmed cell death protein 1 (PD-1), natural killer cell receptor NKG2A, and T cell immunoglobulin mucin 3 (TIM-3) were significantly up-regulated in the peripheral blood of COVID-19 patients compared to healthy subjects[139]. The occurrence of lymphopenia can be explained by several mechanisms. 1) severe acute respiratory syndrome coronavirus 2 (SARS-CoV-2) infects cells via angiotensin-converting enzyme 2 (ACE2) receptor expressed at the membrane surface. Since T cells expressed ACE2[140], the straight infection of T cells by SARS-CoV-2 may lead to cell death [134]. 2) ACE2 is broadly expressed on secondary lymphoid tissues, such as spleen and lymph nodes. Virus infection can cause damage on such tissues, which is supported by the observations of splenic atrophy and lymph node necrosis [141]. 3) Cytokine-mediated depletion and exhaustion of T cells can also occur. 4) T cells can also accumulate in the airways and the lung parenchyma in response to combinations of distinct trafficking signals expressed by airway and alveolar blood vessel endothelial cells.

Other markers of the COVID-19 severity is neutrophilia (Figure 10), the resulting elevated neutrophil: lymphocyte ratio in blood, and has been proposed as a predictive marker of mortality[142]. As part of the first line of innate immune response, neutrophils have a protective role in infections through phagocytosis, reactive oxygen species (ROS) generation, degranulation, neutrophil extracellular traps (NET) formation and cytokine/ chemokine production[143]. However, the overactivation of neutrophils and, particularly, NETs release was shown to activate the coagulation pathways and hence favour DIC[143-145] (Figure 11b). Nevertheless, it is still poorly understood how the virus promotes neutrophil recruitment in COVID-19. Among all the up-regulated cytokines, the level of G-CSF, a major promotor of neutrophil development, and CXCL8 (IL-8), a potent attractant chemokine of neutrophils, were consistently elevated in COVID-19 patients and may promote neutrophil mobilization from the bone marrow to the inflamed lung[146]. Overall, neutrophils likely transit in the blood to accumulate in the lung, which is supported by the increased level of neutrophils observed in the bronchoalveolar lavage fluid (BALF) of COVID-19 patients. Activated neutrophils, in their quest to fight lung infection, can promote damage of the surrounding cells and tissues[147]. Particularly, NETosis, the process that aims at stopping the viral dissemination by capturing it thanks to the released NETs[148], can aggravate damage to the pulmonary endothelia and epithelia, and induce acute lung injury (ALI) and in its more severe form

ARDS[149], as it was also demonstrated in CRS induced by severe influenza[150]. In addition, neutrophils can produce a large amount of CCL2, a potent monocyte attractant, and further amplify the inflammation[151].

Consistently, circulating blood monocytes are also abnormally elevated in CRS (Figure 10). In human, circulating monocytes can be classified according to their CD14 or CD16 expression: classical $CD14^+$ (more than 80%), intermediate $CD14^+CD16^+$ (about 15%) and non-classical $CD16^+$ (less than 5%) monocyte subsets[152]. The latter, also termed 'patrolling monocytes', maintain vascular homeostasis by crawling along endothelial cells to detect signs of injury[153]. In contrast, classic monocytes are recruited from the bone marrow to inflamed tissue where they can differentiate into monocyte-derived DCs or macrophages and initiate an inflammatory response[154]. In COVID-19 patients with severe CRS symptoms[155] (i.e. developing ARDS), classic monocytes were significantly increased, whereas non-classical and intermediate monocytes were reduced (Figure 10). As neutrophils, an increased number of inflammatory monocytes likely transit in the blood to infiltrate the inflamed lung, through a chemotactic gradient. In severe influenza infection, it was shown that the mobilisation of the monocytes from the bone marrow is mediated by the CCR2/CCL2[156], which was also reported in patients with severe COVID-19[163]. Analysis of BALF and circulating monocyte–macrophages from a patient with a severe form of COVID-19 revealed a phenotypic shift of monocytes from $CD16^+$ to $CD14^+$, when moving from the blood to the BALF[155,157]. In addition, activation markers on BALF macrophages[157,158], such as CD64 and HLA-DR, were highly expressed, as well as pro-inflammatory cytokines and chemokines characteristic of activated macrophages[155] . Therefore, monocytes-macrophages are recruited into inflamed tissue to clear viral infection. However, similarly to over-activated neutrophils, they can also contribute to pulmonary damage by secreting elevated levels of inducible nitric oxide synthase, TNF, IL-6[144], which is supported by clinical observations reported that systemic levels of IL-6 also appear to be directly correlated with the severity of COVID-19.

*Vascular dysfunction*

Another complication of COVID-19 is the excessive coagulation, which often degenerates in DIC in the most severe form. Analysis from the original outbreak in Wuhan reported that around 70% of people who died following SARS-CoV-2 infection had all symptoms of DIC, whereas only in 1% of survivors [159]. Similarly with coagulation dysfunction observed in CRS induced by CAR T cells, activated leukocytes, including monocytes and neutrophils, can damage capillary endothelium and disrupt the thromboprotective state of endothelial cells (Figure 11b), resulting in the development of DIC.

Endothelial cells likely take part in the development of the disorder since severe COVID-19 is also associated with systemic endotheliopathy, which is characterised by a severely damaged permeable vascular endothelial barrier and activated endothelial cells[160]. Moreover, while ECs can be activated by cytokines, such as IL-6, IL-1, TNF-$\alpha$[55] (Figure 9), SARS-CoV-2 virus was shown to infect them (Figure 11a) and induce vascular damage both in *in vitro* and *in vivo* studies, resulting in an increase ECs dysfunction[161,162].

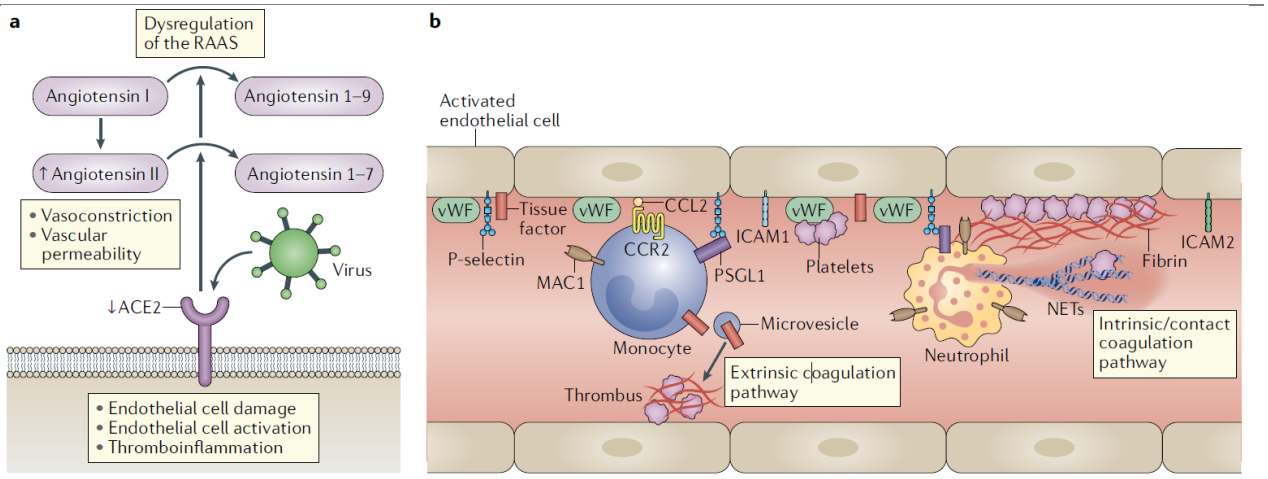


**Figure 11: Activation of endothelial cells, neutrophils and blood monocytes in SARS-CoV-2 infection induces coagulation dysfunction**. A. SARS-CoV-2 infects endothelial cells through its binding to ACE2, inducing a downregulation of the receptor. The decreased level of ACE2 dysregulates the renin–angiotensin–aldosterone system (RAAS), characterised by a reduction of angiotensin I and II cleavage, resulting in elevated vasoconstriction and increased vascular permeability. B. Infected endothelial cells, and endothelial cells activated by the increased level of proinflammatory cytokines, upregulate the expression of adhesion molecules, such as ICAM1 or P-selectin, and of monocyte and neutrophil chemo attractants, such as CCL2 and CXCL1. Recruited monocyte neutrophils released tissue factor-rich micro-vesicles and neutrophil extracellular traps, respectively, which activate the coagulation pathway, leading to massive fibrin deposition and blood clotting. In addition, both neutrophils and monocytes express the integrin macrophage 1 antigen, promoting their binding to the damaged endothelial cells, activated platelets and deposited fibrin. Adapted from Alon *et al.*[163]

### 2.2.2 Role of cytokines

The bronchial and alveolar epithelial cells are the first targets for SARS-CoV-2 infection. Consequently, stressed or infected epithelial cells release a large variety of inflammatory mediators, thereby attracting and activating multiple cell types critical for viral clearance, including B cells, T cells, natural killer cells, macrophages, dendritic cells and monocytes. During infections with SARS-CoV-2, a failure to rapidly clear the infections is thought to be the cause of the cytokine release syndrome, resulting in lung injury and virus spread to other organs[163,164]. The subsequent immune response is exaggerated to compensate for the target clearance failure[165,166]. This concept is supported by *in vitro* and *in vivo* experiments that

reported a profound impairment in type I and III IFNs responses[167], including IFN α/ ß, after the infection by coronavirus, also confirmed in COVID-19 patients who showed a low level of IFN activity and downregulation of IFN stimulated genes[168]. In those pre-clinical and clinical studies, an excessive secretion of pro-inflammatory cytokines from monocytes / macrophages, such as TNF-α, IL-1 and IL-6, was then observed in later stages.

IL-6 is considered as one of the key pathogenic cytokines in the CRS induced by COVID-19 since its level in serum rapidly appeared to be a reliable indicator of disease severity and predictive for patients who will require ICU support[169,170,171,172]. Similarly to CRS induced by CAR T cells, IL-6 is thought to play a critical in role endothelial cell activation, as well as take part to a self-amplification loop increasing the inflammation process. Along with IL-6, IFN-γ was also considered as a reliable indicator of COVID-19 patient deterioration and requiring ICU admission. IFN-γ is thought to be directly produced by $CD4^+$ T and activated $CD8^+$ T cells[164]. IFN-γ, together with IL-6, is also produced by $CD16^+CD14^+$ monocytes which are recruited into the pulmonary environment through the $CD4^+$ T cell-production of GM-CSF. Another cytokine also associated with poor prognosis is TNF-α, which remains elevated throughout the infection[169,173]. Moreover, while blocking IL-6 has had mixed results clinically, a recent mouse model showed that TNF-α and IFN-γ drive the cytokine storm and cell death associated with COVID-19. It was demonstrated that TNF-α and IFN-γ synergize to induce inflammatory cell death and that only the inhibition of both cytokines protected against lethal SARS-CoV-2 infection and other models of CRS such as sepsis or HLH[174].

Interestingly, IL-10 was also highly up-regulated in severe COVID-19 patients in the second week following the CRS symptom-onset. IL-10, a potent anti-inflammatory cytokine, is likely released as a feedback response to the increased levels of IFN-γ and IL-6, and is a biomarker of immune failure in the context of COVID-19 infection[135,169].

## 2.3 THE CYTOKINE STORM OF HEMOPHAGOCYTIC LYMPHOHISTIOCYTOSIS

### 2.3.1 Etiology and immune abnormalities associated with HLH

HLH is a life-threatening, hyperinflammatory disorder, associated to a cytokine release syndrome. It is traditionally divided into a primary or familial form (pHLH or FHLH), and a secondary or acquired form (sHLH) (Table 3)[3,175]. pHLH is typically induced by genetic impairment of the cytotoxic function of both natural killer (NK) and cytotoxic T cells (CTL)[175,176]. While secondary HLH was classically considered to have no genetic background, evidence is currently accumulating for the presence of mutations in the same genes that are altered in the pHLH[175,177]. Therefore, sHLH is more and more determined as a combination of a genetic predisposition, with an underlying chronic inflammatory state (such as in rheumatic diseases), and/or a triggering infection (such as Epstein-Barr virus and cytomegalovirus). Described as sHLH, macrophage activation syndrome (MAS) is a complication seen at times after rheumatic diseases, the most common being children with systemic juvenile idiopathic arthritis (SJIA) and in its adult form, Still's disease[178]. Similarly to pHLH, defects in NK cells and CD8 T cell cytolytic function likely contribute to the development of the CRS associated with sHLH[175].

Distinguishing pHLH from sHLH is difficult since most of the immune abnormalities are common to both syndromes[175]. Overall, HLH is characterised by elevated levels of IFN-γ, IL-1β, IL-6, IL-18, TNF-α, sIL-2Rα, CXCL9, CXCL10 and CXCL11[180]. A massive expansion of IFN-γ-secreting $CD8^+$ T cells and an increased NK cells activity is also common in HLH patients[181]. Moreover, extensive expansion of $CD163^+$ macrophages was reported in the bone marrow of a patient with MAS[182,183]. The CD163 expression identifies macrophages (both M1 pro- and M2 anti-inflammatory macrophages) undergoing differentiation to enhance their phagocytic activity[184]. More generally, hemophagocytosis, which corresponds to the phagocytosis of RBCs, WBCs, and platelets, in the bone marrow or other tissues such as lymph nodes, liver, or spleen, is one of the clinicopathologic criteria associated to HLH[185].

### 2.3.2 Pathogenesis of HLH

HLH comprises a heterogenous spectrum of disease which is induced by different triggers, but resulting in the same upstream events: $CD8^+$ T-cell hyperstimulation. In the case of pHLH, the initiation event is typically an infectious trigger. The inability of $CD8^+$ T cells and NK cells to lyse the infected cells likely increased viral load and prolonged antigen stimulation[186]. The consequence is heightened antigen presentation by antigen presented cells (APC), such as dendritic cells (DC), that continues to activate CTLs and prolong the sustained pro-inflammatory cytokine release[187-189]. Moreover, inadequate downregulation of immune activation is more and more considered as another key mechanism of HLH.

Indeed, CTLs display immunoregulation functions, which mainly rely on the perforin-dependent killing of infected APCs. The defect in the ability of CTLs to kill infected APCs results in continuous antigen presentation and stimulation, enhancing the activation and proliferation of CTLs[190,191]. Similarly, NK cells also display immunoregulatory by limiting hyperactivation of CTL and tissue infiltration by activated macrophages[192] (Figure 12).

The upregulation of $CD8^+$ T cell and NK activity is characterised by the excessive release of TNF-α and IFN-γ, which mediates secondary activation of macrophages and other cell types[198]. The failure to down-regulate activated macrophages further increases their activation and results in chronic macrophage activation, development of haematophagocytosis, and sustained cytokine release[191]. An autocrine engagement between the activated CTLs and macrophages reinforces a positive feedback loop, ultimately resulting in an often-lethal cytokine storm[40,179,191] (Figure 12).

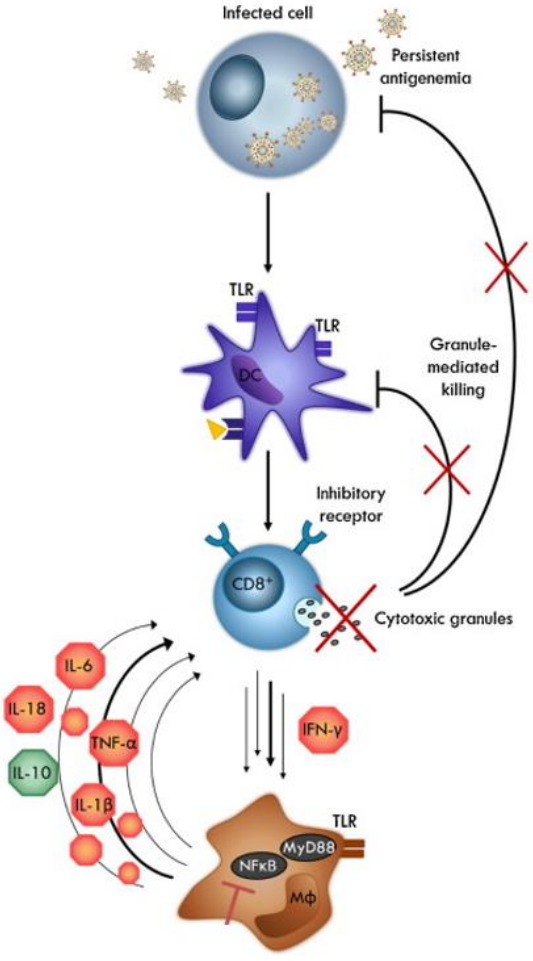


**Figure 12: Pathophysiology of HLH.** Impairment in the cytotoxic function of $CD8^+$ T cells and NK cells results in persistent interaction between the activated DCs, and the cytolytic T cells and NK cells. The activated T cells produce increasing amounts of IFN-γ that mediates activation of macrophages (Mϕ) and other cell types which in turn secrete multiple cytokines. TLR = Toll-like receptor. Adapted from Brisse *et al.*[191]

### 2.3.3 Role of individual cytokines

Several cytokines, including IFN-γ, TNF-α, IL-6, IL-10 and IL-18, are consistently elevated in HLH patients and in several animal models[191]. IFN-γ appears to be the essential cytokine for the disease development[178,191]. Indeed, IFN-γ levels, as well as the IFN-γ-inducible chemokines CXCL9, CXCL10 levels, rise early and quickly in patients with HLH and correlate with the laboratory feature abnormalities characteristic of HLH, including ferritin, alanine transferase levels, neutrophil and platelet counts. The recent FDA approval for the use of emapalumab, an anti-IFN-γ mAb, for primary forms of HLH (pHLH) is clinical validation of its role in CRS[238] .

Several murine models of pHLH and sHLH/MAS reported the high levels of IL-6 and hypothesised that it can play a pathogenic role in HLH[191]. Consistently, IL-6 levels in patient are often elevated and correlate with disease activity[40]. In addition, tocilizumab, an anti-IL-6 receptor antibody, was successfully administered to a patient who developed MAS. Therefore, IL-6 also appears to be a crucial player in the pathogenesis of CRS induced by HLH, although its precise role is not well studied[182].

TNF-α should be, theoretically, a critical actor in the HLH development. Indeed, TNF-α is commonly produced by monocytes/macrophages and $CD8^+$ T cells, which are strongly activated and undergone massive expansion in HLH, respectively[190-192]. Nonetheless, although elevated, TNF-α levels are only slightly higher in MAS compared to those reported in children with active SJIA without severe complications, for instance[40]. In addition, anti-TNF-α agents, such as etanercept, infliximab or adalimumab in different HLH patients, have shown variable success[182,191]. Thus, the role of TNF-α in HLH/MAS remains unclear.

Patients with HLH demonstrated elevated levels of IL-18. The increase in IL-18 levels is accompanied by a decrease in the IL-18 binding protein (IL-18BP), a natural inhibitor of the cytokine, resulting in a high level of biologically active free IL-18[40,182,191]. Moreover, IL-18 was shown to promote IFN-γ production by NK cells and T cells and TNF-α secretion by macrophage[179]. Therefore, its key role in the development of HLH is more and more suggested.

# 3 CURRENT CRS TREATMENT

Severe CRS requires prompt and aggressive treatment that counteract the immune response to avoid life-threatening outcomes. The efficacy of neutralizing specific cytokines, as well as more general immunosuppressive strategies, was proven or are under investigation (Table 4 and Figure 13).

**Table 4: Principal therapeutic options for the treatment of CRS.** Abbreviation: IFN: interferon; IL: interleukin; TNF: tumour necrosis factor; GM-CSF: granulocytes/macrophage colony stimulating factor; JAK: Janus kinase; RA: rheumatoid arthritis; HLH: hemophagocytic lymphohistiocytosis MAS: macrophage activation syndrome; *: US FDA approved. Adapted from Kim *et al.* [206]

| Targeted | Drugs or intervention | Approved indications* and off-label indications |
|---|---|---|
| **IL-1** | Anakinra, Canakinumab | RA*, MAS/HLH, COVID-19 |
| **IL-6** | Tocilizumab, Sarilumab, Siltuximab | RA*, CAR T CRS*, COVID-19, BiTE |
| **TNF-α** | Etanercept | RA*, MAS, Dengue, influenza, SARS-CoV-1, COVID-19 |
| **IFN-γ** | Emapalumab | Primary HLH*, COVID-19 |
| **GM-CSF** | Lenzilumab, Otilimab, Mavrilimumab | CAR T CRS, COVID-19 |
| **JAK** | Baricitinib, Ruxolitinib | RA*, COVID-19, CAR T CRS |
| **Non-selective** | Steroids | Various viral respiratory diseases and hemorrhagic fevers, CAR T, BiTE |

## 3.1 TARGETING SPECIFIC CYTOKINES

### 3.1.1 IL-6 and IL-6R inhibitors

IL-6 has emerged as a critical cytokine in the progression of CRS. Biological drugs against IL-6 can target the cytokine (clazakizumab, olokizumab, sirukumab and siltuximab), its receptor (tocilizumab and sarilumab) or the sIL-6R and hence specifically inhibit the IL-6 *trans*-signalling (olamkicept).

Tocilizumab, an anti-IL-6R mAb, was approved in 2017 for the management of CAR T cell-induced CRS by both US FDA and European Medicines Agency (EMA)[109]. Althought tocilizumab is currently the standard treatment to control the CRS induced by the CAR T cell therapy, its use is not recommended for the highest forms of CRS (grade ≥ 4) and more intense treatments, such as corticosteroid and mechanical ventilation, is recommended to prevent death[200]. In addition, tocilizumab has been relatively poor at controlling neurotoxicity associated with CD19-CAR T cell therapy. Indeed, similarly to most of monoclonal antibodies, tocilizumab does not cross the BBB and therefore could not reduce the

inflammation in the CNS. Moreover, a transient increase of serum IL-6 levels was seen in patients administrated CAR T cells and treated with tocilizumab, likely due to the competitive inhibition IL-6 by the mAb, and may explain the persistence of neurological symptoms, which are even sometimes exacerbated. Therefore, the use of siltuximab, an antibody that directly blocks circulating IL-6, was proposed as an alternative to tocilizumab and could avoid the potential IL-6 increase as observed after IL-6R blockade. However, the evidence for its benefit in ICANS management remains anecdotal and formal studies are needed to test its benefit on both CRS and ICANS[36,48,75,201].

Tocilizumab was also used for the management of blinatumomab-induced CRS, even though its use is more considered as an option if no improvement is noted after drug cessation and treatment with steroids. Indeed, the common treatment strategies for controlling the blinatumomab-induced toxicity rely on using corticosteroids or/and temporary discontinuing the infusions of the BiTE, which is always administered as several-day continuous infusion[202].

Tocilizumab's ability to manage CAR-T cell-induced CRS, prompted many groups across the world to investigate the clinical benefit at blocking IL-6 signalling in severe COVID-19 patients. Although some studies reported a clear benefit in patients treated with tocilizumab, leading to FDA approval of this therapy in patients with COVID-19[144], majority of the clinical trials were underpowered and small-sized. Therefore, the utility of blocking IL-6 signalling in COVID-19 is, to date, still disputed[144,174,217]. Nevertheless, most of the studies (testing either anti-IL-6R or anti-IL-6 mAbs) have shown promise in reducing significantly mechanical ventilation requirement, risk of ICU admission, and mortality of COVID-19 patients[203]. Elevated IL-6 levels are also seen in Ebola virus-induced CRS and may thus also warrant studies aimed at blocking this pathway. Indeed, a mouse model of Ebola disease was used to demonstrate the beneficial effect of IL-6 blockade[204].

IL-6 *trans*-signalling has been shown to be a key pathway in chronic inflammation and cancer development[214,215]. Specific blockade of IL-6 *trans*-signalling is possible using Olamkicept, a molecule resulting from the fusion of sgp130 with the human-IgG1 Fc portion (sgp130-Fc). Olamkicept binds to the IL-6/sIL-6R complex and preventing further binding to membrane gp130[217]. While efficacy of *trans*-signalling blockade was shown in acute inflammatory diseases, such as rheumatoid arthritis, sepsis and malaria, this therapeutic strategy has never been testing in the context of CRS but could be another promising option to control CRS induced by pathogens and drug therapy[216-219].

### 3.1.2 IL-1 inhibitors

IL-1 is one of the major pro-inflammatory cytokines described to recruit immune cells and to induce down-stream cytokine production[220]. Elevated IL-1 level is commonly observed in most CRS settings. Anakinra, a highly effective IL-1 receptor antagonist, is used off label for the treatment of sHLH/MAS in children and adults[221,222], and was shown to resolved clinical symptoms and normalized laboratory features within days post administration[223] and even mortality rate[71]. Both anakinra and canakinumab, a mAb neutralising IL-1β, reduced the systemic inflammatory response and improved the cardiac and respiratory function of COVID-19 patients, although no improvement in morbidity and mortality has been reported so far[40,224-226]. Therefore, further random controlled trials are required to conclude on the benefit of anakinra and canakinumab in COVID-19. Nevertheless, anakinra has the advantage of having a short half-life (4 to 6 hours, *vs* 8 to 14 days for tocilizumab for example). In the context of acute inflammatory response like CRS, this offers the possibility of daily administration of the drug thus allowing better management of patient[227]. In addition in the context of CRS induced by infection, such as COVID-19, since IL-1 is also a key cytokine for viral clearance, the necessity of daily infuse anakinra should allow to find a good balance between attenuate the inflammatory cascade and limit the risks of pathogen proliferation and/or superinfections[227].

As for the potential in managing CRS induced by CAR T cells, two murine models demonstrated that IL-1 blockade by anakinra prevented both CRS and/or ICANS[195,196]. To this end, clinical trials investigating early and/or prophylactic use of anakinra in the context of CAR-T induced CRS are ongoing[228].

### 3.1.3 GM-CSF inhibitors

Elevated GM-CSF was shown in many settings of CRS, in particular, consequent to coronavirus[229], haemorrhagic fevers[12] and CAR T cell-induced toxicity[131,132]. In xenograft mouse models, GM-CSF neutralization prevented CAR-T cell induced CRS and neuroinflammation, without impairing CAR-T cell anti-tumour efficacy[131]. Along these lines, in the ZUMA-19 phase 1b study, it was reported that lenzilumab (anti-GM-CSF mAb) positively impacted the outcome of patients developing severe CRS or neurotoxicity post CAR T cells injection (unpublished data)[230]. Due to the potentially promising effects of GM-CSF blockade in the context of CAR T cell-mediated CRS, several clinical trials are ongoing manage CRS induced by COVID-19. Lenzilumab appeared to improve the oxygenation in severely ill patient, as well as reduce the CRP and IL-6 levels[232]. Therefore, lenzilumab received FDA approval for emergency Investigational New Drug (IND) in severe COVID-19 cases that progress to respiratory failure[231,232].

Surprisingly, a completely opposite approach to the above is under evaluation for reducing CRS in COVID-19 patients. Using sargramostim, a synthetic form GM-CSF. The rational of this approach is based on positive impact of sargramostim in ARDS[233,234]. In response to viral insults, alveolar epithelial cells produce GM-CSF which activates alveolar macrophages to promote clearance of respiratory pathogens. In addition, GM-CSF has beneficial roles, including maintaining the alveolar capillary barrier integrity and enhancing repair of injured lung tissue[231,237]. Pre-treatment with intranasally administered GM-CSF protected mice from lethal influenza-induced lung injury. Therefore, early role of GM-CSF may be protective as it helps limit virus-related injury[234]. For this reason, sargramostim is being tested in patients with COVID-19-related acute respiratory failure, and shown promising results at restoring the oxygen uptake function of the lung, while at the same time effectiveness to fight the virus[235,236]. Of course, careful monitoring will be needed with sargramostim use in the COVID-19 setting, as it could favour neutrophil and monocyte/macrophage maturation and thus exacerbate the SARS-CoV-2-induced hyperinflammatory response.

### 3.1.4 IFN-γ inhibitors

IFN-γ is considered as a major effector cytokine in many examples of CRS[206,174]. The recent FDA approval for the use of emapalumab, an anti-IFN-γ mAb, for primary forms of HLH (pHLH) is clinical validation of its role in CRS[238]. Results of a study, leading in part to the FDA approval, showed a 63% overall response rate, defined as normalization or at least 50% improvement from baseline of fever, splenomegaly, cytopenias, hyperferritinemia, fibrogen or D-Dimer levels and CNS abnormalities, with no sustained worsening of sCD25 serum levels[239]. As follow-on studies, emapalumab is also being further evaluated in MAS associated to systemic juvenile idiopathic arthritis (sJIA)[240]. According to preliminary data, emapalumab treatment results in rapid deactivation of T cells, as indicated by the decrease in sIL-2R levels, and a progressive improvement of clinical and laboratory features, including D-dimer, LDH, ferritin and platelet levels[241]. Additionally, IFN-γ blockade via emapalumab is being tested in COVID-19 patients for patients refractory to other treatment interventions, such as tocilizumab, and JAK inhibitors[242,243].

In the setting of CAR T cell therapy or T cell engagers, an elevated T-cell derived IFN-γ signature has been associated to macrophage activation, leading to secretion of many pro-inflammatory cytokines[298]. Although inhibition of IFN-γ may mitigate toxicity, it may also impair the anti-tumoral efficacy of the immunotherapy. Nonetheless, since inhibiting IFN-γ may reduce the early recruitment and activation of

other factors involved in the CRS, this strategy might be a viable option in severe cases that are refractory to other treatment interventions for example.

### 3.1.5 TNF-α inhibitors

TNF-α is consistently elevated in patients with acute viral diseases, including influenza[8,63], dengue[8,12], Ebola[8,65,66] and corona virus[44,51,144,193,194], as well as in patients experiencing toxicities following T cell-engaging therapies[19,28,56]. TNF-α has an important role in the initiation of the inflammatory cascade, activating T cells, macrophages, monocytes and other cells of the immune system. TNF-α is believed to act upstream to IL-6 and IL-1, and hence, anti-TNF-α strategies may be a promising way to manage various types of CRS. The effectiveness of etanercept, a recombinant soluble TNF receptor, was demonstrated in several clinical case reports in patient suffering from MAS disease and unresponsive to mainstay therapy (corticosteroids and cyclosporin A)[244-246]. In these cases, etanercept was reported to resolve the fever and significantly improve laboratory features, such as CRP, ferritin, and triglycerides levels, within days. In addition, patients remained asymptomatic following the recovery[244-246].

Moreover, management of viral infections were improved following TNF-α blockade, including SARS-CoV-1, respiratory syncytial virus, dengue, and influenza[8,247]. The potential benefit of targeting TNF-α in patients with COVID-19 was also supported in a mouse model of SARS-CoV-2[174]. In this study, researchers demonstrated that the unique combination of neutralizing antibodies to TNF-α and IFN-γ increases survival from up to 50%. Observational human data has shown a possible benefit of anti-TNF-α therapy in patients with COVID-19 but randomized controlled trials (RCTs) are needed to confirm this benefit[247].

In the context of CAR T cell-induced CRS, etanercept as monotherapy permitted the recovery of three patients with relapsed/refractory multiple myeloma who developed CRS after CAR T cell therapy[250]. The benefit at blocking TNF-α in CRS induced by therapies is also supported by pre-clinical experiments. Indeed, in a mouse model of mammary tumours, prophylactic use of anti-TNF-α therapy prevented CRS without compromising antitumour efficacy of the CD3 and HER2 bispecific antibodies therapy[251]. In xenograft model of CRS induced by CAR T cells[195], IL-6 production by myeloid cells and CRS-associated mortality were significantly reduced by TNF blockade, although it could also impair the antitumour activity of CAR T cells depending on the CAR construct[78].

## 3.2 OTHER THERAPIES

### 3.2.1 Steroids

Steroids, such as methylprednisolone or dexamethasone, are frequently used to reduce inflammatory responses. In the setting of CRS associated to HLH/MAS, high doses of dexamethasone, in combination with the cytotoxic drug etoposide, are often utilised as a first line treatment for patients[6,253-255]. Although steroids are standardly used in clinical practice and are considerably more affordable than biologics, they do not target specific cytokines but rather provide broad immunosuppression, which can compromise the effective resolution of the infection or cancer.

Corticosteroids following T-cell engaging therapy is used as second line treatment of CRS, in particular for patients refractory to IL-6 targeted therapies or patients with severe neurotoxicity[201]. Indeed, the well-known negative impact of steroids on antitumour and proliferative efficacy of T cells remains a concern in the management of CRS. Indeed, while some studies reported that steroids do not dampen T cell activation and or response rates in cancer, many studies also report the opposite[75.] However, corticosteroids, such as dexamethasone and prednisone, are more reliable for treatment of CRS-induced neurological disorders due to their ability to permeate the CNS and help resolve oedema and swelling[33,34].

In the context of infectious diseases, the use of steroids is controversial[206]. The main drawbacks are the risk of prolonged viral shedding[206,255] and secondary bacterial infections[256]. In the severe cases of influenza, corticosteroids are considered as empirical drugs, despite the lack of definitive conclusion on their effects and risks. In other severe infections, including dengue, Ebola, SARS-CoV-1, or MERS-CoV infections, the use of steroids failed to improve outcomes[257-259]. Surprisingly, several corticosteroids, especially methylprednisolone and dexamethasone, have demonstrated remarkable efficacy for reducing COVID-19 severity, particularly for patients needing mechanical ventilation[213]. While results from the RECOVERY trial revealed that dexamethasone reduced 28-day mortality in severe COVID-19[260], several studies observed delay in COVID-19 clearance with corticosteroid therapy, suggesting an increased viral replication[261]. To compensate the potential decrease of viral clearance and to avoid the risk of secondary bacterial infections, simultaneous administration of anti-viral agents and/or broad-spectrum antibiotics are essential[264]. For instance, in influenza infection, association of steroid with oseltamivir antibiotic improved outcomes of severe cases of CRS without compromising viral clearance. Nonetheless, since there is no proven effective anti-viral agent for Covid-19, this additional back-up anti-viral strategy cannot be implemented[206].

### 3.2.2 JAK inhibitors

Janus kinases (JAK) are involved in many cytokine signalling pathways such as IL-6 and IFN-γ[110,123]. Therefore, its inhibition and consequent neutralization of cytokine activity, may be highly effective at controlling CRS. Along these lines, studies have reported the effectiveness of JAK-inhibition for patients refractory to IL-6 blockade or steroids in CAR T cell-induced CRS[207-210].

JAK inhibition in COVID-19, and more broadly in infectious diseases, appears to offer promising responses. Several small trials noted a faster clinical improvement in COVID-19 patients treated with ruxolitinib or baricitinib, although the results lacked statistical significance[211,212]. The benefit of JAK inhibitors in infectious disease-induced CRS was also recently demonstrated in mouse model of arenavirus haemorrhagic fever[214]. Conversely, in a recent large clinical trial study, ruxolitinib failed at reducing the number of hospitalized COVID-19 patients with severe complications[40].

### 3.2.3 Blood purification treatments

Blood purification treatments consist of extracorporeal removal of excessive inflammatory factors and therefore may help maintain haemostasis. It is not a novel concept and has already shown promise results in sepsis and septic shock[262,263]. While blood purification is not a standard therapy for CRS in HLH or CAR T-cell therapy, it has been successfully applied in both scenarios[265,266] and is currently used in clinic in COVID-19 patients[55,206].

A wide variety of therapeutical approaches, targeting various aspects of the immune system, are currently investigated to manage CRS (Table 4 and Figure 13). Overall, the main challenge for the development of a therapies against CRS is the risk of compromising the control of the infections or interfering with the efficacy of immunotherapeutic approaches in cancer and even promoting the appearance of a secondary infections.

Moreover, future research should focus on identifying drugs that can be used in all cytokine storm-induced disorders. Advances in precision diagnostics should help establish biomarker signatures and thus select the right drugs for the right patients, regardless of the underlying disease.

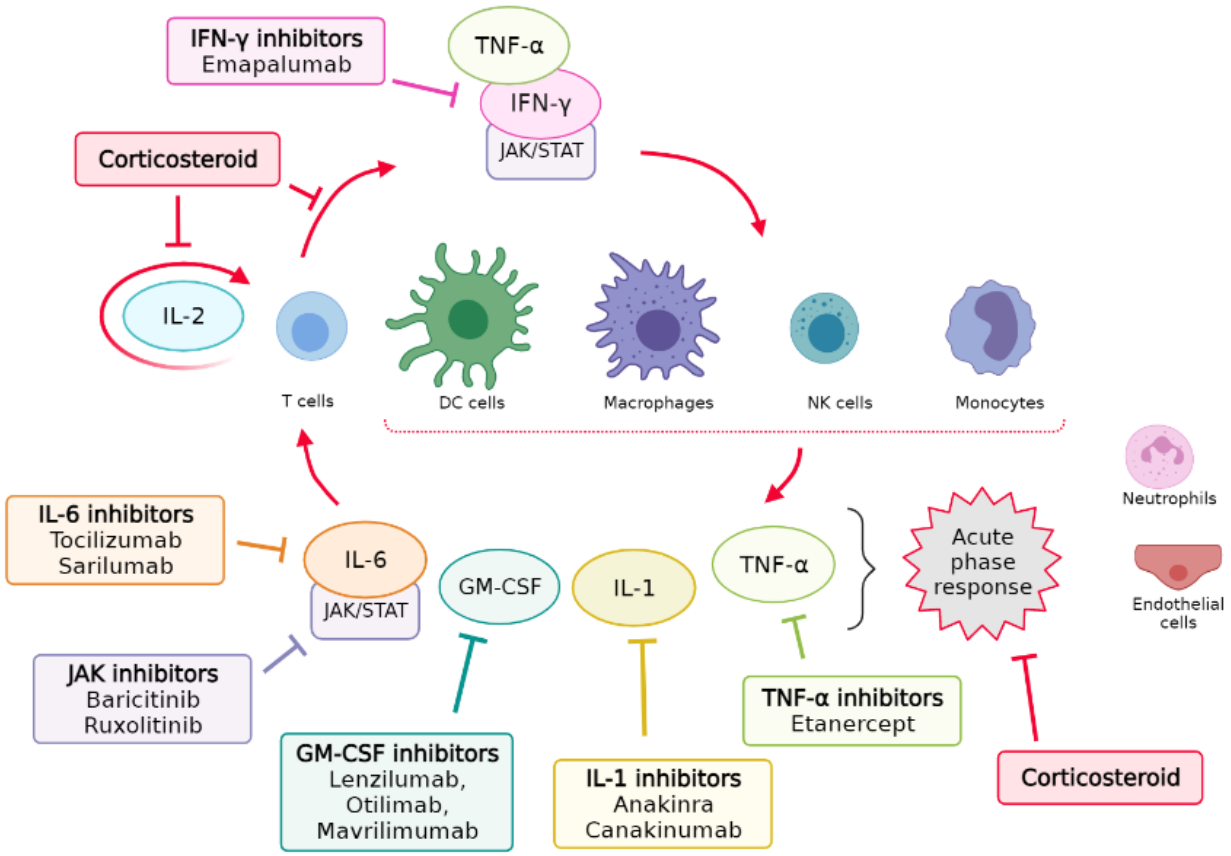


**Figure 13: Different treatment strategies to manage the cytokine release syndrome**. Once activated through recognition of an antigen cytokine stimulation and/or genetic deficiency, T cells, dendritic cells, monocytes and macrophages induce an acute phase response through pro-inflammatory cytokines such as IFN-γ, IL-6, IL-1, and TNF-α. Corticosteroids and/or novel cytokine blockades should inhibit immune responses and prevent cytokine storm. Adapted from Kim *et al*.[206]

# 4 MURINE MODELS OF CRS

## 4.1 MURINE MODELS FOR HUMAN INFECTIOUS DISEASES

Immunocompetent mice are very sensitive to certain influenza strains, such as the 1918 H1N1 and the 2009 H1N1 pandemic strains, and have been extensively used for studying T-cell responses against these viruses[269,270]. However, these mice are not naturally susceptible to many other strains of influenza, and more commonly, to most human pathogens which exhibit a unique human tropism. This includes Zika and Ebola haemorrhagic fever viruses, dengue, coronaviruses, malaria. Therefore, surrogate pathogens need to be developed, but often differ significantly from highly restricted human counterparts[271]. For example, mice are only semi-permissive to SARS-CoV-1 and -2 because murine ACE2, the cellular surface protein used by virus to enter cells, does not effectively bind the virus in comparison to human ACE2[23,272]. To circumvent this issue, one approach consisted of modifying SARS-CoV to gain more effective binding to mouse ACE2. Nonetheless, although mice were more sensitive for infection, they develop only very mild disease[272].

Progress in genetic engineering allow the development of transgenic mice, in whom specific genes are silenced or expressed, which represents a powerful tool for investigating human infectious diseases[274]. For instance, transgenic mice that express human ACE2 and infected with SARS-CoV-2 develop typical interstitial pneumonia and pathology resembling COVID-19 patients and, therefore, may be useful for pathogenesis studies[272,273]. For respiratory infections, it is also possible to increase sensitivity of the respiratory tract of mice through transduction with adenovirus virus that expresses human viral target. Instead of having permanent genetic modifications, a transient and localised expression of the human protein occurs. Sensitising the respiratory tract has the advantage to be easily and rapidly implemented in different mouse strains and for various pathogens, as it relies on intranasal injection of the adenovirus and of the pathogens few days after[273,275,278]. This system was first used in the context of MERS[275], and successfully applied to SARS-Cov-2[273]. Adenoviral vectors expressing the human receptor dipeptidyl peptidase 4 or ACE2 were injected in the respiratory tract of mice to favour sensitivity to MERS or SARS-CoV-2, respectively[273,275]. In both models, sensitised mice developed clinical signs of disease, characterized by weight loss, as well as histopathological changes that are consistent with viral pneumonia observed in humans[273,278].

'Humanized' mouse models also represent tools of choice for studying plethora of human infections, such as Ebola, Dengue virus, yellow fever virus, and malaria[274,276-277]. For generating humanized mice, immunodeficient mice are engrafted with peripheral blood mononuclear cells (PBMCs), or human hematopoietic stem cells (HSCs), to reconstitute a human immune system[274]. However, a major limitation of this type of model is that pathogens only infect cells derived from human PBMCs or HSCs due to their unique human tropism, whereas most pathogens usually target other human cell types, including epithelial, endothelial and mesenchymal cells. More complex models, such as mice engrafted with human hepatocytes (HuHep), bone marrow-liver-thymus (BLT) humanised mice and BLT-Lung mice can overcome this limitation and allow the study of hepatotropic viruses and respiratory viruses in models which better reflect clinical situation[277,278] (Figure 14).

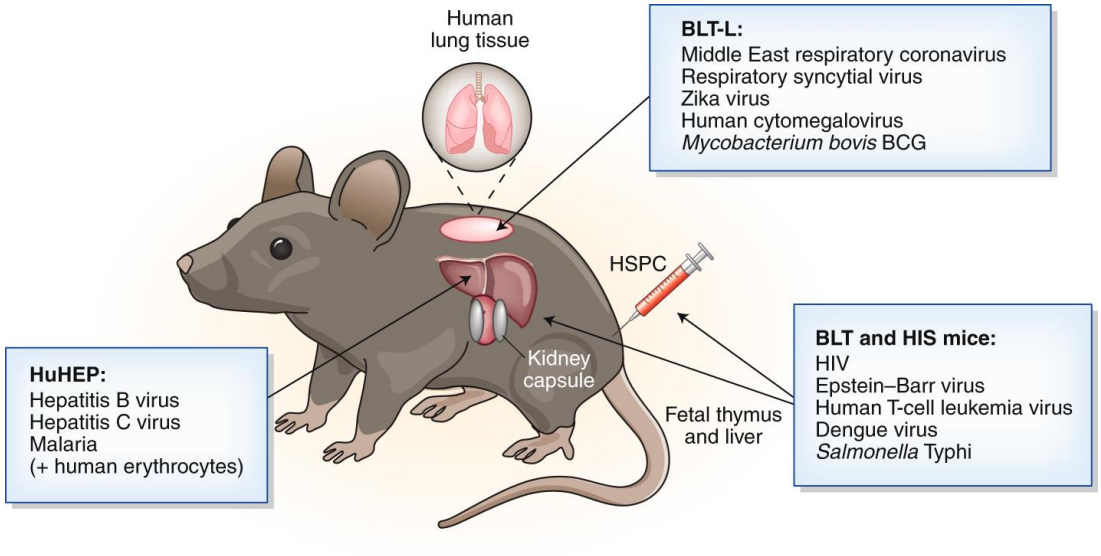


**Figure 14: Humanized mice to study human-tropic pathogens.** Various human cell types have been transplanted into immunodeficient mice to study diverse pathogens and diseases. Human immune system (HIS) mice are engrafted with hematopoietic stem cells. Bone marrow–liver–thymic (BLT) mice are engrafted with hematopoietic stem cells, fetal liver and fetal thymus from the same donor. HuHEP mice are engrafted with human liver cells to study hepatotropic viruses and, when combined with human erythrocytes, the replication cycle of the malaria parasite. BLT-L mice engrafted with lung cells, with or without autologous immune cells, to study respiratory viruses. Adapted from Spits *et al.*[278]

## 4.2 MURINE MODELS OF CAR-T CELL THERAPY-INDUCED CRS

Preclinical evaluation of CAR T cell therapy has, for the most part, been performed with xenograft models[281-283]. In those models, immunocompromised mice are transplanted with human tumour cells. Xenograft models have allowed to dissect the impacts of different costimulatory domain inserted in the CAR, CD28 and 4-1BB co-stimulatory domains being the most studied[268,284,287]. While these models were useful at demonstrating the efficacy of T cell-engaging therapy to eradicate human malignancies, they often failed at reproducing severe CRS and neurotoxicity[285-289].

To date, only two studies have described models reproducing the toxicities induced by CD19-CAR T cells in humans [195,196]. One model, described by Giavridis *et al.*[195], relied on immunodeficient SCID-beige mouse intraperitoneally engrafted with human Burkitt lymphoma Raji cells. Injection of human CD19-CAR T cells induced a severe CRS 2–3 days after infusion, characterised by reduced activity, general presentation of malaise, piloerection, weight loss and elevated serum cytokines concentration of human origin, including IL-2, IL-6, IFN-γ, and GM-CSF. Authors also identified macrophages as key producers of IL-6, IL-1 and inducible nitric oxide synthase (iNOS). In this model, anakinra treatment inhibited CRS-related mortality and reduced iNOS expression levels, without compromising antitumour activity[195,].

In the second study, Norelli *et al.* first developed a xenotolerant humanised mouse model to avoid xenogeneic graft-versus-host disease (X-GVHD)[196] which often occurred in humanised mouse model[268,293]. Since X-GVHD symptoms are similar to symptoms of CRS, distinguishing the two toxicities is critical. To do so, newborn NSG mice triple transgenic for human stem cell factor, GM-CSF and IL-3 (nSGM3) were transplanted with human hematopoietic stem and progenitor cells (HSPCs). Human T cells purified from the human transplanted newborn SGM3 (nHuSGM3) mice and transferred in secondary recipients persisted up to 200 days without causing X-GVHD, whereas in 'classical' humanised mouse models, X-GVHD often occurs a couple of weeks following human T cells transferred. Therefore, nHuSGM3-derived T cells were transduced *ex vivo* to express the CAR and then injected into secondary HuSGM3 recipients bearing patient-derived acute lymphoblastic leukaemia (ALL) cells. CAR T cell-injected mice developed a systemic inflammatory syndrome, characterized by weight loss, high fever and increased serum levels of pro-inflammatory cytokines, such as IL-6 and TNF-α. In addition, a sudden (24-hours duration) neurological disorder, characterized by generalized paralysis and seizures, was also documented. In this model, the severity of CRS and neurotoxicity was associated with increased number of circulating monocytes, also identified as the main producers of IL-1 and IL-6. Finally, whereas blocking

of either IL-1 or IL-6 prevented CRS without affecting CAR T cell efficacy, only anakinra protected against the subsequent development of lethal neurotoxicity[196].

While both previously described mouse model nicely recapitulated majority of human CRS features, some limitations can be highlighted. In the Giavridis *et al.* model, neurotoxicity was not reproduced[195]. In addition, SCID-Beige mouse, characterized by defective B, T and NK cells and competent myeloid cells, were injected with human CAR T cells. Due to the lack of cross-reactivity of certain cytokines between human and murine receptors, interactions between transferred human CAR T cells and the murine cells, such as myeloid cells or endothelial cells, are impaired. In the Norelli *et al.* study[196], authors reported that mouse IL-6 did not appear to play a substantial role in their model and acknowledged this was likely due cytokine dysregulation inherited from the NOD background, as also reported by others[290]. Moreover, although immunodeficient mice were engrafted with human stem cells and reconstituted an immune system, there are still defects in the myeloid compartment[294]. Therefore, as mentioned above, all the interactions between transferred CAR T cells and the patients are not reproduced in these models.

Overall, syngeneic mouse models remain the single type of model with fully functional immune system and in which all biological processes and crosstalk are present. While CRS is a systemic disease, likely resulting of the interplay between the CAR T cells and immune and non-immune/bystander cells, immunocompetent syngeneic mouse models should be the most powerful tool to reflect the human clinical situation. However, there is a lack of adequate methodologies for efficient transduction and expansion of murine T cell *in vitro*[291], resulting in shorter persistence and higher susceptibility to activation-induced cell death in comparison to the human CAR T cells when injected into mice[292,293]. Therefore, only few syngeneic mouse models of CAR T cells have been described thus far. One of them reported the occurrence of two distinct toxicities over time in BALB/c mice receiving CD19-CAR T cells containing the full-length CD28 protein (extracellular, transmembrane, and intracellular parts). The first toxicity occurred within days following CAR T cells infusion and could correlate with a mild CRS observed in patients, the second toxicity happened later, > 30 days after infusion, and was rarely observed in patients. In this study, when using CAR with a truncated extracellular domain of CD28 (corresponding to CAR construct used in clinical trials), only chronic toxicity was observed in mice, which do not reflect CRS observed in patients [296]. Moreover, in this study, no evidence of acute and chronic toxicities was apparent when C57BL/6 or C3H mice were used as recipient. Consistently, another pre-clinical study using C3H mice reported no toxicity after murine CD19-CAR T cells[296], suggesting a mouse-strain

dependent induction of toxicity. This discrepancy has been also described in the context of cytokine release induced by anti-CD3 mAb. Amongst NZW, CBA/J, C3H/HeJ and BALB/c mouse strains, the latter were the most affected by the anti-CD3 injection, showing higher level of Th1 cytokines (IFN-γ and TNF-α), stronger hypothermia and hypomotility[297].

Awareness of the importance and usefulness of syngeneic models has encouraged the development of additional immunocompetent mouse models. Recently, an efficient and reproducible protocol for the development of potent murine CAR T cell was reported, although the study focuses more on the importance of syngeneic mouse model in the field of solid tumours than understanding the induced toxicity[291].

Similarly, bispecific T cell engagers are mainly investigated in xenograft and humanized mouse models, which poorly recapitulate features of CRS. The same challenges exist when studying toxicities related to T cell engagers, thus the development of surrogate approaches is often required[295,298].

There is no one perfect model to evaluate toxicities induced by the above-mentioned therapeutic modalities or by an infectious trigger. All models discussed (i.e., syngeneic, transgenic, or humanised) have brought novel insights on CRS physiopathology, and on efficacy and safety of novel therapeutic approaches. For instance, syngeneic mouse models have been invaluable for the study of how certain strains of influenza virus lead to hyper-inflammatory states. In the setting of CRS induced by CAR T cells, xenograft mouse models have been successfully used to assess the efficacy of the therapy but failed to reproduce the toxicity. The critical role of monocytes and macrophages in CAR-T cell induced CRS was demonstrated using humanized mouse models. Appreciating the limitations of each model will help investigators chose the appropriate system to address the appropriate questions.

# 5 AIM OF THE STUDY

CRS is an acute inflammatory syndrome caused by the activation of immune cells and release of proinflammatory cytokines. Starting as a fever, it can rapidly progress to hypotension, hypoxia, multiple-organ dysfunction, and death. CRS is observed in a wide variety of settings; it is associated to severe form of infectious diseases as well as to the side effects of immunotherapies. Understanding of the CRS pathophysiology has greatly progressed since the advent of CAR T cell therapy and consequent to infectious diseases such as the ongoing COVID-19 pandemic. The pro-inflammatory cytokines involved in the CRS is now well described and often include IFN-γ, IL-6, IL-1 and TNF-α. An accumulation of evidence also incriminates monocytes and macrophages as key drivers of the life-threatening syndrome.

Therapeutic approaches relying on neutralisation of a specific cytokines have been successful at managing some near fatal cases of CRS. For instance, tocilizumab, an anti-IL-6R, and emapalumab, an anti-IFN-γ, has been approved by the FDA for the treatment of CRS associated with CAR T cells and HLH, respectively. However, these treatments are not effective in all cases, suggesting there are other cytokines/mechanisms at play.

The lack of animal models that faithfully recapitulate the toxicities is a major hindrance to the understanding of the CRS and the development of safe therapeutic approach. Preclinical evaluation of CRS has been performed using immunodeficient xenograft or humanised models, for the most part. While these models have offered insights, the limitation is that they are not evaluating disease progression in the context of a fully competent immune system. Therefore, the mechanisms underlying the CRS are still poorly understood, which hampers the development of effective treatment targeting the right mediator(s).

Two models of CRS have been developed herein. The first relies on potent *in vivo* T cell activation mediated by an anti-CD3ε mAb. A second model was developed to investigate CAR T cell-induced CRS in mice transplanted with A20 B cell lymphoma cells. The model systems were dissected to further understand the hierarchy and orchestration of the cytokine release leading to disease and highlight immune cells that may have key role in the initiation and propagation of the exaggerated immune response.

An important aspect of the project was to address whether blockade of proinflammatory cytokines, single or in combination, impacted clinical and laboratory features of CRS. Distinguishing between protective *versus* pathologic role of cytokines is critical for development of novel treatments. Indeed,

the CAR T cell-model of CRS investigated the contribution of the cytokines to CAR-T cell efficacy and to the development of CRS.

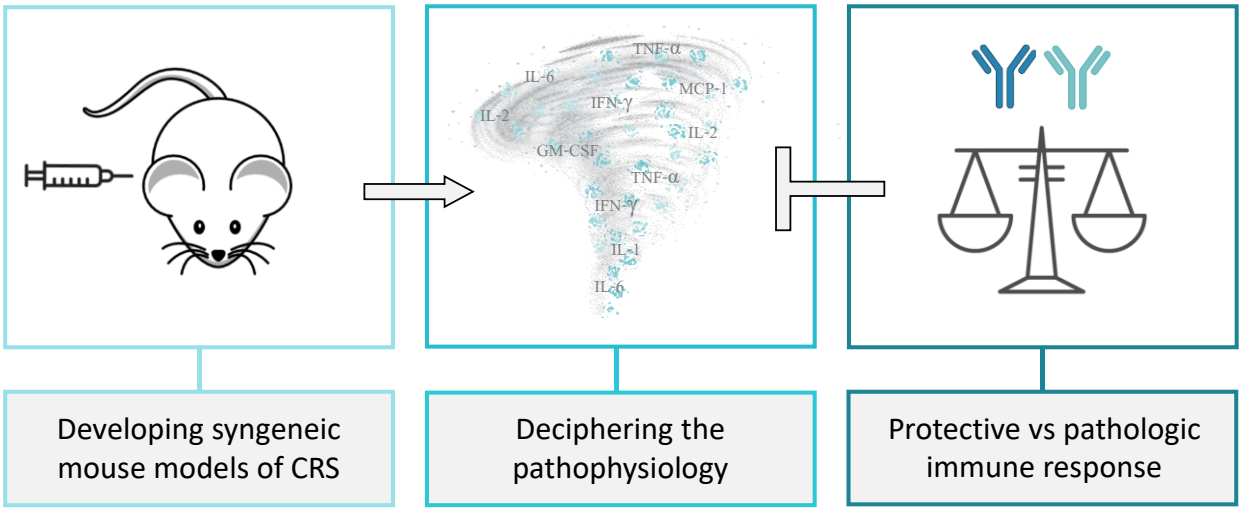


**Figure 15: Aims of the thesis**.

# CHAPTER II: ANTI-CD3 MOUSE MODEL OF CRS

Muromonab-CD3 (trade name Orthoclone OKT3) is a murine IgG2a mAb recognizing CD3 on human T cells. OKT3 was the first murine mAb available for therapy in humans in the context of solid-organ transplantation and was approved by the US FDA in 1986. However, clinical development was halted due to considerable side effects. Indeed, OKT3 is a potent mitogen, promoting T-cell proliferation and cytokine secretion, triggering a wide spectrum of side effects that include fever, chills nausea, vomiting and headaches, and life-threatening symptoms like hypotension, respiratory distress, and neurotoxicity, summarized as 'flu-like,' 'cytokine-release' or 'first-dose' syndrome[299]. It wasn't until 1990 that Chatenoud and colleagues first demonstrated that mice administered the hamster anti-mouse CD3 mAb (clone 145-2C11) developed CRS including piloerection, diarrhoea, hypothermia, hypomotility[300]. The CRS correlated with high transient release of pro-inflammatory cytokines (i.e., TNF-α, IL-6, IFN-γ, IL-2), as observed in human patients infused with OKT3. Several strategies to manage the CRS were investigated, including anti-TNF-α, anti-IFN-γ or high doses of corticosteroids[299,301-306]. None of the afore-mentioned efficiently reversed the toxicity induced by the anti-CD3 in mice. We took advantage of this model to further dissect the molecular and cellular events leading to CRS and to investigate the potential benefit of simultaneously neutralizing key cytokines.

## 1 MATERIEL AND METHODS

### 1.1 Mice

All animal procedures were performed in accordance with the Swiss Veterinary Office guidelines and authorized by the Cantonal Veterinary Office. Studies were conducted in 6- to 8-week-old male BALB/cByJ, mice obtained from Charles River Laboratories (Saint-Germain-Nuelles, France). The animals were reared under conventional conditions temperature-controlled room (25 ± 2°C) under a 12 hours light/dark cycle.

### 1.2 Antibodies used for *in vivo* studies

The anti-CD3ε (hamster IgG, clone 145-2C11) mAb and the anti-IL2 (Rat IgG2a, clone JES6-1A12) were obtained from BioXCell (Lebanon, NH, USA). The Armenian hamster IgG isotype control (clone HTK888) was obtained from BioLegend® (CA, USA). To induce CRS, mice were injected intravenously (i.v.) with the indicated dose of anti-CD3 mAb. Mice were weighed and then euthanized by $CO_2$ inhalation at different

time points. Spleen weight were recorded and samples of spleen and lung tissue were stored in RNA later (Sigma-Aldrich, Saint-Louis, MO) for gene expression analysis.

## 1.3 Measurement of cytokines and chemokines in plasma

The plasma concentrations of cytokines and chemokines were measured using MILLIPLEX MAP multiplex immunodetection kits (Merck Millipore, Burlington, MA, USA) and analysed on the Luminex® 200TM immunoassay analyser (Luminex®, TX, USA), according to manufacturer's instructions.

## 1.4 Gene expression

Spleen and lung RNA isolated using RNeasy mini-Kit (Qiagen, Hilden, Germany) was reverse transcribed using High-Capacity cDNA Reverse Transcription kit (Applied Biosystems®, Foster City, CAL, USA). Quantitative PCR (qPCR) was performed using SYBR® Green Master Mix (Applied Biosystems®) on the 7900HT Fast Real-Time PCR System from Applied Biosystems®. The $\Delta\Delta Ct$ method was used to calculate the relative gene expression levels (RQ) with β-actin gene as housekeeping gene. The primer sequences are listed Table 5.

**Table 5: Primer sequences for qPCR analysis.**

| | **Sequence primers (5'-3')** | |
|---|---|---|
| | **Forward** | **Reverse** |
| **β-actin** | AGCCTTCCTTCTTGGGTATGG | CAACGTCACACTTCATGATGGAAT |
| **CXCL1** | CATGCAGGCAGCACTCAGA | ATCCATGGTGGCACACAGACT |
| **CXCL9** | AGCCTTCCTTCTTGGGTATGG | AGGTCTTTGAGGGATTTGTAGTGG |
| **CXCL10** | GACGGTCCGCTGCAACTG | GCTTCCCTATGGCCCTCATT |
| **IFN-γ** | CAACAGCAAGGCGAAAAAGG | CCTGTGGGTTGTTGACCTCAA |
| **IL-2** | AACTGTTGTAAAACTAAAGGGCTCTGA | CACCACAGTTGCTGACTCATCA |
| **IL-6** | TCGGAGGCTTAATTACACATGTTC | TGCCATTGCACAACTCTTTTCT |
| **IL-10** | TTTGAATTCCCTGGGTGAGAA | GCTCCACTGCCTTGCTCTTATT |
| **TNF-α** | GCCACCACGCTCTTCTGTCT | GGTCTGGGCCATAGAACTGATG |

# 2 RESULTS

## 2.1 HIGH DOSES OF ANTI-CD3 INDUCED SEVERE AND LONG-LASTING CLINICAL FEATURES OF CRS

The first objective was to confirm that the i.v. injection of the anti-CD3 induced clinical signs of CRS. Mice were i.v. administrated single doses of anti-CD3 mAb ranging from 1-25 µg. Almost all anti-CD3 doses induced clinical features of CRS within the first hours post injection, including piloerection, prostration (hypomotility) and diarrhoea (data not shown) (Table 6). At the highest 25µg dose, the CRS was acute and severe, mice failed to recover from the single dose and continued to loss body weight (Figure 16A and Table 6). At lower doses (5, 10 or 15 µg), the syndrome was reversible, with a faster recovery for the lowest dose (Table 6 and Figure 16A). Interestingly, mice at all doses developed splenomegaly equivalently (Figure 16B).

**Table 6: Clinical features after anti-CD3 injection.** Mice were injected with 1, 5, 10, 15 or 25 µg of anti-CD3. Data representative of N=2 independent experiments with n=5 mice per time point.

| αCD3 / hpi | Prostration | | | | | Piloerection | | | | |
|---|---|---|---|---|---|---|---|---|---|---|
| | 1 µg | 5 µg | 10 µg | 15 µg | 25 µg | 1 µg | 5 µg | 10 µg | 15 µg | 25 µg |
| 2h | 0% | 20% | 30% | 30% | 50% | no | no | low | low | low |
| 6h | 0% | 50% | 50% | 60% | 70% | no | low | low | low | medium |
| 24h | 0% | 100% | 100% | 100% | 100% | no | medium | high | high | high |
| 48h | 0% | 30% | 60% | 60% | 90% | no | low | medium | medium | high |
| 72h | 0% | 5% | 10% | 10% | 90% | no | no | low | low | high |

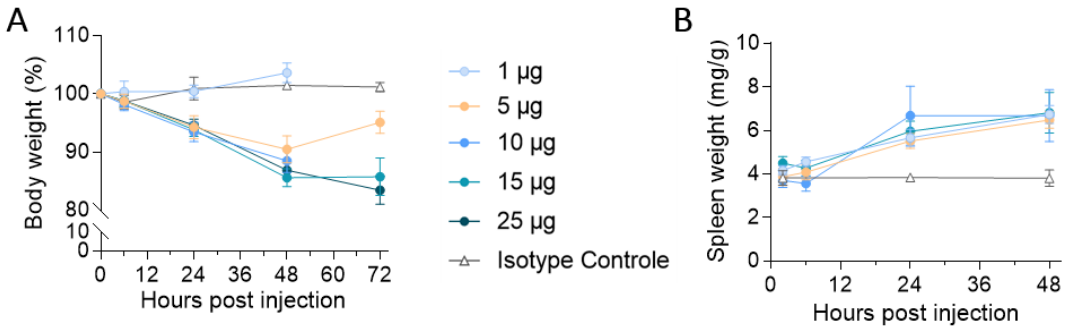


**Figure 16: High dose of anti-CD3 induced prolonged body weight loss**. Mice were injected i.v. with the indicated dose of anti-CD3 mAb. Body (A) and spleen (B) weight follow-up. Data representative of N=2 experiments with n= 5 mice per time point. Data are indicated as mean ± SD.

## 2.2 DOSE RESPONSE OF CYTOKINE RELEASE INDUCED BY ANTI-CD3.

As previously reported[299-306] and confirmed here, anti-CD3 injection to mice resulted in a high transient release of pro-inflammatory cytokines, including TNF-α, IL-6, IFN-γ, IL-2 (Figure 17A-top). Accordingly, CXCL9 and CXCL10, biomarkers of IFN-γ, were also up-regulated. CXCL1, a strong mediator of neutrophilia and IL-10, often described as an anti-inflammatory cytokine were also rapidly released following anti-CD3 injection (Figure 17A-bottom). Surprisingly, the dose of anti-CD3 did not correlate with cytokine levels in plasma. Indeed, whatever the dose, the cytokine release kinetics was similar peaking either 2 or 6 hours post injection and returning to basal level at 24 or 48 hours. Of note, the highest anti-CD3 dose (25 µg) resulted in a second plasma TNF-α peak 48 hours post-injection (Figure 17A-top), confirming a previous study by Bemelmans *et al.*[301] As cytokine levels in plasma most certainly reflect what is being produced in tissues and organs, *de novo* messenger RNA (mRNA) was quantified by qPCR in the spleen and the lung. As expected, anti-CD3 injection resulted mRNA synthesis of inflammatory mediators in both studied organs (Figure 17B and C). As observed for plasma cytokine quantification, the anti-CD3 dose had minimal differentiating impact on the early mRNA level response in tissues. Nonetheless, at 48 hours, mice administrated the highest anti-CD3 dose developed a second wave of mRNA synthesis, including *Ifn-γ*, *Cxcl9*, *Cxcl10*, *Il-2*, *Tnf-α* and to a lesser extent, *Il-6* in the spleen, as well as *Tnf-α* and *Il-6* in the lung (Figure 17B and C).

Taken together, the clinical and laboratory features induced at the 25 µg dose resulted in a lethal form of CRS, characterised by a prolonged cytokine release in two waves. Lower doses (ie, 5, 10 and 15 µg) of anti-CD3 resulted in similar clinical outcomes in mice. The 5 µg and 25 µg doses of anti-CD3-were selected to study further as a reflection of a mild and more severe CRS.

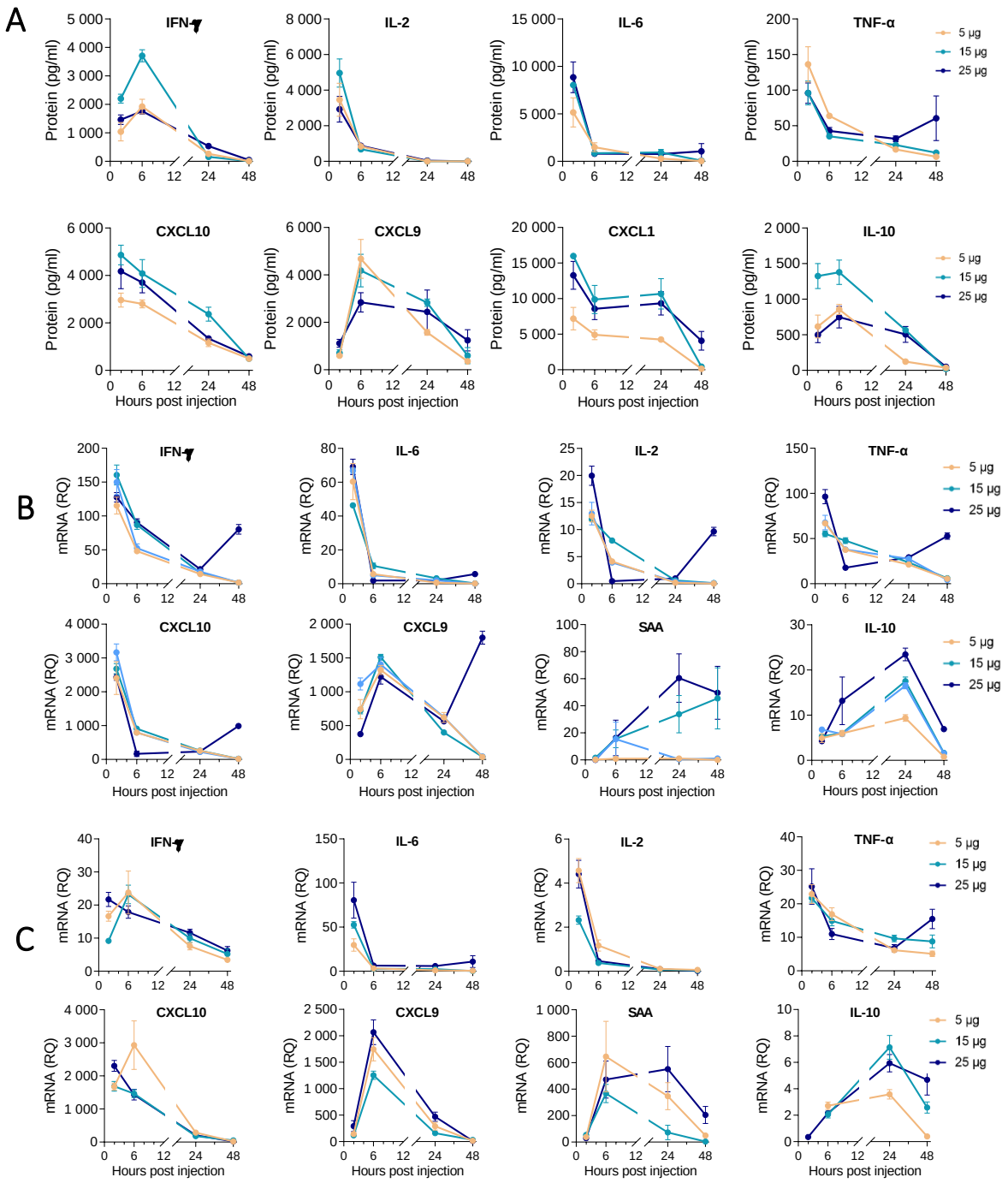


**Figure 17: High dose of anti-CD3 induced two waves of cytokine release.** Mice were injected i.v. with the indicated dose of anti-CD3 mAb. (A) Plasma concentration of cytokines and chemokines was quantified using a multiplex assay using Luminex. Quantification of tissue-derived cytokine and chemokine mRNA levels evaluated by qPCR in (B) the spleen and (C) the lung. n=4-5 mice per time point from a single experiment. Data are indicated as mean ± SEM.

## 2.3 IMMUNOLOGICAL ANALYSIS OF THE MURINE ANTI-CD3-INDUCED CYTOKINE RELEASE SYNDROME MODEL AND THERAPEUTIC EFFICACY OF ANTI-CYTOKINE ANTIBODIES

*Note: The following research work led to a publication in European Journal of Immunology early this year. I conducted all the in vitro and in vivo experiments, and prepared the figures and the core text for the manuscript.*

In the aim to develop an *in vivo* model of CRS, an agonistic anti-CD3 monoclonal antibody was administered to mice to induce an acute and polyclonal T cell activation. The severity of CRS was shown to depend on the anti-CD3 dose, closely replicating clinical and laboratory features of CRS seen in human conditions. A detailed analysis of how organs respond in the context of a CRS is described in detail offering new insights to how CRS may differ in humans depending on the intensity of the trigger. Moreover, the study investigated the impact of an anti-cytokine antibody cocktail on managing the CRS. A transient efficacy at decreasing critical CRS parameters is seen when using an anti-cytokine therapy. It mirrors that only drastic dexamethasone option works to some extent in severe indications such as COVID-19. Hence, this model is useful for further deciphering the CRS and acting sufficiently early to reduce mortality.

European Journal of Immunology

Immunomodulation and immune therapies

Research Article

# Immunological analysis of the murine anti-CD3-induced cytokine release syndrome model and therapeutic efficacy of anti-cytokine antibodies

*Lise Nouveau, Vanessa Buatois, Laura Cons, Laurence Chatel, Guillemette Pontini, Nicolas Pleche and Walter G. Ferlin*

Light Chain Bioscience-Novimmune S.A., Geneva, Switzerland

**The aberrant release of inflammatory mediators often referred to as a cytokine storm or cytokine release syndrome (CRS), is a common and sometimes fatal complication in acute infectious diseases including Ebola, dengue, COVID-19, and influenza. Fatal CRS occurrences have also plagued the development of highly promising cancer therapies based on T-cell engagers and chimeric antigen receptor (CAR) T cells. CRS is intimately linked with dysregulated and excessive cytokine release, including IFN-γ, TNF-α, IL 1, IL-6, and IL-10, resulting in a systemic inflammatory response leading to multiple organ failure. Here, we show that mice intravenously administered the agonistic hamster anti-mouse CD3ε monoclonal antibody 145-2C11 develop clinical and laboratory manifestations seen in patients afflicted with CRS, including body weight loss, hepatosplenomegaly, thrombocytopenia, increased vascular permeability, lung inflammation, and hypercytokinemia. Blood cytokine levels and gene expression analysis from lung, liver, and spleen demonstrated a hierarchy of inflammatory cytokine production and infiltrating immune cells with differentiating organ-dependent kinetics. IL-2, IFN-γ, TNF-α, and IL-6 up-regulation preceded clinical signs of CRS. The co-treatment of mice with a neutralizing anti-cytokine antibody cocktail transiently improved early clinical and laboratory features of CRS. We discuss the predictive use of this model in the context of new anti-cytokine strategies to treat human CRS.**

**Keywords:** Anti-CD3 · Anti-cytokine therapy · Cytokine release syndrome · Inflammatory cytokines · T-cell activation in vivo

Additional supporting information may be found online in the Supporting Information section at the end of the article.

## Introduction

The 21st century has ushered in spectacular progress in the field of immunotherapy for cancer. T-cell engagers, immune checkpoint inhibitors, and chimeric antigen receptor (CAR) T cells represent a new era of remarkable therapeutic options extending life for cancer patients [1–3]. The pharmacology of these therapies, however, has at times led to severe cytokine release syndrome (CRS) and neurotoxicity [4]. Bach and colleagues first described a CRS following the administration of an agonistic anti-cluster differentiation 3 (CD3) mAb, OKT3, in patients undergoing renal transplantation [5], when excess TNF-α and IFN-γ was produced following the first injection of OKT3. This cytokine release, albeit transient, was characterized by high fever, headaches, and gastrointestinal symptoms. The syndrome's underlying "cytokine

*Correspondence:* Walter G. Ferlin
e-mail: walter.ferlin@lightchainbio.com

storm," the unrestrained release of proinflammatory mediators in response to a trigger, has also been seen across multiple infectious diseases including dengue [6,7], Lassa fever [8], Ebola [9], influenza [10,11], SARS, and in the recent COVID-19 outbreak [12,13]. Indeed, COVID-19-associated mortality is also characterized by excessive production of proinflammatory cytokines, thrombosis, and acute lung damage [13–17]. The CRS observed in all the above is often characterized by features seen in patients afflicted with hemophagocytic lymphohistiocytosis (HLH) and macrophage activation syndrome [18]. The recent approval for the use of mAbs blocking IFN-γ for primary forms of HLH [19] and IL-6 signaling in COVID-19 patients and following CAR T-cell treatments [20] is a clinical validation of cytokine storms causing CRS.

The cytokine storm induced in six healthy subjects in a 2006 Phase I clinical trial following administration of the CD28 superagonist antibody TGN1412 was the first demonstration of near-fatal consequences subsequent to excessive T-cell activation [21]. Within 90 min after a single i.v. dose of TGN1412, all six volunteers had a systemic inflammatory response characterized by the rapid induction of proinflammatory cytokines (especially IFN-γ and TNF-α), accompanied by other clinical manifestations of CRS, including nausea, diarrhea, erythema, vasodilatation, hypotension, and multiorgan failure [22].

In this study, we evaluated the role of proinflammatory cytokines up-regulated in an anti-CD3 mouse model of CRS leading to systemic inflammation and mortality. Mice administered the agonist anti-CD3ε antibody (herein called anti-CD3) developed an acute CRS characterized by weight loss, hepatosplenomegaly, leucopenia, and hemotoxicity. A single i.v. administration of anti-CD3 led to a rapid up-regulation of inflammatory mediators associated with T cell and macrophage activation. In particular, a sharp increase of TNF-α, IL-2, IL-6, and IFN-γ preceded the development of CRS features. We describe a hierarchical organ-dependent cytokine induction and production kinetics in the lung, the liver, and the spleen, driving the mobilization of a plethora of activated immune cells. CRS severity was particularly correlated with a prolonged neutrophil and macrophage infiltration in the lung. Coadministration of a neutralizing anti-cytokine antibody cocktail, targeting TNF-α, IL-2, IL-6, and IFN-γ, reduced early features of CRS, including body weight loss, prostration, piloerection, and hemotoxicity, as well as lung inflammation. However, the protection afforded by the anti-cytokine cocktail was not extended beyond 24 h after administration. These data suggest that early monitoring of blood biomarkers in CRS-susceptible patients may help identify risk profiles and those who might benefit from a multispecific neutralizing antibody-based treatment, an approach that may be applicable to a plethora of infectious and inflammatory diseases driven by a T-cell-mediated cytokine storm.

## Results

### Clinical and laboratory features of CRS resulting from CD3 agonism in mice

T-cell activation after in vivo administration of anti-CD3 to mice, results in increased cytokine secretion and extramedullary hematopoiesis in the spleen, was described over 30 years ago by Bluestone and colleagues [23]. We reproduced this model to dissect and comprehensively describe the clinical and laboratory features of CRS induced by CD3 agonism.

Within 2 h post anti-CD3 injection (2 hpi), the first symptoms, including piloerection and prostration, were observed in 20% of mice. At 6 hpi, 50% of the mice exhibited signs of clinical illness reaching a peak at 24 hpi with animals presenting also significant body weight loss and splenomegaly (Table 1 and Fig. 1A and B). Acute leucopenia (Fig. 1C), evidenced by a marked lymphopenia (Fig. 1D), was observed within 30 min after anti-CD3 injection lasting up to 24 hpi. The transient recovery in leucocyte count between 4 and 8 hpi was surprisingly correlated with an acute and transient neutrophilia (Fig. 1E). Monocyte count also increased at 6 hpi and remained above baseline levels for at least 48 hpi (Fig. 1F). A short-lived decrease in platelet numbers (Fig. 1G) with a concurrent increase in RBC counts occurred within the first hours post anti-CD3 injection, with an unexpected RBC drop 24 hpi with return to baseline levels (Fig. 1H). At the 5 μg anti-CD3 dose tested here, mice started to recover 48 hpi.

### CD3 agonism leads to systemic hypercytokinemia with organ-specific cytokine production kinetics

Here, we describe a model of CRS caused by the activation of T cells leading to hypercytokinemia within the first hours following anti-CD3 injection. Th1 cytokines IFN-γ and IL-2 were rapidly

**Table 1.** Anti-CD3-injected mice present clinical features of CRS and anti-cytokine antibody cocktail alleviated early signs

| | | Hours post anti-CD3 injection (hpi) | | | | | | |
|---|---|---|---|---|---|---|---|---|
| | | 0.5 | 1 | 2 | 6 | 24 | 48 | 72 |
| Anti-CD3 + PBS | Piloerection | No | Low | Low | Medium | High | Medium | Low |
| | Prostration (% of mice) | 0% | 0% | 20% | 50% | 100% | 30% | 0% |
| Anti-CD3 + anti-cytokines | Piloerection | No | No | No | No | High | Medium | Low |
| | Prostration (% of mice) | 0% | 0% | 0% | 0% | 90% | 30% | 0% |

Mice were injected with 5 μg of anti-CD3 plus PBS or plus an anti-cytokine cocktail. Data representative of N = 3 independent experiments with n = 5 mice per time point per experiment.

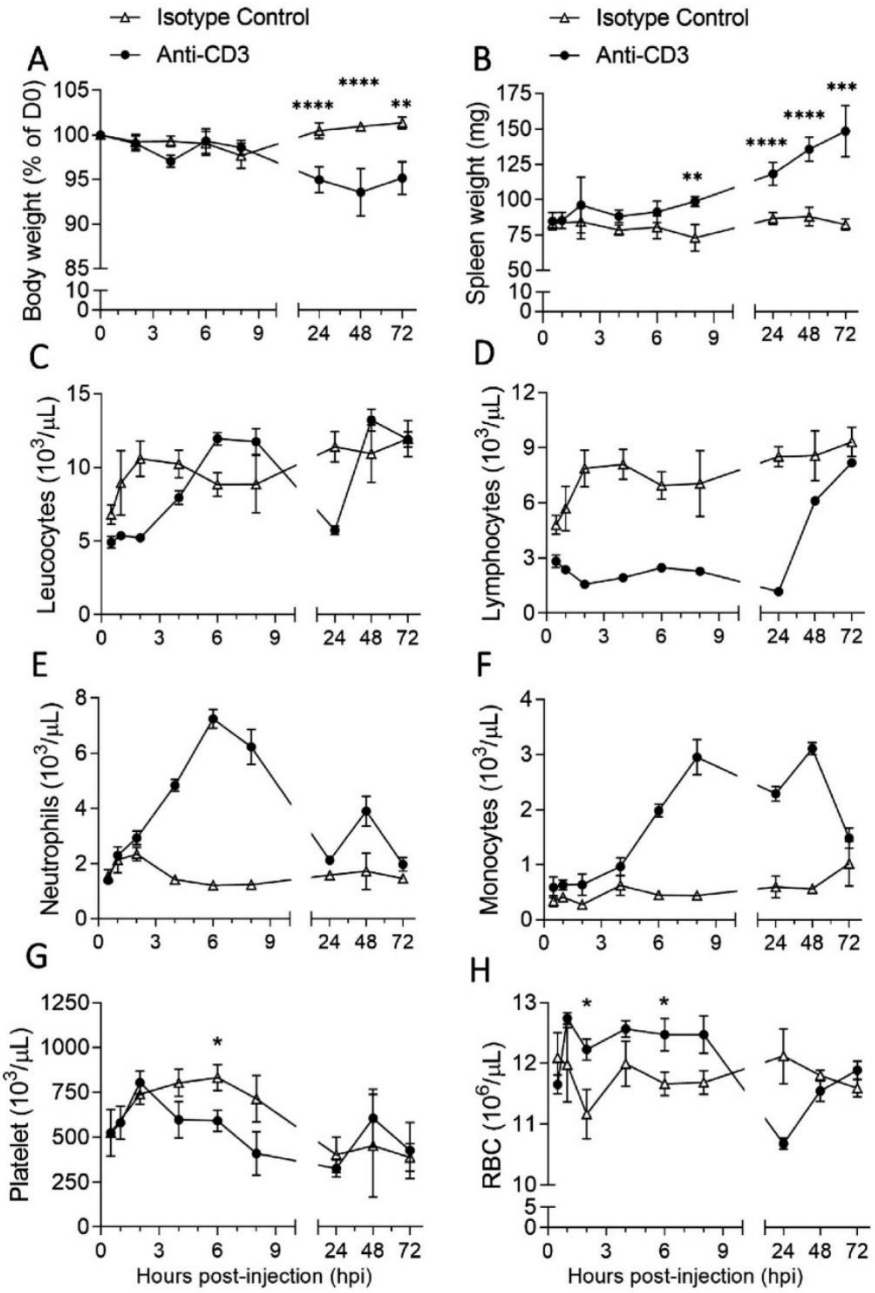


**Figure 1.** Clinical and laboratory features of CRS resulting from CD3 agonism in mice. Mice were injected i.v. with 5 µg of anti-CD3 or with 5 µg of isotype control. Body (**A**) and spleen (**B**) weight follow-up. Blood parameters including leucocyte (**C**), lymphocyte (**D**), neutrophil (**E**), monocyte (**F**), platelet (**G**), and RBC (**H**) counts. n = 4-15 mice per time point from N = 3 independent experiments. $^{*}p < 0.05$, $^{**}p < 0.01$, $^{***}p < 0.001$, and $^{****}p < 0.0001$ were obtained using the unpaired *t*-test. Values are displayed as mean ± SEM.

(i.e. 0.5 hpi) up-regulated in the blood to 40- and 10-fold levels above isotype control-injected mice (Table 2 and Fig. 2A and B), respectively. Cytokines often associated with macrophage activation syndrome, TNF-α and IL-6, were also rapidly up-regulated, with the former reaching a 75-fold peak at 1 hpi (Table 2 and Fig. 2C and D). These four cytokines were significantly up-regulated before the appearance of clinical symptoms (Table 1). The peak levels of IL-2 and IL-6 were observed at 2 hpi, with a 1200-fold (3500 pg/mL) and 300-fold (7500 pg/mL) increases, respectively and decreasing at 6 hpi (Table 2 and Fig. 2B and C).

 

In contrast, IFN-γ persisted at peak levels of 2000 pg/mL 6 hpi, a 2600-fold increase above baseline (Table 2 and Fig. 2A). Accordingly, IFN-γ-induced proteins CXCL9 and CXCL10 were also up-regulated, peaking at 6 and 2 hpi, respectively (Table 2 and Fig. 2F and G). Often described as anti-inflammatory, IL-10 was observed to be rapidly up-regulated within 1 hpi and peaked at 6 hpi, with a 80-fold increase above control (baseline) levels (Table 2 and Fig. 2E). Unexpectedly, only moderate increases in IL-1β (two fold increase) and IL-12p40 (18-fold increase) were observed at 1 and 2 hpi, respectively (Table 2). Inflammatory mediators frequently associated with macrophage activation and neutrophilia, including peaks of GM-CSF (1 hpi, 23-fold increase), CCL4/MIP-1β (2 hpi, 17-fold increase), and CXCL1 (2 hpi, 34-fold increase), were differentially up-regulated (Table 2 and Fig. 2H to J). The hypercytokinemia was accompanied by *de novo* mRNA synthesis in the spleen, the liver, and the lung (Fig. 2K-S). Interestingly, an organ-specific inflammatory gene signature was observed. The liver was the site where an increased gene expression profile was observed for *Ifn-γ* (Fig. 2K) and related *Cxcl9* and *Cxcl10* genes (Fig. 2P and Q), as well as *Tnf-α* (Fig. 2N), *Cxcl1* (Fig. 2R) and IL-6-induced protein *Saa* (Fig. 2S), but interestingly not *Il-6* (Fig. 2E). Indeed, the latter was instead significantly up-regulated in the spleen and in the lung following anti-CD3 administration (Fig. 2M). The spleen was the main site where *Il-2* gene up-regulation was observed (Fig. 2L), whereas *Il-10* was significantly up-regulated in the lung (Fig. 2O) as well as, albeit earlier, *Cxcl9, Cxcl10, Il-6*, *Saa*, and *Il-2* (Fig. 2L, M, P, Q, and S).

## Mobilization of inflammatory cells after CD3 activation in vivo

The organ-specific cytokine signature, the drop in circulating lymphocyte count, and the increase in neutrophil and monocyte counts following anti-CD3 administration, suggested a potential differential mobilization of immune cells to the respective tissues. To further investigate this, the spleen, lungs, and liver were excised at 24 and 48 hpi (corresponding to peak of illness and initiation of recovery) and the infiltrating immune cells characterized (see Supporting information Fig. S1 to S4 for gating strategies). We noted a decrease in the proportion of $CD4^+$ and $CD8^+$ T cells in the spleen and lungs from mice treated with anti-CD3 although a marginal increase in the liver was observed at 24 hpi (Fig. 3A and E). The lung and spleen T cells were activated, as characterized by an up-regulation of CD25 and CD69 (Fig. 3B, C, F, G) and the down-regulation of CD62L at 24 hpi (Fig. 3D and H). Hepatic $CD8^+$ T cells, on the other hand, showed an increased expression of CD62L at 24 hpi (Fig. 3D and H). At 48 hpi however, overall, the $CD4^+$ and $CD8^+$ T cell proportions and activation state returned to normal levels (Fig. 3A-H). In addition, the proportion of NK cells increased in the liver, whereas a decrease was observed in the spleen and lung following anti-CD3 injection (Fig. 3I). On the other hand, myeloid subsets also fluctuated significantly in the studied organs. The frequency of neutrophils was increased in all three organs analyzed at 24 hpi, returning to basal levels in the spleen and the liver 48 hpi while remaining elevated in the lungs (Fig. 3J). A decrease in macrophage numbers was observed in the spleen and the liver whereas in lung, the frequency of alveolar-macrophages and interstitial-macrophages increased at 24 hpi, respectively (Fig. 3K). Taken together, systemic T-cell activation in vivo resulted in a cytokine and chemokine cascade driving the mobilization of a plethora of activated immune cells to the lung, liver, and spleen.

## An anti-cytokine antibody cocktail alleviated early signs of CRS

We next tested if a cocktail of neutralizing antibodies targeting up-regulated cytokines (IL-2, IL-6, IFN-γ, and TNF-α) would ameliorate the anti-CD3-induced CRS in mice. To this end, anti-CD3 mice were co-treated with a combination of anti-cytokine mAbs

**Table 2.** Anti-CD3 injection induced a hypercytokinemia

| | Hours post anti-CD3 injection (hpi) | | | | | | |
|---|---|---|---|---|---|---|---|
| | 0.5 | 1 | 2 | 6 | 24 | 48 | 72 |
| IFN-γ | **40** ± 3.0 | **459** ± 55 | **1 410** ± 436 | **2 610** ± 346 | **359** ± 56 | **13.5** ± 3 | **2** ± 0.7 |
| IL-2 | **10** ± 1.4 | **1 193** ± 106 | **1 264** ± 338 | **308** ± 50 | **1** ± 0 | **1** ± 0.1 | **1** ± 0.1 |
| TNF-α | **22** ± 1.2 | **75** ± 4 | **45** ± 8 | **21** ± 1 | **5.5** ± 1.2 | **2** ± 1 | **1** ± 0 |
| IL-6 | **3** ± 0.9 | **118** ± 21 | **306** ± 91 | **88** ± 27 | **17** ± 5 | **2.5** ± 1.5 | **0.2** ± 0.1 |
| CXCL9 | **1** ± 0.1 | **2** ± 0.4 | **16** ± 3 | **131** ± 23 | **44** ± 3 | **10** ± 1.2 | **3** ± 0.3 |
| CXCL10 | **1** ± 0.1 | **8** ± 1 | **22** ± 2 | **20** ± 1 | **8.5** ± 1.2 | **3.5** ± 0.3 | **1.5** ± 0.1 |
| IL-10 | **2** ± 0.4 | **23** ± 3 | **58** ± 15 | **82** ± 6 | **12** ± 3 | **3** ± 2 | **0.4** ± 0.1 |
| IL-1β | **1** ± 0.1 | **2** ± 0.3 | **1.5** ± 0.3 | **1** ± 0.03 | **1** ± 0 | **1.5** ± 0.5 | **1** ± 0 |
| IL12p40 | **6** ± 4.9 | **1** ± 1 | **18** ± 11 | **6** ± 2.5 | **1** ± 0 | **1** ± 0 | **1** ± 0 |
| GM-CSF | **5** ± 3.3 | **23** ± 2.6 | **11** ± 4 | **4** ± 2.4 | **1** ± 0.0 | **1** ± 0.1 | **1** ± 0 |
| CCL4 | **2** ± 0.3 | **14** ± 1.7 | **17** ± 4 | **8.** ± 1.3 | **1.5** ± 0.1 | **1** ± 0.1 | **0.5** ± 0.1 |
| CXCL1 | **3** ± 1.4 | **30** ± 6 | **34** ± 7 | **24** ± 3 | **21** ± 1.4 | **0.7** ± 0.1 | **0.5** ± 0.1 |

Mice were injected with 5 μg of anti-CD3. Plasma concentration of cytokines was quantified using a multiplex assay using Luminex. Fold increase above baseline (i.e. mean of plasma levels from isotype control injected mice) was calculated. Data are indicated as mean ± SEM.

 

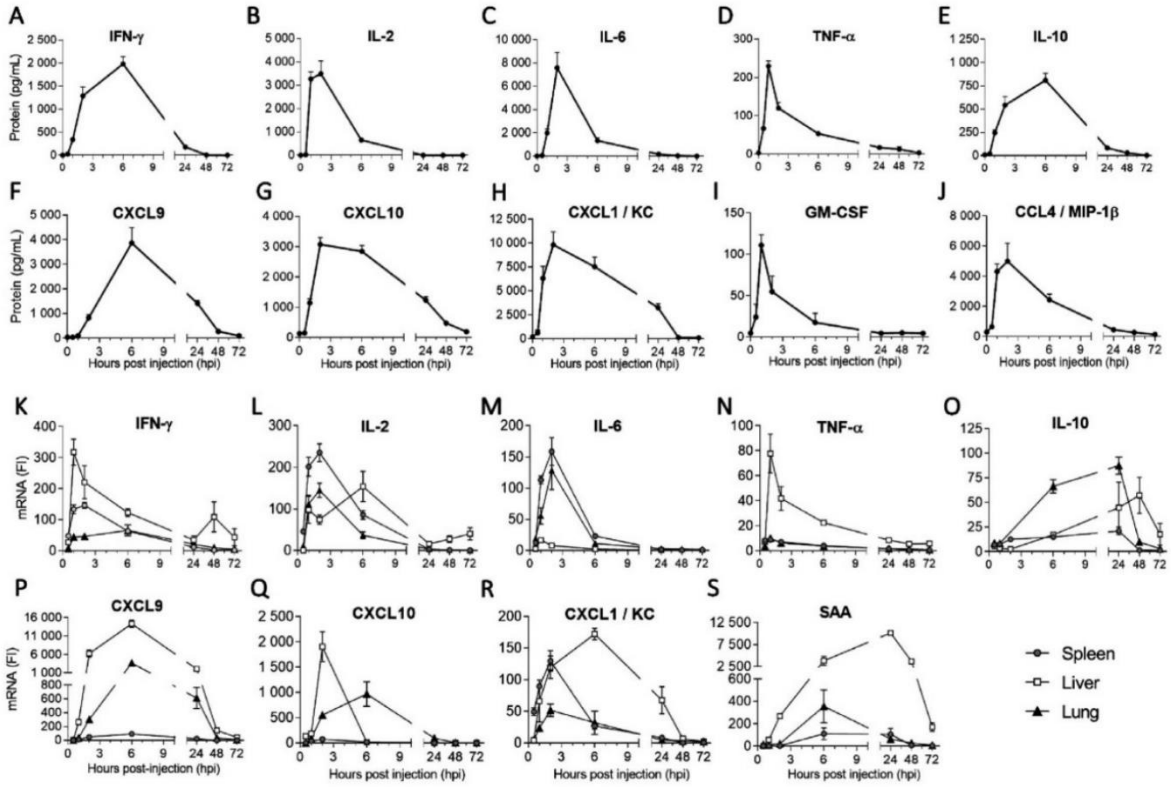


**Figure 2.** Anti-CD3-induced CRS leads to systemic hypercytokinemia with an organ-specific cytokine production kinetics. Mice were injected i.v. with 5 μg of anti-CD3 or isotype control. Graphs **A-J** represent Luminex-based quantification of plasma cytokines and chemokines. The baseline (*t* = 0 h) corresponds to the mean of isotype control injected mice. Graphs **K-S** represent the quantification of tissue-derived cytokine and chemokine mRNA levels evaluated by qPCR in the organs, expressed as fold increase above baseline. For plasma and spleen qPCR data, n = 9-10 from N = 2 independent experiments; for lungs and liver qPCR data n = 4-5 mice per time point from a single experiment. Values are displayed as mean ± SEM.

(anti-IL-2, -IL-6, -IFN-γ, -TNF-α mAbs). Mice administered the anti-cytokine antibody cocktail presented no clinical signs of CRS for up to 6 hpi, in contrast to 50% of the animals injected with anti-CD3 alone, who showed piloerection and prostration (Table 1). The severity of acute leucopenia, thrombocytopenia, erythrocytosis, and body weight loss seen in anti-CD3- treated mice was also significantly improved by the anti-cytokine antibody cocktail, while neutrophilia and monocytosis remained unchanged (Fig. 4A and B). As a measure of increased vascular permeability [24], Angiopoietin-2 (Ang-2) was up-regulated in anti-CD3-treated mice and was significantly reduced by the anti-cytokine cocktail (Fig. 4C). Analysis of bronchoalveolar lavage (BAL) also confirmed the amelioration in inflammatory parameters afforded by the anti-cytokine antibody cocktail (Fig. 4D and E). Here, cytokine blockade resulted in a decreased activation marker MHCII on F4/80$^+$ macrophages in the BAL at 24 hpi (Fig. 4D) and decreasing levels of inflammatory chemokines CXCL1 and CXCL10 (Fig. 4E). G-CSF was surprisingly up-regulated in the BAL in all treated groups (Fig. 4E). Interestingly, while G-CSF and CXCL1 are described to enhance neutrophil attraction, survival, and proliferation, this population was significantly diminished in the BAL across all treated groups (Fig. 4D) while an increase was observed in whole-lung cell suspensions (Fig. 3J). While the anti-cytokine antibody cocktail alleviated early signs of CRS, this was no longer the case 24 h post anti-CD3 injection. Nonetheless, the anti-cytokine cocktail afforded an increased benefit as compared to the monotherapy administration of the anti-cytokine mAbs (see Supporting information Table S1).

## CRS severity is associated with sustained neutrophil and monocyte infiltration in lungs

To further understand the mechanisms underpinning CRS severity, we analyzed mice treated with a low (5 μg) or high (25 μg) dose of anti-CD3. Body weight loss, temperature loss, hepatomegaly and, to a lesser extent, splenomegaly aggravated in high-dose anti-CD3- treated mice (Fig. 5A to D). Indeed, while the low-dose anti-CD3 mice recovered spontaneously, mice receiving 25 μg anti-CD3 were sacrificed at 72 hpi for ethical reasons. Interestingly, the two anti-CD3 doses induced equivalent levels of hypercytokinemia (Fig. 5E and Supporting

 

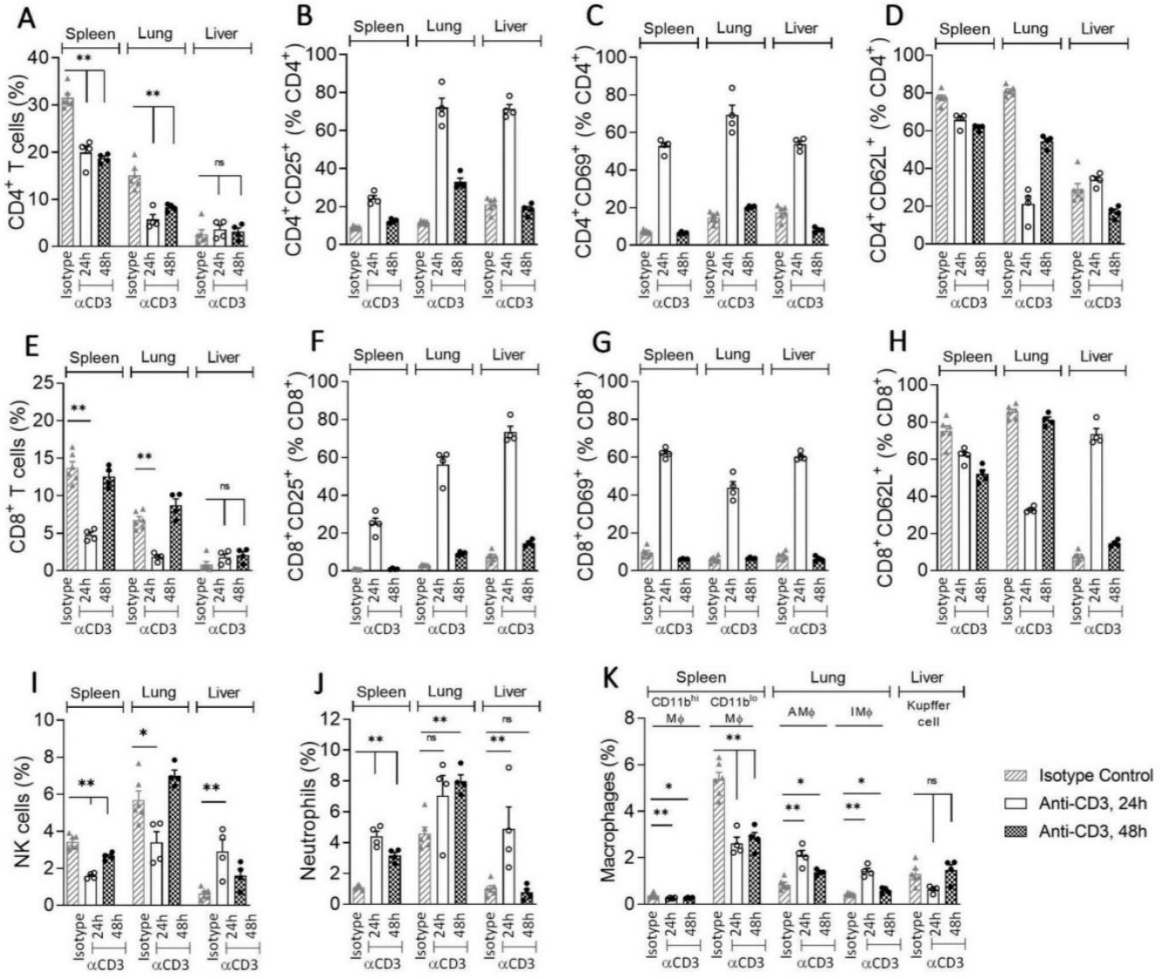


**Figure 3.** Organ-specific mobilization of inflammatory cells after CD3 activation. Mice were injected i.v. with 5 μg of anti-CD3 or with 5 μg of isotype control. Single cell-suspensions from the spleen, liver, and lungs were prepared 24 or 48 h postinjection, followed by immunophenotyping. Bar graphs **A** and **E** represent frequencies of $CD4^+$ and $CD8^+$ T cells expressed as percentage of total viable cells and up-regulation of CD25, CD69, and CD62L markers on $CD4^+$ (**B** & **D**) and $CD8^+$ (**F**-**H**) T cells. Plot **I** shows frequencies of NK cells and plots **J** and **K** show frequencies of myeloid cells expressed as a percentage of viable cells. Gating strategies and relative number of cells are available in Supporting information Fig. S1 to S4 and Supporting information Table S5. NK, natural killer; Mϕ, macrophages; AMϕ and IMϕ, alveolar and interstitial macrophages. Representative data of N = 2 independent experiments, n = 4-6 mice/organ per time point. $^*p < 0.05$, $^{**}p < 0.01$, and $^{***}p < 0.001$ as determined by one-tailed nonparametric Mann–Whitney U t-test. Values are displayed as the mean ± SEM.

information Table S2), whereas clinical signs of CRS (piloerection and prostration) occurred earlier and were more severe in mice given the higher dose. Blood levels of IFN-γ, TNF-α, and CXCL9 were still detectable in mice developing severe CRS at 48 hpi (Supporting information Table S2). Significant differences were observed only for circulating levels for IL-6 and CXCL1 at 48 hpi, when they were 25- and 30-fold higher, respectively, in high-dose anti-CD3- treated mice (Fig. 5E and Supporting information Table S2). Mobilization of inflammatory cells in tissues was equivalent across the two dose levels, normalizing at 48 hpi (see Supporting information Fig. S2 and S3 for gating strategies). Nonetheless, notable differences were observed in the proportions of lung monocytes and neutrophils (Fig. 5F). Indeed, the neutrophils in the severe form of CRS remained significantly higher at 48 hpi as compared to the low-dose anti-CD3- treated mice. In addition, this sustained increase correlated with an equally persistent elevated plasma concentration of CXCL1 (Fig. 5E). Similarly, $Ly6C^{low}$ resident monocytes were significantly persistent in lungs from severe CRS-afflicted mice (Fig. 5F). We next attempted to deplete neutrophils or macrophages to further investigate their contribution to the anti-CD3-induced CRS. While the anti-Ly6G antibody significantly depleted neutrophils from the lung and the spleen, only a 60% reduction was achieved in the liver. The treatment failed to significantly reverse CRS in mice

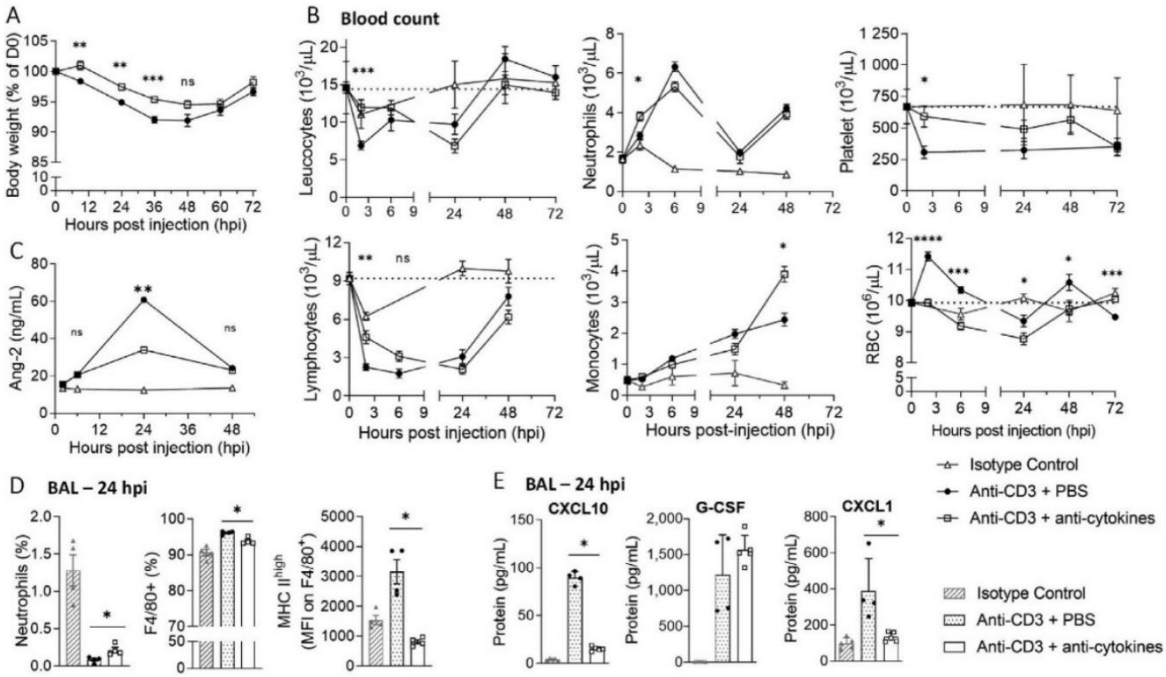


**Figure 4.** An anti-cytokine antibody cocktail alleviates early signs of CRS. Mice were i.v. co-injected with 5 µg of anti-CD3 plus either control PBS or an anti-cytokine cocktail (composed of an anti-IL-2, -IL-6, -IFN-γ, and -TNF-α mAbs, 30 mg/kg each), or with 5 µg of isotype control. Graphs show body weight (**A**) and blood parameters blood cell counts (**B**). Plasma concentration of Angiopoietin-2 (Ang-2) was determined by ELISA (**C**). Frequencies of neutrophils and F4/80$^+$ cells were expressed as percentage of viable cells (**D**). Cytokine concentrations were quantified in BAL at 24 hpi (**E**). RBC, red blood cell. n = 8-10 mice per time point, data from N = 2 independent experiments, except for **C** and **E** n = 4-5 mice per time point, data from a single experiment. $^*p < 0.05$, $^{**}p < 0.01$, $^{***}p < 0.001$, and $^{****}p < 0.0001$ as determined by one-tailed nonparametric Mann–Whitney U t-test. Values are displayed as the mean ± SEM.

(Supporting information Fig. S5). On the other hand, while clodronate liposome treatment was very efficient at depleting macrophages from the spleen and liver, it was ineffective at diminishing the cells from the lung. Here too, the treatment failed to reverse the anti-CD3-induced CRS (Supporting information Fig. S6). Taken together, data highlight a potential role of neutrophils and monocytes/macrophages in the physiopathology of severe CRS.

## Discussion

In this study, an agonistic anti-CD3 was used to mimic severe forms of CRS induced by polyclonal T-cell activation in mice. Within 60 min and up to 24 hpi, a rapid and severe lymphopenia, erythrocytosis, thrombocytopenia, and neutrophilia was observed in mice following anti-CD3 injection. Interestingly, monocytosis occurred in mice, whereas monocytopenia was reported in healthy volunteers given the superagonist CD28 antibody TGN1412 [22]. These divergent responses could be explained by the differentiating ability to engage FcγRs of a hamster IgG1-Fc domain of the anti-CD3 in mice, as compared to the attenuated human IgG4 domain of TGN1412 in humans. Akin to CRS in mice, however, monocytosis, neutrophilia, and a marked lymphopenia were observed in patients severely ill with SARS-Cov-1 and -2 infections [25, 26]. In parallel, an induction of hypercytokinemia, characterized by type I cytokines and anti-inflammatory type II cytokines, was observed in mice. Of note, an up-regulation of CXCR3 ligands, CXCL9 and CXCL10, was seen in blood and in tissues of anti-CD3-treated mice within 1 hpi.

IFN-γ has been described as a main contributor to CRS in a plethora of preclinical models leading to sharp increases in CXCL9/CXCL10 [7,18,26,27]. Elevated levels of IFN-γ-induced chemokines have also been measured in patients with SARS and HLH [27–29]. IFN-γ is central to CpG-induced CRS in mice [30] and we have shown that tissue-derived levels of the cytokine are 500- to 2000-fold higher in organs than those measured in the blood [18]. Likewise, CXCL9/CXCL10 levels in pediatric secondary HLH patients correlated with key disease parameters and severity [18]. In the present study, type I cytokines *Tnf*-α, *Ifn*-γ, *Cxcl10*, and *Cxcl9* were rapidly induced in the liver following anti-CD3 administration. Within the first hpi, *de novo Ifn*-γ gene transcript levels peaked in the liver and spleen but to a lesser extent in the lung, with blood levels of the cytokine climaxing at 6 hpi. Interestingly, a second *Ifn*-γ spike was observed at 48 hpi only in the liver and correlated with a second wave of neutrophils in blood. While an IFNγ-mediated role in recruitment of neutrophils is described [31], the role for these cells in the CRS manifestations

 

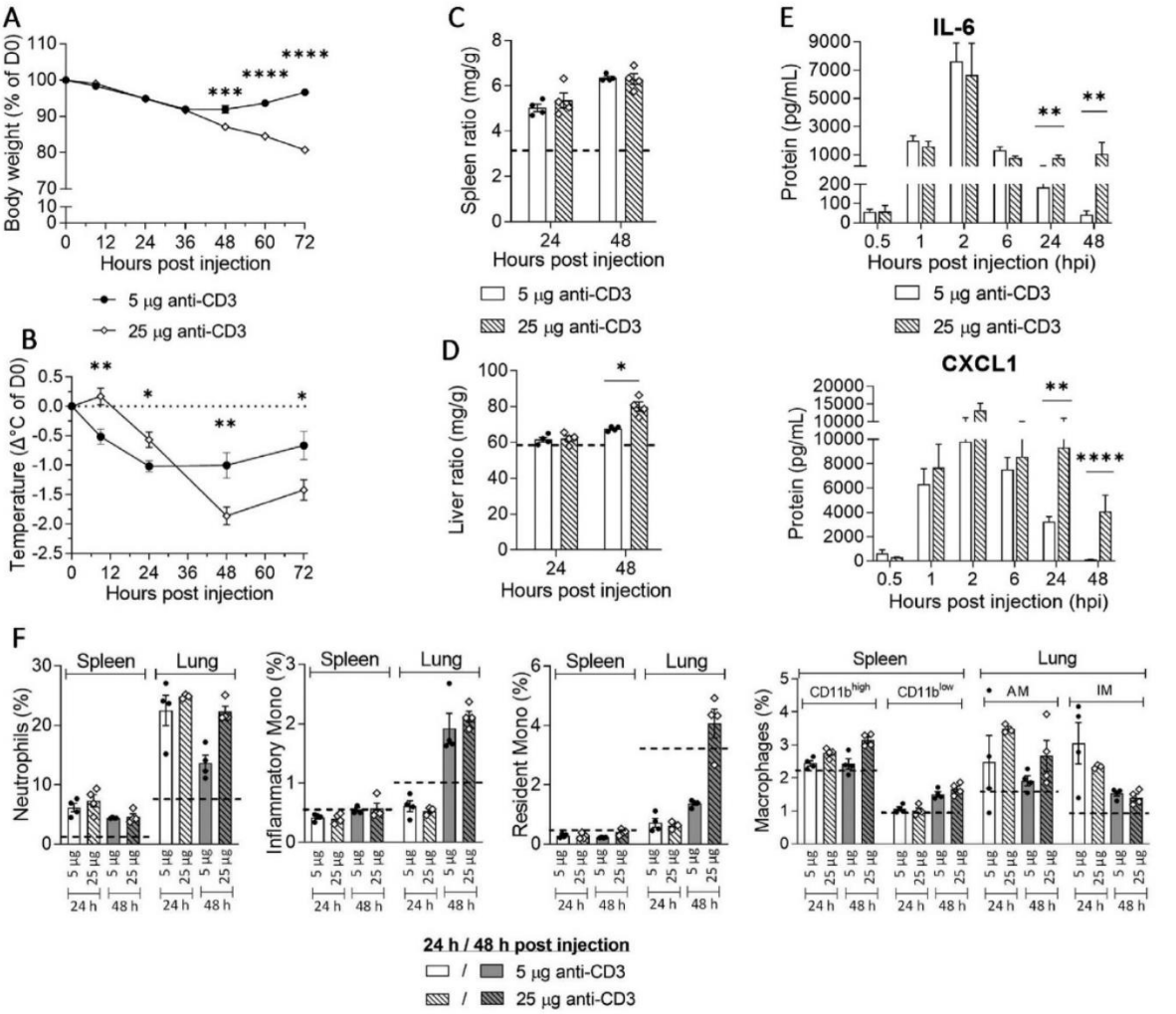


**Figure 5.** CRS severity is associated with sustained neutrophil and monocyte infiltration in lungs. Mice were i.v. injected with either 5 µg or 25 µg of anti-CD3. Body weight (**A**), temperature (**B**), spleen/body weight ratio (**C**), liver/body weight ratio (**D**), and IL-6 and CXCL1 plasma concentration (**E**) is shown. Immunophenotyping of single-cell suspensions from the spleen and the lungs (**F**). Gating strategies and relative number of cells are available in supporting information Fig. S2 and S3 and Table S5. Dotted lines on graphs in (**C**), (**D**), and (**F**) represent the mean of corresponding values of isotype control injected mice. n = 9-10 per time point from N = 2 independent experiments, except for C, D, and F n = 4-5 mice per time point, data from a single experiment representative of three experiments. $^{*}p < 0.05$, $^{**}p < 0.01$, $^{***}p < 0.001$, and $^{****}p < 0.0001$ as determined by one-tailed nonparametric Mann–Whitney U t-test. Values are displayed as the mean ± SEM.

described here remain unclear. Indeed, the co-administration of a neutrophil-depleting antibody, anti-Ly6G, failed to significantly reverse CRS features in mice. Nonetheless, a contribution of neutrophils to the anti-CD3-induced CRS manifestations should not be discounted, as the depleting efficacy of anti-Ly6G was not absolute, as evidenced here and by others [32]. As neutrophils have been shown to be important mediators of tissue damage in inflammatory diseases, potentially detrimental in the pathophysiology of COVID-19 [33], we do not rule out a pathogenic role for these cells in the anti-CD3-induced CRS in mice. The significant increase of *Ifn-γ* in the liver within minutes post anti-CD3 injection resulted in the local and sustained production of CXCL9 and CXCL10 as evidenced in the protein exudates and mRNA transcript up-regulation. As a consequence, CXCR3-expressing neutrophils [34], macrophages [35, 36], T cells [37], and NK cells [38] rapidly infiltrated the liver. While *Cxcl10* returned to baseline levels more rapidly, *Cxcl9* production was sustained at 2000-fold levels above homeostatic levels at 24 hpi in the liver.

Lungs from anti-CD3-treated mice presented a rapid and prolonged induction of proinflammatory cytokines/chemokines. Within 1 hpi, *Ifn-γ* production was increased 40-fold coinciding with a subsequent 3600-fold induction of *Cxcl9* and 1000-fold induction of *Cxcl10* mRNA transcripts with the former remaining at that level for at least 24 h. CXCL9/10 protein levels in the

lung remained high up to 48 hpi, certainly accounting for the infiltration of CXCR3-expressing neutrophils and activated T cells. CXCL1 and G-CSF may also induce significant neutrophil recruitment to the lung [39, 40], the BAL from anti-CD3-treated mice presented with high levels of these soluble factors, contributing to the sustained neutrophil infiltration at 48 hpi.

Severe CRS disease manifested by fever and pneumonia, leading to acute respiratory distress syndrome (ARDS) has been described in up to 20% of COVID-19 patients [41]. Additionally, CRS is common in patients with COVID-19 where elevated plasma IL-6 correlated with respiratory failure, ARDS, and adverse clinical outcomes [42,43]. High plasma levels of IL-6, CXCL10, GM-CSF, and increased lung neutrophil infiltrate, hallmarks of ARDS [44], were observed in our animal study as well as an increased proportion of activated alveolar macrophages ($MHCII^{high}$). Significant neutrophil and macrophage infiltration is also observed in pulmonary interstitium and alveoli from SARS-induced ARDS patients [26]. Interestingly, a prolonged neutrophil and monocyte infiltration in the pulmonary interstitium, but not in the alveoli, was observed in our study. In contrast to ARDS patients, we failed to observe histological differences in terms of lung architecture, cellularity in the alveolar cavities and interalveolar septal walls. This observation contrasted with the erythrocytosis and thrombocytopenia observed, thought to indicate disseminated intravascular coagulation and/or capillary leakage and also seen in humans administered Muromonab-CD3 or TGN1412 [22, 45]. Nonetheless, elevated Ang-2 plasma concentration in anti-CD3-treated mice suggests endothelial dysfunction and increased vascular permeability disorders [46]. Up-regulated levels of plasma Ang-2 is observed in COVID-19 and ARDS patients and correlated with mortality in the latter [16, 24, 47].The use of anti-cytokine approaches to manage CRS is validated by recent approvals of tocilizumab (anti-IL6R) and emapalumab (anti-IFN-γ) by the US Food and Drug Administration in the context CAR-T-cell-therapy and primary HLH [48, 49], respectively. Additionally, clinical trials with therapies, including a device designed to remove cytokines from blood using hemadsorption [50] and the blockade of IL-1 [51], GM-CSF, [52] and JAK1/JAK2 signaling [53,54], are ongoing. To this end, our anti-cytokine Ab cocktail, targeting IFN-γ, IL-6, TNF-α, and IL-2 (herein called anti-cytokine cocktail) reduced the clinical features of CRS induced by anti-CD3 injection in the first 24 hpi including body weight, prostration, and piloerection. Blood parameters remained in normal ranges in mice co-treated with the anti-CD3 and the anti-cytokine cocktail although neutrophilia and monocytosis persisted. Ang-2 plasma levels were significantly reduced by the anti-cytokine cocktail suggesting a reduction in vascular leakage supported by observed improvements in RBC and platelet counts. In addition, the lung inflammation induced by anti-CD3 treatment was improved as shown by the reduced BAL levels of CXCL1 and CXCL10, and decreased MHCII expression on alveolar macrophages. The anti-cytokine cocktail afforded an increased benefit as compared to the monotherapy administration of the anti-cytokine mAbs. Nonetheless, the benefit of the anti-cytokine cocktail was transient. A second injection of the cocktail at 12 hpi of anti-CD3 failed to prolong the protective benefit. IL-1 receptor antagonist, Anakinra®, or an anti-IL-15 neutralizing mAb (clone AIO.3, BioXCell) offered no improvement to the anti-cytokine cocktail. The failure to control CRS features beyond the initial 24 h post anti-CD3 administration was unexpected. In a mouse model recapitulating key features of CAR-T-cell-mediated CRS and neurotoxicity, human monocytes were the major source of IL-1 and IL-6 [55]. Accordingly, the authors observed that the syndrome was prevented by monocyte depletion or IL-6 blockade, but the latter failed to protect mice from delayed lethal neurotoxicity caused by meningeal inflammation. Anakinra®, however, diminished CRS and neurotoxicity, a finding corroborated by others [51]. The challenge to interrupt a cytokine storm by targeting IL-6 was made more evident in a recent clinical study where tocilizumab was ineffective at reducing COVID-19 mortality [56]. Nonetheless, co-administration of TNF-α and IFN-γ-neutralizing antibodies provided superior protection over monotherapy in a mouse SARS-CoV-2 infection model, highlighting a benefit of anti-cytokine combination therapy [14]. The limited benefit we observed in anti-CD3-treated mice by the cytokine-blocking antibody cocktail, and from efforts by others depleting inflammatory cells, parallel challenges faced in the clinical setting with patients suffering from severe forms of CRS. While cytokine activity was ablated by the high-dose antibody therapy we used in mice, cellular infiltration was not entirely abrogated. While clodronate liposome treatment was very efficient at depleting macrophages from spleen and liver, the treatment was ineffective at diminishing the cells from the lung. We cannot rule out a role for macrophages as their capacity for proinflammatory cytokine production have been shown to promote further leucocytosis and immune cell infiltrates in COVID-19- induced lung damage [57]. Similarly, we saw in our severe CRS model (using a higher dose of anti-CD3), increased body weight loss and an acute decrease in body temperature, confirming a critical role for the increased presence of neutrophils and macrophages in the lung.

The severe CRS induced by in vivo T-cell activation after anti-CD3 administration to mice highlights the central role of the subsequent cytokine storm and recruitment of pathogenic neutrophils and macrophages. The challenges encountered to halt disease relate to the complexities of severe T-cell-mediated CRS, while potentially advocating an anti-cytokine therapy as a therapeutic option for less-severe cases.

## Materials and methods

### Mice

All animal procedures were performed in accordance with the Swiss Veterinary Office guidelines and authorized by the Cantonal Veterinary Office. Studies were conducted with 6- to 8-week-old male BALB/cByJ, mice obtained from Charles River Laboratories (Saint-Germain-Nuelles, France). The animals were reared under conventional conditions temperature-controlled room (25 ± 2°C) under a 12 h light/dark cycle.

### Antibodies used for in vivo studies in mice

The anti-CD3ε (hamster IgG), clone 145-2C11) mAb and the anti-IL2 (Rat IgG2a, clone JES6-1A12), anti-IFN-γ (Rat IgG1, clone XMG1.2) and anti-TNF-α (Rat IgG1, clone XT3.11) neutralizing mAbs were obtained from BioXCell (Lebanon, NH, USA). The Armenian hamster IgG isotype control (clone HTK888) was obtained from BioLegend® (CA, USA). The anti-IL6 neutralizing mAb, clone 1F7 [58], was produced inhouse.

### Mouse model of CRS

Mice were injected i.v. with a single 5 μg anti-CD3 mAb, unless otherwise mentioned. Neutralizing mAbs were injected i.v. at 30 mg/kg simultaneously with the anti-CD3 mAb. At indicated time points, mice were euthanized by $CO_2$ inhalation, unless indicated. Blood cell count was performed with a ProCyte Dx analyzer (IDEXX Laboratories, Inc., ME, USA) or with a Hemavet analyzer (Drew Scientific, FL, USA). Samples of spleen, lung, and liver tissue were stored in RNA later (Sigma-Aldrich, St.-Louis, MO, USA) for gene expression analysis. Whole-lung, -liver, and -spleen were harvested for immune cell infiltration analysis.

### Bronchoalveolar lavages analysis

Mice were sacrificed by lethal injection of pentobarbital (Streuli Pharma AG, Uznach, Switzerland). Bronchoalveolar lavage (BAL) was performed twice with sterile PBS. BAL fluids were centrifuged, supernatants were kept at −20°C for cytokines analysis and cell pellets were resuspended for immunophenotyping analysis.

### Measurement of cytokines and chemokines in plasma

The plasma concentrations of cytokines and chemokines were measured using MILLIPLEX MAP multiplex immunodetection kits (Merck Millipore, Burlington, MA, USA) and analyzed on the Luminex® 200™ immunoassay analyzer (Luminex®, TX, USA), according to manufacturer's instructions. Plasma level of Ang-2 was quantified with the Ang-2 Mouse ELISA Kit (Abcam, Cambridge, UK) according to manufacturer's instructions.

### Gene expression

Spleen, liver, and lung RNA isolated using RNeasy mini-Kit (Qiagen, Hilden, Germany) was reverse transcribed using High-Capacity cDNA Reverse Transcription kit (Applied Biosystems®, Foster City, CAL, USA). Quantitative PCR (qPCR) was performed using SYBR® Green Master Mix (Applied Biosystems®) on the 7900HT Fast Real-Time PCR System from Applied Biosystems®. The $\Delta\Delta Ct$ method was used to calculate the relative gene expression levels (RQ) with β-actin gene as housekeeping gene. The primer sequences are listed in Supporting information Table S3.

### Cell preparation

Single-cell suspension of liver was performed using a dissociation kit (Miltenyi Biotec, Bergisch Gladbach, Germany) and the gentleMACS™ Dissociator (Miltenyi Biotec) according to the manufacturer's protocol. Single-cell suspension from spleen and lungs were prepared by enzymatic digestion in collagenase IV (Gibco) and DNase I (Sigma-Aldrich) for 20 min at 37°C, followed by mechanical digestion with the gentleMACS™ Dissociator (Miltenyi Biotech). RBC lysis was performed using ACK buffer (Ammonium-Chloride-Potassium). Cell suspensions were filtered through a 70 μM Nylon filter (BD Falcon™) and counted using a cell viability analyzer (Vi-CELL XR, Beckman Coulter, CAL, USA).

### Flow cytometry

After cells were counted, $2 \times 10^6$ cells per sample were stained with Fixable Viability Stain 620 (BD Biosciences) according to manufacturer's instructions. Cells were then incubated with Mouse BD Fc Block™ and surface staining was directly performed in the dark for 20 min at 4°C (see Supporting information Table S4 for a list of antibodies, clones, fluorochromes, manufacturers). Cells were then washed twice with FACS buffer and acquired on the CytoFLEX S flow cytometer (Beckman Coulter). Data analyses were performed using FlowJo software (Tree Star Inc., OR, USA). Flow cytometry experiments were done in accordance with the guidelines of the journal [59].

### Statistical analysis

GraphPad Prism (GraphPad Software, CA, USA) was used for all statistical analysis. The unpaired *t*-test or one-tailed nonparametric Mann–Whitney U *t*-test were used for statistical comparison. *p*-value of $<0.05$ was considered significant.

Acknowledgments: The authors would like to thank Drs. X. Chauchet, E. Hatterer, and D. Merkler, for scientific input and the former for help in the setup of flow cytometry panels; Y.R. Donati for BAL and lung perfusion methodologies and E. Eggimann for animal husbandry.

Conflict of Interest: The authors declare no commercial or financial conflict of interest.

 

**Author Contributions:** VB and WGF designed and conceived the project. LN and WGF analyzed the data and wrote the manuscript. LN, LCo, and LCh performed the mouse experiments. GP produced the antibody and NP performed the analytics. LN performed in vitro experiments and prepared the figures for the manuscript. All the authors revised the manuscript and approved the final version.

**Peer review:** The peer review history for this article is available at https://publons.com/publon/10.1002/eji.202149181.

**Data availability statement:** Data available on request from the authors.

## References

1 **Zhang, Y.** and **Zhang, Z.**, The history and advances in cancer immunotherapy: understanding the characteristics of tumor-infiltrating immune cells and their therapeutic implications. *Cell. Mol. Immunol.* 2020. **17**: 807–821

2 **Robert, C.**, A decade of immune-checkpoint inhibitors in cancer therapy. *Nat. Commun.* 2020. **11**: 3801.

3 **Gupta, S., Gupta, S. C., Hunter, K. D.** and **Pant, A. B.**, Immunotherapy: a new hope for cancer patients. *J. Oncol.* 2020. https://doi.org/10.1155/2020/3548603

4 **Shimabukuro-Vornhagen, A., Gödel, P., Subklewe, M., Stemmler, H. J., Schlößer, H. A., Schlaak, M., Kochanek, M.** et al., Cytokine release syndrome. *J. Immunother. Cancer.* 2018. **6**: 56

5 **Chatenoud, L., Ferran, C., Legendre, C., Thouard, I., Merite, S., Reuter, A., Gevaert, Y.** et al., In vivo cell activation following OKT3 administration. Systemic cytokine release and modulation by corticosteroids. *Transplantation*. 1990. **49**: 697–702

6 **Srikiatkhachorn, A., Mathew, A.** and **Rothman, A. L.**, Immune-mediated cytokine storm and its role in severe dengue. *Semin. Immunopathol*. 2017. **39**: 563–574.

7 **Patro, A. R. K, Mohanty, S., Prusty, B. K., Singh, D. K., Gaikwad, S., Saswat, T., Chattopadhyay, S.** et al., Cytokine signature associated with disease severity in dengue. *Viruses*. 2019. **11**: 34.

8 **Prescott, J. B., Marzi, A., Safronetz, D., Robertson, S. J., Feldmann, H.** and **Best, S. M.**, Immunobiology of Ebola and Lassa virus infections. *Nat. Rev. Immunol.* 2017. **17**: 195–207

9 **Wauquier, N., Becquart, P., Padilla, C., Baize, S.** and **Leroy, E. M.** Human fatal zaire ebola virus infection is associated with an aberrant innate immunity and with massive lymphocyte apoptosis. *PLoS Negl. Trop. Dis*. 2010. **4**: e837.

10 **Tisoncik, J. R., Korth, M. J., Simmons, C. P., Farrar, J., Martin, T. R.** and **Katze, M. G.**, Into the eye of the cytokine storm. *Microbiol. Mol. Biol. Rev.* 2012. **76**: 16–32

11 **Liu, Q., Zhou, Y. -H.** and **Yang, Z. -. Q.**, The cytokine storm of severe influenza and development of immunomodulatory therapy. *Cell. Mol. Immunol.* 2016. **13**: 3–10

12 **Mehta, P., Mcauley, D. F., Brown, M., Sanchez, E., Tattersall, R. S.** and **Manson, J. J.**, COVID-19: consider cytokine storm syndromes and immunosuppression. *Lancet North Am. Ed.* 2020. **395**: 1033–1034

13 **Vaninov, N.**, In the eye of the COVID-19 cytokine storm. *Nat. Rev. Immunol.* 2020; 277.

14 **Karki, R., Sharma, B. R., Tuladhar, S., Williams, E. P., Zalduondo, L., Samir, P., Zheng, M.** et al., Synergism of TNF-α and IFN-γ triggers inflammatory cell death, tissue damage, and mortality in SARS-CoV-2 infection and cytokine shock syndromes. *Cell* 2020. **184**:149-168.

15 **Huang, C., Wang, Y., Li, X., Ren, L., Zhao, J., Hu, Yi, Zhang, Li** et al., Clinical features of patients infected with 2019 novel coronavirus in Wuhan, China. *Lancet North Am. Ed.* 2020. **395**: 497–506.

16 **Smadja, D. M., Guerin, C. L., Chocron, R., Yatim, N., Boussier, J., Gendron, N., Khider, L.** et al., Angiopoietin-2 as a marker of endothelial activation is a good predictor factor for intensive care unit admission of COVID-19 patients. *Angiogenesis* 2020. **23**: 611–610.

17 **Gibson, P. G., Qin, L.** and **Puah, S. H.**, COVID-19 acute respiratory distress syndrome (ARDS): clinical features and differences from typical pre-COVID-19 ARDS. *Med. J. Aust.* 2020. **213**: 54–56.

18 **Buatois, V., Chatel, L., Cons, L., Lory, S., Richard, F., Guilhot, F., Johnson, Z.** et al., Use of a mouse model to identify a blood biomarker for IFNγ activity in pediatric secondary hemophagocytic lymphohistiocytosis. *Transltinl. Res.* 2017. **180**: 37–52.

19 **Locatelli, F., Jordan, M. B., Allen, C., Cesaro, S., Rizzari, C., Rao, A., Degar, B.** et al., Emapalumab in children with primary hemophagocytic lymphohistiocytosis. *N. Engl. J. Med.* 2020. **382**: 1811–1822.

20 **Neelapu, S. S., Tummala, S., Kebriaei, P., Wierda, W., Gutierrez, C., Locke, F. L., Komanduri, K. V.** et al., Chimeric antigen receptor T cell therapy: assessment and management of toxicities. *Nat. Rev. Clin. Oncol.* 2018. **15**: 47–62.

21 **Hünig, T.**, The storm has cleared: lessons from the CD28 superagonist TGN1412 trial. *Nat. Rev. Immunol.* 2012. **12**: 317–318.

22 **Suntharalingam, G., Perry, M. R., Ward, S., Brett, S. J., Castello-Cortes, A., Brunner, M. D.** and **Panoskaltsis, N.**, Cytokine storm in a phase 1 trial of the anti-CD28 monoclonal antibody TGN1412. *N. Engl. J. Med.* 2006. **355**: 1018–1028.

23 **Hirsch, R., Gress, R. E., Pluznik, D. H., Eckhaus, M.** and **Bluestone, J. A.** Effects of in vivo administration of anti-CD3 monoclonal antibody on T cell function in mice. II. In vivo activation of T cells. *J. Immunol.* 1989. **142**: 737–743.

24 **Hashimoto, T.** and **Pittet, J. -. F.**, Angiopoietin-2: modulator of vascular permeability in acute lung injury? *PLoS Med.*. 2006. **3**: e113.

25 **Liu, J., Li, S., Liu, J., Liang, B., Wang, X., Wang, H., Li, W.** et al., Longitudinal characteristics of lymphocyte responses and cytokine profiles in the peripheral blood of SARS-CoV-2 infected patients. *EBioMedicine* 2020. **55**, 102763.

26 **Channappanavar, R.** and **Perlman, S.**, Pathogenic human coronavirus infections: causes and consequences of cytokine storm and immunopathology. *Semin. Immunopathol.* 2017. **39**: 529–539.

27 **Takada, H., Takahata, Y., Nomura, A., Ohga, S., Mizuno, Y.** and **Hara, T.**, Increased serum levels of interferon-gamma-inducible protein 10 and monokine induced by gamma interferon in patients with haemophagocytic lymphohistiocytosis. *Clin. Exp. Immunol.* 2003. **133**: 448–453.

28 **Henter, Ji, Elinder, G., Soder, O., Hansson, M., Andersson, B.** and **Andersson, U.**, Hypercytokinemia in familial hemophagocytic lymphohistiocytosis. *Blood*. 1991. **78**: 2918–2922.

29 **Osugi, Y., Hara, J., Tagawa, S., Takai, K., Hosoi, G., Matsuda, Y., Ohta, H.** et al., Cytokine production regulating Th1 and Th2 cytokines in hemophagocytic lymphohistiocytosis. *Blood*. 1997. **89**: 4100–4103.

30 **Behrens, E. M., Canna, S. W., Slade, K., Rao, S., Kreiger, P. A., Paessler, M., Kambayashi, T.** et al., Repeated TLR9 stimulation results in macrophage activation syndrome–like disease in mice. *J. Clin. Invest.* 2011. **121**: 2264–2277.

 

31 **Bonville, C. A., Percopo, C. M., Dyer, K. D., Gao, J., Prussin, C., Foster, B., Rosenberg, H. F.** et al., Interferon-gamma coordinates CCL3-mediated neutrophil recruitment in vivo. *BMC Immunol.* 2019. **10**: 14.

32 **Pollenus, E., Malengier-Devlies, B., Vandermosten, L., Pham, T. -T., Mitera, T., Possemiers, H., Boon, L.** et al., Limitations of neutrophil depletion by anti-Ly6G antibodies in two heterogenic immunological models. *Immunol. Lett.* 2019. **212**: 30–36.

33 **Veras, F. P., Pontelli, M. C., Silva, C. M., Toller-Kawahisa, J. E., de Lima, M., Nascimento, D. C., Schneider, A. H.** et al. SARS-CoV-2-triggered neutrophil extracellular traps mediate COVID-19 pathology. *J. Exp. Med.* 2020. **217**: 20201129.

34 **Hartl, D., Krauss-Etschmann, S., Koller, B., Hordijk, P. L., Kuijpers, T. W., Hoffmann, F., Hector, A.** et al., Infiltrated neutrophils acquire novel chemokine receptor expression and chemokine responsiveness in chronic inflammatory lung diseases. *J. Immunol.* 2008. **181**: 8053–8067.

35 **Luster, A. D.** and **Leder, P.**, IP-10, a -C-X-C- chemokine, elicits a potent thymus-dependent antitumor response *in vivo*. *J. Exp. Med.* 1993. **178**: 1057–1065.

36 **Luster, A. D., Greenberg, S. M.** and **Leder, P.**, The IP-10 chemokine binds to a specific cell surface heparan sulfate site shared with platelet factor 4 and inhibits endothelial cell proliferation. *J. Exp. Med.* 1995. **182**: 219–231.

37 **Qin, S., Rottman, J. B., Myers, P., Kassam, N., Weinblatt, M., Loetscher, M., Koch, A. E.** et al., The chemokine receptors CXCR3 and CCR5 mark subsets of T cells associated with certain inflammatory reactions. *J. Clin. Invest.* 1998. **101**: 746–754.

38 **Thomas, S. Y., Hou, R., Boyson, J. E., Means, T. K., Hess, C., Olson, D. P., Strominger, J. L.** et al., CD1d-restricted NKT cells express a chemokine receptor profile indicative of Th1-type inflammatory homing cells. *J. Immunol.* 2003. **171**: 2571–2580.

39 **Capucetti, A., Albano, F.** and **Bonecchi, R.**, Multiple roles for chemokines in neutrophil biology. *Front. Immunol.* 2020. **11**: 1259.

40 **Sawant, K. V., Poluri, K. M., Dutta, A. K., Sepuru, K. M., Troshkina, A., Garofalo, R. P.** and **Rajarathnam, K.**, Chemokine CXCL1 mediated neutrophil recruitment: role of glycosaminoglycan interactions. *Sci. Rep.* 2016. **6**: 1–8.

41 **Moore, J. B.** and **June, C. H.**, Cytokine release syndrome in severe COVID-19. *Science*. 2020. **368**: 473–474.

42 **Chen, G., Wu, Di, Guo, W., Cao, Y., Huang, Da, Wang, H., Wang, T.** et al., Clinical and immunological features of severe and moderate coronavirus disease 2019. *J. Clin. Invest.* 2020. **130**: 2620–2629.

43 **Ruan, Q., Yang, K., Wang, W., Jiang, L.** and **Song, J.**, Clinical predictors of mortality due to COVID-19 based on an analysis of data of 150 patients from Wuhan, China. *Intensive Care Med.* 2020. **46**: 846–848.

44 **De Wit, E., Van Doremalen, N., Falzarano, D.** and **Munster, V. J.**, SARS and MERS: recent insights into emerging coronaviruses. *Nat. Rev. Microbiol.* 2016. **14**: 523–534.

45 **Hansel, T. T., Kropshofer, H., Singer, T., Mitchell, J. A.** and **George, A. J. T.**, The safety and side effects of monoclonal antibodies. *Nat. Rev. Drug Discov.* 2010. **9**: 325–338.

46 **Akwii, R. G., Sajib, M. S., Zahra, F. T.** and **Mikelis, C. M.**, Role of angiopoietin-2 in vascular physiology and pathophysiology. *Cells* 2019. **8**: 471.

47 **Li, F., Yin, R.** and **Guo, Q.**, Circulating angiopoietin-2 and the risk of mortality in patients with acute respiratory distress syndrome: a systematic review and meta-analysis of 10 prospective cohort studies. *Ther. Adv. Respir. Dis.* 2020. **14**. https://doi.org/10.1177/1753466620905274

48 **Le, R. Q., Li, L., Yuan, W., Shord, S. S., Nie, L., Habtemariam, B. A., Przepiorka, D.** et al., FDA approval summary: tocilizumab for treatment of chimeric antigen receptor T cell-induced severe or life-threatening cytokine release syndrome. *Oncologist*. 2018. **23**: 943–947.

49 **Al-Salama, Z. T.**, Emapalumab: first global approval. *Drugs*. 2019. **79**: 99–103.

50 **Tomescu, D. R., Dima, S. O., Ungureanu, D., Popescu, M., Tulbure, D.** and **Popescu, I.**, First report of cytokine removal using CytoSorb® in severe noninfectious inflammatory syndrome after liver transplantation. *Int. J. Artif. Organs* 2016. **39**: 336–340.

51 **Giavridis, T., Van Der Stegen, S. J. C., Eyquem, J., Hamieh, M., Piersigilli, A.** and **Sadelain, M.**, CAR T cell–induced cytokine release syndrome is mediated by macrophages and abated by IL-1 blockade. *Nat. Med.* 2018. **24**: 731–738.

52 **Sterner, R. M., Sakemura, R., Cox, M. J., Yang, N., Khadka, R. H., Forsman, C. L., Hansen, M. J.** et al., GM-CSF inhibition reduces cytokine release syndrome and neuroinflammation but enhances CAR-T cell function in xenografts. *Blood* 2019. **133**: 697–709

53 **Huarte, E., O'connor, R. S., Peel, M. T., Nunez-Cruz, S., Leferovich, J., Juvekar, A., Yang, Y-Ou** et al., Itacitinib (INCB039110), a JAK1 inhibitor, reduces cytokines associated with cytokine release syndrome induced by CAR T cell therapy. *Clin. Cancer Res.* 2020. **26**: 6299–6309

54 **Yeleswaram, S., Smith, P., Burn, T., Covington, M., Juvekar, A., Li, Y., Squier, P.** et al., Inhibition of cytokine signaling by ruxolitinib and implications for COVID-19 treatment. *Clin. Immunol.* 2020. **218**: 108517.

55 **Norelli, M., Camisa, B., Barbiera, G., Falcone, L., Purevdorj, A., Genua, M., Sanvito, F.** et al., Monocyte-derived IL-1 and IL-6 are differentially required for cytokine-release syndrome and neurotoxicity due to CAR T cells. *Nat. Med.* 2018. **24**: 739–748

56 **Stone, J. H., Frigault, M. J., Serling-Boyd, N. J., Fernandes, A. D., Harvey, L., Foulkes, A. S., Horick, N. K.** et al., Efficacy of tocilizumab in patients hospitalized with Covid-19. *N. Engl. J. Med.* 2020. **383**: 2333–2344

57 **Panigrahy, D., Gilligan, M. M., Huang, S., Gartung, A., Cortés-Puch, I., Sime, P. J., Phipps, R. P.** et al., Inflammation resolution: a dual-pronged approach to averting cytokine storms in COVID-19? *Cancer Metastasis Rev.* 2020. **39**: 337–340

58 **Lacroix, M., Rousseau, F., Guilhot, F., Malinge, P., Magistrelli, G., Herren, S., Jones, S. A.** et al., Novel insights into interleukin 6 (IL-6) Cis- and trans-signaling pathways by differentially manipulating the assembly of the IL-6 signaling complex. *J. Biol. Chem.* 2015. **290**: 26943–26953

59 **Cossarizza, A., Chang, H. -. D., Radbruch, A., Acs, A., Adam, D., Adam-Klages, S., Agace, W. W.** et al., Guidelines for the use of flow cytometry and cell sorting in immunological studies (second edition). *Eur. J. Immunol.* 2019. **49**: 1457–1973


*Abbreviations:* **Ang-2**: angiopoietin-2 · **BAL**: Bronchoalveolar lavage · **CAR**: chimeric antigen receptor · **CD**: cluster differentiation · **CRS**: cytokine release syndrome · **HLH**: hemophagocytic lymphohistiocytosis · **hpi**: hour post injection · **IgG**: immunoglobulin gamma · **qPCR**: quantitative polymerase chain reaction

*Full correspondence:* Walter G. Ferlin, Light Chain
Bioscience-Novimmune S.A., Chemin du Pré-Fleuri 15, 1228
Plan-Les-Ouates, Geneva, Switzerland
e-mail: walter.ferlin@lightchainbio.com

Received: 15/1/2021
Revised: 23/3/2021
Accepted: 28/4/2021
Accepted article online: 4/5/2021

Supporting information for:

# IMMUNOLOGICAL ANALYSIS OF THE MURINE ANTI-CD3-INDUCED CYTOKINE RELEASE SYNDROME MODEL AND THERAPEUTIC EFFICACY OF ANTI-CYTOKINE ANTIBODIES

Lise Nouveau, Vanessa Buatois, Laura Cons, Laurence Chatel, Guillemette Pontini, Nicolas Pleche and Walter G. Ferlin*

Light Chain Bioscience-Novimmune S.A., Chemin du Pré-Fleuri 15, 1228 Plan-Les-Ouates Geneva, Switzerland.

***Correspondence:**

Walter Ferlin, Light Chain Bioscience-Novimmune S.A., Chemin du Pré-Fleuri 15, 1228 Plan-Les-Ouates Geneva, Switzerland; E-mail: walter.ferlin@lightchainbio.com

**This PDF file includes:**

Tables S1 to S5

Figs. S1 to S6

**Supplemental Table S1: Summary of the impact of monotherapy on key CRS parameters.** Comparison is done against anti-CD3 + PBS injected mice. Statistical data performed with Kruskal-Wallis test, comparing all the six groups together (anti-CD3 + PBS, or + Cocktail, + anti-IL2, + anti-IL-6, + anti-TNF-α, or + anti-IFN-γ), and indicated when significative for each time point. (*P<0.05, **P<0.01, ***P<0.001, ns: not significant but obvious visual trend). In green: Benefit of the therapy on a given CRS feature; in red: Therapy worsened a given CRS feature.

| | Cocktail | Anti-IL-2 | Anti-IL-6 | Anti-IFN-γ | Anti-TNF-α |
|---|---|---|---|---|---|
| **Body weight** | **6h: Reduced loss<br>*24h: Reduced loss<br>ns48h: Reduced loss | 6h: No difference<br>24h: No difference<br>48h: Start to recover | 6h: No difference<br>24h: No difference<br>48h: Start to recover | 6h: No difference<br>24h: No difference<br>48h: Start to recover | *6h: Reduced loss<br>***24h: Reduced loss<br>**48h: Reduced loss |
| **Tempe-rature** | 6h: No difference<br>**24h: worsened loss<br>ns48h: Faster recovery | ns6h: Reduced loss<br>24h: No difference<br>48h: No difference | 6h: No difference<br>24h: No difference<br>48h: No difference | 6h: No difference<br>*24h: worsened loss<br>ns48h: Faster recovery | 6h: No difference<br>24h: No difference<br>48h: No difference |
| **RBC increase** | *6h: Managed<br>24h: No difference<br>48h: No difference | 6h: Managed<br>24h: No difference<br>48h: No difference | 6h: No difference<br>24h: No difference<br>48h: No difference | *6h: Managed<br>24h: No difference<br>48h: No difference | 6h: Lower increase<br>24h: No difference<br>48h: No difference |
| **Lympho-penia** | ns6h: Lower lympho-penia<br>*24h: Start to recover<br>ns48h: Faster recovery | *6h: Worsened<br>24h: No difference<br>48h: No difference | *6h: Worsened<br>24h: No difference<br>ns48h: Start to recover | ns6h: Lower lympho-penia<br>24h: No difference<br>48h: No difference | 6h: No difference<br>24h: No difference<br>48h: No difference |
| **Neutro-philia** | 6h: No difference<br>24h: No difference<br>48h: No difference | **6h: Reduced<br>ns24h: Managed<br>48h: No difference | 6h: No difference<br>24h: Worsened<br>48h: No difference | 6h: No difference<br>24h: No difference<br>48h: No difference | ns6h: Reduced<br>24h: No difference<br>48h: No difference |
| **Mono-cytopenia** | 6h: No difference<br>24h: No difference<br>48h: Worsened | 6h: No difference<br>24h: No difference<br>48h: No difference | 6h: No difference<br>24h: No difference<br>48h: No difference | *6h: Worsened<br>24h: No difference<br>48h: No difference | 6h: No difference<br>24h: No difference<br>48h: No difference |
| **Clinical aspect** | 6h: No CRS features<br>24h: Medium CRS features<br>48h: Good recovery | 6h: No difference<br>24h: No difference<br>48h: No difference | 6h: No difference<br>24h: No difference<br>48h: Relative recovery | 6h: No difference<br>24h: No difference<br>48h: No difference | 6h: Reduced CRS features<br>24h: Medium CRS features<br>48h: Relative recovery |

**Supplemental Table S2: CRS severity is associated with prolonged IL-6 and CXCL1 plasma concentration.** Mice were injected i.v. with 5 µg or 25 µg of anti-CD3. Cytokines and chemokines concentration was quantified using Luminex technology and fold increase between mild (5 µg) and severe (25 µg) CRS was calculated.

| | Hours post injection | | | | | |
|---|---|---|---|---|---|---|
| | **0.5** | **1** | **2** | **6** | **24** | **48** |
| **IFN-γ** | 0.6 | 0.9 | 1.1 | 1.3 | 3.4 | 4.0 |
| **IL-2** | 1.1 | 1.2 | 0.8 | 1.3 | 14.2 | 1.0 |
| **IL-6** | 1.0 | 0.8 | 0.9 | 0.6 | 4.3 | 25.1 |
| **TNF-α** | 0.9 | 0.6 | 0.8 | 0.8 | 1.9 | 4.8 |
| **CXCL9** | 1.9 | 1.1 | 1.3 | 0.7 | 1.7 | 4.5 |
| **CXCL10** | 1.0 | 1.1 | 1.4 | 1.3 | 1.1 | 1.2 |
| **CXCL1** | 0.5 | 1.2 | 1.4 | 1.1 | 2.9 | 31.7 |
| **IL-10** | 0.6 | 0.5 | 0.9 | 0.9 | 6.0 | 1.6 |

**Supplemental Table S3: Primer sequences for qPCR analysis.**

| | **Sequence primers (5'-3')** | |
|---|---|---|
| | **Forward** | **Reverse** |
| **β-actin** | AGCCTTCCTTCTTGGGTATGG | CAACGTCACACTTCATGATGGAAT |
| **CXCL1** | CATGCAGGCAGCACTCAGA | ATCCATGGTGGCACACAGACT |
| **CXCL9** | AGCCTTCCTTCTTGGGTATGG | AGGTCTTTGAGGGATTTGTAGTGG |
| **CXCL10** | GACGGTCCGCTGCAACTG | GCTTCCCTATGGCCCTCATT |
| **IFN-γ** | CAACAGCAAGGCGAAAAAGG | CCTGTGGGTTGTTGACCTCAA |
| **IL-2** | AACTGTTGTAAAACTAAAGGGCTCTGA | CACCACAGTTGCTGACTCATCA |
| **IL-6** | TCGGAGGCTTAATTACACATGTTC | TGCCATTGCACAACTCTTTTCT |
| **IL-10** | TTTGAATTCCCTGGGTGAGAA | GCTCCACTGCCTTGCTCTTATT |
| **SAA** | GCTGAGAAAATCAGTGATGGAAGA | TCAGCAATGGTGTCCTCATGTC |
| **TNF-α** | GCCACCACGCTCTTCTGTCT | GGTCTGGGCCATAGAACTGATG |

**Supplemental Table S4: Antibodies used for immunophenotyping analysis.**

| Fluorochrome | Marker | Clone | Manufacturer |
|---|---|---|---|
| PerCP-Cy5.5 | CD69 | H1.2F3 | BD Biosciences |
| APC | CD8 | QA17A07 | Biolegend |
| APC-R700 | CD25 | PC61 | BD Biosciences |
| BV421 | CD45 | 30-F11 | BD Biosciences |
| BV510 | CD4 | RM4-5 | Biolegend |
| BV711 | CD62L | MEL-14 | Biolegend |
| PerCP-Cy5.5 | Ly6g | 1A8 | BD Biosciences |
| APC | MHCII IA/IE | M5/114.15.2 | Biolegend |
| APC-R700 | CD11b | M1/70 | BD Biosciences |
| APC-Cy7 | CD11c | N418 | Biolegend |
| BV421 | CD45 | 30-F11 | BD Biosciences |
| BV605 | Ly6c | HK1.4 | Biolegend |
| PE | NKp46 | 29A1.4 | eBioscience |
| PE-Cy7 | F4/80 | BM8 | invitrogen |

**Supplemental Table S5: Average number of cells analysed by flow cytometry.** Surface staining was performed according to the Materials and Methods and the same volume per well was acquired. For each immune cell subtype, the average number of cells is displayed in the table.

| Fig. 3 | $CD4^+$ T cell | | | $CD8^+$ T cell | | |
|---|---|---|---|---|---|---|
| | Spleen | Lung | Liver | Spleen | Lung | Liver |
| 24h - 5 µg αCD3 | 31053 | 7679 | 2963 | 7532 | 589 | 1580 |
| 48h - 5 µg αCD3 | 36996 | 4454 | 3466 | 25045 | 2570 | 2535 |
| 5 µg Isotype | 64503 | 12160 | 1273 | 27732 | 3951 | 438 |

| Fig.3 | Natural Killer | | | Neutrophil | | | $CD11b^{low}$ | $CD11b^{high}$ | AM | IM | KC |
|---|---|---|---|---|---|---|---|---|---|---|---|
| | Spleen | Lung | Liver | Spleen | Lung | Liver | Spleen | Spleen | Lung | Lung | Liver |
| 24h - 5 µg αCD3 | 2316 | 3764 | 2334 | 6778 | 8660 | 4456 | 2687 | 345 | 5078 | 2021 | 709 |
| 48h - 5 µg αCD3 | 5763 | 7109 | 2443 | 7889 | 7945 | 1499 | 4782 | 509 | 3064 | 950 | 2917 |
| 5 µg Isotype | 5976 | 5687 | 809 | 2723 | 4640 | 1423 | 7158 | 588 | 2012 | 1015 | 2246 |

| Fig. 4 | $F4\_80^+$ | $MHC\ II^+$ | Neutrophil |
|---|---|---|---|
| 5 µg αCD3 | 32676 | 8378 | 49 |
| 5 µg αCD3 + α-cytokines | 18535 | 1200 | 55 |
| Isotype | 20904 | 1732 | 474 |

| Fig. 5F | Neutrophil | | Inf. Monocyte | | Res. Monocyte | | $CD11b^-$ | $CD11b^+$ | AM | IM |
|---|---|---|---|---|---|---|---|---|---|---|
| | Spleen | Lung | Spleen | Lung | Spleen | Lung | Spleen | Spleen | Lung | Lung |
| 24h - 5 µg αCD3 | 23642 | 18983 | 1627 | 341 | 1088 | 628 | 4087 | 9381 | 5147 | 2826 |
| 24h - 25 µg αCD3 | 30187 | 18366 | 1687 | 275 | 1105 | 507 | 4190 | 11368 | 6785 | 2363 |
| 48h - 5 µg αCD3 | 19277 | 20542 | 2434 | 1941 | 965 | 1814 | 6566 | 10591 | 8851 | 3475 |
| 48h - 25 µg αCD3 | 19369 | 17469 | 2420 | 1304 | 1707 | 3927 | 7039 | 13307 | 4745 | 1580 |

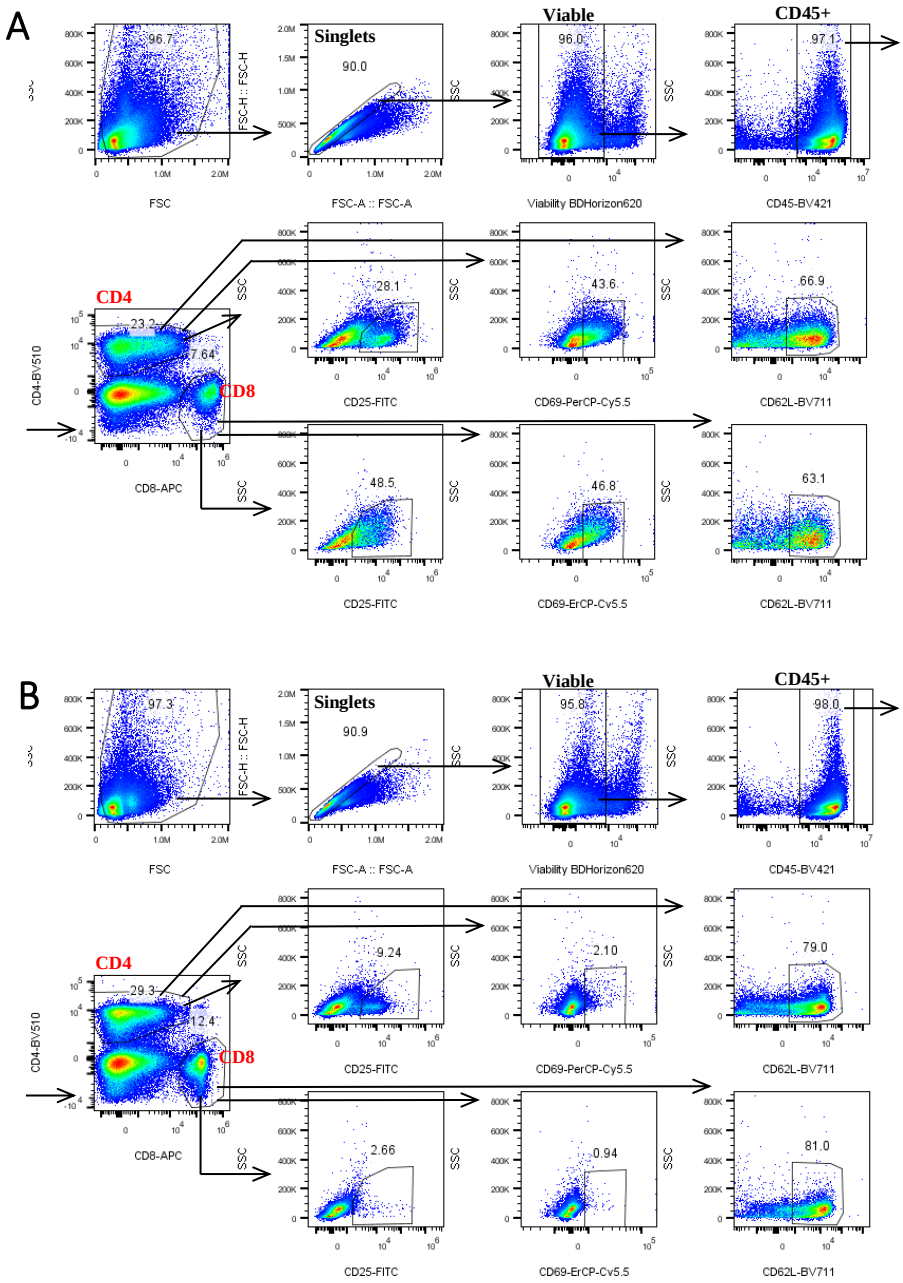


**Supplemental Figure S1: Gating strategy to identify lymphoid-cell subsets in mice.** Single-cell suspension were prepared from organs of isotype control-injected mice (**A**) or anti-CD3-injected mice (**B**). After the exclusion of debris, doublets and dead cells, lymphocytes T cells were identified by CD45, CD4 and CD8 staining. Activation level of each T cells subset was appreciated by determining the proportion of $CD25^{+}$, $CD69^{+}$ and $CD62L^{-}$ T cells. Definition of abbreviations: FSC, forward scatter; SSC, side scatter.

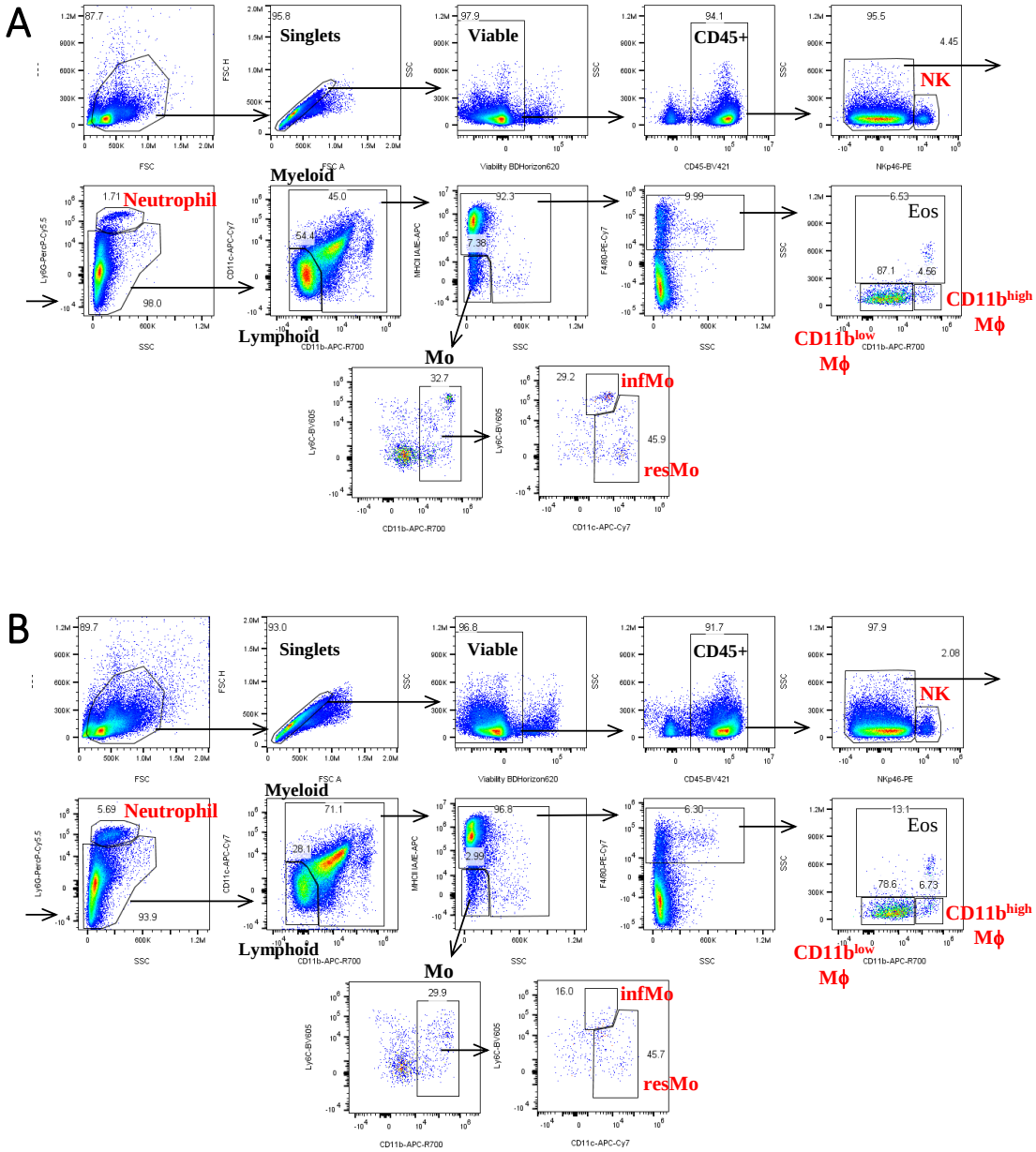


**Supplemental Figure S2: Gating strategy to identify myeloid-cell subsets in the spleen.** Single-cells suspension were prepared from spleen of isotype control-injected mice (**A**) or anti-CD3-injected mice (**B**). After the exclusion of debris, doublets and dead cells, immune cells were identified by CD45 staining. A sequential gating strategy was first used to identify populations expressing specific markers: natural killer (NK) cells (NKp46$^{+}$), neutrophils (Ly6G$^{+}$). Identification of populations with overlapping expression patterns was done as followed: lymphoid cells, CD11c$^{-}$CD11b$^{-}$; myeloid cells, CD11c$^{pos}$CD11b$^{pos}$; monocytes, CD11b$^{+}$ CD11c$^{+}$ MHCII$^{-/low}$; macrophage CD11b$^{+}$CD11c$^{+}$F4/80$^{pos}$MHCII$^{pos}$. Using Ly6C marker, distinction between inflammatory vs resident monocytes was done, Ly6C$^{high}$ and Ly6C$^{-/low}$ respectively. Eosinophils and macrophages were dissociated respectively as SSC$^{high}$CD11b$^{+}$ and SSC$^{low}$CD11b$^{-/low}$ or CD11b$^{high}$. Definition of abbreviations: NK, natural killer; infMo, inflammatory monocytes; resMo, resident monocytes; Mϕ, macrophages; MHCII, major histocompatibility complex class II; FSC, forward scatter; SSC, side scatter.

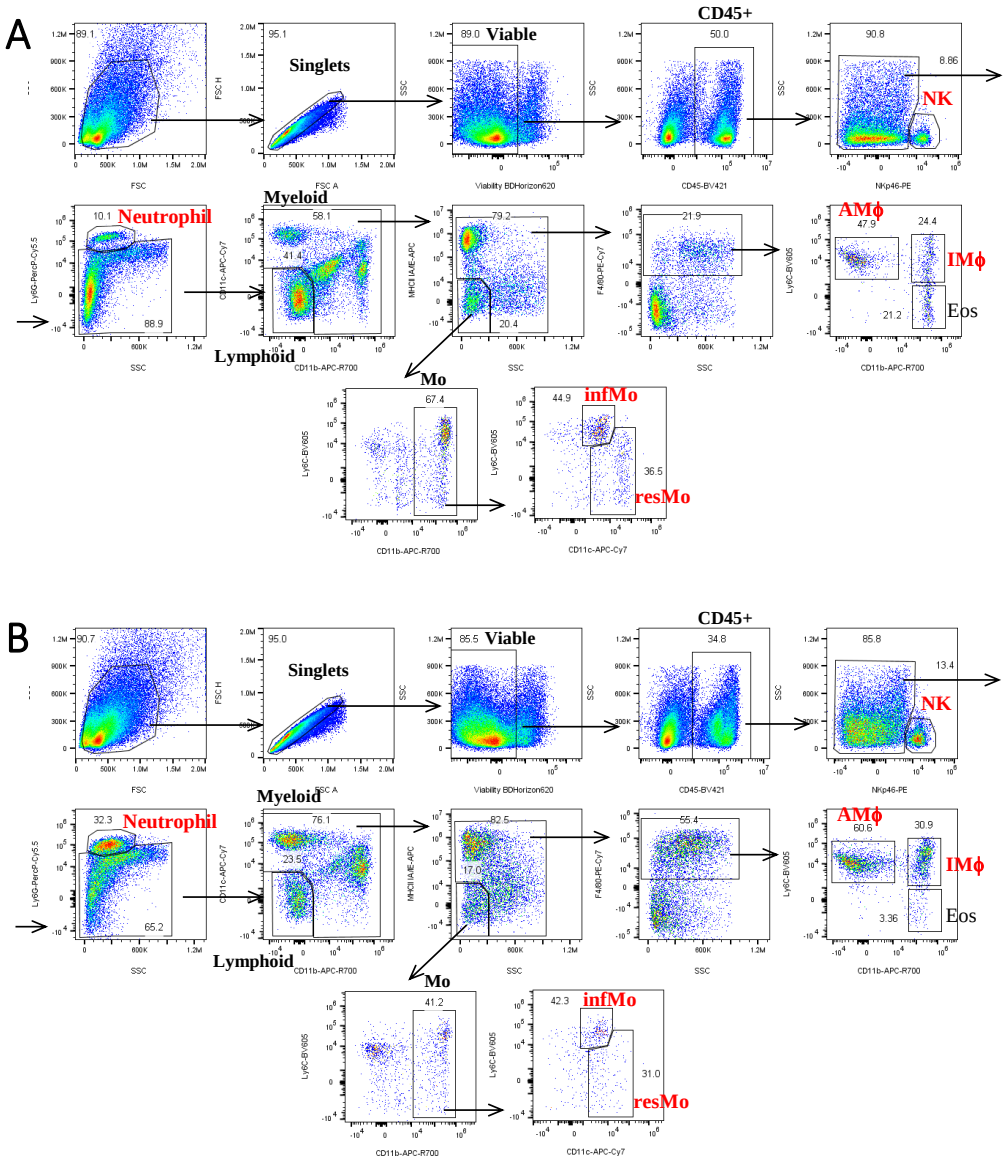


**Supplemental Figure S3: Gating strategy to identify myeloid-cell subsets in the lungs.** Single-cells suspension were prepared from lungs of isotype control-injected mice (**A**) or anti-CD3-injected mice (**B**). After the exclusion of debris, doublets and dead cells, immune cells were identified by CD45 staining. A sequential gating strategy was first used to identify populations expressing specific markers: natural killer (NK) cells (NKp46$^{+}$), neutrophils (Ly6G$^{+}$). Identification of populations with overlapping expression patterns was done as followed: lymphoid cells, CD11c$^{-}$CD11b$^{-}$; myeloid cells, CD11c$^{pos}$CD11b$^{pos}$; monocytes, CD11b$^{+}$CD11c$^{+}$MHCII$^{-/low}$; macrophage, CD11b$^{pos}$CD11c$^{pos}$F4/80$^{pos}$MHCII$^{pos}$. Using Ly6c marker, distinction between inflammatory vs resident monocytes was done, Ly6c$^{high}$ and Ly6c$^{-/low}$ respectively. Alveolar macrophages (AMϕ) were characterized as CD11b$^{-}$Ly6C$^{high}$ population, and interstitial macrophages (IMϕ) were dissociated respectively as Ly6C$^{low}$CD11b$^{+}$ and Ly6C$^{high}$CD11b$^{+}$. Definition of abbreviations: NK, natural killer; Eos, eosinophil; AMϕ, alveolar macrophages; IMϕ, interstitial macrophages; Mo, monocytes; infMo, inflammatory monocytes; resMo, resident monocytes; MHCII, major histocompatibility complex class II; FSC, forward scatter; SSC, side scatter.

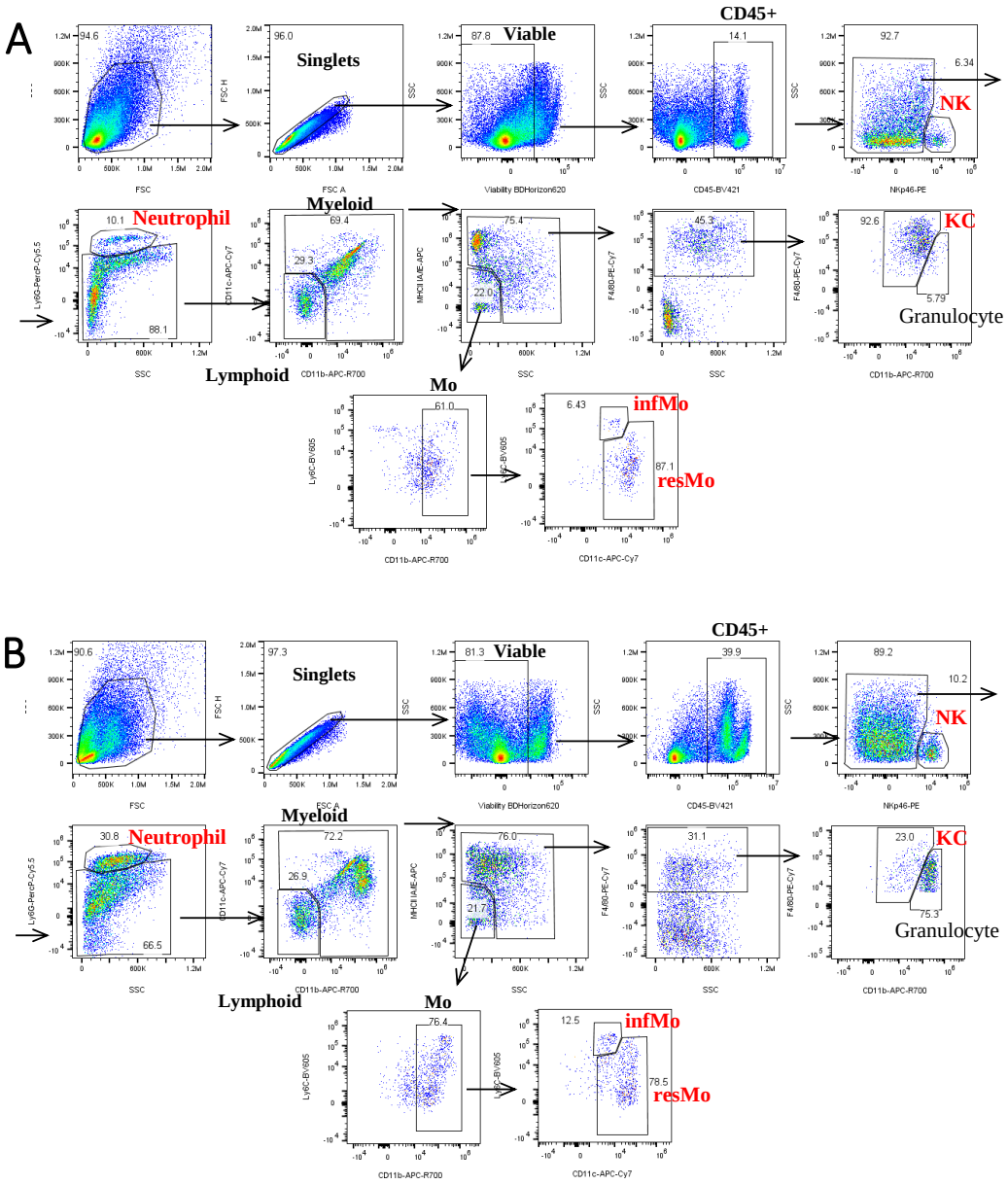


**Supplemental Figure S4: Gating strategy to identify myeloid-cell subsets in the liver.** Single-cells suspension were prepared from liver of isotype control-injected mice livers (**A**) or anti-CD3-injected mice livers (**B**). After the exclusion of debris, doublets and dead cells, immune cells were identified by CD45 staining. A sequential gating strategy was first used to identify populations expressing specific markers: natural killer (NK) cells (NKp46$^{+}$), neutrophils (Ly6G$^{+}$). Identification of populations with overlapping expression patterns was done as followed: lymphoid cells, CD11c$^{-}$CD11b$^{-}$; myeloid cells, CD11c$^{pos}$CD11b$^{pos}$; monocytes, CD11b$^{+}$CD11c$^{+}$MHCII$^{-/low}$; macrophage, CD11b$^{pos}$CD11c$^{pos}$F4/80$^{pos}$MHCII$^{pos}$. Using Ly6c marker, distinction between inflammatory vs resident monocytes was done; Ly6c$^{high}$ and Ly6c$^{-/low}$ respectively. Kupffer cell macrophages (KC) CD11b$^{low}$ and granulocytes CD11b$^{high}$, were discriminated according CD11b expression. Definition of abbreviations: NK, natural killer; infMo, inflammatory monocytes; resMo, resident monocytes; KC, Kupffer cell; MHCII, major histocompatibility complex class II; FSC, forward scatter; SSC, side scatter.

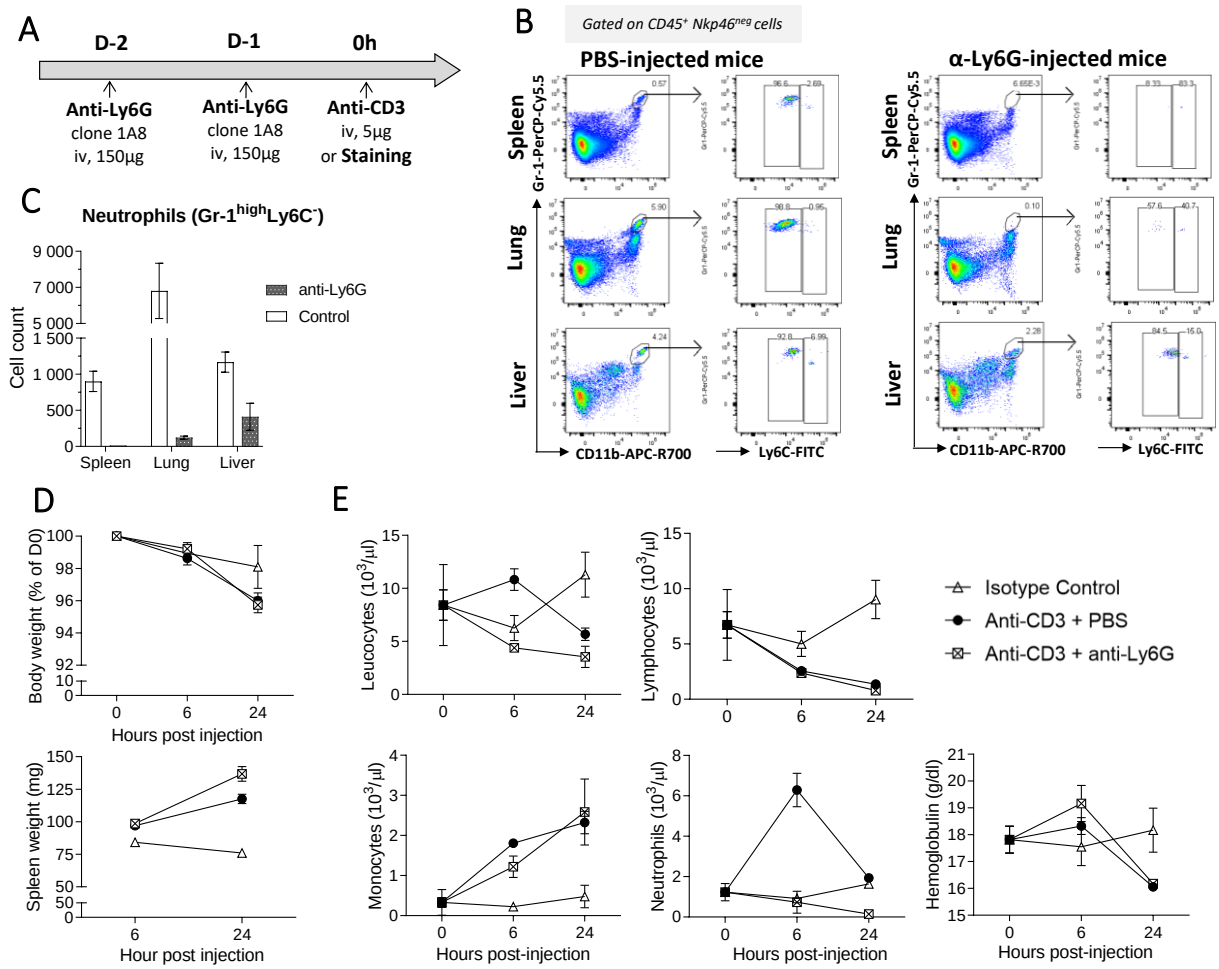


**Supplemental Figure S5: Reduced neutrophils number does not help to manage CRS in anti-Ly6G mAb treated mice**. PBS or anti-Ly6G mAb (BioXCell) treated-mice were i.v. injected with 5 µg of anti-CD3 as detailed in **A**. (**B**-**C**) FACS plots and scatter plots show complete or partial neutrophils depletion in anti-Ly6G mAb treated mice in comparison to BALB/c mice, in the spleen, lung and liver. (**D**) Body and spleen weight were recorded. (**E**). Blood cell count was done using the Procytes DX, IDEXX. N=5 from N = 1 experience. Data are displayed as mean ± SEM.

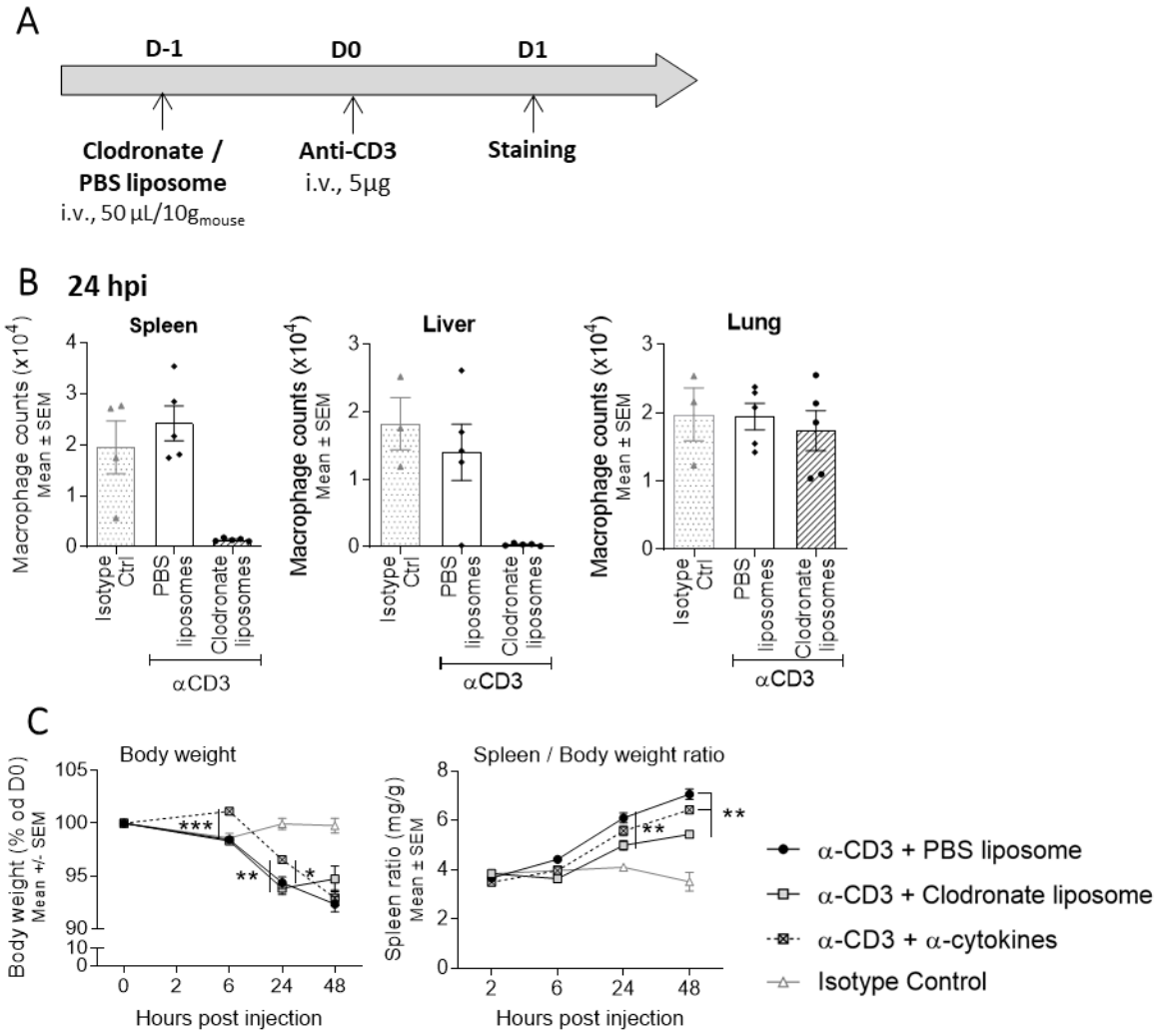


**Supplemental Figure S6: Reduced phagocytic cells number does not help to manage anti-CD3-induced CRS in mice.** Mice were treated with wither PBS liposome or clodronate liposome before being intravenously injected with 5µg of anti-CD3 as detailed in **A**. (**B**) Macrophages in the spleen, liver and lung. (**C**) Body and spleen weight follow up. n=4-6 mice per time point, from a single experiment. **P*<0.05, ***P*<0.01, ****P*<0.001 as determined by Mann–Whitney U t-test between PBS vs clodronate-treated mice. Data are displayed as mean ± SEM.

# CHAPTER III: CAR T CELL MOUSE MODEL

The anti-CD3 model of CRS relies on robust T cell activation *in vivo*, resulting in a sharp and severe cytokine storm. The goal above was to understand if this acute model of *in vivo* T cell activation reflected CRS typically seen in the context of infectious diseases, for example, consequent to Corona, Ebola and Lassa virus. Here, the aim was to develop a syngeneic mouse model to investigate mechanisms of CRS following CAR-T cell therapy.

Unfortunately, CRS is not uncommon in patients treated with CAR T cell therapy, leading to severe neurotoxicity in some cases. Almost all preclinical studies to dissect CAR T cell-induced CRS have been performed in 'humanized' mouse models[195,196,281-283]. While offering valuable insight, the limitation has been that these models do not evaluate disease progression in the context of a fully competent immune system, mainly due to the inability for complete differentiation of certain human hematopoietic cell lineages in mice[294]. As such, this work describes the development and use of a syngeneic mouse model of CAR T cell-induced CRS.

## 1 MATERIEL AND METHODS

### 1.1 SYNGENEIC A20 B CELL-LYMPHOMA MOUSE MODEL

#### 1.1.1 A20, mouse B lymphoma cells

A20 cells (B lymphoma cells derived from BALB/c) cells were obtained from ATCC (Manassas, VA) and cultured in RPMI 1640 supplemented with 10 % heat-inactivated fetal bovine serum, 2 mM L-glutamine, 10 mM 4-(2-hydroxyethyl)-1-piperazineethanesulfonic acid (HEPES), 1 mM sodium pyruvate, 2.6 g/l glucose and 50 µM 2-mercaptoethanol (all from Sigma, St Louis, MO). Cells were cultured at 37°C and 5 % $CO_2$.

#### 1.1.2 A20-Luciferase-mCherry generation

A20 cells were genetically modified to express luciferase, an enzyme that catalyzes the bioluminescence reaction in the presence of a luciferin, and mCherry. A20-Luciferase-mCherry (herein called A20-Luc) were derived from original A20 cells by targeting the Rosa 26 locus using clustered regularly interspaced short palindromic repeats (CRISPR)/Cas9 technology. The guide RNA sequence gRNA-Rosa26: 5' CGCTTCCTGCCACGTTGCGC 3' was inserted into the GeneArt CRISPR Nuclease Vector with OFP from Invitrogen (Figure 18A). Luciferase-IRES-mCherry DNA sequence was inserted into pEAK8 plasmid (Figure

18B), flanked by the two homology arms (see Annex 1). Nuclease and donor DNA vectors were transferred by electroporation using Gene Pulser MXcell™ Electroporation System (Bio-Rad, Hercules, CA). Cells were then let for recovery and growth for 2 weeks. According to mCherry expression, clones were sorted using the S3e™ Cell Sorter (Bio-Rad) and stability was studied for up to 2 months. *In vitro* analysis of bioluminescence for each clone was assessed before *in vivo* testing of engraftment capability.

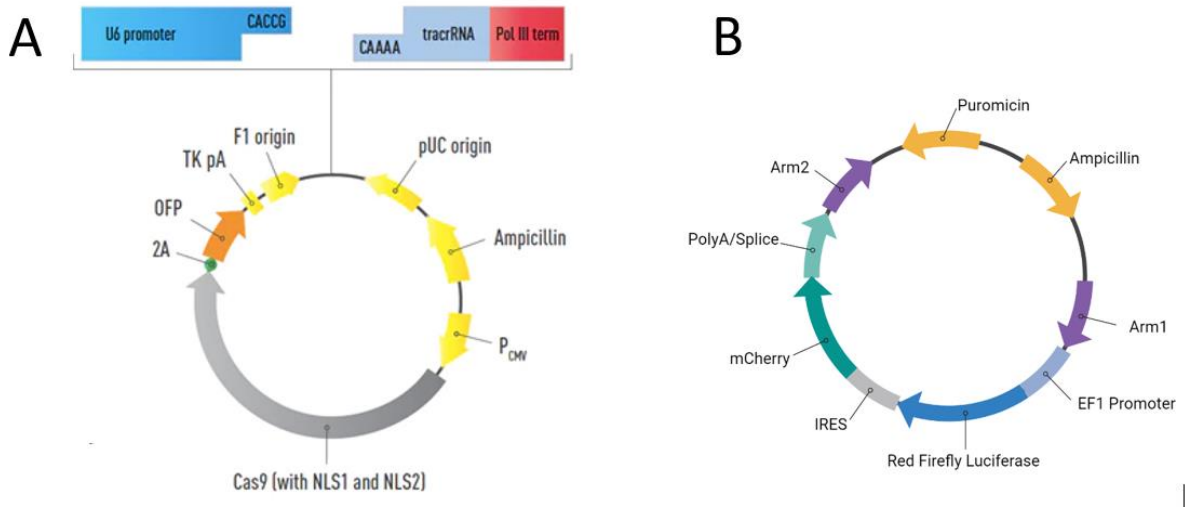


**Figure 18: Vectors used for genetically modified A20 cells.** (A) GeneArt CRISPR Nuclease Vectors. *Adapted from www.thermofisher.com.* (B) PEAK8 donor DNA vector containing the DNA sequence of Luciferase-IRES-mCherry.

### 1.1.3 Mice

All animal procedures were performed in accordance with the Swiss Veterinary Office guidelines and as authorized by the Cantonal Veterinary Office. Studies were conducted with six- to eight-week-old female BALB/cByJ, obtained from Charles River Laboratories (Saint-Germain-Nuelles, France).

### 1.1.4 Syngeneic mouse model of A20 B-cell lymphoma

One day prior to A20-Luc engraftment, mice were pre-conditioned with an intravenous injection of 150 mg/kg of Cyclophosphamide (Sandoz, Germany). A20-Luc were washed twice and diluted into sterile PBS before i.v. injecting $0.5x10^6$ cells per mouse. Every day of BLI acquisition, mice were intraperitoneally (i.p.) injected with 3 mg XenoLight D-Luciferin (PerkinElmer AG, Switzerland) and, anesthetized with 3 % isoflurane (Verflurane®, Virbac, France) 5 minutes prior to imaging. Bioluminescence signal was converted to photon/s (p/s). Mice were culled by $CO_2$ inhalation if weight loss was > 15% or if they developed symptoms such as swollen distended abdomens, laboured breathing, tail or leg paralysis or other signs of ill-health.

## 1.2 MOUSE MODEL OF CAR T CELL

### 1.2.1 Design and construction of the CARs

The DNA sequence of the 1D3-28z CAR construct has been described[311] and the sequence available at GenBank under accession number HM754222. The sequence encodes the following components in-frame from the 5' to the 3': the signal sequence of the single-chain variable fragment (scFv) of the 1D3 antibody (that specifically recognizes murine CD19), a portion of the murine CD28 molecule from amino-acids IEFMY to the 3' terminus, and the cytoplasmic region of the murine CD3-ζ molecule from amino-acids RAKFS to the 3' terminus. Kochenderfer *et al.* changed both tyrosine (Y) residues in the first and third ITAMs to phenylalanine (F) with the aim to decrease T-cell apoptosis and toxicity[311]. Here, the wild-type CD3-ζ DNA sequence was restored (Figure 19). This DNA sequence was ordered for synthesis by Eurofins Genomics (Germany), then amplified and flanked by restriction enzymes sites by PCR with the following primers:

P1: Fwd_HindIII-BglII-*Kozak*-1D3: 5' GCCGGAAGCTTAGATCT*GCCGCCACC*ATGGGTGTCCCTACCCAG 3'

P2: Rev-EcoRI-*Stop*-CD3z: 5'CGCCGAATTCA*TTA*TCTGGGGGCCAGGGTC 3'

PCR products were loaded on 1.2% agarose gel (Invitrogen) and DNA from agarose gel band were purified using QIAquick Gel Extraction Kit (Quiagen, Germany) and cloned in the PCR4TOPO vector (Invitrogen, Basel, Switzerland). The construct was then sub-cloned into the pMIG retroviral backbone (kindly provided by the Doron's lab from the University of Geneva) to form the pMIG-1D3-28z retroviral vector.

```
MGVPTQLLGLLLLWITDAICDIQMTQSPASLSTSLGETVTIQCQASEDIYSGLAWYQQKPGKSPQLLIYGASDLQDG
Peptide signal                          1D3-VL
VPSRFSGSGSGTQYSLKITSMQTEDEGVYFCQQGLTYPRTFGGGTKLELKGGGGSGGGGSGGGGSEVQLQQSGAELV
                                                      linker
RPGTSVKLSCKVSGDTITFYYMHFVKQRPGQGLEWIGRIDPEDESTKYSEKFKNKATLTADTSSNTAYLKLSSLTSE
        1D3-VH
DTATYFCIYGGYYFDYWGQGVMVTVSSIEFMYPPPYLDNERSNGTIIHIKEKHLCHTQSSPKLFWALVVVAGVLFCY
                                mCD28 extracellular                     mCD28
GLLVTVALCVIWTNSRRNRGGQSDYMNMTPRRPGLTRKPYQPYAPARDFAAYRPRAKFSRSAETAANLQDPNQLYNE
Transmembranaire       mCD28 cytoplasmic                                 itam1
LNLGRREEFDVLEKKRARDPEMGGKQQRRRNPQEGVYNALQKDKMAEAYSEIGTKGERRRGKGHDGLYQGLSTATKD
               mCD3zeta        itam2                          itam3
TFDALHMQTLAPR
```

**Figure 19: Annotated amino acid sequence of the 1D3-28z CAR construct.** The two tyrosine residues of the 1st and 3rd itams changed in phenylalanines in Kochenderfer *et al.* are highlighted in grey.

A second recombinant retroviral vector, pMIG-1D3-BBz, was designed consisting of the same pMIG-1D3-28z DNA sequence, except that the CD28 cytoplasmic domain was exchanged for the 4-1BB cytoplasmic domain from KWIRKK to the 3' end[308]. A third vector was also created, pMIG-1D3-28-BBz, and composed of the same DNA of the pMIG-1D3-28z, plus the part of the 4-1BB cytoplasmic domain sequence inserted in frame between the CD28 cytoplasmic domain and CD3-ζ part. Fragments encoding the 4-1BB flanked with the appropriated DNA sequences were generated using an overlapping PCR method (Figure 20) with the following primers:

P3: Fwd_$CD28_{TM}$-$BB_{Cyto}$: 5'CAGTGGCCCTGTGCGTGATCTGGACCAAATGGATCAGGAAAAAATTC3'

P3: Rev_$CD28_{TM}$-$BB_{Cyto}$ : 5'GGGGAATTTTTTCCTGATCCATTTGGGTCTGTAGGCGGCGAAGTCTCTG3'

P4: Fwd_$CD28_{Cyto}$-$BB_{Cyto}$: 5'CAGAGACTTCGCCGCCTACAGACCCAAATGGATCAGGAAAAAATTCCCC3'

P4: Rev_$CD28_{Cyto}$-$BB_{Cyto}$: 5'GGGGAATTTTTTCCTGATCCATTTGGGTCTGTAGGCGGCGAAGTCTCTG3'

P5: Fwd_$BB_{Cyto}$-CD3z: 5'GAAGGAGGAGGAGGAGGCTATGAGCTGAGAGCCAAGTTCAGCAGATCCGCCGAGAC 3'

P5: Fwd_$BB_{Cyto}$-CD3z: 5'GTCTCGGCGGATCTGCTGAACTTGGCTCTCAGCTCATAGCCTCCTCCTCCTCCTTC 3'

Amplification of the retroviral vectors was done by transformation of STBL3 *E. coli* bacteria (ThermoFischer Scientific) followed by growth at 30°C. All constructs were verified by DNA sequencing to ensure the absence of any undesirable mutations (Fasteris, Geneva, Switzerland).

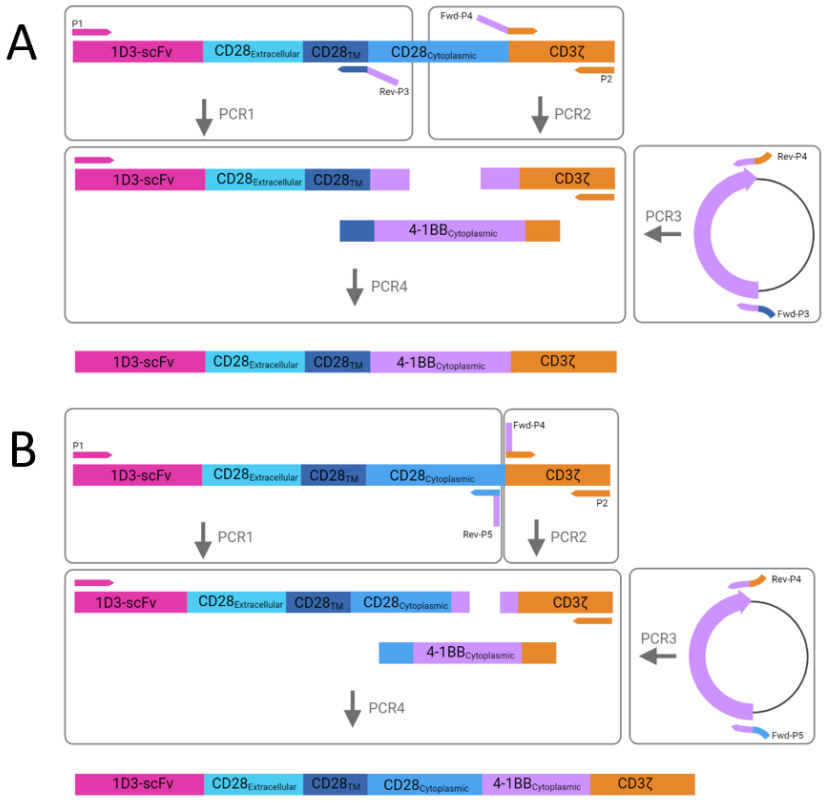


**Figure 20: Overlapping PCR method to generate 1D3-BBz (A) and 1D3-28-BBz (B) DNA sequence.**

### 1.2.2 Cells and Culture Media

Mouse T cells were purified from splenocytes of naïve BALB/cByJ mice using EasySep™ Mouse T Cell Isolation Kit (StemCell Technologies) and cultured either in complete Gibco medium, composed of Gibco™ AIM V® Medium (Invitrogen; Waltham, MA) supplemented with 50 µM 2-mercaptoethanol, or in complete RPMI medium, composed of RPMI 1640 supplemented with 10 % heat-inactivated fetal bovine serum, 2 mM L-glutamine, 10 mM 4-(2-hydroxyethyl)-1-piperazineethanesulfonic acid (HEPES), 1 mM sodium pyruvate and 50 µM 2-mercaptoethanol (all from Sigma-Aldrich, St Louis, MO, except mentioned). Media was supplemented with either 100 UI/mL of recombinant murine IL-2 (Peprotech, Rocky Hill, NJ) or 10 ng/mL of recombinant murine IL-7 (Peprotech) and 5ng/mL of recombinant murine IL-15 (Peprotech), as indicated. PEAK cells (Edge Biosystems, Gaithersburg, MD) were maintained in DMEM, 10% FBS, and 2 mM L-glutamine. The wild-type (WT) A20 cells and in-house generated A20-Luc cells were cultured in RPMI 1640 supplemented with 10 % FBS, 2 mM L-glutamine, 10 mM HEPES, 1 mM sodium pyruvate, 2.6 g/l glucose and 50 µM 2-mercaptoethanol. Cells were cultured at 37°C and 5% $CO_2$.

### 1.2.3 Retrovirus Production

PEAK cells (Edge Biosystems, Gaithersburg, MD) were plated at a density of $8\times10^6$ cells per T175 flask. The day after, cells were transfected with a mix of DMEM containing Lipofectamine 2 000 (Invitrogen) and 40 µg of DNA composed 1:1 (w/w) of either the pMIG-1D3-28z plasmid, the pMIG-1D3-BBz plasmid, or the pMIG-1D3-28-BBz plasmid and a pCl-Eco plasmid encoding the retroviral envelope protein. The transfected cells were incubated at 37°C, 5% $CO_2$ for 48 hours. Supernatant containing retroviruses was collected, passed through a 0.45-µm filter (MerckMillipore; Burlington, MA) and concentrated 4-folds with Amicon® Centrifugal Filter Unit (Merck Millipore) before immediate use.

### 1.2.4 Mouse T Cell Transduction

Purified mouse T cells were activated for 18h at 37°C using anti-CD3 and anti-CD28 mAbs (BD Biosciences, Franklin Lakes, NJ) at 1 µg/mL, in a 96 well-plate pre-coated with 5 µg of goat anti-hamster IgG (Jackson ImmunoResearch, West Grove, PA). Activated T cells were transduced by spinoculation at 2 000 rpm at 37°C for 1 hour using freshly produced concentrated retroviral supernatants supplemented with 8 µg/mL polybrene (Sigma-Aldrich) and 50 µM of β-Mercaptoethanol. The retroviral supernatant was removed 4 hours later and replaced with fresh T cell medium and let for recovery 24 hours before being amplified in T-flask. Cell viability was followed using the ViCell cell count (Beckman).

### 1.2.5 Cytotoxicity Assay

The CD19-CAR T cells or empty vector transduced T cells (control CAR T) were co-cultured overnight with A20-Luciferase cells, at indicated effector/target ratios (E:T, T = $1\times10^4$ A20-Luciferase cells) in a 96-well plate. Following co-culture, plates were centrifuged at 500 g for 5 minutes, supernatant collected for protein quantification analysis, and cells were resuspended in PBS with 300 µg/ml of XenoLight D-Luciferin. The bioluminescence was acquired 5 minutes later using SpectraMax-i3x (Molecular Devices, San Jose, CA).

### 1.2.6 Mice

All animal procedures were performed in accordance with the Swiss Veterinary Office guidelines and authorized by the Cantonal Veterinary Office. Studies were conducted with six- to eight-week-old female BALB/cByJ, mice obtained from Charles River Laboratories (Saint-Germain-Nuelles, France). The animals were reared under conventional conditions temperature-controlled room (25 ± 2°C) under a 12 hours light/dark cycle.

### 1.2.7 *In vivo* mouse model

Mice were i.v. treated with 150 mg/kg of cyclophosphamide (CTX) a day before i.v. engraftement of $5x10^5$ A20-Luc or A20-WT B cell lymphoma cells. 8-9 days post-engraftment, $8\text{-}12x10^6$ T cells were i.v. injected, corresponding to $5\text{-}7x10^6$ CAR T cells depending on transduction efficacy. One day prior to CAR T cell infusion, mice were pre-conditioned with a single i.p. administration of CTX. Tumour burden or *in vivo* T-Luc expansion was monitored by i.p. injection of 3 mg XenoLight D-Luciferin and an *in vivo* imaging system.

Anti-IFN-γ (Rat IgG1, clone XMG1.2) neutralizing mAb was obtained from BioXCell (Lebanon, NH, USA) and anti-IL6R rat IgG1 mAbs, clone 2B10 and $25F10^{310}$, were produced in-house. Neutralizing mAbs were injected i.v. at the indicated doses, simultaneously with the CAR T cell infusion. Two additional anti-cytokine mAb doses were injected 2-days and 4- or 5-days post CAR T cell infusion.

At indicated time points, mice were euthanized by $CO_2$ inhalation. Blood cell count was performed with a ProCyte Dx analyser (IDEXX Laboratories, Inc., ME, USA). Samples of spleen, lung and liver tissue were stored in RNA later (Sigma-Aldrich, Saint-Louis, MO, USA) for gene expression analysis. Whole-liver and -spleen were harvested for immune cell infiltration analysis.

### 1.2.8 Cytokine quantification

The cytokines and chemokines concentration in supernatant from cytotoxicity assay was measured using MILLIPLEX MAP multiplex immunodetection kits (Merck Millipore, Burlington, MA, USA) and analysed on the Luminex® 200™ immunoassay analyser (Luminex®, TX, USA), according to manufacturer's instructions.

The plasma concentrations of cytokines and chemokines were measured using either MILLIPLEX MAP multiplex immunodetection kits or MSD U-PLEX assay kits and analysed respectively on the Luminex® 200™ or MESO SECTOR S 600 (Meso Scale Discovery, MSD; Kenilworth, NJ) immunoassay analyser, according to manufacturer's instructions. Plasma level of Angiopoetin-2 (Ang-2) and SAA were quantified with mouse Ang-2 and mouse SAA ELISA Kit (Abcam, Cambridge, UK), according to manufacturer's instructions.

### 1.2.9 Gene expression

**Table 7: Primer sequences for qPCR analysis.**

| | **Sequence primers (5'-3')** | |
|---|---|---|
| | **Forward** | **Reverse** |
| β-actin | AGCCTTCCTTCTTGGGTATGG | CAACGTCACACTTCATGATGGAAT |
| CXCL1 | CATGCAGGCAGCACTCAGA | ATCCATGGTGGCACACAGACT |
| CXCL9 | AGCCTTCCTTCTTGGGTATGG | AGGTCTTTGAGGGATTTGTAGTGG |
| CXCL10 | GACGGTCCGCTGCAACTG | GCTTCCCTATGGCCCTCATT |
| IFN-γ | CAACAGCAAGGCGAAAAAGG | CCTGTGGGTTGTTGACCTCAA |
| IL-2 | AACTGTTGTAAAACTAAAGGGCTCTGA | CACCACAGTTGCTGACTCATCA |
| IL-6 | TCGGAGGCTTAATTACACATGTTC | TGCCATTGCACAACTCTTTTCT |
| IL-10 | TTTGAATTCCCTGGGTGAGAA | GCTCCACTGCCTTGCTCTTATT |
| SAA | GCTGAGAAAATCAGTGATGGAAGA | TCAGCAATGGTGTCCTCATGTC |
| TNF-α | GCCACCACGCTCTTCTGTCT | GGTCTGGGCCATAGAACTGATG |
| MCP-1 | GCAGCAGGTGTCCCAAAGAA | GGGTCAGCACAGACCTCTCTCT |
| Ang-1 | CATTCTTCGCTGCCATTCTG | GCACATTGCCCATGTTGAATC |
| Ang-2 | TTAGCACAAAGGATTCGGACAAT | TTTTGTGGGTAGTACTGTCCATTCA |
| VEGF | GGAGATCCTTCGAGGAGCACTT | GGCGATTTAGCAGCAGATATAAGAA |

Spleen, liver and lung RNA isolated using RNeasy mini-Kit (Qiagen) was reverse transcribed using High-Capacity cDNA Reverse Transcription kit (Applied Biosystems®, Foster City, CAL, USA). Quantitative PCR (qPCR) was performed using SYBR® Green I Master Mix (Roche; Mannheim, Germany) on the LightCycler® 480 System from Roche. The ΔΔCt method was used to calculate the relative gene expression levels (RQ) with β-actin gene as housekeeping gene. The primer sequences are listed in Table 7.

### 1.2.10 Flow cytometry

*In vitro analysis - CAR detection and binding assay*

Surface expression of CAR on transduced T cells was detected with Alexa Fluor 687 (AF687) labelled goat anti-rat-F(ab)$_2$ antibodies (Jackson Immunoresearch, West Grove, PA). Briefly, transduced T cells were washed and resuspended in FACs buffer (PBS plus 1% BSA). Cells were then incubated with Mouse BD Fc Block™ (BD Biosciences; San Jose, CA). Surface staining was directly performed in the dark for 20 min at 4°C.

Transduced T cells were incubated in FACS buffer with a recombinant murine CD19 His-tagged protein (Creative Biomart; Shirley, NY) for 10 minutes at 4°C. Fc receptors were blocked as previously described and T cells-CD19-His protein mix was stained with AF647 Penta-His (dilution 1/400, Qiagen) for 20 minutes at 4°C. Cells were then washed twice with FACS buffer and acquired on the CytoFLEX S flow cytometer (Beckman Coulter). Data analyses were performed using FlowJo software (Tree Star Inc., OR, USA).

*Ex-vivo analysis - Organ single-cell suspension preparation and analysis*

Single-cell suspension of liver was performed using the liver dissociation kit from Miltenyi Biotec and the gentleMACS™ Dissociator (Miltenyi Biotec) according to the manufacturer's protocol. Single-cell suspension from spleen was prepared by enzymatic digestion in collagenase IV (Gibco) and DNase I (Sigma-Aldrich) for 20 min at 37°C, followed by mechanical digestion with the gentleMACS™ Dissociator. Red blood cell lysis was performed using ACK buffer (Ammonium-Chloride-Potassium). Cell suspensions were filtered through a 70 µM Nylon filter (BD Falcon™) and counted using a cell viability analyser (Vi-CELL).

After cells were counted, 2x10$^6$ cells per sample were stained with Fixable Viability Dye eFluor™ 780 (eBioscience™) according to manufacturer's instructions. Cells were then incubated with Mouse BD Fc Block™ and surface staining was directly performed in the dark for 20 min at 4°C (see Table 8 for

details). Cells were then washed twice with FACS buffer and acquired on the CytoFLEX S flow cytometer (Beckman Coulter). Data analysis were performed using FlowJo software.

**Table 8: Antibodies used for immunophenotyping analysis.**

| Fluorochrome | Marker | Clone | Manufacturer |
|---|---|---|---|
| PerCP-Cy5.5 | CD69 | H1.2F3 | BD Biosciences |
| APC | CD8 | QA17A07 | Biolegend |
| APC-R700 | CD25 | PC61 | BD Biosciences |
| BV421 | CD45 | 30-F11 | BD Biosciences |
| BV510 | CD4 | RM4-5 | Biolegend |
| BV711 | CD62L | MEL-14 | Biolegend |
| PE | CD19 | 1D3 | BD Biosciences |
| PE-Cy5 | CD3 | 145-2C11 | Biolegend |
| PE-Cy7 | CD44 | IM7 | Invitrogen |
| PerCP-Cy5.5 | Ly6g | 1A8 | BD Biosciences |
| APC | MHCII IA/IE | M5/114.15.2 | Biolegend |
| APC-Cy7 | CD11c | N418 | Biolegend |
| BV421 | CD45 | 30-F11 | BD Biosciences |
| BV605 | Ly6c | HK1.4 | Biolegend |
| BV711 | CD64 | X54-5/7.1 | Biolegend |
| PE | NKp46 | 29A1.4 | eBioscience |
| PE-Cy5 | CD11c | N418 | Biolegend |
| PE-Cy7 | F4/80 | BM8 | invitrogen |

*Ex-vivo analysis - Detection of mouse anti-CAR antibodies*

Mouse bearing A20-Luc lymphoma and treated with 30 mg/kg of CTX plus Control or CD19-CAR T cells were euthanised and plasma was collected and stored at -20°C. Freshly produced Control or CAR T cells were incubated for 1 hour at RT with 1/100 diluted sera. Samples were then washed twice with FACS buffer and incubated for 30 minutes at RT in the dark with an AF647 Goat Anti-Mouse IgG (sub-classes 1+2a+2b+3), Fcγ Fragment Specific (Jackson ImmunoResearch), 1/400 diluted. Samples were washed twice with FACS buffer and acquired on the CytoFLEX S flow cytometer.

### 1.2.11 Statistics

GraphPad Prism (GraphPad Software, CA, USA) was used for all statistical analysis. The unpaired t-test or unpaired non-parametric Mann–Whitney t-test were used for statistical comparison. p-value of $<0.05$ was considered significant.

# 2 RESULTS

## 2.1 ESTABLISHMENT OF A20 MURINE B LYMPHOMA MODEL LABELLED WITH LUCIFERASE

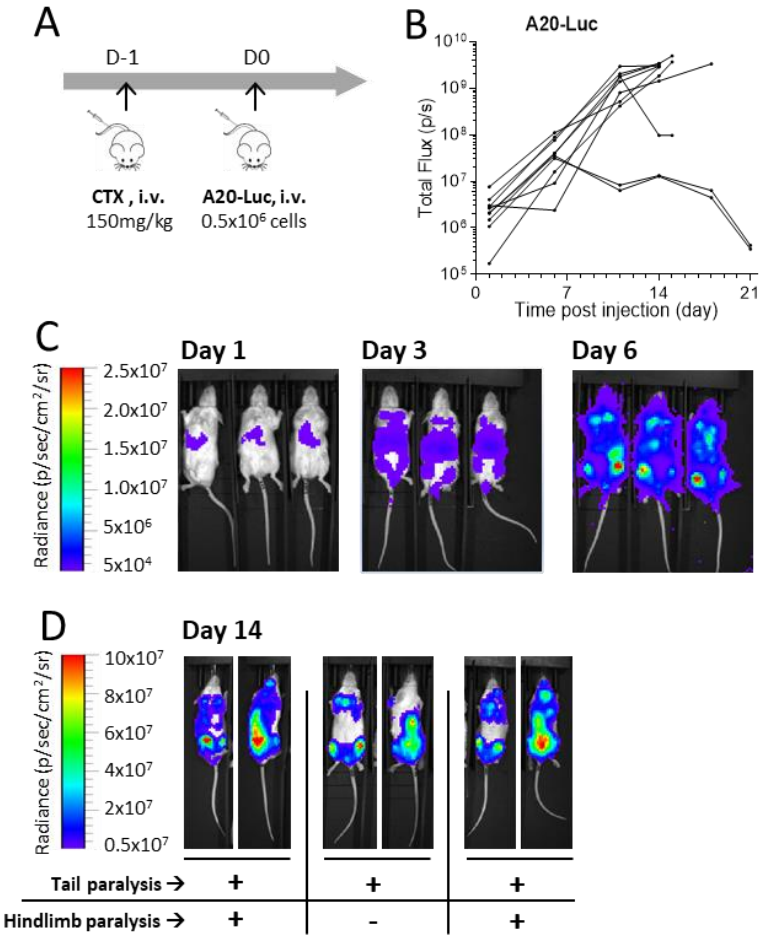


**Figure 21: *In vivo* engraftment of A20-Luc lymphoma cells.** (A) 0.5x10$^6$ A20-Luc cells were injected intravenously into BALB/c mice pre-conditioned with 150 mg/kg cyclophosphamide (CTX). (B) Quantification of tumour growth by measuring light emission from BALB/c mice. (C, D) Bioluminescence imaging of pre-conditioned mice i.v. injected with A20-Luc. The scale to the left of the images describes the color map for the photon count. (D) At day 14, mice were exposed on the ventral side first and immediately flipped over to image dorsal to pick up tumour masses on both sides of the bodies.

Several A20-Luc clones were selected and tested *in vivo* for engraftment capability without success. A20 cells are highly immunogenic by themselves, even free of genome-editing. Tolerance to A20-luc cells was challenging, decreasing the number of A20-Luc cells per injection has no impact (data not shown). The administration one day prior to tumour cell engraftment of immune-depleting agent allowed for successful tumour engraftment. A20-Luc clone A7 cells were injected intravenously into BALB/c

recipient mice pre-conditioned with cyclophosphamide (Figure 21A). Almost all recipient mice showed tumour engraftment (8 mice out of 10, 80%) (Figure 21B). One day after tumour injection, a bioluminescent signal was detectable from the lungs and, after 6 days, in spleen and lymph nodes (Figure 21C). An infiltration of lungs, lymph nodes, spinal cord and brain was observed in final disease stages (Figure 21D). As for mice bearing A20 wild type cells, clinical signs of disease included tail paralysis rapidly followed by hind-limb paralysis (Figure 21D).

## 2.2 *IN VITRO* EFFICACY OF CD19-CAR T CELL THERAPY

### *2.2.1* Comparison of murine CAR T cells having different costimulatory domains

Several CARs sharing the same structure except for the costimulatory domain were studied (Figure 22A). The first construct, 1D3-28z, was designed by Kochenderfer *et al.* to specifically recognize the murine CD19 and contained the costimulatory domain of CD28[311]. To investigate the impact of the 4-1BB costimulatory domain, a second CAR was designed, 1D3-BBz, in which the CD28 costimulatory part was exchanged for the 4-1BB costimulatory domain (Figure 22A). In addition, this kind of construct containing 4-1BB as the costimulatory domain was used by Chadwick *et al.* to study toxicity and neuroinflammation induced by CAR T-cells in a syngeneic mouse model of lymphoma[307]. A third-generation of CAR was also created, 1D3-28-BBz, in which the two costimulatory domains of CD28 and 4-1BB were expressed. All the retroviral vectors contained the DNA sequence of GFP in order to assess transduction efficacy (Figure 22A).

Whatever the retroviral vector, T cell transduction efficacy was over 60% as determined by GFP expression. If the transduction efficacy of vectors containing the first-generation of CAR (meaning, 1D3-28z or 1D3-BBz) was similar and around 75-80% of $GFP^+$ T cells, the CAR expression at the surface membrane was significantly different, over 60% and around 35% of $CAR^+$ T cells, respectively (Figure 22B). Interestingly, the percentage of $CAR^+$ T cells transduced with the second-generation of CAR was similar as the T cells transduced with the 1D3-BBz, despite the percentage of $GFP^+$ T cells being lower (Figure 22B).

The ability of the CAR to bind the murine CD19 was investigated by flow cytometry using recombinant murine CD19-His tagged protein (Figure 22C). All the T cells transduced with retroviral vectors containing CAR DNA sequence bound to the recombinant murine CD19 as expected, the 1D3-scFv being identical between the CAR constructs. The percentage of T cells bound to the murine CD19 was proportional to the $CAR^+$ T cells. Indeed, 1D3-28z transduced T cells shared the highest percentage of $CAR^+$ T cells (Figure 22B) and the highest binding capacity (Figure 22C). Nonetheless, despite same $CAR^+$

percentage of T cells, 1D3-BBz CAR T cells showed better binding to murine CD19 than 1D3-28-BBz CAR T cells (Figure 22C). While the different CAR T cell cultures showed difference regarding CAR expression and binding capacity, all the transduced T cells demonstrated strong and equivalent killing efficacy (Figure 22D). To investigate if one CAR construct would be more potent to induce cytokine release, cytokine production was quantified when transduced T cells were cultured with A20 cells (Figure 22D). Transduced T cell cultures exhibited robust levels of IFN-γ, TNF-α, GM-CSF, IL-10 and CXCL10 whatever the costimulatory domain of the CAR.

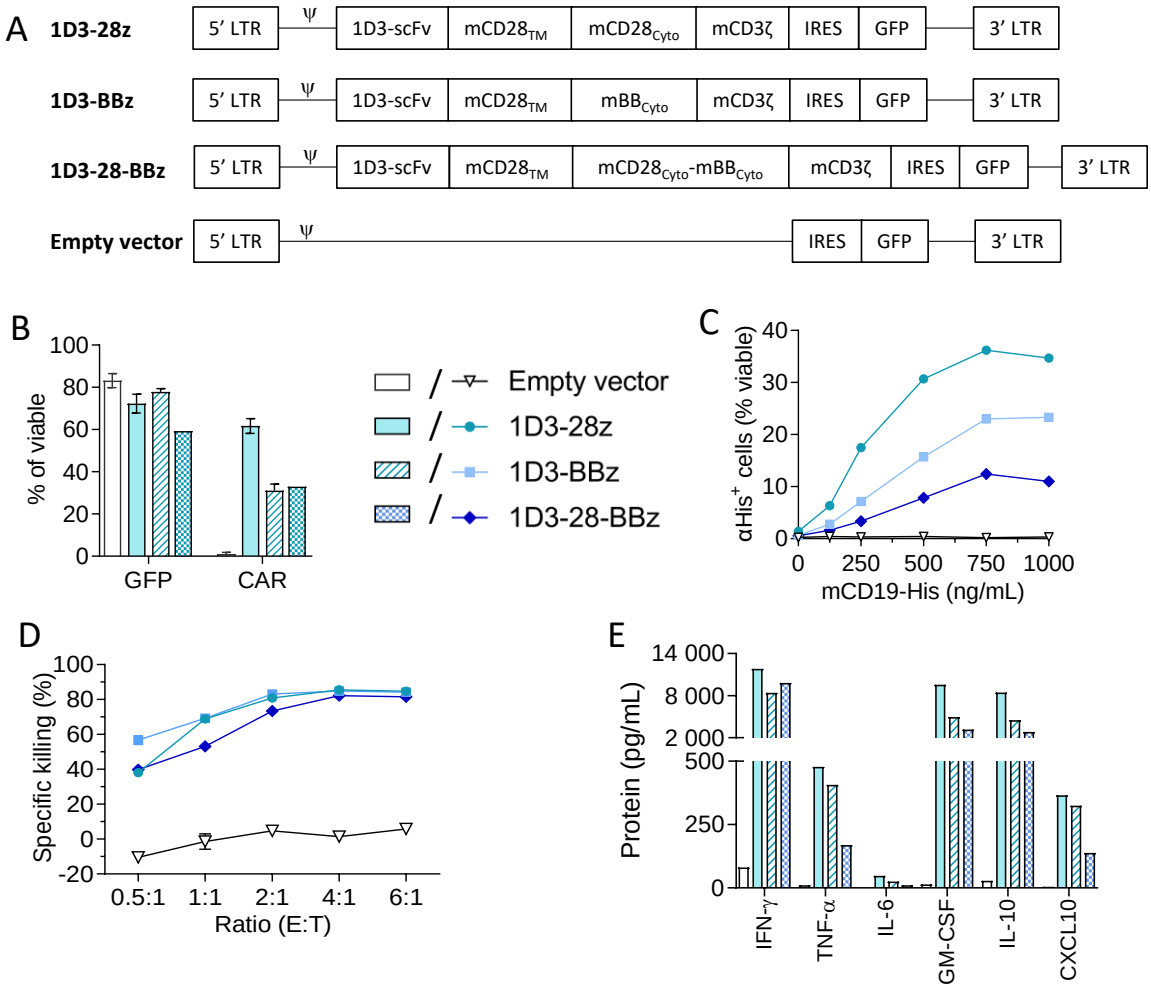


**Figure 22: In-house CD19-CAR constructs are differentially expressed but share same killing efficacy.** (A) Diagram of the DNA encoding the 1D3-28z, 1D3-BBz and 1D3-28-BBz CAR (ψ, retroviral packaging signal). T cells were purified from spleen, activated for 18 hours with anti-CD3/anti-CD28 antibodies and then transduced with retroviruses encoding the different CARs. Five days post transduction, (B) GFP and CAR expressions, as well as (C) the capability of the CD19-CARs to bind the murine CD19 protein were assessed by flow cytometry. The CAR T cells were co-cultured with A20-Luc cells at indicated E:T ratios. (D) Cytotoxicity was investigated 24 hours later by acquiring bioluminescence and (E) cytokines from the supernatant were quantified by Luminex. Data are representative of N=3 experiments, except for (E) N=1. Data are represented as mean ± SEM.

### 2.2.2 Complete RPMI medium is superior to complete Gibco medium for preserving CAR T cells population

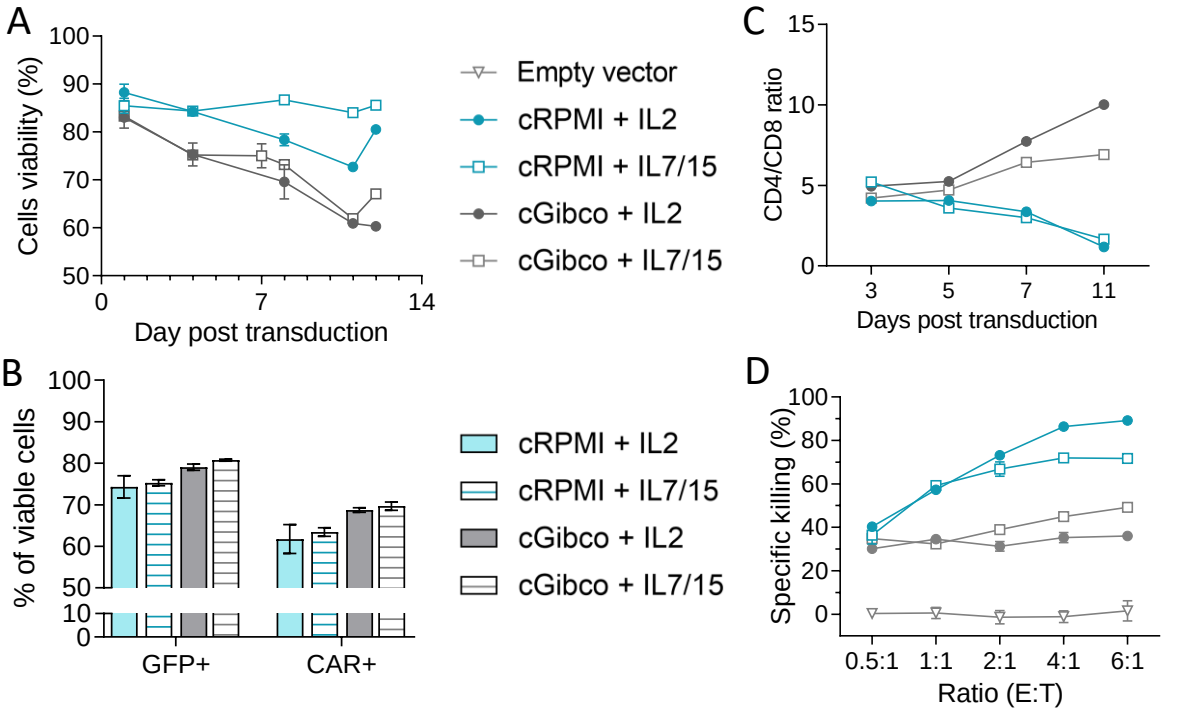


**Figure 23: Complete RPMI medium supplemented with IL-2 better preserved viability and cytotoxic activity of the CD19-CAR T cells.** T cells were purified from spleen and cultured either in complete RPMI or complete Gibco medium, supplemented with either IL-2 or IL-7 plus IL-15 cytokines. After 18 hours of activation, T cells were transduced with 1D3-28z retrovirus. (A) Viability of T cell cultures was followed for up to 12 days of culture, (B) GFP and CD19-CAR expression, and (C) CD4/CD8 ratio were investigated by flow cytometry. (D) CAR T cells from each culture condition were co-culture with A20-Luc cells at indicated E:T ratio. Cytotoxicity of the CAR T cells was assessed 24 hours later by quantifying the bioluminescence (triplicates). Data are representative of N=2 experiments. Data are represented as mean ± SEM.

Survival of CAR T cells in complete RPMI (cRPMI) medium was better compared to CAR T cells grown in cGibco medium, whatever the supplemented cytokine(s) (Figure 23A). Nonetheless, cGibco medium provided better transduction efficiency and CAR expression at the membrane (Figure 23B). Interestingly, culture medium impacted CD4/CD8 ratios: cRPMI favoured $CD8^+$ T cell proliferation whereas cGibco favoured $CD4^+$ T cell proliferation (Figure 23C). Most importantly, CAR T cell grown in cGibco medium demonstrated an impaired killing activity (Figure 23D). Globally, survival, CAR expression and CD4/CD8 ratio of CAR T cells in the presence of IL-7 plus IL-15 were similar with CAR T cells grown in the presence of IL-2. Although, when grown in cRPMI, the efficacy of CAR T cells in presence of IL-2 is better than CAR T cells grown with IL-7 plus IL-15, at highest E:T ratios (Figure 23D). Therefore, the cRPMI supplemented with IL-2 was selected for all the following experiments.

## 2.3 CRS INDUCED BY CD19-CAR T CELL IN A20-LYMPHOMA MODEL

### 2.3.1 Transient depletion of immune cell populations is required for optimal CAR-T cell mediated tumour control

*Long term survival of A20-lymphoma bearing mice treated with CD19-CAR T cells*

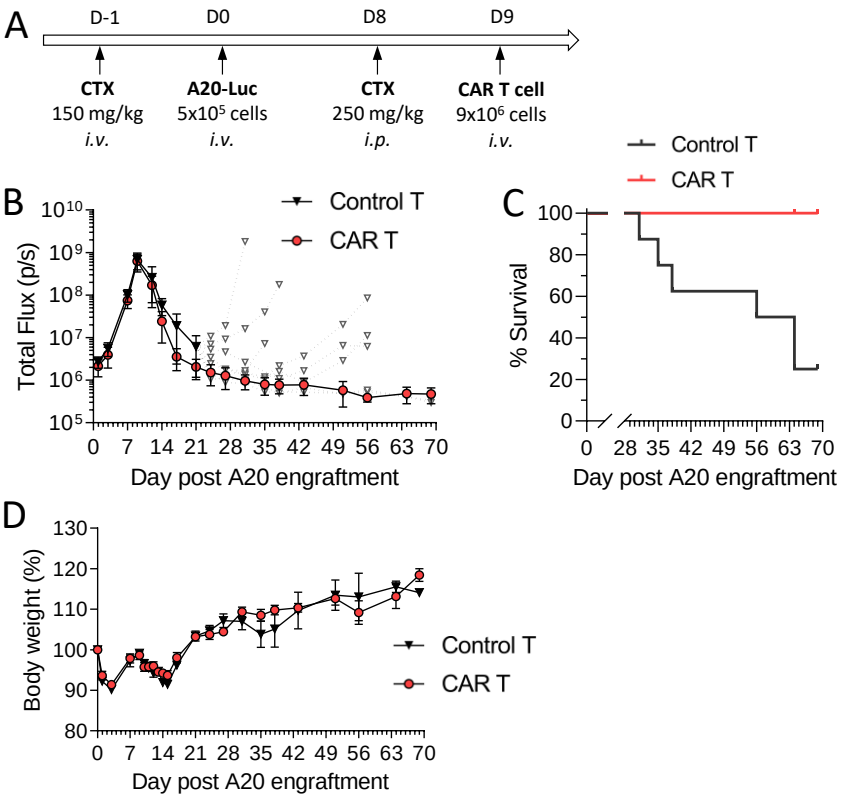


**Figure 24: CD19-CAR T cell therapy allowed long term survival.** (A) Mice were pre-conditioned with i.v. injection of CTX one day prior to A20-Luc lymphoma engraftment. Eight days later, mice were imaged, randomized, and received 250 mg/kg i.p. of CTX. The day after, mice were infused with either CD19-CAR T cells or Control-CAR T cells. (B) Mean of bioluminescence and (C) survival of mice with established A20-Luc lymphoma. After Day 21, individual bioluminescence signal of mice treated with Control-CAR T cells was represented. (D) Percent of body weight from D-1. Data representative of N=2 experiments, n=7-8 mice per group.

A pilot experiment was designed to investigate the efficacy of the CAR T cell therapy *in vivo*. Based on the experimental procedure provided by Chadwick *et al.*[307], 250 mg/kg of CTX was administrated i.p. to mice bearing A20-Luc lymphoma B cells (A20-Luc) one day prior to CAR T cell injection (Figure 23A). At this CTX dose, control-CAR (i.e. T cells transduced with retroviral empty vector) and CD19-CAR T cell therapy controlled A20-Luc growth in the days following treatment administration, as demonstrated by the reduction of bioluminescence signal (Figure 23B). However, only mice treated with CD19-CAR T cell therapy showed a complete response over time whereas 75% of mice treated with control-CAR T relapsed within the 28 to 56 days post tumour engraftment (Figure 23B and C).

In lymphoreplete patients (i.e., in presence of endogenous T cells), adoptive T cell therapy showed poor persistence and limited anti-cancer efficacy without prior immune cell depletion[312,313]. Indeed, endogenous T cells are much more abundant than adoptively transferred T cells, leading to competition for cytokines that induce proliferation. However, agents used to induce immune depletion, often chemotherapy or radiotherapy, also induce toxic side effects. As observed in this experiment, mice lost weight after each administration of CTX, whatever the administration route (Figure 23D). In addition, the potent efficacy of CTX plus Control T cells at killing A20-Luc cells the days following injection was not expected. Therefore, a set of experiments was performed to refine the CTX dose.

*Pre-conditioning immunomodulation is essential for potent CAR T cells engraftment*

To find the right balance between efficient engraftment of T cell therapy and reduced toxicity of the immune depleting agent, doses from 30 to 170 mg/kg of CTX one day prior to T cells infusion were tested in mice bearing A20-Luc lymphoma (Figure 25A and Annex 2). The combination of low CTX doses (30 or 43 mg/kg) with Control-CAR T cells had a light anti-tumour effect (Figure 25B). With higher doses (> 63 mg/kg), a CTX dose-dependent killing of A20 cells was observed the days following treatment (Figure 25B). However, whatever the CTX dose, mice treated with Control-CAR T cell relapsed within the 14 to 56 days post tumour engraftment (Figure 25B and C), with a maximum of 30% survival rate for mice pre-treated with the highest CTX dose plus Control-CAR T cells (Figure 25C).

As expected, CTX administration pre-CAR T cell infusion significantly impacted the efficacy potential of CAR T cell therapy. In short, the higher the CTX dose injected, the better the CAR T cell survival rate (Figure 25D). As previously observed with Control-CAR T cell therapy, pre-conditioned CTX dose of 30 mg/kg afforded no benefit to control A20-Luc lymphoma, even combined with CD19-CAR T cell therapy. A CTX dose of 43 mg/kg, resulted in a positive CD19-CAR T cell effect on tumour growth: reduction of bioluminescence signal was noticed for several days post treatment only in the CD19-CAR T cell treatment group (Figure 25B and E). However, at this CTX dose, CD19-CAR T cell therapy afforded a survival rate of only 40% (Figure 25D). With CTX doses > 63 mg/kg, CD19-CAR T cells demonstrated a potent therapeutic efficacy to control A20-luc cell growth, with a survival rate over 75% and up-to 100% for the highest tested CTX dose of 170 mg/kg (Figure 25D and E).

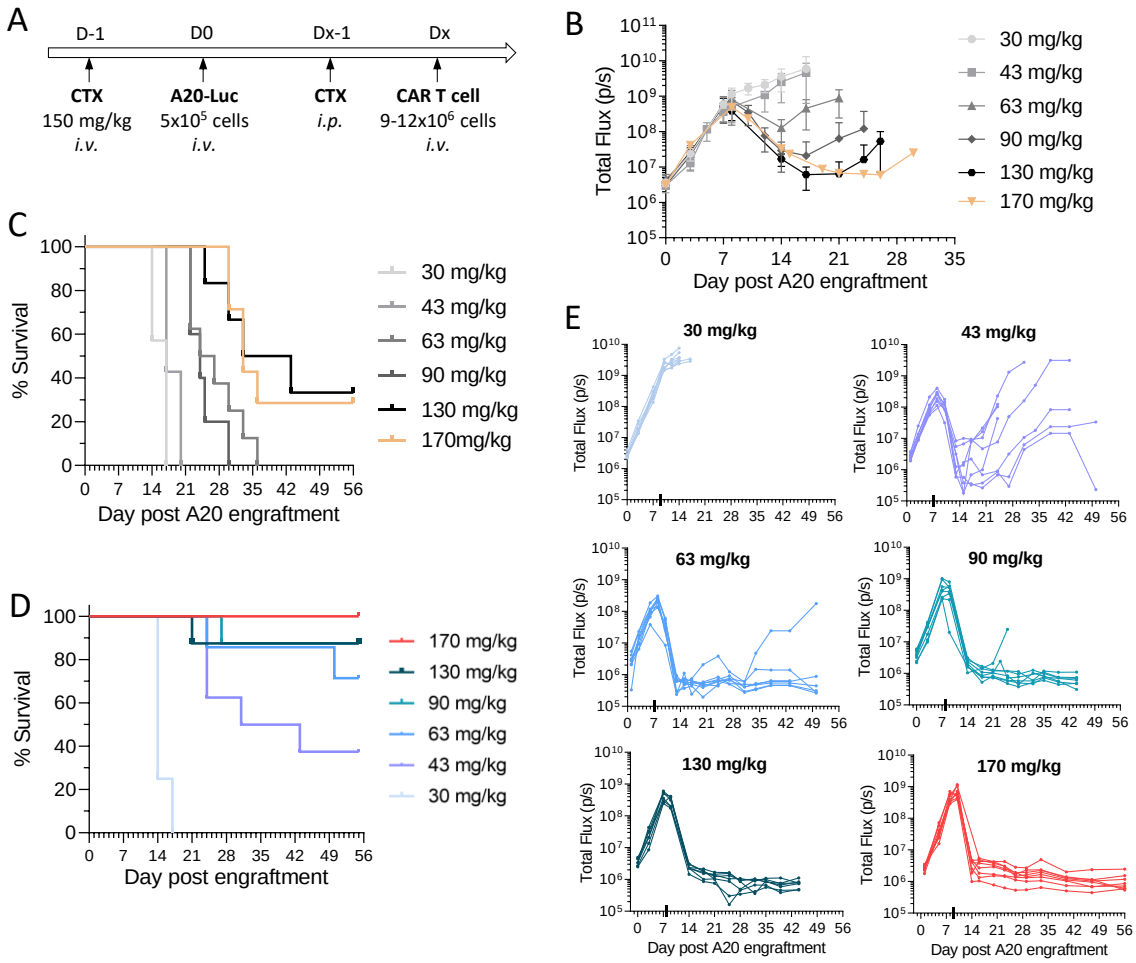


**Figure 25: Immunomodulation is mandatory for CAR T cell therapy efficacy.** (A) Mice were pre-conditioned with i.v. injection of CTX one day prior to A20-Luc lymphoma engraftment. Seven or eight days later, mice were imaged, randomized, and received i.p. indicated dose of CTX. The day after, mice were infused with (B and C) Control-CAR or (D and E) CD19-CAR T cells. (B) Bioluminescence and (C) survival of Control-CAR T cell injected mice following indicated doses of CTX pre-treatment. (D) Survival and (E) individual bioluminescence of mice treated with indicated dose of CTX plus CD19-CAR T cell therapy. Data representative of two independent experiments, n=7-8 mice per group.

To further understand the lack of CD19-CAR T cell efficacy when administered following a low dose of CTX (30 mg/kg), the presence of anti-CAR-T cell antibodies was investigated from mouse plasma (Figure 26A). While no antibodies were detected in mice given Control-CAR-T cells (Figure 26B), a positive signal was detected from sera of mice administered CD19-CAR T cells (Figure 26C). This data suggests that at CTX doses < 43 mg/kg, host mice are able to recognize and mount an immune response to adoptively transferred CD19-CAR T cells, most likely directed to the rat origin of the 1D3-scFv CD19-CAR construct.

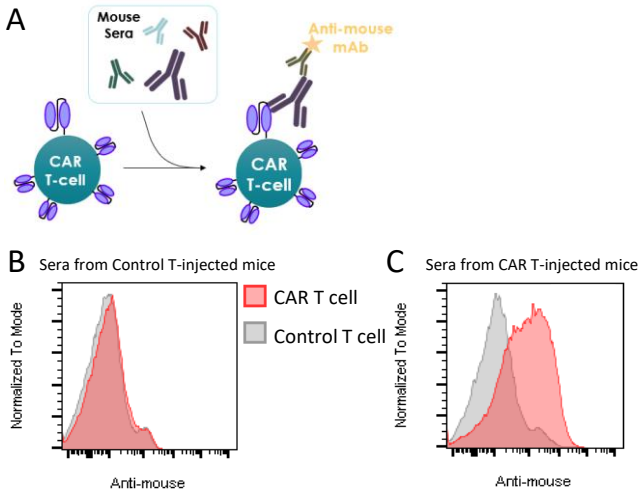


**Figure 26: *In vivo* immune response against CAR T cells with low CTX doses.** (A) Fresh Control-CAR and CD19-CAR T cells were reproduced *in vitro* and incubated with sera from mouse injected with 30 mg/kg of CTX plus (B) Control-CAR or (C) CD19-CAR T cells. Murine anti-CAR Ab from sera were detected by flow cytometry using anti-mouse antibody. Data representative of several samples from a single experiment.

*Proliferation of CD19-CAR T cell infused in mice bearing A20 lymphoma*

Robust CAR T cell proliferation *in vivo* was shown to coincide with CRS[48,67,80]. Therefore, to monitor CAR T cell expansion *in vivo*, luciferase-expressing Control-CAR T and CD19-CAR T cells were produced. Expression of the luciferase was checked *in vitro and* the bioluminescence signal of the luciferase-expressing Control-CAR T and CD19-CAR T-Luc cells was similar (Figure 27A). In addition, the cytoplasmic expression of luciferase does not impair expression of the CAR at the membrane surface (Figure 27B). Control-CAR and CD19-CAR T-Luc cells were infused in in mice bearing A20-WT lymphoma (Figure 27C) and cells were monitored via bioluminescence imaging (Figure 27E and F). To compare A20-Luc tumour cell growth kinetics *in vivo*, $2x10^6$ A20-WT cells were also transplanted. Mice were euthanized 15- or 16-days post A20-WT engraftment due to tail paralysis (Figure 27D), at a similar time point to mice given A20-Luc cells (Figure 21). In addition, Control-CAR T cells afforded a survival rate of 40% whereas CD19-CAR T cell administered mice displayed a 100% survival rate (Figure 27D). Whereas Control-CAR T-Luc cells persisted for 2 weeks *in vivo* without showing evidence of proliferation, CD19-CAR T-Luc cells proliferated the 4 first days post infusion and remained at high concentration as of 11 days post-infusion (Figure 27E and F). At the peak of expansion, CD19-CAR T-Luc cells appeared to be localized mainly in the liver and the spleen, whereas Control-CAR T-Luc cells were disseminated in the body (Figure 27F). CD19-CAR T-Luc cells then migrated to secondary lymphoid organs (Figure 27F), most probably due to the increased presence of A20 tumour cells (Figure 21). A decrease of the bioluminescence signal was noted around 11 days post infusion of Control- and CD19-CAR T-Luc cell groups (Figure 27E). It is important to note that the decrease in luciferase expression was observed *in vitro* over time (data not shown). This observation may explain the 'rapid' reduction of the bioluminescence signal *in vivo* which

may reflect the true reason for the disappearance of transferred CAR T-Luc cells over time. Nonetheless, the early clearance of CD19-CAR T-Luc cells may also be due to host immune responses returning to normal following early CTX-treatment.

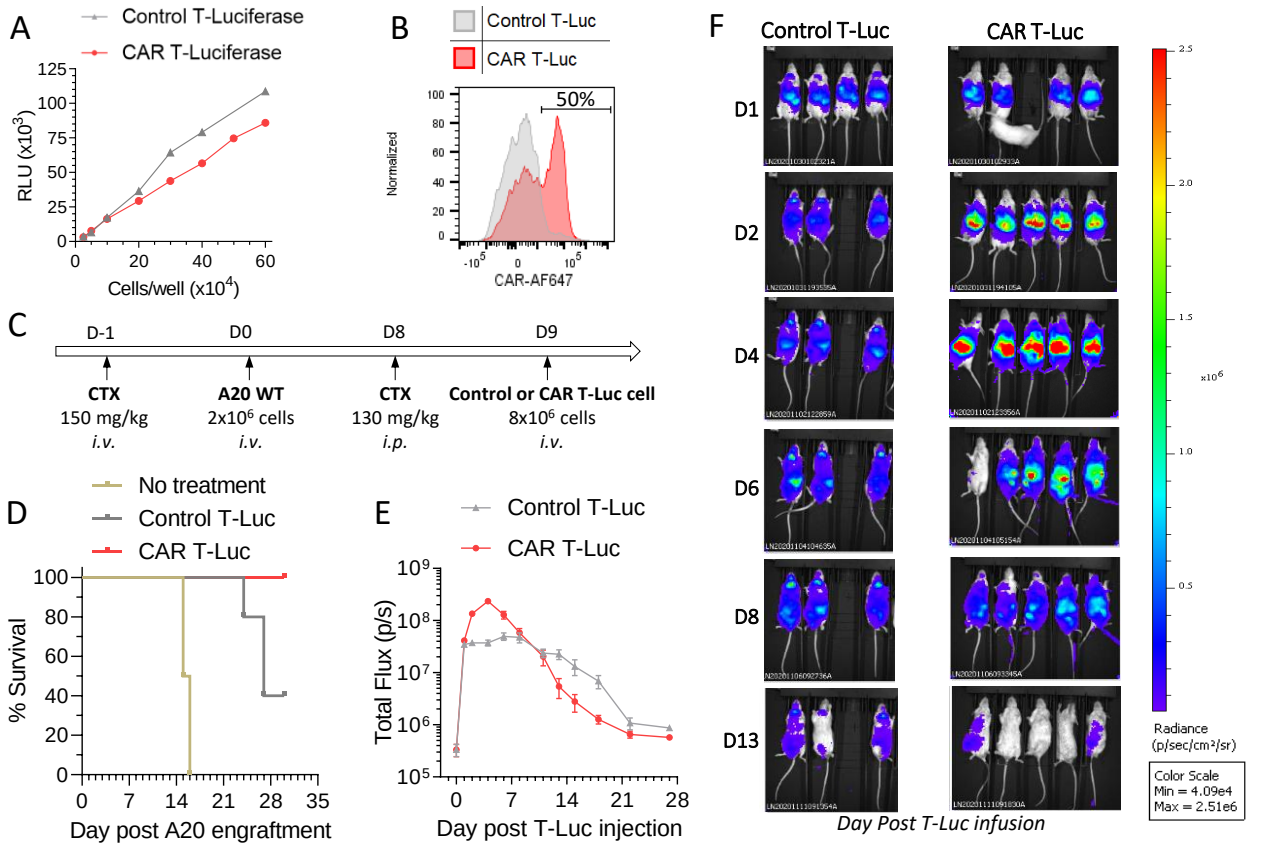


**Figure 27: *In vivo* proliferation of CD19-CAR T-Luc cells in mice with established A20 lymphoma.** Murine T cells were transduced with retroviral vector expressing the Luciferase and Control- or CD19-CAR. Four days post transduction, (A) luminescence signal was assessed using SpectraMax-i3x device, and (B) CD19-CAR expression was investigated by flow cytometry. (C) Mice were pre-conditioned with i.v. injection of CTX one day prior to A20-WT lymphoma engraftment. Eight days later, mice were imaged, randomized, and received i.p. indicated dose of CTX. The day after, mice were infused with engineered T cells. (D) Survival of mice with established A20-WT lymphoma, treated with Control- or CD19-CAR T cell therapy. (E and F) Following of Control- and CD19-CAR T-Luc cells by bioluminescence. (E) Mean of bioluminescence signal and (F) mouse images during bioluminescence acquisition. Data from single experiment. Values are displayed as mean ± SD.

Taken together, these data supported the rational to use a high dose of immune-depleting agent prior to adoptive transfer of CAR T cells. Indeed, high dose CTX allowed a good tumour engraftment and provided an optimal milieu for CAR-T cell proliferation. In addition, preliminary data (Annex 3) demonstrated that the pre-conditioning dose of CTX positively impacted cytokine production; i.e., the highest CTX dose resulted in the highest cytokine release. As such, the CTX at 170 mg/kg was chosen as the pre-conditioning dose prior CAR T cells infusion in the subsequent experiments.

### 2.3.2 Mouse CD19-CAR T cell induced CRS

*CAR T-cell model of CRS reproduces features of CRS*

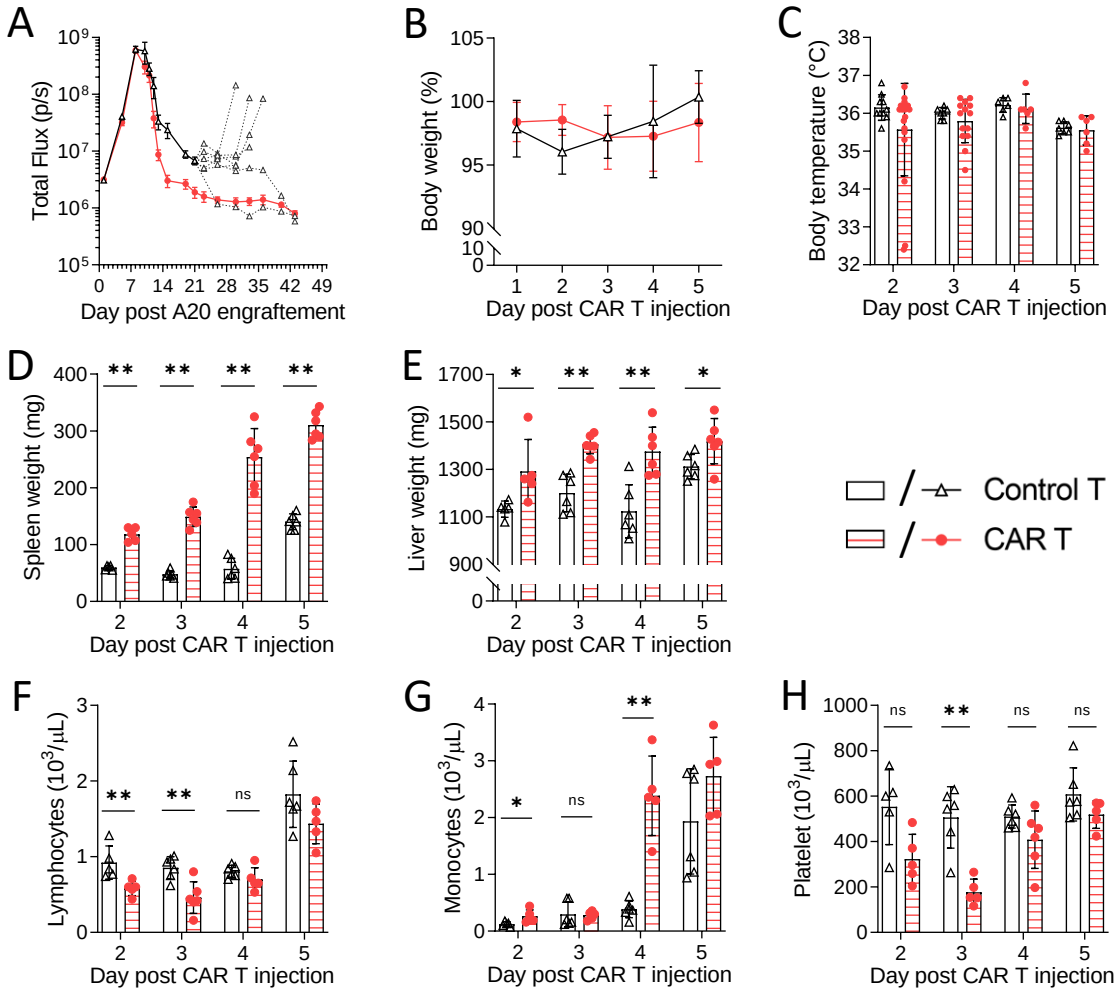


**Figure 28: Lymphoma killing by murine CD19-CAR T cells induced CRS.** Mice were pre-conditioned with i.v. injection of CTX one day prior to A20-Luc lymphoma engraftment. 8 days later, mice were imaged, randomized, and received 170 mg/kg of CTX on day prior Control-CAR or CD19-CAR T cells infusion. (A) Tumour growth, body (B) weight and (C) temperature, (D) spleen and (E) liver weight follow-up. Blood parameters including leucocyte (E) lymphocyte, (F) monocyte, and (G) platelet, counts. (H) Plasma angiopeitin-2 quantification. n=5-6 mice per time point and representative of N=3 independent experiments. *P<0.05, **P<0.01, were obtained using the unpaired Mann-Whitney t-test. Values are displayed as mean ± SD.

To investigate the potential toxicities associated with CAR T cells, mice were injected with A20-Luc lymphoma cells and 8 days later treated with 170 mg/kg of CTX, one day pre-Control-CAR or CD19-CAR T cell infusion. After initial tumour remission, almost all A20-lymphoma–bearing mice treated with Control-CAR T cells relapsed, whereas mice having received CD19-CAR T cells showed long term tumour control (Figure 28A). At first sight, mice did not demonstrate common signs of CAR T-toxicities, such as body weight and body temperature loss, that remained stable (Figure 28B and C). Nonetheless, body

temperature measurements of mice given CD19-CAR T cells were more heterogenous with a tendency to be lower than Control-CAR T cell-injected mice (Figure 28C). As a robust expansion of CD19-CAR T cells was observed during 4 days following infusion (Figure 27E), mice were euthanized at those time points to further study the impact of the CAR T therapy. Mice developed several CRS features including hepatosplenomegaly (Figure 28D and E) and blood disorders (Figure 28F to H). Indeed, the spleen and liver weights from CD19-CAR T cell-injected mice significantly increased in days post injection. Although lymphopenia was observed in both Control-CAR and CD19-CAR T cell administered mice, a more severe phenotype developed following the latter (Figure 28F). Monocytosis (Figure 28G) and thrombocytopenia (Figure 28H) was also observed.

*CD19-CAR T cell induced systemic hypercytokinemia with an IL-6 and IFN-γ signature*

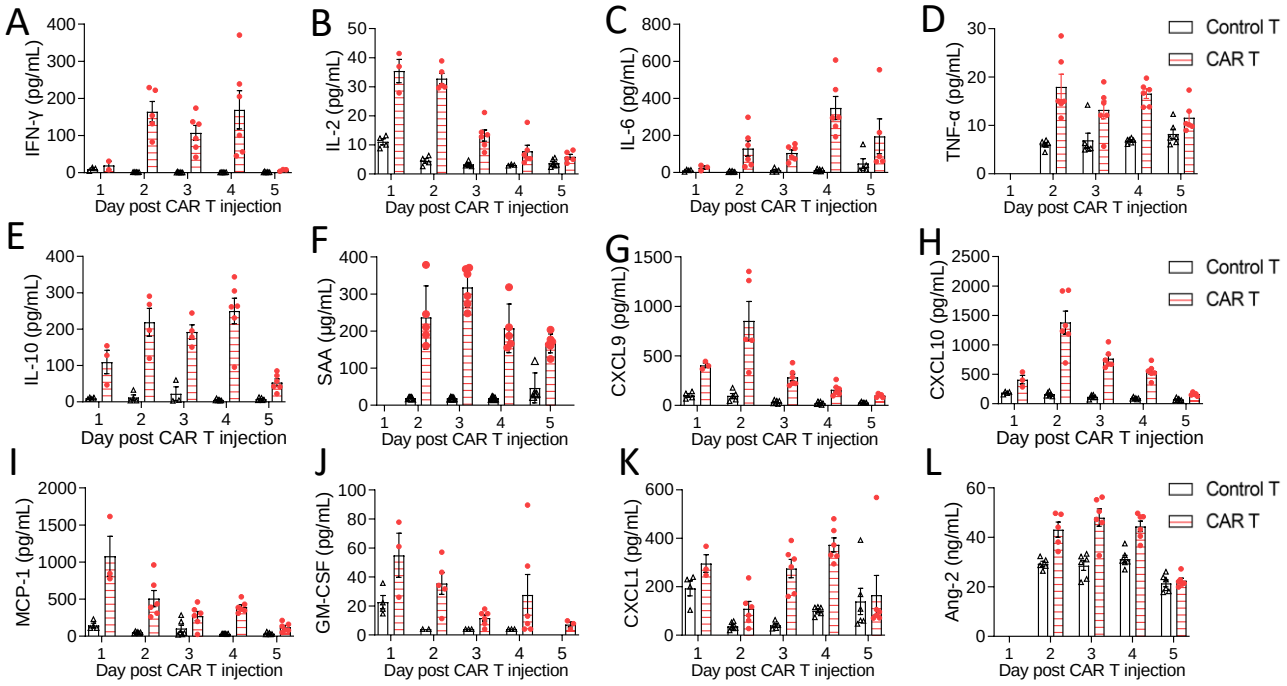


**Figure 29: CD19-CAR T cells induced systemic hypercytokinemia characteristic of CRS.** Mice were pre-conditioned with i.v. injection of CTX one day prior to A20-Luc lymphoma engraftment. 8 days later, mice were imaged, randomized, and received 170 mg/kg of CTX on day prior Control-CAR or CD19-CAR T cells infusion. Mice were euthanized at the indicated days post treatment and plasma cytokines and chemokines were quantified using MSD U-PLEX assay kits or ELISA assays. Data are representative of N=3 independent experiments, n=4-6 mice per time point. Values are displayed as mean ± SEM.

The above observed toxicities induced by CD19-CAR T therapy was associated with a transient increase of inflammatory cytokines and chemokines, starting immediately after the CAR T injection and lasting almost 5 days. As observed in human patients developing CRS, plasma levels of IFN-γ, IL-6, TNF-α, IL-2

and IL-10 were up-regulated (Figure 29A to E). The kinetics of production was cytokine dependent. IL-2 was first to peak followed by IFN-γ and then IL-6, one-, two- and four-day post CD19-CAR T injection (Figure 29A to C), respectively. Levels of SAA, a biomarker often associated with IL-6 signalling, was up-regulated in plasma as early as day 2 post CD19-CAR-T transfer and remained high until at least day 5 (Figure 29F). In contrast, CXCL9 and CXCL10, two well-described biomarkers of IFN-γ activity[330], peaked at day 2 and then rapidly returned to basal level (Figure 29G and H). Monocyte chemoattractant protein-1 (MCP-1), and granulocyte-macrophage colony-stimulating factor (GM-CSF), inflammatory mediators frequently associated with life-threatening CRS[64], were also significantly and rapidly up-regulated, peaking at day 1 (Figure 29I and J), as well as CXCL1, chemokine described to enhance neutrophil attraction[163], survival, and proliferation, progressively peaking at day 4 (Figure 29K). Finally, and as a measure of increased vascular permeability[74], Angiopoietin-2 (Ang-2) was also over-expressed following CD19-CAR T cell infusion (Figure 29L). Elevations of the above cytokines closely mirrored the kinetics of *de novo* mRNA synthesis in the spleen, the liver, and the lung (Figure 30), although the latter analysis was only performed once.

The mRNA signature for *Ifn-γ* was sharply up regulated in the spleen and, in a sustained manner, in the lung (Figure 30A). Accordingly, *Cxcl10* and *Cxcl9* were mainly up regulated in the lung (Figure 30B and C). As expected, the liver was the site where the *Saa* gene expression was the highest (Figure 30E), whereas *Il-6* was similarly up-regulated in the three studied organs (Figure 30D). The liver also presented the highest fold increase for *Mcp-1* and *Tnf-α* gene expression level (Figure 30F and G). Interestingly, *Ang*-2 was up regulated only in the liver, whereas it was down-regulated in the spleen and the lung (Figure 30H). In addition, *Ang-1*, a key component in blood vessel maturation and stabilization[72,74], was down-regulated in the three organs (Figure 30I), as well as vascular endothelial growth factor VEGF (Figure 30J). Globally, the lung and the spleen behaved relatively in a same way, reflecting a Th1 gene expression signature. Conversely, the liver presented with an up-regulation of inflammatory genes associated with monocyte/macrophage attraction and activation, as well as vascular permeability (Figure 30).

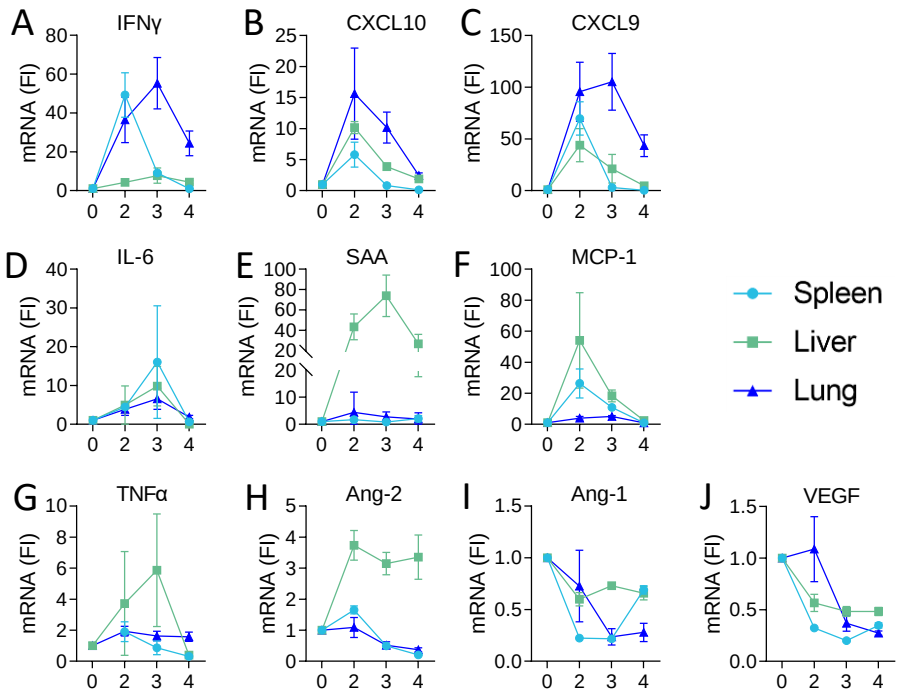


**Figure 30: Organ-specific inflammatory gene signature induced by CD19-CAR T therapy.** Mice were pre-conditioned with i.v. injection of CTX one day prior to A20-Luc lymphoma engraftment. 8 days later, mice were imaged, randomized, and received 170 mg/kg of CTX on day prior Control-CAR or CD19-CAR T cells infusion. Mice were euthanized at the indicated days post treatment. Graphs A to I represents the quantification of tissue-derived cytokine and chemokine mRNA levels evaluated by qPCR in the spleen, the liver, and the lung. Data are expressed as fold increase (FI) above mean of Control-CAR T-injected mice. n=4-6 mice per time point from a single experiment. Values are displayed as mean ± SEM.

*Organ-specific mobilization of inflammatory cells*

The organ-specific cytokine signature, hepatosplenomegaly, the drop in circulating lymphocyte count, and the increase in monocyte count following CD19-CAR T cell injection, suggested a potential differential mobilization of immune cells to respective tissues. To further characterize this observation, infiltrating immune cells from spleen and liver were excised 2-, 3- and 4-days post CAR T injection and characterized (see Annex 4 for gating strategies). A differentiating homing pattern was observed between Control- and CD19-CAR T cells. Indeed, while Control-CAR T cell frequency was higher than CD19-CAR T cell frequency in the spleen, the opposite was observed in the liver (Figure 31A and B). Secondly, myeloid subsets also fluctuated significantly in the studied organs. A lower frequency of NK cells was seen in the spleens from mice injected with CD19-CAR T cells as compared to Control-CAR T cell administered mice (Figure 31C) whereas the opposite was observed in the liver (Figure 31D). In both organs, an increased frequency of neutrophils, inflammatory and resident monocytes/macrophages was seen (Figure 31E to J). The frequency of the latter remained stable over time (Figure 31J). Frequency of

myeloid subsets in the organs increased with time and correlated with the growing hepatosplenomegaly previously observed (Figure 31D and E). This was particularly obvious for NK cells in the liver (Figure 31D) and both neutrophils and inflammatory monocytes/macrophages in the spleen (Figure 31G and I).

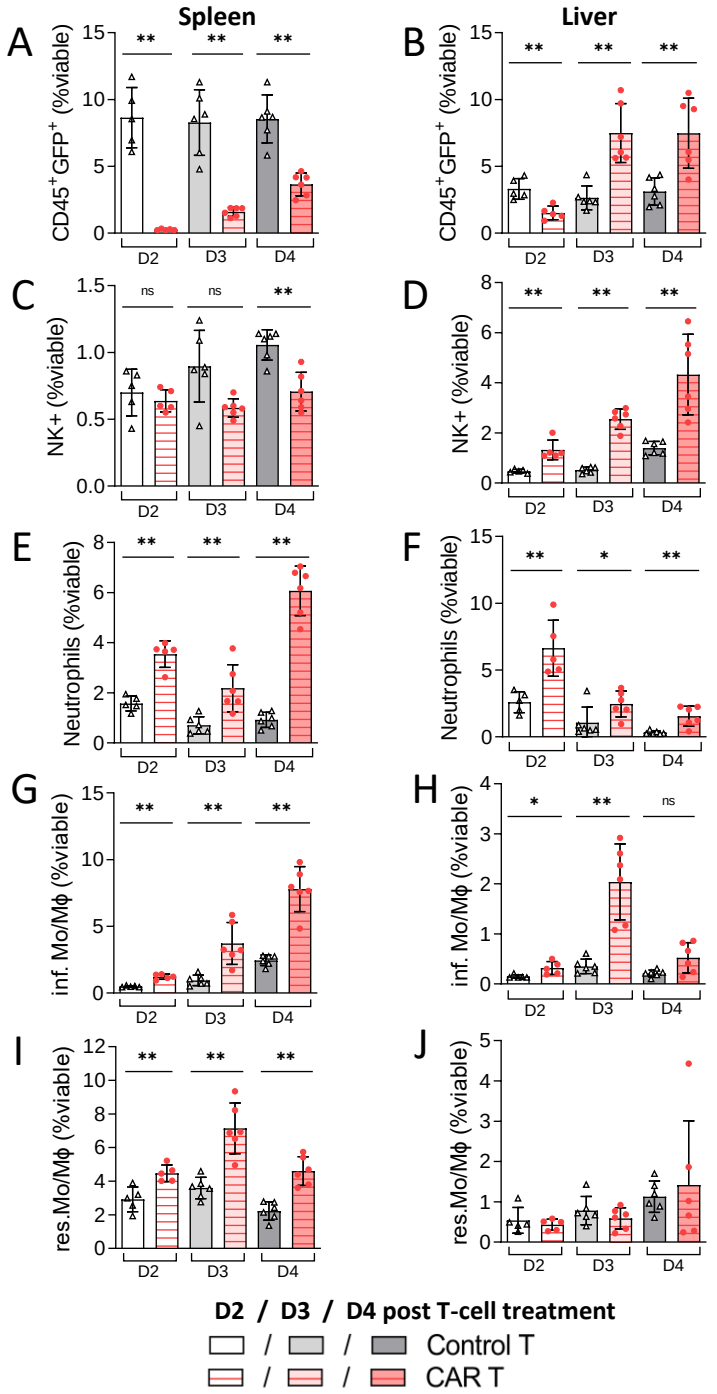


**Figure 31: Monocytes and neutrophils are major contributor to hepatosplenomegaly.** Mice bearing lymphoma model were treated with Control- or CD19-CAR T cell therapy. Single cell-suspensions from the spleen and liver were prepared 2-, 3- or 4-days post treatment, followed by immunophenotyping. Left bar graphs and right bar graphs represent frequencies of cells population from spleen and liver respectively. Cells frequencies are expressed as a percentage of viable cells. Gating strategies are available in Annex 4. NK, Natural Killer; Mϕ, macrophages. Data are representative of N=2 independent experiments, n=5-6 mice/organ per time point. *P<0.05, **P<0.01, were obtained using the unpaired Mann-Whitney t-test Values are displayed as mean ± SD.

## 2.4 INVESTIGATING ROLE FOR IFN-Γ AND IL-6 IN CAR-T INDUCED CRS

### 2.4.1 Neutralizing IL-6 affords partial benefit at reducing CRS features

As a significant increase of IFN-γ and IL-6 was observed following CD19-CAR T cell infusion, mice were treated with mAbs neutralizing IFN-γ and IL-6-mediated signalling. Anti-cytokine mAbs were injected at 30 mg/kg simultaneously with the CAR T therapy, followed up by two additional doses administrated 2 and 5 days later (Figure 32A). Interestingly, the efficacy afforded by CD19-CAR T therapy was not impair by neutralizing IL-6-signalling or IFN-γ. All mice administered anti-IL-6R or anti-IFN-γ mAbs with CD19-CAR T cells controlled A20 tumour growth over time whereas only 25% of mice treated with Control-CAR T cells survived (Figure 32B). In addition, anti-cytokine treatment did not impair the killing efficacy of CD19-CAR T cells (Figure 32C). Interestingly, while mice administered the neutralizing antibodies recovered more rapidly from lymphopenia compared to untreated mice (Figure 32D), only IL-6 blockade significantly ameliorated the observed monocytosis (Figure 32E) as well as the hepatosplenomegaly (Figure 32F and G). Accordingly, IL-6 neutralization reduced the frequency of myeloid subsets previously shown to be increased in the spleen and liver of CD19-CAR T cells injected-mice developing hepatosplenomegaly (Figure 31). Indeed, the IL-6 blockade resulted in a decreased frequency of neutrophils in the spleen and the liver (Figure 32H and I), and of inflammatory monocytes/macrophages in the spleen (Figure 32I) in comparison to CD19-CAR T cells injected-alone mice. Taken together, the data herein suggests that IL-6 and IFN-γ are obligate cytokines for CAR-T cell induced tumour control and that IL-6 may be linked to CRS parameters.

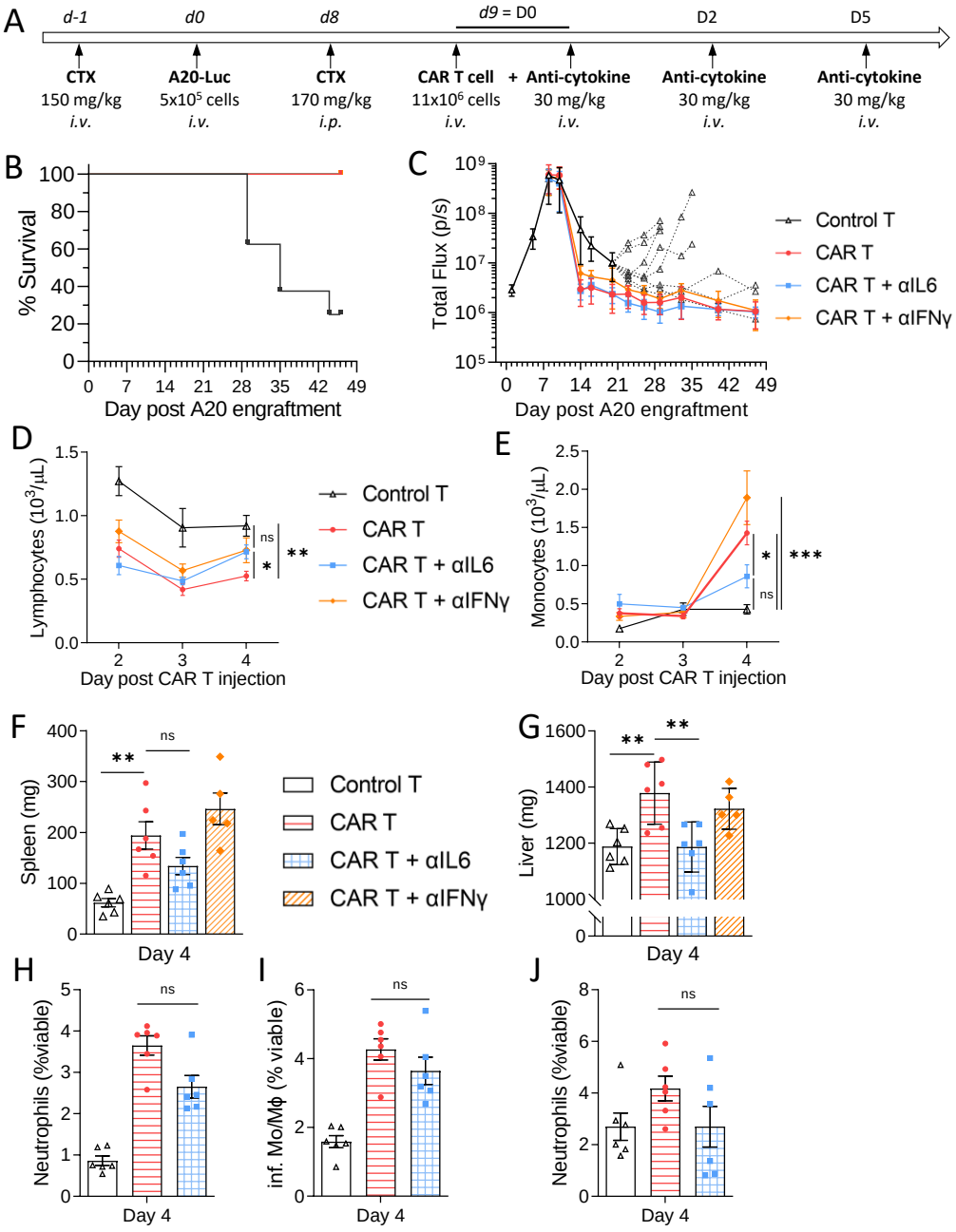


**Figure 32: Neutralizing IL-6, but not IFN-γ, affords benefit at reducing CRS features.** (A) Mice bearing lymphoma model were treated with Control-CAR or CD19-CAR T cell therapy and an anti-IL-6R or anti-IFN-γ. (B) Survival and (C) bioluminescence of mice. Blood parameters including (D) lymphocyte and (E) monocyte counts. (F) Spleen and (G) liver weight. Single cell-suspensions from the (H and I) spleen and (J) liver were prepared 4 days post treatment, followed by immunophenotyping. Neutrophils (H and J) and inflammatory monocytes/macrophages (I) frequencies are expressed as a percentage of viable cells. Gating strategies are available in Annex 4. Data are representative of N=2 independent experiments, n=5-6 mice per group. *P<0.05, **P<0.01 and ***P<0.001 were obtained using unpaired t-test or one-way ANOVA. Values are displayed as mean ± SEM.

### 2.4.2 Investigating IL-6-cis and -trans signalling pathways in CAR T-induced efficacy and toxicity

IL-6 is a pleiotropic cytokine utilizing two different pathways to mediate its biological effects: the classical pathway, and the *trans*-signalling pathway. While the classical pathway appears to mediate the homeostatic and protective activities of IL-6, the *trans*-signalling pathway is emerging as a driver of dysregulated inflammatory responses leading to disease[111-116,124]. Previously developed anti-IL-6R antibodies were tested in the CD19-CAR T cell/A20 model. 25F10 exclusively inhibits the *trans*-signalling pathway, whereas 2B10 (a tocilizumab-like antibody) blocks both cis- and *trans*-signalling pathway (Figure 33A and B). With the aim to investigate the impact of IL-6 *trans*-signalling on CAR-T therapy efficacy and toxicity, mice bearing A20 lymphoma were treated with CD19-CAR T cells and administrated 25F10 or 2B10, as detailed in Figure 33C. While blockade of IL-6-signalling pathways via the two mAbs did not impair CD19-CAR T efficacy (Figure 33D), 25F10 (*trans*-signalling blocker) afforded an improved control of hepatosplenomegaly (Figure 33E) and hemotoxicity (Figure 33F). Accordingly, 25F10 reduced the infiltration of neutrophils and monocytes/macrophages in the spleen and the liver (Figure 33G), although not reaching statistical significance. Differential blockade of the IL-6-signalling pathways impacted the cytokine production (Figure 33H). Whereas both 25F10 and 2B10 did not reduce the early cytokine up-regulation in plasma (Figure 33H – Day 3), 25F10 treatment resulted in a more rapid return to baseline (ie, Control-CAR T cells mice) plasma cytokine levels, of IFN-$\gamma$, TNF-$\alpha$, IL-2, CXCL10, MCP-1, as compared to 2B10 administrated CD19-CAR T cells mice or anti-IL6R-mAb untreated CD19-CAR T cells mice (Figure 33H). Interestingly, over-expression of CXCL1 was controlled by 2B10 and 25F10 (Figure 33H). Contrary to the previous trend, only 2B10 significantly reduced the SAA level, which may point to an inefficient blockade of IL-6 signalling by the mAbs (Figure 33H). Taken together, a role of IL-6-trans signalling in toxicity induced by CAR T therapy was suggested in these first experiments. In an effort to reproduce the data, mice were administrated with higher doses of anti-IL-6R mAbs. Due to technical reasons, the 30 mg/kg was administrated i.v. and the 60 mg/kg doses administrated ip. In addition, the third anti-IL-6R injection was given D4 (instead of D5 in the previous experiment) (Annex 5A). If the higher doses of anti-IL-6R did not impair CAR T therapy (Annex 5B), the positive impact of 25F10 at reducing CAR T cell-toxicities was not reproduced (Annex 5). This discrepancy may be due to different batches of anti-IL-6R mAbs used between the two experiments. In addition, the mAbs were stored for a long period at -80°C (since 2012) that might impact their activity.

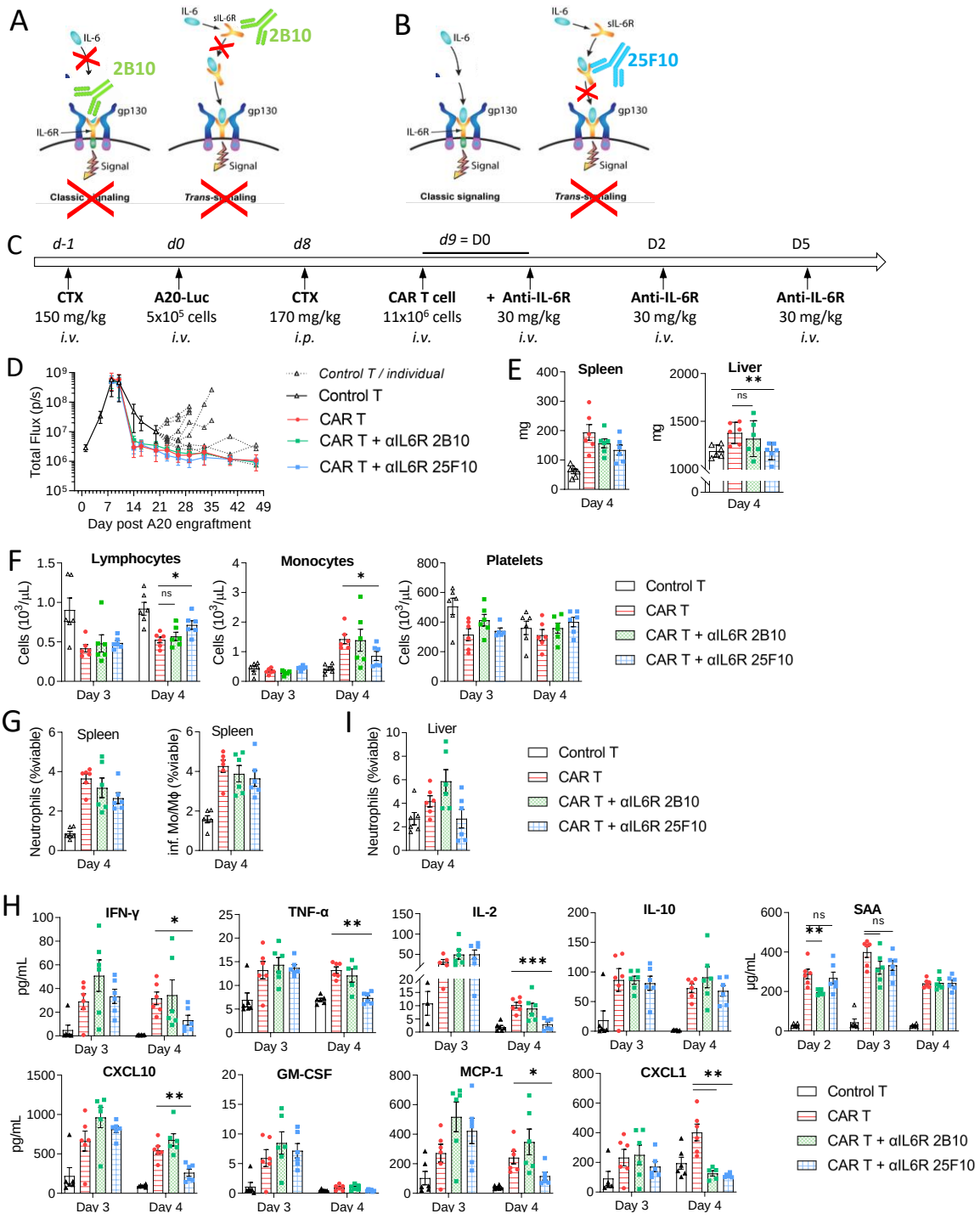


**Figure 33: Differential role of IL-6-*trans*- and cis-signalling pathways in toxicities mediated by CD19-CAR T cells.** Downstream pathways of IL-6 signalling, and specific blocking of (A) 2B10 and (B) 25F10. (C) Mice bearing lymphoma model were treated with Control-CAR or CD19-CAR T cell therapy and 25F10 or 2B10. (D) bioluminescence follow-up. (E) Spleen and liver weight. (F) Blood parameters including lymphocyte, monocyte and platelet counts. (G) Single cell-suspensions from the spleen and liver were prepared 4 days post CAR T infusion, followed by immunophenotyping. Neutrophils and inflammatory monocytes/macrophages (inf. Mo/MΦ) frequencies are expressed as a percentage of viable cells. Gating strategies are available in Annex 4. (H) Plasma cytokines and chemokines quantification using MSD U-PLEX assay kits or ELISA assays. Preliminary data from of one single experiment, n=5-6 mice per group. *P<0.05, **P<0.01 and ***P<0.001 were obtained using unpaired t-test. Values are displayed as mean ± SEM. (A) and (B) are adapted from Lee *et al.*[114]

# 3 CONCLUDING REMARKS

Several factors affect the efficacy and safety of CD19-CAR T cells, such as composition of the CAR (for instance, nature and number of costimulatory domains), the culture methods prior infusion, the number of T cells transferred, the tumour burden[33].

In order to determine the optimal CAR for *in vivo* studies three CAR constructs were generated; two containing a single costimulatory domain, either CD28 or 4-1BB, and the third containing the both costimulatory domains. All CAR constructs included the same anti-CD19-scFv component and the CD3-ζ activation domain. The CD19-CAR T cells were shown to bind to the recombinant murine CD19, although with different capacity that correlated with CAR expression levels. Importantly, all transduced CAR-T cells demonstrated equivalent *in vitro* cytotoxicity activity. Whatever the CAR construct, the activation of the CD19-CAR T cells upon co-culture with target A20 B lymphoma cells resulted in abundant Th1 (IFN-γ, TNF-α) and Th2 (IL-10) cytokine production. Although the high production level of Th1 cytokines is expected, it was shown by other that the incorporation of the 4-1BB domain into CARs decreased the production of Th2 cytokines[314].

The efficacy of CAR T cell therapy is dependent on the ability of T cells to engraft, expand and persist after adoptive transfer[46]. The culturing conditions during *ex vivo* CAR T cell generation and expansion play a crucial role for producing an effective therapeutic activity[315]. Furthermore, the degree of T cell expansion also correlates with the severity of CRS[33]. T cell culture media is often supplemented with cytokines, the most commonly used being IL-2. However, IL-7 and IL-15 have also been used due to their ability to enhance the survival and proliferation of T cells[315,316]. Hence, two culture mediums were screened herein, the serum-free Gibco medium known to enhance T cells expansion, and the more widely used RPMI medium[321], supplemented with either IL-2 or IL-7/IL-15. In contrast to the majority of studies describing the Gibco medium to be better for T cell culture conditions, the work described here found that RPMI medium allows a better maintenance of the viability and a superior killing capacity of T cells in comparison to Gibco medium[321]. Surprisingly, while the IL7/15 cytokine supplementation in the medium was shown to impact the maintenance and cytotoxic activity of the T cells culture, the addition of recombinant cytokines failed to enhance the CAR-T cell antitumor activity and the *in vivo* expansion (data not shown), as commonly reported[316,318-321]. Nonetheless, the impact of cytokine supplementation on CAR T cells vary from one study to another. Indeed, contradictory reports described that murine T cell function *in vitro* following culture in IL-7/IL-15 is lower than following culture in IL-2. The method of

T cell stimulation used, differences in the cytokine concentration used, and the duration of expansion are reasons among others that may explain this discrepancy[322,323].

The ability of the murine 1D3-28z-CAR T cells (named after CD19-CAR T cells), to control A20 B lymphoma in syngeneic mice and to induce CRS was evaluated. Multiple studies have demonstrated that host lymphocytes can reduce the antitumor efficacy of transferred T cells and therefore lymphodepletion prior to the adoptive T cell transfer enhances antitumor activity in mouse and in humans[311,3327-329]. Most-importantly, intensity of lymphodepleting regimen was associated with the severity of CRS mediated by CAR T cells[48,64,80]. Consistently, it was shown herein that the dose of cyclophosphamide (CTX) administrated one day prior to CAR T cell infusion positively impacted the efficacy of the CD19-CAR T cells and the cytokine production *in vivo*. Mice transplanted with A20 B lymphoma cells, pre-conditioned with CTX and then administered the CD19-CAR T cells demonstrated long-term survival. Although the mice did not exhibit visual clinical symptoms of CRS such as piloerection or prostration, the CD19-CAR T cells induced a robust systemic inflammatory response and other symptoms characteristic of CRS such as splenomegaly and hemotoxicity.

# CHAPTER IV: GENERAL DISCUSSION, CONCLUSION & PERSPECTIVES

*Note: The results obtained from the mouse model of anti-CD3-induced CRS has been already discussed in the published paper inserted in the Chapter II. Therefore, the general discussion will be more focussed on the data of the model of CRS mediated by CAR T cells. Nevertheless, similarity and differences between the two models will be highlighted.*

Cytokine release syndrome (CRS) is an acute inflammatory syndrome caused by the activation of immune cells and release of proinflammatory cytokines. Symptomatically starting off as a fever, clinical signs rapidly progress to hypotension, hypoxia, multiple-organ dysfunction, and death[3,33,34,121]. Initially described in patients receiving muromonab-CD3[17,18], a mouse anti-human mAb, CRS is now commonly seen in HLH patients[175-180], following T-cell engager therapies, such as BiTE[26,27] and CAR T cells[28-30], and plethora of infectious diseases[5-14], the most recent example being COVID-19[15,16]. Under certain circumstances, the inflammatory response to a pathogen or consequent to an immune-boosting cancer therapy is unrestrained leading to collateral damage including organ dysfunction. To date, it is unclear what determinants of the host response triggers the amplification of the immune response to a potential lethal cytokine release syndrome rather than contracting to static levels. Although valuable insights on the pathophysiology have been elucidated in these last years, in particular following the advent of CAR T cell therapy for cancer, the key cellular and molecular players involved in the life-threatening toxicities remain poorly understood. Improved preclinical models of CRS may help further the understanding of the mechanisms driving disease and, potentially, offer new insights to novel therapies.

## 1 SYNGENEIC MOUSE MODELS OF CRS

Although the clinical presentation of CRS is often similar whatever the trigger, caution should be used when extrapolating and comparing the results from one study to another. Two mouse models of CRS, induced by different triggers, were set up to better understand the key mediators involved in the syndrome. To this end, models were developed relying on either an agonistic anti-CD3 mAb to trigger polyclonal T cell activation *in vivo* or CAR-T cells in tumour bearing mice. The anti-CD3 model results in an acute *in vivo* T cell activation mimicking CRS typically seen in the context of infectious diseases, for example, consequent to Corona, Ebola and Lassa virus. On the other hand, CD19-CAR T cell therapy,

albeit having shown to considerably improve the survival of patients with haematological malignancies, it is often associated with a spectrum of cytokine-mediated toxicities, such as CRS and even neurotoxicity in some cases. Almost all preclinical studies to dissect CAR T cell-induced CRS have been performed in 'humanized' mouse models[281-283]. The main drawback of these models is they do not evaluate disease progression in the context of a fully competent immune system. While CRS is a systemic disease, likely resulting of the interplay between the CAR T cells and immune and non-immune/bystander cells, immunocompetent syngeneic mouse model is the most powerful tool to reflect the human clinical situation.

Body weight loss and fever are common clinical features observed in patients afflicted with CRS[3,33]. A consistent feature see in the anti-CD3 model was the rapid loss of weight and decreased body temperature within the first 24 hours post anti-CD3 injection. In contrast to the anti-CD3 model and published data[195,196,307], the afore mentioned symptoms were not observed in mice transplanted with tumour and administered CD19-CAR T cells. Nonetheless, in the first days after CD19-CAR-T injection, body temperature in mice was heterogenous and, on average, lower than in Control-CAR- T cell treated mice, although not reaching statistical significance. CD19-CAR T cell-treated mice did present with hemotoxicities, including lymphopenia, monocytosis and thrombocytopenia, akin to what was observed in the anti-CD3-injected mice. Lymphopenia and thrombocytopenia are features commonly observed in CRS patients and are associated with disease severity across almost all settings[64]. Monocytopenia is also often documented and was a striking feature seen in the healthy volunteers given the super-agonist CD28 antibody, TGN1412[19], and in patients infused with CAR T cell therapy[64]. Interestingly, monocytosis was observed in both the anti-CD3 and CAR-T cell models described herein. The efficiency and potency at engaging FcγRs between TGN1412 (hu-IgG4) and anti-CD3-(hamster IgG1) may explain the discrepancy on monocyte populations seen between human subjects treated with the former and mice with the latter. Nonetheless, in a humanized mouse model of CRS, a surge in human monocyte counts was also observed following CAR T cells administration, although this was dependent on the antigen targeted by the cellular therapy[196]. In the study herein, an acute spike in MCP-1 levels was also observed in mice injected with CAR T cells. MCP-1 is one of the key chemokines that regulates the migration and infiltration of monocytes/macrophages[331]. This increased in MCP-1 levels may help explain the migration of monocytes from the blood to tissues, given the observed increase of monocytes/macrophages observed in the spleen and the livers from mice injected with CD19-CAR T cells. Moreover, a recent

study reported that early elevated MCP-1 levels was the most accurate feature in predicting severe CRS development induced by CAR T cell therapy[64].

Infiltration of monocytes/macrophages in the spleen and the liver progressively increased the days following injection of the CD19-CAR T cells in mice, correlating with the observed hepatosplenomegaly, also a common clinical feature in patients afflicted with CRS[3,33]. In the anti-CD3 model, splenomegaly was observed, accompanied by hepatomegaly in the more severe forms of CRS. The frequency of neutrophils was increased in both organs. Similarly, in the CAR T cell model, in addition to the monocytes/macrophages, neutrophils were also shown to infiltrate both liver and spleen, although to a lesser degree in the former. While the pathologic role of monocytes and macrophages in CRS has been documented[191, 195,196,198], the role of neutrophils remains unclear and poorly explored. Lymphoid subsets also fluctuated significantly in the studied tissues. CD19-CAR T cells egressed from the spleen migrating to the liver, as also reported in study with human CAR T cells[196]. Why CD19-CAR T cells predominantly infiltrated the liver instead of the spleen remains unclear, especially since $CD19^{+}$ A20 cells were more present in spleen according to bioluminescence imaging (Annex 2).

Several studies have identified T-cell derived IFN-γ and TNF-α as key cytokines in the development of CRS mediated by CAR T cells and T cell-engaging therapies[28,33,122,251]. In agreement, a robust induction of IFN-γ, TNF-α was observed in mice injected with CD19-CAR T cells in the *in vivo* model here. Concomitantly, de-novo *Ifn-γ* and *Tnf-α* gene expression was rapidly up-regulated, and in an organ-dependant manner. In the spleen and the lung, *Ifn-γ* was up regulated, peaking 2- and 3-days post injection respectively, whereas *Tnf-α* was unchanged. In contrast for the liver, *Ifn-γ* was unchanged whereas *Tnf-α*, was up-regulated. As a consequence of the IFN-γ up-regulation, a sharp increase in CXCL9 and CXCL10 chemokine was detected in the plasma, and in the three organs as evidenced by the mRNA transcript up-regulation. The local tissue production of CXCL9 and CXCL10 most probably was key at driving the infiltration of CXCR3-expressing cells, such as neutrophils, macrophages, T cells and NK cells. IFN-γ signature associated with high CXCL9/CXCL10 levels was also seen in the studied anti-CD3 model, and in paediatric HLH patients, correlating in the latter with key disease parameters and severity[187,330].

In the setting of T-cell engaging immunotherapy, the acute production of T-cell derived IFN-γ and TNF-α induced the activation of bystander cells, such as monocytes and macrophages well described as producers of IL-1, IL-6[196,197,251]. In the CAR T cell study herein, IL-6 peaked 4 days post CAR T cell

injection, concomitantly with a sharp increase of monocytes in the blood. The level of plasma amyloid A (SAA), a murine homolog of human C-reactive protein[46], is often considered IL-6-dependant and rapidly up-regulated, although peaking earlier than detectable plasma IL-6. Nonetheless, de-novo *Il-6* gene transcript levels was increased in the liver, spleen and the lung, 2 days post injection and peaking 3 days post CAR T cell injection. While an increased production of IL-6 was observed, IL-1 level was unchanged (data not shown), similar to observations in the anti-CD3 mouse model. The lack of IL-1 production in both studied models in this project was unexpected, especially in the CAR T cell model of CRS as IL-1 cytokine was shown to be a key mediator in CRS and neurotoxicity mediated by this therapy[196,197]. Nonetheless, IL-1 up-regulation in pre-clinical models was observed only in studies using immunodeficient mouse engrafted with human immune system cells and may explain the discrepancy. In agreement with the data from the CD19-CAR T model presented herein, others have also not mentioned an increase IL-1 in syngeneic models of CD19-CAR T cell-induced CRS[307].

More severe forms of CRS leading to neurotoxicity are often correlated with hemodynamic instability, capillary leakage, and consumptive coagulopathy[3,33,34,121]. Angiopoietin (Ang)-2 is a biomarker of endothelial activation and promotes microvascular permeability[72,73,78]. In contrast, Ang-1 acts to stabilize the endothelium[80,105]. Increased Ang-2 levels were observed in serum of patients treated with the CD3/CD19 T cell engager, blinatumomab[332], or CAR T cell therapy[104] and was correlated to CRS severity in the later[104]. In both CRS models presented here, an increase level of Ang-2 was also observed, suggesting endothelial activation. Interestingly, prolonged up-regulation of *Ang-2* transcript was observed only in the liver of mice injected with CAR T cells, whereas it remained unchanged in the spleen and the lung. In contrast *Ang-1* was down-regulated in all organs. Since platelets are considered a main source of the Ang-1, thrombocytopenia observed in mice injected with CAR T cell may explain this decrease, and favour the observed hemodynamic instability[105]. The mechanisms that lead to endothelial activation in all setting of CRS have not been characterized. However, the high serum concentrations of endothelium-activating cytokines, such as IL-6 and IFN-γ, also observed in patients with severe CRS, suggest that these cytokines may contribute to the phenomena in the animal models[55] .

# 2 MANAGING CRS

A significant IL-6 and IFN-γ signature was observed in the syngeneic model of CD19-CAR T cell-induced CRS. Of particular interest, IL-6 has been shown to be highly up-regulated and is considered as one of

the major biomarkers of CRS in patients across a plethora of indications[117]. In addition, the anti-IL-6 receptor (IL-6R) mAb, tocilizumab, is to date the only biologic approved by the Food and Drug Administration (FDA) for the treatment of CRS associated with CAR T therapy. While effective at reducing some CRS features, such as fever and hypotension, neurotoxicity, for example, is not reversed[78]. Additionally, tocilizumab is not recommended for severe forms of CRS and more intense treatments, such as methylprednisolone and mechanical ventilation is recommended to prevent death[333]. IL-6 is a well-described and often studied pleiotropic cytokine key for anti-inflammatory and pro-inflammatory responses. IL-6 classic (or cis) signalling is mediated by the binding of the cytokine to the membrane bound IL-6R (mIL-6R). Classic signalling, therefore, drives the activation of a restricted number of cell-subtypes expressing the mIL-6R, including macrophages, neutrophils, hepatocytes, and some T cells. In conditions of low IL-6 levels, this signalling pathway predominates. However, when IL-6 levels are elevated, such as in inflammatory conditions, IL-6 will bind to soluble (s) IL-6R, produced upon shedding of mIL-6R from cell surfaces. The IL-6 *trans*-signalling pathway is then initiated through coupling the IL-6/sIL-6R complex to gp130, the ubiquitously expressed, signal-transducing receptor that forms part of the receptor complex for several cytokines[110-115]. IL-6 *trans*-signalling, therefore, is able to occur systematically due to the wide-spread expression pattern of gp130. While IL-6 cis-signalling appears to mediate the homeostatic and protective activities, the *trans*-signalling pathway is considered as a key driver of dysregulated inflammatory responses leading to disease[111].

To further dissect the potential role for IL-6 signalling for anti-tumour responses and CRS development in the CD19-CAR T cell model, two previously described anti-mouse-IL6R mAbs (mAb 2B10, tocilizumab-like; and the IL-6 *trans*-signalling blocking mAb, 25F10[310]) were used *in vivo*. In a first set of experiments, data suggested that 25F10 was more efficient than 2B10 at reducing CD19-CAR T-induced toxicity, in particular, hepatosplenomegaly. In parallel, IL-6 *trans*-signalling blockade decreased the level of MCP-1 and CXCL10 4 days post CAR T cell injection and may explain the lower infiltration of monocytes/macrophages and neutrophils in the spleen and liver. In addition, levels of IL-2, IFN-$\gamma$, TNF-$\alpha$ were reduced only in mice treated with 25F10, suggesting that blockade of *trans*-signalling reduced the activation potential of monocytes/macrophages and T cells. Importantly, the CD19-CAR T cell mediated anti-tumour activity was not impaired. This set of data was intriguing and suggested that *trans*-signalling may indeed drive CAR-T cell toxicities but may not be needed for effective tumour control, whereas a recent study proposed that IL-6 *trans*-signalling drives the expansion and antitumor activity of CAR T cells in a mouse model[334]. In addition, a subsequent follow up experiment failed to reproduce findings related to the reduction in toxicity with 25F10, albeit tumour control was maintained notwithstanding.

Additional studies are warranted to confirm initial findings that blockade of IL-6 *trans*-signalling affords protection from CAR-T cell induced CRS.

Intriguingly, the level of SAA in serum was only marginally impacted by the anti-IL6R mAb treatments. Since up-regulation of SAA is often considered as a biomarker of IL-6 activity, it suggests here that either the anti-IL6R mAbs did not efficiently inhibit all IL-6 activity, or SAA production was induced by an IL-6-independent pathway. In this study, plasma level of SAA peaked earlier than detectable plasma IL-6, which tends to suggest the second hypothesis.

Although several reports have suggested that IFN-γ plays an important role CAR-T-mediated CRS[56,123], no conclusive studies have directly shown a role of IFN-γ in the syndrome. Nonetheless, the benefit at blocking IFN-γ was demonstrated in other CRS settings. For instance, the prophylactic blockade of IFN-γ in murine model of CRS induced by anti-CD3 mAb protected mice from disease[238,240,241,243]. In addition, emapalumab, an anti-IFN-γ mAb, was approved by the FDA for the treatment of primary HLH, a CRS[243]. In agreement with a putative role for the cytokine in CRS, a significant up-regulation of IFN-γ was also observed in the CD19-CAR T model system herein. Surprisingly, IFN-γ blockade did not impair the anti-tumour CD19-CAR T cell efficacy. Nevertheless, little benefit was observed at reducing CRS features, despite the absence of CXCL9 and CXCL10 production testifying the efficient blockage of IFN-γ *in vivo*. Interestingly, mice injected with the anti-IFN-γ developed unexpected acute sign of illness, characterised by weight lost and hypomobility, 7 days after the last treatment injection (data shown). This result was surprising considering the benefit afforded by IFN-γ blockade in other preclinical models of CRS and where no toxicity was observed[187,330].

In the CD19-CAR T cell mouse model of CRS, the single blockade of IFN-γ or IL-6, both cytokines thought to be the major drivers of the CRS in this model, offered respectively no or weak benefit at reducing CRS symptoms. The failure at controlling CRS features with anti-IL-6R mAbs post CD19-CAR T cell administration was unexpected, since in a humanized mouse models recapitulating key features of CAR-T-cell-mediated CRS, IL-6 blockade protected mice from CRS and neurotoxicity[195,196]. The challenge to interrupt a cytokine storm by targeting IL-6 is still topical as tocilizumab is not universally effective in reversing symptoms of CRS induced by CAR T cells[200]. In addition, this concern was made more evident in a recent clinical study where tocilizumab was ineffective at reducing COVID-19 mortality[203]. Nonetheless, coadministration of TNF-α and IFN-γ-neutralizing antibodies provided superior protection over monotherapy in a mouse SARS-CoV-2 infection model, highlighting a benefit of anti-cytokine

combination therapy[174]. In the anti-CD3 mouse model of CRS studied here, IL-6, IL-2, IFN-γ and TNF-α were shown to precede clinical signs of CRS[300,301]. Akin in the CD19-CAR T cell model of CRS studied, monotherapy blocking of the afore-mentioned cytokines provided poor improvement in mice. However, anti-cytokine mAb cocktail, targeting IFN-γ, IL-6, TNF-α, and IL-2 (herein called anti-cytokine cocktail) significantly reduced the clinical features of CRS induced by anti-CD3 in the first 24 hpi including body weight, prostration, piloerection, and some blood parameters disorders. Ang-2 plasma levels were also significantly reduced by the anti-cytokine cocktail suggesting a reduction in endothelial activation and vascular leakage. Nonetheless, the anti-cytokine cocktail offered transient protective benefit. To prolong the efficacy of the anti-cytokine cocktail, several strategies, such as performed a second injection of the cocktail 12 hours later, or supplemented the anti-cytokine cocktail with IL-1 receptor antagonist or anti-IL-15 mAbs, were investigated without success.

The limited benefit of the anti-IL6R at controlling CD19-CAR T cells-induced CRS, and the difficulties encountered to extend the window of the therapy efficacy in the anti-CD3 mouse model of CRS, parallel challenges faced in the clinical setting with patients suffering from severe forms of CRS.

# 3 CONCLUSION AND PERSPECTIVES

Inherent biological differences between syngeneic mouse systems and humans exist and limit the direct translation from mouse studies to human disease settings. Clinical CRS manifestations of inflammatory toxicities, such as weight and temperature loss, decreased activity, are difficult to reproduce in mice. Hence in the model of moderate CRS induced by CAR T cells, clinical features did not develop in mice. In contrast, the acute inflammatory response induced by the anti-CD3 in mice allowed to recapitulate majority of clinical features observed in human patients.

An infiltration of monocytes/macrophages in the spleen and the liver was observed following injection of the CAR T cells or the anti-CD3 mAb, together with a systemic up-regulation of chemoattractants, such as MCP-1. The impact of depleting monocytes and macrophages in the anti-CD3 was investigated using clodronate liposome. While macrophages were efficiently depleted from spleen and liver, the treatment was ineffective at diminishing the cells from the lung, making the experiment inconclusive. This was disappointing particularly as key role for monocytes/macrophages was demonstrated in mouse models of CRS induced by CAR T cells[195,196].

Another widespread concern in CAR T cell therapy is the development of neurotoxicity[33,34]. In the CAR T cell model studied here, mice injected with the CD19-CAR T cells did not show overt neurological

symptoms, such as seizures, limb dyskinesia or paralysis. Nonetheless, efforts were done for investigating inflammation in the brain, by flow cytometric and mRNA analysis, but without success due to technical issue. The absence of obvious neurological disorders may be explained by the absence of IL-1 up-regulation. Indeed, it was shown by others that IL-1 has a pivotal role in the development of neurotoxicity during CAR-T therapy[195,196] and only IL-1 blockade by anakinra (an IL-1RA) was effective at controlling neurotoxicity[196]. Nonetheless, clinical alterations and/or structural morphological changes were not investigated. Therefore, the occurrence of neurotoxicity mediated by CAR T cells in this model cannot be excluded.

The pathophysiology of CRS is poorly understood, largely because of the lack of experimental models that recapitulate all toxicities seen in patients. Two models were developed in the aim of bridging this knowledge gap; the first relying on potent *in vivo* T cell activation mediated by an anti-CD3ε mAb, while the second investigated CAR T cell-induced CRS in mice transplanted with A20 B cell lymphoma cells. The anti-CD3 mAbs-induced CRS syndrome in mice is characterized by acute weight loss, splenomegaly and hemotoxicity. The cytokine hierarchy in this CRS mouse model was described with inflammatory mediators associated with T-cell and macrophage activation rapidly upregulated. In particular IL-2, IFN-γ and IL-6 preceded the development of several clinical and laboratory features of CRS. In addition, the central role of the recruitment of pathogenic neutrophils and macrophages in organs was highlighted. CRS mediated by mouse CD19-CAR T cells is also characterized by an up-regulation of pro-inflammatory mediators, including Th1 cytokines (IFN-γ and TNF-α) and IL-6, most likely produced by monocytes/macrophages. The latter, together with neutrophils, were also shown to infiltrate the spleen and the liver, resulting in development of hepatosplenomegaly, a hallmark of human CRS.

Another important aim of the project was to address whether blockade of proinflammatory cytokines, impacted clinical and laboratory features of CRS. In the anti-CD3 model, an anti-cytokine mAb cocktail, targeting IFN-γ, IL-6, TNF-α, and IL-2, reduced the clinical features of CRS in the first 24 hours, including body weight loss, prostration, piloerection, some hemotoxicity parameters and lung inflammation. While the benefit of the anti-cytokine cocktail was transient, it afforded a superior benefit as compared to the monotherapy administration of the anti-cytokine mAbs. Monotherapy targeting either IL-6 or IFN-γ in the CAR T cells model of CRS also afforded benefit but the finding was not reproducible upon a repeated experiment. Surprisingly, blockade of IL-6 or IFN-γ did not impair the CAR T cell therapy efficacy. Moreover, to further elucidate a beneficial vs pathogenic role for IL-6 in the model, the impact

of an anti-IL6R mAb that specifically inhibits the *trans*-signalling pathway was investigated. Preliminary data suggested that the blockade of IL-6 *trans*-signalling reduced some CRS features including monocytosis, hepatomegaly, and the associated myeloid cells infiltration. Hence, it suggests that IL-6-trans-signalling may be linked to CRS parameters, but is not obligate for CAR-T cell induced tumour control, since control of the tumour growth by CD19-CAR T cells was not impacted.

The systemic immune changes occurring during toxicity induced by anti-CD3-mediated activation of T cells or CD19-CAR T cells were investigated in this project. It was shown that activation of T cells drove subsequent activation of myeloid cells, resulting in an up-regulation of T cell- and monocytes/macrophages-derived cytokines, including IFN-γ, TNF-α, IL-2 and IL-6, and the recruitment of those immune cells to organs. Hence, the data suggest that the early monitoring of blood biomarkers in CRS-susceptible patients may help to identify risk profiles patients.

The challenge to abrogate disease with an anti-cytokine approach highlighted the complexities of severe T cell mediated CRS. This limitation also suggests that while an anti-cytokine therapy is a therapeutic option for less-severe cases, the addition of potent corticosteroids may be needed as an option to manage severe forms of CRS.

Taken together, this work describes two models of CRS which may offer insights to further decipher mechanisms underpinning the CRS across multiple indications. Most importantly, these models could be use as predictive tools for evaluation of novel anti-cytokine and additional innovative strategies (such as JAK inhibitors) to manage CRS in patients.

# ABBREVIATIONS

CRS: cytokine release syndromes
CAR: chimeric antigen receptor
IFN: interferon
IL: interleukin
TNF: tumour necrosis factor
mAb: monoclonal antibody
ARDS: acute respiratory distress syndrome
ICANS: immune effector cell-associated neurotoxicity syndrome
HLH: hemophagocytic lymphohistiocytosis
MAS: macrophage activation syndrome
CRP: C-reactive protein
LDH: lactate dehydrogenase
DIC: disseminated intravascular coagulation
Ang: angiopoietin
RBC: red blood cells
SAA: serum amyloid A
MCP: monocyte chemoattractant protein
GM-CSF: granulocyte-macrophage colony-stimulating factor
NO: nitric oxide
iNOS: inducible nitric oxide synthases
CD40L: CD40 ligand
IL1-RA: IL-1 receptor antagonist
NOD: non-obese diabetic
SCID: severe combined immunodeficiency
NSG: NOD SCID gamma
MIP: macrophage inflammatory protein
EC: endothelial cell
CSF: cerebral spinal fluid
CNS: central nervous system
TIM-3: T cell immunoglobulin mucin 3
PD-1: programmed cell death protein 1
SARS-CoV-2: severe acute respiratory syndrome coronavirus 2
ACE2: angiotensin-converting enzyme 2
ROS: reactive oxygen species
NET: neutrophil extracellular traps
BALF: bronchoalveolar lavage fluid
APC: antigen presented cell
SJIA: systemic juvenile idiopathic arthritis
PBMC: peripheral blood mononuclear cell
HSC: human hematopoietic stem cells
HuHep: human hepatocytes
BLT: bone marrow-liver-thymus
X-GVHD: xenogeneic graft-versus-host disease
HSPC: hematopoietic stem and progenitor cell
nHuSGM3: newborn SGM3 mice transplanted with HSPCs
RA: rheumatoid arthritis
EMA: European Medicines Agency
BiTE: bispecific T cell engager
FDA: Food and Drug Administration
mIL-6R: membrane IL-6 receptor
sIL-6R: soluble IL-6 receptor

# ANNEX

Arm1:
ACTAGTGCTTACATAGTCTAACTCGCGACACTGTAATTTCATACTGTAGTAAGGATCTCAAGCAGGAGAGTATAAA
ACTCGGGTGAGCATGTCTTTAATCTACCTCGATGGAAAATACTCCGAGGCGGATCACAAGCAATAATAACCTGTAG
TTTTGCTGCATAAAACCCCAGATGACTACCTATCCTCCCATTTTCCTTATTTGCCCCTATTAAAAAACTTCCCGACAA
AACCGAAAATCTGTGGGAAGTCTTGTCCCTCCAATTTTACACCTGTTCAATTCCCCTGCAGGACAACGCCCACACAC
CAGGTTAGCCTTTAAGCCTGCCCAGAAGACTCCCGCCCATCTTCTAGAAAGACTGGAGTTGCAGATCACGAGGGA
AGAGGGGGAAGGGATTCTCCCAGGCCCAGGGCGGTCCTCAGAAGCCAGGAGGCAGCAGAGAACTCCCAGAAAG
GTATTGCAACACTCCCCTCCCCCCTCCGGAGAAGGGTGCGGCCTTCTCCCCGCCTACTCCACTGCAGCTCCCTTACT
GATAACAACTCAGAGCGACTTTGGGAGAGCAAGTGCTTCCTGCCTCCAAAACAGCCCAACTGAGCCCTCGCTCCTT
CCCTCCACTCCCCGGAGTGCGCGATGGAGGTCTGGCTCAGCACGCCCCTCTTGAGGCAACTCAAGTCGGAAACGT
GCTTGCACCCGCCCCGCAGCCGCTCAGCCCTACTGCCCGTCCCCGCCCCCAGCGCGCGCTTCCTGCCACGTCGGCA
TAA

Arm2:
GATCCAGGGGCGCGCGGCCAGACTCTGCGGCGCGGGGCCGAGGGGAGGGCCGGAACCTGGGAGCGCCTCCTCG
CCGCCCCCGCTGGCCGGCGGATGGACTCAACTTGCACGAACACGAGCCAATGGCAAGGGCCAGTTTTCTGGGCCC
CGAGAGCCAATCAGACGACGAGGCCCGGCCGGCGGCGGGTAAAACGACTCCCCCAGAGGAAGGGGAGGGTGG
GCGGCCGCTCGCGCGCGAGCTACTTTCGCTGACCCTCCCTCCCCTCCCCCGCCCCGCCAGAGGCCGACCGCGCCCG
CACGTCCAGCTCGCCTCACCCCACCTACCTCCCGCCCCACCCAGTGGGCAGAGCGAGGCTGCCGGCGGCTGCGCA
CTCCGGCTGCCGTTAACTGACAGGCGCCTTACGCCAACCAAAACACGCCATTTGTGTTTTCACACACGGCGGGAGG
AAAAGAAGCCAATCAGCGACGAGACGTCGGCCGGAAGCGCTCCTCCGCTGCCCCCCCCCCCCCGAGCCATGGCCG
CGTCCGGTGGAGACTTTTCCGCTCCCTTCTCCCTCCCCCTCCGGTTGCTGCAGGGCGGACCGCATTCCTGCCCACCA
CCCGCTTGCCCCTTCCAGCGTCACGACTCGTACCCGGCTGTCTCACAGAACGGCTCCACCACGCTCGGAGGGCCTG
CCGCGGCCGCCCATCCCCGCAAACGCACCAAGCCGCCCTCCCGCCAGAGTCCCGATCCCCTACCTAGCCGAGGCTC
TCTGAGGAGCCG

Annex 1: DNA sequence of the homology arms for A20 genome editing into Rosa26 locus.

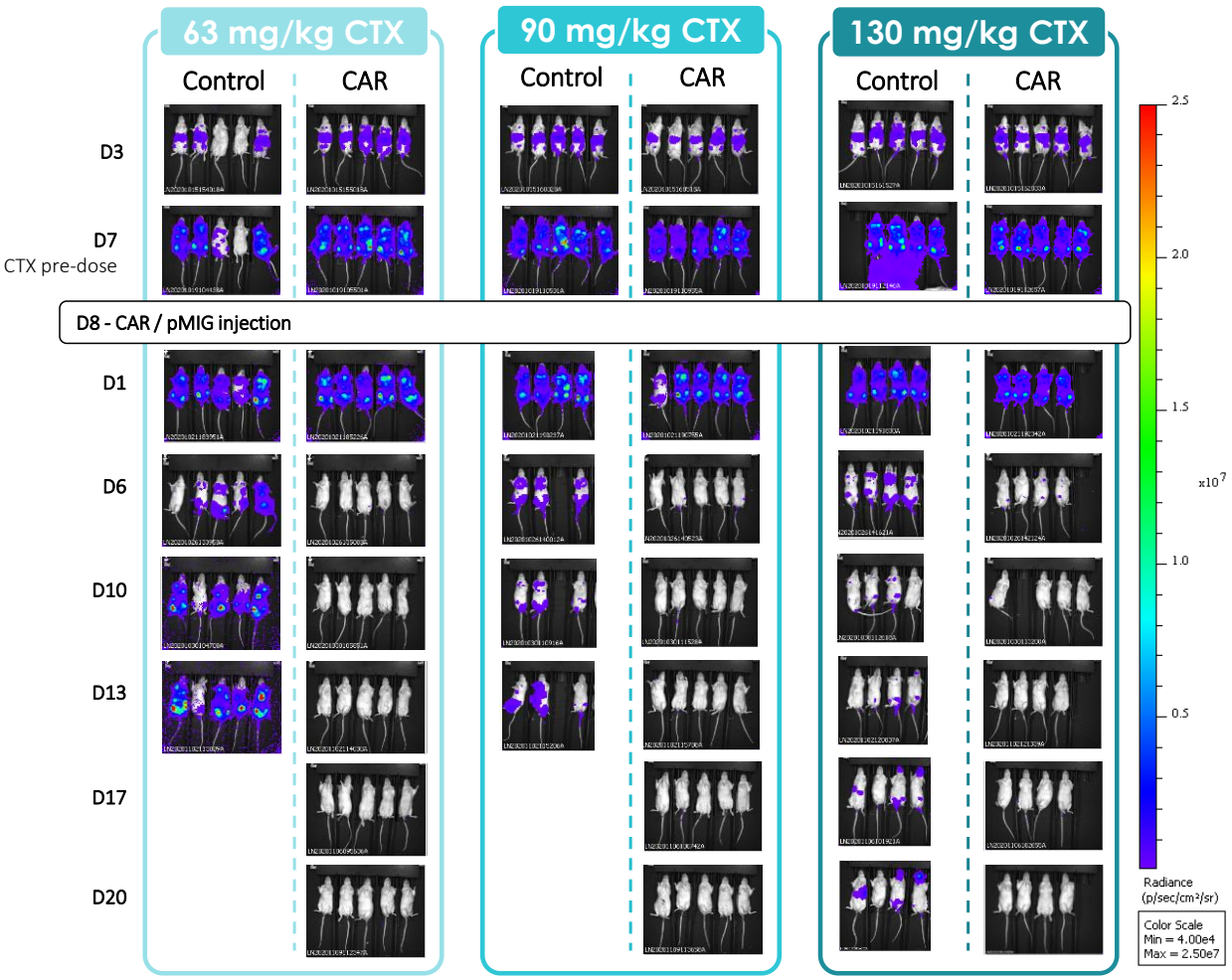


Annex 2: Bioluminescence images of mouse bearing A20-Luc lymphoma treated with CAR T cell therapy. Seven days post A20-Luc lymphoma engraftment, mice were imaged, randomized, and received i.p. indicated dose of CTX. The day after, mice were infused with Control-CAR or CD19-CAR T cells. Tumour growth was followed by bioluminescence.

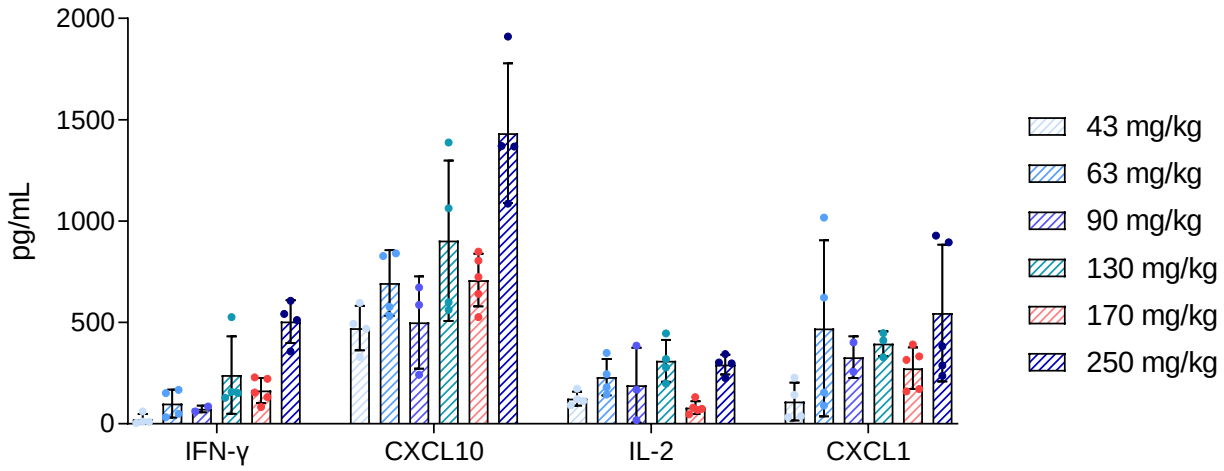


Annex 3: Cytokine expression depends on the CTX-pre-conditioning dose prior CAR T cells infusion. Mice bearing A20 lymphome model were treated with CAR T cell therapy. On day prior treatment administration, different CTX doses were i.p. administrated. Two- or three-days post treatment, plasma was collected by tail vein micro-bleeding and cytokines quantified using a multiplex assay. Data representative of two experiments, n=3-5 mice per condition.

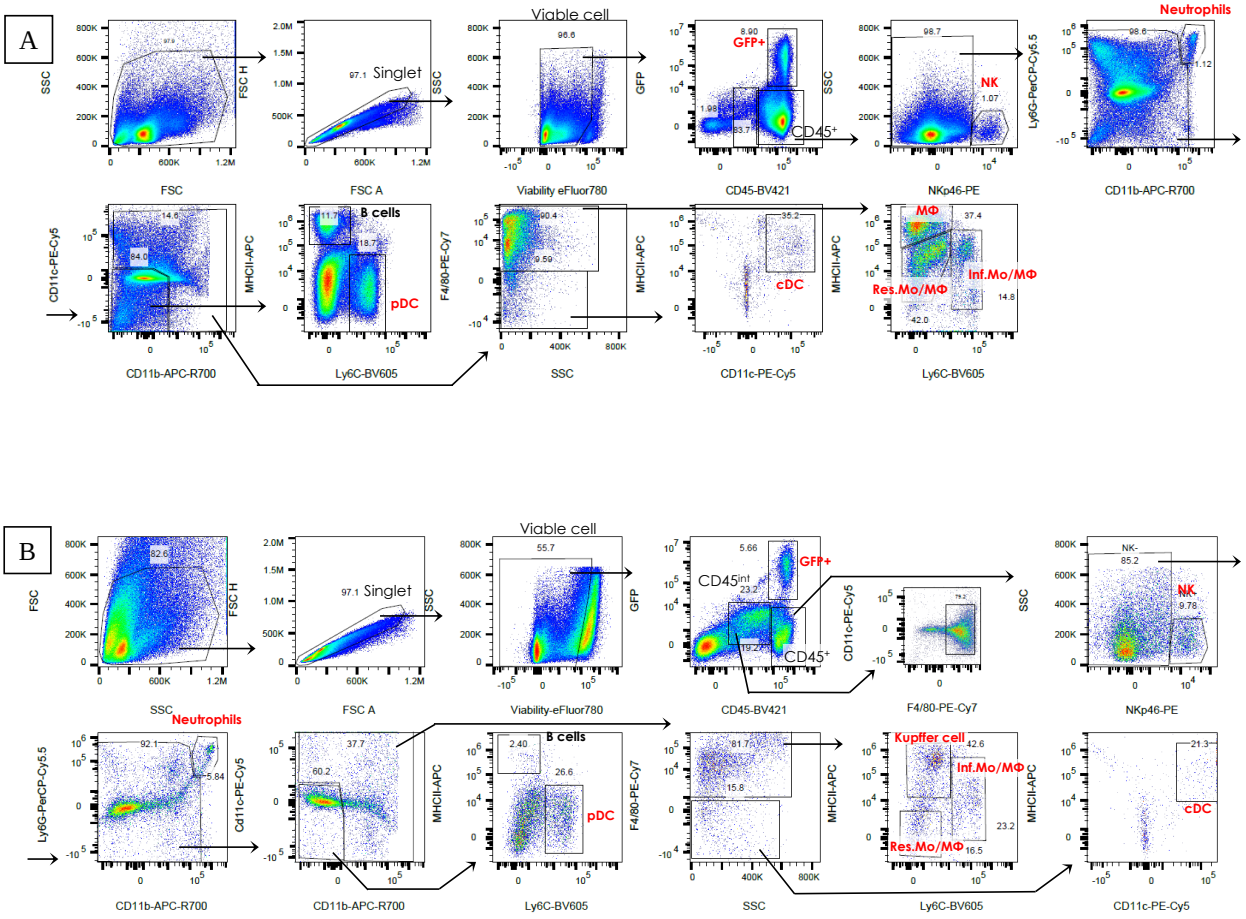


Annex 4: Gating strategies for flow cytometry analysis. Single-cells suspension were prepared from spleen (A) and liver (B). After the exclusion of debris, doublets and dead cells, Control- and CD19-CAR T cells were identified as $CD45^{+}GFP^{+}$ cells and other immune cells were identified by CD45 positive staining. A sequential gating strategy was then used to identify populations expressing specific markers: natural killer (NK) cells ($NKp46^{+}$), neutrophils ($CD11b^{high}Ly6G^{+}$). Identification of populations with overlapping expression patterns was done as followed: lymphoid cells, $CD11c^{-}CD11b^{-}$; myeloid cells, $CD11c^{pos}CD11b^{pos}$. From myeloid cells, subtypes distinction was done as followed: macrophage (or Kupffer cell) $F4/80^{pos}MHCII^{pos}Ly6C^{low}$; inflammatory monocytes/macrophages $MHCII^{int/high}Ly6C^{high}$; resident monocytes/macrophages, $MHCII^{low}Ly6C^{-/low}$. Definition of abbreviations: NK, natural killer; Mϕ, macrophages; inf.Mo/Mϕ, inflammatory monocytes/Mϕ; res.Mo/Mϕ, resident monocytes/Mϕ; MHCII, major histocompatibility complex class II; FSC, forward scatter; SSC, side scatter.

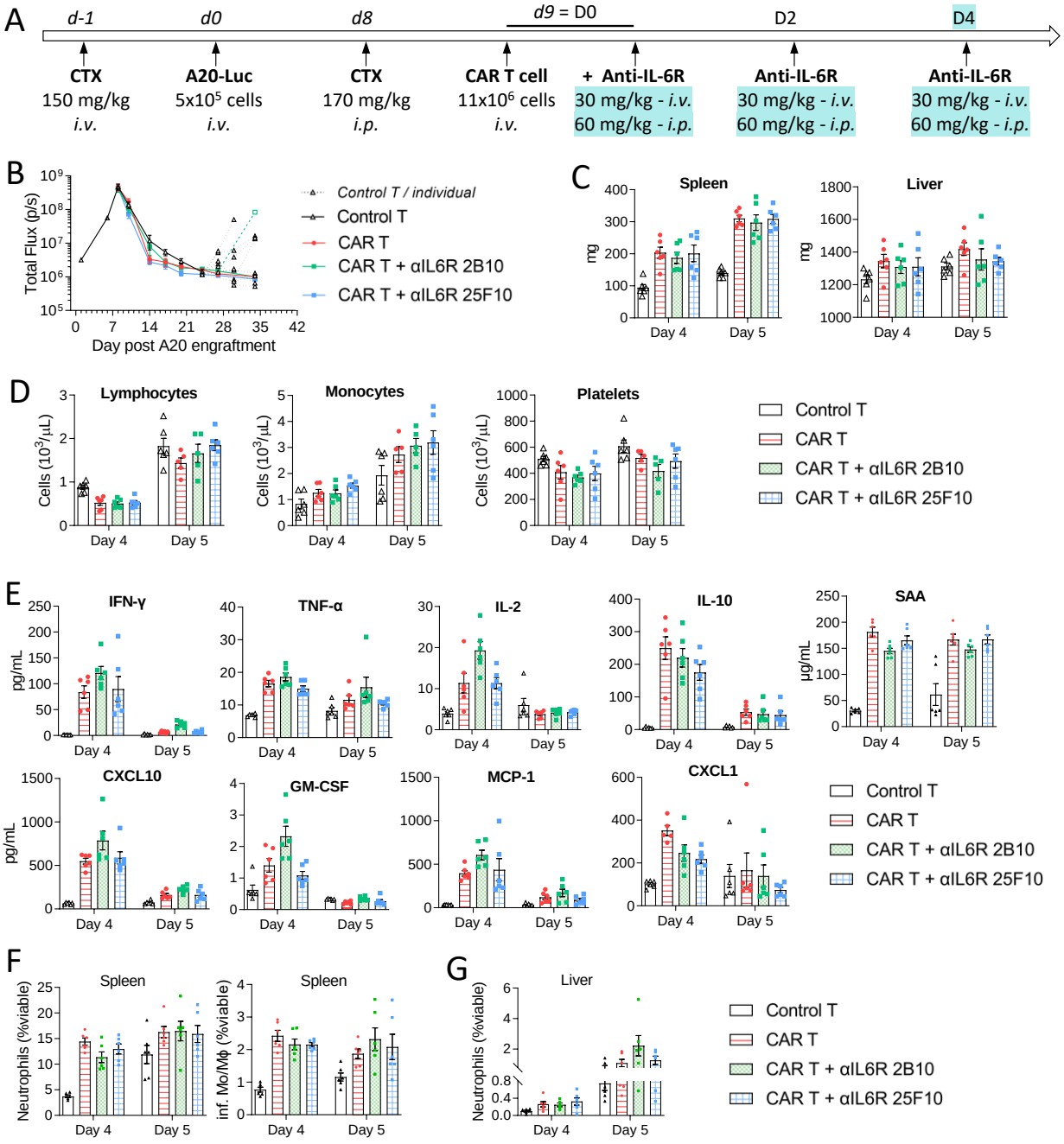


Annex 5: Highest dose of anti-IL-6R did not improve therapy benefit. (A) Mice bearing lymphoma model were treated with Control- or CD19-CAR T cell therapy and anti-IL-6R mAbs, clone 25F10 or 2B10. (B) bioluminescence follow-up. (C) Spleen and liver weight. (D) Blood parameters including lymphocyte, monocyte and platelet counts. (E) Plasma cytokines and chemokines quantification using MSD U-PLEX assay kits or ELISA assays. (F) Single cell-suspensions from the spleen and liver were prepared 4 days post CAR T infusion, followed by immunophenotyping. Neutrophils and inflammatory monocytes/macrophages (inf. Mo/MΦ) frequencies are expressed as a percentage of viable cells. Gating strategies are available in Annex 4. Preliminary data from of one single experiment, n=5-6 mice per group. Values are displayed as mean ± SEM.

# BIBLIOGRAPHY


1 Ferrara JL, Abhyankar S, Gilliland DG. Cytokine storm of graft-versus-host disease: a critical effector role for interleukin-1. *Transplant Proc.* 1993;25:1216–1217.

2 Tisoncik JR, Korth MJ, Simmons CP, Farrar J, Martin TR and Katze MG. Into the eye of the cytokine storm. *Microbiol Mol Biol Rev.* 2012;76:16–32.

3 Fajgenbaum DC, June CH. Cytokine Storm. *New England Journal of Medicine*. 2020 Dec 3;383(23):2255–73.

4 Ian A Clark. The advent of the cytokine storm. *Immunology and Cell Biology*. 2007;85:271–273.

5 Barry SM, Johnson MA, Janossy G. 2000. Cytopathology or immunopathology? The puzzle of cytomegalovirus pneumonitis revisited. *Bone Marrow Transplant*. 2000;26:591–597.

6 Imashuku S. Clinical features and treatment strategies of Epstein-Barr virus-associated hemophagocytic lymphohistiocytosis. *Crit. Rev. Oncol. Hematol.* 2002;44:259 –272.

7 Bisno AL, Brito MO, Collins CM. Molecular basis of group A streptococcal virulence. *Lancet Infect. Dis*. 2003;3:191–200.

8 Liu Q, Zhou YH and Yang ZQ. The cytokine storm of severe influenza and development of immunomodulatory therapy. *Cell Mol Immunol.* 2016;13:3–10.

9 Yuen KY, Wong SS. Human infection by avian influenza A H5N1. *Hong Kong Med J.* 2005;11:189–199.

10 Jahrling PB, Hensley LE, Martinez MJ, et al. Exploring the potential of variola virus infection of cynomolgus macaques as a model for human smallpox. *Proc Natl Acad Sci USA.* 2004;101:15196–15200.

11 Srikiatkhachorn A, Mathew A and Rothman AL. Immune-mediated cytokine storm and its role in severe dengue. *Semin Immunopathol.* 2017;39:563–574.

12 Patro ARK, Mohanty S, Prusty BK, et al. Cytokine signature associated with disease severity in dengue. *Viruses*. 2019;11:34.

13 Prescott JB, Marzi A, Safronetz D, et al. Immunobiology of Ebola and Lassa virus infections. *Nat Rev Immunol*. 2017;17:195–207.

14 Wauquier N, Becquart P, Padilla C, Baize S and Leroy EM. Human fatal zaire ebola virus infection is associated with an aberrant innate immunity and with massive lymphocyte apoptosis. *PLoS Negl Trop Dis*. 2010;4(10):e837.

15 Mehta P, Mcauley DF, Brown M, Sanchez E, Tattersall RS and Manson JJ. COVID-19: consider cytokine storm syndromes and immunosuppression. *Lancet*. 2020;395(10229):1033–1034.

16 Vaninov N. In the eye of the COVID-19 cytokine storm. *Nat Rev Immunol*. 2020;20(5):277.

17 Chatenoud L, Ferran C, Reuter A, et al. Systemic reaction to the anti-T-cell monoclonal antibody OKT3 in relation to serum levels of tumour necrosis factor and interferon-gamma. *N Engl J Med*. 1989;320(21):1420–1421.

18 Chatenoud L, Ferran C, Legendre C, et al. In vivo cell activation following OKT3 administration. Systemic cytokine release and modulation by corticosteroids. *Transplantation*. 1990;49(4):697–702.

19 Suntharalingam G, Perry MR, Ward S, et al. Cytokine storm in a phase 1 trial of the anti-CD28 monoclonal antibody TGN1412. *N Engl J Med*. 2006;355(10):1018–1028.

20 Winkler U, Jensen M, Manzke O, Schulz H, Diehl V, Engert A. Cytokine-release syndrome in patients with B-cell chronic lymphocytic leukemia and high lymphocyte counts after treatment with an anti-CD20 monoclonal antibody (rituximab, IDEC-C2B8). *Blood*. 1999;94(7):2217-2224.

21 Freeman CL, Morschhauser F, Sehn L, et al. Cytokine release in patients with CLL treated with obinutuzumab and possible relationship with infusion-related reactions. *Blood*. 2015;126(24):2646-2649.

22 Wing MG, Moreau T, Greenwood J, et al. Mechanism of first-dose cytokine-release syndrome by CAMPATH 1-H: involvement of CD16 (FcgammaRIII) and CD11a/CD18 (LFA-1) on NK cells. *J Clin Invest*. 1996;98(12):2819–2826.

23 Alig SK, Dreyling M, Seppi B, Aulinger B, Witkowski L, Rieger CT. Severe cytokine release syndrome after the first dose of Brentuximab Vedotin in a patient with relapsed systemic anaplastic large cell lymphoma (sALCL): a case report and review of literature. *Eur J Haematol*. 2015;94(6):554–557.

24 de Vos S, Forero-Torres A, Ansell SM, et al. A phase II study of dacetuzumab (SGN-40) in patients with relapsed diffuse large B-cell lymphoma (DLBCL) and correlative analyses of patient-specific factors. *J Hematol Oncol*. 2014;7:44.

25 Rotz SJ, Leino D, Szabo S, Mangino JL, Turpin BK, Pressey JG. Severe cytokine release syndrome in a patient receiving PD-1-directed therapy. *Pediatr Blood Cancer*. 2017;64(12):e26642.

26 Topp MS, Gökbuget N, Stein AS, et al. Safety and activity of blinatumomab for adult patients with relapsed or refractory B-precursor acute lymphoblastic leukaemia: a multicentre, single-arm, phase 2 study. *Lancet Oncol.* 2015;16(1):57-66.

27 Teachey DT, Rheingold SR, Maude SL, et al. Cytokine release syndrome after blinatumomab treatment related to abnormal macrophage activation and ameliorated with cytokine-directed therapy. *Blood*. 2013 Jun 27;121(26):5154–5157.

28 Teachey DT, Lacey SF, Shaw PA, et al. Identification of Predictive Biomarkers for Cytokine Release Syndrome after Chimeric Antigen Receptor T-cell Therapy for Acute Lymphoblastic Leukemia. *Cancer Discov*. 2016;6(6):664–679.

29 Morgan RA, Yang JC, Kitano M, Dudley ME, Laurencot CM, Rosenberg SA. Case report of a serious adverse event following the administration of T cells transduced with a chimeric antigen receptor recognizing ERBB2. *Mol Ther*. 2010;18(4):843–851.

30 Brudno JN, Kochenderfer JN. Toxicities of chimeric antigen receptor T cells: recognition and management. *Blood*. 2016;127(26):3321-3330.

31 JCAR015 in ALL: A Root-Cause Investigation. *Cancer Discov*. 2018; 8(1):4-5.

32 D'Elia RV, Harrison K, Oyston PC, Lukaszewski RA, Clark GC. Targeting the "Cytokine Storm" for Therapeutic Benefit. *Clin Vaccine Immunol*. 2013;20(3):319–327.

33 Shimabukuro-Vornhagen A, Gödel P, Subklewe M, et al. Cytokine release syndrome. *J Immunother Cancer*. 2018 Jun 15;6(1):56.

34 Lee DW, Santomasso BD, Locke FL, et al. ASTCT consensus grading for cytokine release syndrome and neurologic toxicity associated with immune effector cells. *Biol Blood Marrow Transplant*. 2019;25(4):625-638.

35 Moradian N, Gouravani M, Salehi MA, et al. Cytokine release syndrome: inhibition of pro-inflammatory cytokines as a solution for reducing COVID-19 mortality. *Eur Cytokine Netw*. 2020;31(3):81–93.

36 Neelapu SS, Tummala S, Kebriaei P, et al. Chimeric antigen receptor T-cell therapy - assessment and management of toxicities. *Nat Rev Clin Oncol*. 2018 Jan;15(1):47–62.

37 Brudno JN, Kochenderfer JN. Recent advances in CAR T-cell toxicity: Mechanisms, manifestations and management. *Blood Reviews*. 2019 Mar 1;34:45–55.

38 Black S, Kushner I, Samols D. C-reactive protein. *J Biol Chem*. 2004;279(47):48487–48490.

39 Schuster SJ, Maziarz RT, Rusch ES, et al. Grading and management of cytokine release syndrome in patients treated with tisagenlecleucel in the JULIET trial. *Blood Adv*. 2020 Apr 9;4(7):1432–9.

40 Morris G, Bortolasci CC, Puri BK, et al. The cytokine storms of COVID-19, H1N1 influenza, CRS and MAS compared. Can one sized treatment fit all? *Cytokine*. 2021;144:155593.

41 Reisler RB, Yu C, Donofrio MJ, et al. Clinical Laboratory Values as Early Indicators of Ebola Virus Infection in Nonhuman Primates. *Emerg Infect Dis*. 2017 Aug;23(8):1316–24.

42 Vuong NL, Le Duyen HT, Lam PK, et al. C-reactive protein as a potential biomarker for disease progression in dengue: a multi-country observational study. *BMC Med.* 2020 Feb 17;18(1):35.

43 Vasileva D, Badawi A. C-reactive protein as a biomarker of severe H1N1 influenza. *Inflamm Res*. 2019;68(1):39–46.

44 Cappanera S, Palumbo M, Kwan SH, et al. When Does the Cytokine Storm Begin in COVID-19 Patients? A Quick Score to Recognize It. *J Clin Med.* 2021 Jan 15;10(2):297.

45 Chen G, Wu D, Guo W, et al. Clinical and immunological features of severe and moderate coronavirus disease 2019. *J Clin Invest*. 2020 May 1;130(5):2620–2629.

46 Davila ML, Riviere I, Wang X, et al. Efficacy and toxicity management of 19-28z CAR T cell therapy in B cell acute lymphoblastic leukemia. *Sci Transl Med*. 2014 Feb 19;6(224):224ra25.

47 Mei H, Jiang H, Wu Y, et al. Neurological toxicities and coagulation disorders in the cytokine release syndrome during CAR-T therapy. *British Journal of Haematology*. 2018;181(5):689–692.

48 Lee DW, Gardner R, Porter DL, et al. Current concepts in the diagnosis and management of cytokine release syndrome. *Blood*. 2014 Jul 10;124(2):188–95.

49 Nägele V, Kratzer A, Zugmaier G, Holland C, Hijazi Y, Topp MS, *et al.* Changes in clinical laboratory parameters and pharmacodynamic markers in response to blinatumomab treatment of patients with relapsed/refractory ALL. *Exp Hematol Oncol*. 2017 May 18;6:14.

50 Poggiali E, Zaino D, Immovilli P, Rovero L, Losi G, Dacrema A, *et al.* Lactate dehydrogenase and C-reactive protein as predictors of respiratory failure in CoVID-19 patients. *Clin Chim Acta*. 2020 Oct; 509:135–138.

51 Velavan TP, Meyer CG. "Mild versus severe COVID-19: laboratory markers". *Int of Infect Dis.* 2020;95:304–307.

52 Litton E, Lim J. Iron Metabolism: An Emerging Therapeutic Target in Critical Illness. *Critical Care*. 2019 Mar 9;23(1):81.

53 Banchini F, Cattaneo GM, Capelli P. Serum ferritin levels in inflammation: a retrospective comparative analysis between COVID-19 and emergency surgical non-COVID-19 patients. *World J Emerg Surg*. 2021 Mar 8;16(1):9.

54 Zhang Z, Wang J, Ji B, et al. Clinical presentation of hemophagocytic lymphohistiocytosis in adults is less typical than in children. *Clinics (Sao Paulo).* 2016 Apr;71(4):205–209.

55 Wang J, Doran J. The Many Faces of Cytokine Release Syndrome-Related Coagulopathy. *Clinical Hematology International*. 2021 Jan;3(1):3–12.

56 Wang Z, & Han W. Biomarkers of cytokine release syndrome and neurotoxicity related to CAR-T cell therapy. *Biomark Res*. 2018 Jan 22;6(1):4.

57 Rollin PE, Bausch DG, Sanchez A. Blood chemistry measurements and D-Dimer levels associated with fatal and nonfatal outcomes in humans infected with Sudan Ebola virus. *J Infect Dis*. 2007 Nov 15;196 Suppl 2:S364-2371.

58 Wang Y, Qi K, Cheng H, et al. Coagulation Disorders after Chimeric Antigen Receptor T Cell Therapy: Analysis of 100 Patients with Relapsed and Refractory Hematologic Malignancies. *Biol Blood Marrow Transplant*. 2020 May;26(5):865–75.

59 Keller TT, Mairuhu ATA, de Kruif MD, et al. Infections and endothelial cells. *Cardiovascular Research*. 2003 Oct 15;60(1):40–48.

60 Fosse JH, Haraldsen G, Falk K, Edelmann R. Endothelial Cells in Emerging Viral Infections. *Front Cardiovasc Med*. 2021;8:619690.

61 Wahl-Jensen VM, Afanasieva TA, Seebach J, Ströher U, Feldmann H, Schnittler H-J. Effects of Ebola Virus Glycoproteins on Endothelial Cell Activation and Barrier Function. *J Virol*. 2005 Aug;79(16):10442–1050.

62 Spiropoulou CF, Srikiatkhachorn A. The role of endothelial activation in dengue haemorrhagic fever and hantavirus pulmonary syndrome. *Virulence*. 2013 Jul 10;4(6):525–536.

63 Teijaro JR, Walsh KB, Cahalan S et al. Endothelial cells are central orchestrators of cytokine amplification during influenza virus infection. *Cell.* 2011 Sep 16;146(6):980–991.

64 Hay KA, Hanafi L-A, Li D, et al. Kinetics and biomarkers of severe cytokine release syndrome after CD19 chimeric antigen receptor–modified T-cell therapy. *Blood*. 2017 Nov 23;130(21):2295–2306.

65 Falasca L, Agrati A, Petrosillo N, et al. Molecular mechanisms of Ebola virus pathogenesis: focus on cell death. *Cell Death Differ*. 2015;22(8):1250–1259.

66 Lalle E, Biava M, Nicastri E et al. Pulmonary Involvement during the Ebola Virus Disease. *Viruses*. 2019 Aug 24;11(9):780.

67 de Wit E, van Doremalen N, Falzarano D, Munster VJ. SARS and MERS: recent insights into emerging coronaviruses. *Nat Rev Microbiol.* 2016 Aug;14(8):523–534.

68 Kernan KF, Carcillo JA. Hyperferritinemia and inflammation. *Int Immunol*. 2017;29(9):401–409.

69 Cassat JE, Skaar EP. Iron in Infection and Immunity. *Cell Host Microbe*. 2013 May 15;13(5):509–519.

70 Allen CE, Yu X, Kozinetz CA, McClain KL. Highly elevated ferritin levels and the diagnosis of hemophagocytic lymphohistiocytosis. *Pediatr Blood Cancer*. 2008;50(6):1227–1355.

71 Eloseily EM, Weiser P, Crayne CB, et al. Benefit of anakinra in treating pediatric secondary hemophagocytic lymphohistiocytosis. *Arthritis Rheumatol*. 2020;72(2):326–334.

72 Nicolini G, Forini F, Kusmic C, Iervasi G, Balzan S. Angiopoietin 2 signal complexity in cardiovascular disease and cancer. *Life Sci*. 2019;239:117080.

73 Li F, Yin R, Guo Q. Circulating angiopoietin-2 and the risk of mortality in patients with acute respiratory distress syndrome: a systematic review and meta-analysis of 10 prospective cohort studies. *Ther Adv Respir* Dis. 2020;14:1753466620905274 .

74 Smadja DM, Guerin CL, Chocron R, et al. Angiopoietin-2 as a marker of endothelial activation is a good predictor factor for intensive care unit admission of COVID-19 patients. *Angiogenesis*. 2020;23(4):611–620.

75 Yildizhan E, Kaynar L. Cytokine release syndrome. *Journal of Oncological Sciences*. 2018;4(3):134–41.

76 Chandra H, Chandra S, Kaushik R, Bhat N, Shrivastava V. Hemophagocytosis on bone marrow aspirate cytology: single center experience in north himalayan region of india. *Ann Med Health Sci. Res*. 2014;4(5):692–696.

77 Cosenza, M.; Sacchi, S.; Pozzi, S. Cytokine release syndrome associated with T-cell-based therapies for hematological malignancies: pathophysiology, clinical presentation, and treatment. Int. J. Mol. Sci. 2021; 22:7652.

78 Morris EC, Neelapu SS, Giavridis T, Sadelain M. Cytokine release syndrome and associated neurotoxicity in cancer immunotherapy. *Nat Rev Immunol*. 2021 May 17;1–12.

79 Siegler EL, Kenderian SS. Neurotoxicity and Cytokine Release Syndrome After Chimeric Antigen Receptor T Cell Therapy: Insights Into Mechanisms and Novel Therapies. *Front Immunol*. 2020 Aug 28;11:1973.

80 Hay KA. Cytokine release syndrome and neurotoxicity after CD19 chimeric antigen receptor-modified (CAR-) T cell therapy. *British J Haematol.* 2018;183(3):364–74.

81 Brudno JN, Maric I, Hartman SD, et al. T cells genetically modified to express an anti-B-cell maturation antigen chimeric antigen receptor cause remissions of poor-prognosis relapsed multiple myeloma. *J Clin Oncol*. 2018;36(22):2267–2280.

82 Alfred L, Garfall E, Edward A, et al. Posterior reversible encephalopathy syndrome (PRES) after infusion of anti-Bcma CAR T Cells (CART-BCMA) for multiple myeloma: successful treatment with cyclophosphamide. *Blood*. 2016;128:5702.

83 Liang A, Ye S, Li P, et al. Safety and efficacy of a novel anti-CD20 chimeric antigen receptor (CAR)-T cell therapy in relapsed/refractory (r/r) B-cell non-Hodgkin lymphoma (B-NHL) patients after failing CD19 CAR-T therapy. *JCO*. 2021;39(15):2508–2508.

84 Fry TJ, Shah NN, Orentas RJ, et al. CD22-targeted CAR T cells induce remission in B-ALL that is naive or resistant to CD19-targeted CAR immunotherapy. *Nat Med.* 2018;24(1):20–28.

85 Santomasso B, Bachier C, Westin J, Rezvani K, Shpall EJ. The other side of car t-cell therapy: cytokine release syndrome, neurologic toxicity, and financial burden. *Am Soc Cl. Onc Educ Book*. 2019;39:433–444.

86 Ruella M, Kenderian SS, Shestova O, et al. The addition of the BTK inhibitor Ibrutinib to anti-CD19 chimeric antigen receptor T cells (CART19) improves responses against mantle cell lymphoma. *Clin Cancer Res*. 2016;22(11):2684–2696.

87 Ruella M, Kenderian SS, Shestova O, et al. Kinase inhibitor ibrutinib to prevent cytokine-release syndrome after anti-CD19 chimeric antigen receptor T cells for B-cell neoplasms. *Leukemia*. 2017;31(1):246–248.

88 Murthy H, Iqbal M, Chavez JC, Kharfan-Dabaja MA. Cytokine release syndrome: current perspectives. *Immunotargets Ther*. 2019 Oct 29;8:43–52.

89 Lee DW, Kochenderfer JN, Stetler-Stevenson M, et al. T cells expressing CD19 chimeric antigen receptors for acute lymphoblastic leukaemia in children and young adults: a phase 1 dose-escalation trial. *Lancet*. 2015 Feb 7;385(9967):517–528.

90 van der Stegen SJC, Hamieh M, Sadelain M. The pharmacology of second-generation chimeric antigen receptors. *Nat Rev Drug Discov*. 2015;14(7):499–509.

91 Neelapu SS, Locke FL, Bartlett NL, et al. Axicabtagene Ciloleucel CAR T-cell therapy in refractory large B-cell lymphoma. *N Engl J Med*. 2017;377:2531–2544.

92 Schuster RA, Hong SY, Arnold RM, White DB. Investigating conflict in ICUs-is the clinicians' perspective enough? *Crit Care Med*. 2014;42(2):328–335.

93 Santomasso BD, Park JH, Salloum D, et al. Clinical and biological correlates of neurotoxicity associated with CAR T-cell therapy in patients with B-cell acute lymphoblastic leukemia. *Canc Disc*. 2018 Aug 8;8(8):958–971.

94 Turtle CJ, Hudecek M, Jensen MC, Riddell SR. Engineered T cells for anti-cancer therapy. *Curr Opin Immunol*. 2012;24(5):633–639.

95 Turtle CJ, Hanafi LA, Berger C, et al. CD19 CAR-T cells of defined CD4+:CD8+ composition in adult B cell ALL patients. *J Clin Invest*. 2016 Jun 1;126(6):2123–2138.

96 Turtle CJ, Hanafi LA, Berger C, et al. Immunotherapy of non-Hodgkin's lymphoma with a defined ratio of CD8+ and CD4+ CD19-specific chimeric antigen receptor–modified T cells. *Sc Trans Med*. 2016;8(355):355ra116.

97 Ohashi Y, Kawashima S, Hirata K, et al. Hypotension and reduced nitric oxide-elicited vasorelaxation in transgenic mice overexpressing endothelial nitric oxide synthase. *J Clin Investig*. 1998;102(12):2061–2071.

98 Thakar MS, Kearl TJ, Malarkannan S. Controlling cytokine release syndrome to harness the full potential of CAR-based cellular therapy. *Front Oncol*. 2020;9:1529.

99 Zhang Y, Zhang W, Dai H, et al. An analytical biomarker for treatment of patients with recurrent B-ALL after remission induced by infusion of anti-CD19 chimeric antigen receptor T (CAR-T) cells. *Sci China Life Sci*. 2016;59(4):379-385.

100 Bossen C, Ingold K, Tardivel A, et al. Interactions of tumor necrosis factor (TNF) and TNF receptor family members in the mouse and human. *J Biol Chem*. 2006;281(20):13964–71.

101 Martinez FO, Helming L, Gordon S. Alternative activation of macrophages: an immunologic functional perspective. *Annu Rev Immunol*. 2009;27:451-483.

102 Hao Z, Li R, Meng L, Han Z, Hong Z. Macrophage, the potential key mediator in CAR-T related CRS. *Exp Hematol Oncol*. 2020;9(1):1-12.

103 Staedtke V, Bai RY, Kim K, et al. Disruption of a self-amplifying catecholamine loop reduces cytokine release syndrome. *Nature*. 2018;564(7735):273–277.

104 Gust J, Hay KA, Hanafi LA, et al. Endothelial activation and blood-brain barrier disruption in neurotoxicity after adoptive immunotherapy with CD19 CAR-T cells. *Cancer Discov*. 2017;7:1404-1419.

105 Page AV, Liles WC. Biomarkers of endothelial activation/dysfunction in infectious diseases. *Virulence*. 2013;4:507–516.

106 Obstfeld AE, Frey NV, Mansfield K, et al. Cytokine release syndrome associated with chimeric-antigen receptor T-cell therapy: clinicopathological insights. *Blood*. 2017;130:2569-2572.

107 Taraseviciute A, Tkachev V, Ponce R, et al. Chimeric antigen receptor T cell-mediated neurotoxicity in nonhuman primates. *Cancer Discov*. 2018;8:750–763.

108 Torre M, Solomon IH, Sutherland CL, et al. Neuropathology of a case with fatal CAR T-cell-associated cerebral edema. *J Neuropathol Exp Neurol*. 2018;77(10):877-882.

109 Le RQ, Li L, Yuan W, et al. FDA approval summary: tocilizumab for treatment of chimeric antigen receptor T cell-induced severe or life-threatening cytokine release syndrome. *Oncologist*. 2018;23:943–947.

110 Hunter CA, Jones SA. IL-6 as a keystone cytokine in health and disease. *Nat Immunol*. 2015;16:448-457.

111 Rose-John S, Neurath MF. IL-6 *trans*-signaling: the heat is on. *Immunity* 2004;20(1):2-4.

112 Jostock T, Mullberg J, Ozbek S, et al. Soluble gp130 is the natural inhibitor of soluble interleukin-6 receptor trans signaling responses. *Eur J Biochem*. 2001;268(1):160-7.

113 Kang S, Tanaka T, Narazaki M, Kishimoto T. Targeting Interleukin-6 Signaling in Clinic. *Immunity*. 2019 Apr 16;50(4):1007–23.

114 Lee SY, Buhimschi IA, Dulay AT, et al. IL-6 *trans*-signaling system in intra-amniotic inflammation, preterm birth, and preterm premature rupture of the membranes. *J Immunol*. 2011 Mar 1;186(5):3226–3236.

115 Heinrich PC, Castell JV, Andus T. Interleukin-6 and the acute phase response. *Biochem J*. 1990;265:621–636.

116 Kang S, Kishimoto T. Interplay between interleukin-6 signaling and the vascular endothelium in cytokine storms. *Exp Mol Med*. 2021;53(7):1116–1123.

117 Tanaka T, Narazaki M, Kishimoto T. Immunotherapeutic implications of IL-6 blockade for cytokine storm. *Immunotherapy*. 2016;8(8):959–970.

118 Szotowski B, Antoniak S, Poller W, Schultheiss HP, and Rauch U. Procoagulant soluble tissue factor is released from endothelial cells in response to inflammatory cytokines. *Circ Res*. 2005 Jun 24;96(12):1233-1239.

119 Neumann FJ, Ott I, Marx N, et al. Effect of human recombinant interleukin-6 and interleukin-8 on monocyte procoagulant activity. *Arterioscler Thromb Vasc Biol.* 1997;17(12):3399–3405.

120 Witkowski M, Landmesser U, Rauch U. Tissue factor as a link between inflammation and coagulation. *Trends Cardiovasc Med*. 2016;26(4):297-303.

121 Marin V, Montero-Julian FA, Grès S, et al. The IL-6-soluble IL-6Rα autocrine loop of endothelial activation as an intermediate between acute and chronic inflammation: an experimental model involving thrombin. *J Immunol*. 2001;167(6):3435-3442.

122 Matthys P, Dillen C, Proost P, Heremans H, Van Damme J, Billiau A. Modification of the anti-CD3-induced cytokine release syndrome by anti-interferon-gamma or anti-interleukin-6 antibody treatment: Protective effects and biphasic changes in blood cytokine levels. *Eur J Immunol*. 1993;23(9):2209–2216.

123 Saha B, Jyothi Prasanna S, Chandrasekar B, Nandi D. Gene modulation and immunoregulatory roles of interferon gamma. *Cytokine*. 2010 Apr;50(1):1–14.

124 Bernardo A, Ball C, Nolasco L, Moake JF, Dong JF. Effects of inflammatory cytokines on the release and cleavage of the endothelial cell-derived ultralarge von Willebrand factor multimers under flow. *Blood*. 2004 Jul 1;104(1):100-106.

125 Khan MM, Liu Y, Khan ME, et al. Upregulation of tissue factor in monocytes by cleaved high molecular weight kininogen is dependent on TNF-alpha and IL-1beta. *Am J Physiol Heart Circ Physiol*. 2010 Feb;298(2):H652-H658.

126 Choy E, Rose-John S. Interleukin-6 as a multifunctional regulator: inflammation, immune response, and fibrosis. *J Scleroderma Related Disord*. 2017;2:S1-S5.

127 Murakami M, Hirano T. The pathological and physiological roles of IL-6 amplifier activation. *Int J Biol Sci*. 2012;8(9):1267-1280.

128 Kim HJ, Tsao JW, Stanfill AG. The current state of biomarkers of mild traumatic brain injury. *JCI Insight.* 2018;3:e97105.

129 Sofroniew MV. Multiple roles for astrocytes as effectors of cytokines and inflammatory mediators. *Neuroscientist*. 2014;20:160–172.

130 Becher B, Tugues S, Greter M. GM-CSF: From growth factor to central mediator of tissue inflammation. *Immunity*. 2016;45(5):963-973.

131 Sterner RM, Sakemura R, Cox MJ, et al. GM-CSF inhibition reduces cytokine release syndrome and neuroinflammation but enhances CAR-T cell function in xenografts. *Blood*. 2019;133(7):697–709.

132 Sachdeva M, Duchateau P, Depil S, Poirot L, Valton J. Granulocyte-macrophage colony-stimulating factor inactivation in CAR T-cells prevents monocyte-dependent release of key cytokine release syndrome mediators. *J Biol Chem*. 2019;294(14):5430–5437.

133 Vogel DY, Kooij G, Heijnen PD, et al. GM-CSF promotes migration of human monocytes across the blood brain barrier. *Eur J Immunol*. 2015;45(6):1808–1819.

134 Yang L, Xie X, Tu Z, Fu J, Xu D, Zhou Y. The signal pathways and treatment of cytokine storm in COVID-19. *Signal Transduct Target Ther*. 2021 Jul 7;6(1):255.

135 Huang C, Wang Y, Li X, et al. Clinical features of patients infected with 2019 novel coronavirus in Wuhan, China. *Lancet*. 2020 Feb 15;395(10223):497-506.

136 Hou H, Zhang B, Huang H, et al. Using IL-2R/lymphocytes for predicting the clinical progression of patients with COVID-19. *Clin Exp Immunol*. 2020;201(1):76-84.

137 Yang L, Liu S, Liu J, et al. COVID-19: immunopathogenesis and Immunotherapeutics. *Signal Transduct Target Ther*. 2020;5(1):128.

138 Zhang JJ, Dong X, Cao YY et al. Clinical characteristics of 140 patients infected with SARS-CoV-2 in Wuhan, China. *Allergy*. 2020;75(7):1730–1741.

139 Zheng M, Gao Y, Wang G et al. Functional exhaustion of antiviral lymphocytes in COVID-19 patients. *Cell Mol Immunol*. 2020;17(5):533–535.

140 Wang X, Xu W, Hu G, et al. Retraction Note to: SARS-CoV-2 infects T lymphocytes through its spike protein-mediated membrane fusion. *Cell Mol Immunol.* 2020;17(8):894.

141 Xu Z, Shi L, Wang Y, et al. Pathological findings of COVID-19 associated with acute respiratory distress syndrome. *Lancet Respir Med*. 2020;8(4):420–422.

142 Liu Y, Du X, Chen J, et al. Neutrophil-to-lymphocyte ratio as an independent risk factor for mortality in hospitalized patients with COVID-19. *J Infect*. 2020;81(1):e6-e12.

143 Zuo Y, Yalavarthi S, Shi H, et al. Neutrophil extracellular traps in COVID-19. *JCI Insight*. 2020;5(11): e138999.

144 Merad M, Martin JC. Pathological inflammation in patients with COVID-19: a key role for monocytes and macrophages. *Nat Rev Immunol*. 2020;20:355–362.

145 Iliadi V, Konstantinidou I, Aftzoglou K, Iliadis S, Konstantinidis TG, Tsigalou C. the emerging role of neutrophils in the pathogenesis of thrombosis in COVID-19. *Int J Mol Sci.* 2021 May 20;22(10):5368.

146 Luster AD, Alon R, von Andrian UH. Immune cell migration in inflammation: present and future therapeutic targets. *Nat Immunol.* 2005;6(12):1182–90.

147 Weiss, SJ. Tissue destruction by neutrophils. *N Engl J Med*. 1989 Feb 9;320(6):365–376.

148 Jenne CN, Wong CHY, Zemp FJ et al. Neutrophils recruited to sites of infection protect from virus challenge by releasing neutrophil extracellular traps. *Cell Host Microbe*. 2013 Feb 13;13(2):169–180.

149 Johansson C, Kirsebom FCM. Neutrophils in respiratory viral infections. *Mucosal Immunol.* 2021;14(4):815–27.

150 Zhu L, Liu L, Zhang Y et al. High level of neutrophil extracellular traps correlates with poor prognosis of severe influenza A infection. *J Infect Dis.* 2018 Jan 17;217(3):428–437.

151 Soehnlein O, Lindbom L, Weber C. Mechanisms underlying neutrophil-mediated monocyte recruitment. *Blood*. 2009 Nov 19;114(21):4613-4623.

152 Guilliams M, Mildner A, Yona S. Developmental and functional heterogeneity of monocytes. *Immunity*. 2018 Oct 16;49(4):595–613.

153 Narasimhan PB, Marcovecchio P, Hamers AAJ, Hedrick CC. Nonclassical monocytes in health and disease. *Annu Rev Immunol*. 2019 Apr 26;37:439–456.

154 Guilliams M, Lambrecht BN, Hammad H. Division of labor between lung dendritic cells and macrophages in the defense against pulmonary infections. *Mucosal Immunol*. 2013 May;6(3):464–473.

155 Xu G, Qi F, Li H, et al. The differential immune responses to COVID-19 in peripheral and lung revealed by single-cell RNA sequencing. *Cell Discov*. 2020 Oct 20;6:73.

156 Maus UA, Waelsch K, Kuziel WA, et al. Monocytes are potent facilitators of alveolar neutrophil emigration during lung inflammation: role of the CCL2-CCR2 axis. *J Immunol*. 2003 Mar 15;170(6):3273–3278.

157 Wilk AJ, Rustagi A, Zhao NQ, et al. A single-cell atlas of the peripheral immune response in patients with severe COVID-19. *Nat Med*. 2020 Jul;26(7):1070–1076.

158 Saris A, Reijnders TDY, Nossent EJ, et al. Distinct cellular immune profiles in the airways and blood of critically ill patients with COVID-19. *Thorax*. 2021 Apr 12;thoraxjnl-2020-216256.

159 Wang F, Hou H, Luo Y, et al. The laboratory tests and host immunity of COVID-19 patients with different severity of illness. *JCI Insight*. 2020 May 21;5(10):e137799.

160 Ackermann M, Verleden SE, Kuehnel M, et al. Pulmonary vascular endothelialitis, thrombosis, and angiogenesis in Covid-19. *N Engl J Med*. 2020 Jul 9;383(2):120-128.

161 Lillicrap D. Disseminated intravascular coagulation in patients with 2019-nCoV pneumonia. *J Thromb Haemost*. 2020 Apr;18(4):786-787.

162 Varga Z, Flammer AJ, Steiger P, et al. Endothelial cell infection and endotheliitis in COVID-19. *Lancet*: 2020 May 2;395(10234):1417-1418.

163 Alon R, Sportiello M, Kozlovski S, et al. Leukocyte trafficking to the lungs and beyond: lessons from influenza for COVID-19. *Nat Rev Immunol*. 2021;21(1):49-64.

164 Fara A, Mitrev Z, Rosalia RA, Assas BM. Cytokine storm and COVID-19: a chronicle of pro-inflammatory cytokines. *Open Biology*. 2020;10(9):200160.

165 McGonagle D, Sharif K, O'Regan A, Bridgewood C. The role of cytokines including interleukin-6 in COVID-19 induced pneumonia and macrophage activation syndrome-like disease. *Autoimmun Rev.* 2020 Jun;19(6):102537.

166 Ye Q, Wang B, Mao J. The pathogenesis and treatment of the `Cytokine Storm' in COVID-19. *The Journal of infection*. 2020;80(6):607-613.

167 Blanco-Melo D, Nilsson-Payant BE, Liu WC, et al. Imbalanced Host Response to SARS-CoV-2 Drives Development of COVID-19. *Cell*. 2020;181(5):1036-45.e9.

168 Hadjadj J, Yatim N, Barnabei L, et al. Impaired type I interferon activity and inflammatory responses in severe Covid-19 patients. *Science*. 2020;369(6504):718-724.

169 Pedersen SF, Ho YC. SARS-CoV-2: a storm is raging. *J Clin Invest*. 2020;130:2202-2205.

170 Herold T, Jurinovic V, Arnreich C, et al. Elevated levels of IL-6 and CRP predict the need for mechanical ventilation in COVID-19. *J Allergy Clin Immunol*. 2020 Jul;146(1):128-136.

171 Lin L, Lu L, Cao W, Li T. Hypothesis for potential pathogenesis of SARS-CoV-2 infection-a review of immune changes in patients with viral pneumonia. *Emerg Microbes Infect*. 2020 Dec;9(1):727-732.

172 Gubernatorova EO, Gorshkova EA, Polinova AI, Drutskaya MS. IL-6: relevance for immunopathology of SARS-CoV-2. *Cytokine Growth Factor Rev.* 2020 Jun;53:13-24.

173 Zhou Y, Fu B, Zheng X, et al. Pathogenic T-cells and inflammatory monocytes incite inflammatory storms in severe COVID-19 patients. *Natl Sci Rev*. 2020 Mar 13;nwaa041.

174 Karki R, Sharma BR, Tuladhar S, Williams EP, Zalduondo L, Samir P, *et al.* Synergism of TNF-α and IFN-γ triggers inflammatory cell death, tissue damage, and mortality in SARS-CoV-2 infection and cytokine shock syndromes. *Cell*. 2021; 184(1):149-168.e17.

175 Kim YR, Kim D-Y. Current status of the diagnosis and treatment of hemophagocytic lymphohistiocytosis in adults. *Blood Res*. 2021 Apr 30; 56(Suppl 1):17–25.

176 Zhang K, Jordan MB, Marsh RA, et al. Hypomorphic mutations in PRF1, MUNC13-4, and STXBP2 are associated with adult-onset familial HLH. *Blood*. 2011;118:5794–5798.

177 Kaufman KM, Linghu B, Szustakowski JD, et al. Whole-exome sequencing reveals overlap between macrophage activation syndrome in systemic juvenile idiopathic arthritis and familial hemophagocytic lymphohistiocytosis. *Arthritis Rheumatol* 2014;66:3486-3495.

178 Ravelli A, Grom AA, Behrens EM, Cron RQ. Macrophage activation syndrome as part of systemic juvenile idiopathic arthritis: diagnosis, genetics, pathophysiology and treatment. *Genes Immun.* 2012 Jun; 13(4):289–98.

179 Put K, Avau A, Brisse E, et al. Cytokines in systemic juvenile idiopathic arthritis and haemophagocytic lymphohistiocytosis: tipping the balance between interleukin-18 and interferon-γ. *Rheumatology (Oxford).* 2015 Aug;54(8):1507-1517.

180 Takada H, Takahata Y, Nomura A, Ohga S, Mizuno Y, Hara T. Increased serum levels of interferon-gamma-inducible protein 10 and monokine induced by gamma interferon in patients with haemophagocytic lymphohistiocytosis. *Clin Exp Immunol*. 2003;133:448-453.

181 Ruscitti P, Cipriani P, Benedetto PDi, et al. H-ferritin and proinflammatory cytokines are increased in the bone marrow of patients affected by macrophage activation syndrome. *Clin Exp Immunol*. 2018 Feb;191(2):220-228.

182 Schulert JS, Grom AA. Pathogenesis of macrophage activation syndrome and potential for cytokine-directed therapies. *Annu Rev Med*. 2015;66:145-159.

183 Avcin T, Tse SM, Schneider R, Ngan B, Silverman ED. Macrophage activation syndrome as the presenting manifestation of rheumatic diseases in childhood. *J Pediatr*. 2006 May;148(5):683-686.

184 Moller HJ, Aerts H, Gronbaek H, et al. Soluble CD163: a marker molecule for monocyte/macrophage activity in disease. *Scand J Clin Lab Invest Suppl.* 2002; 237:29-33.

185 Henter JI, Elinder G, Ost A. Diagnostic guidelines for hemophagocytic lymphohistiocytosis. The FHL Study Group of the Histiocyte Society. *Semin Oncol*. 1991 Feb;18(1):29-33.

186 Janka GE, Lehmberg K. Hemophagocytic syndromes–an update. *Blood Re*v. 2014;28:135–42.

187 Jordan MB, Hildeman D, Kappler J, Marrack P. An animal model of hemophagocytic lymphohistiocytosis (HLH): CD8+ T cells and interferon gamma are essential for the disorder. *Blood* 2004 Aug 1;104(3):735-43.

188 Janka GE, Lehmberg K. Hemophagocytic lymphohistiocytosis: pathogenesis and treatment. *Hematol Am Soc Hematol Educ Program*. 2013;2013:605-11.

189 Sepulveda FE, de Saint Basile G. Hemophagocytic syndrome: primary forms and predisposing conditions. *Curr Opin Immunol*. 2017;49:20-26.

190 Terrell CE, Jordan MB. Perforin deficiency impairs a critical immunoregulatory loop involving murine CD8(+) T cells and dendritic cells. *Blood*. 2013;121:5184-91.

191 Brisse E, Wouters CH, Matthys P. Hemophagocytic lymphohistiocytosis (HLH): A heterogeneous spectrum of cytokine-driven immune disorders. *Cytokine Growth Factor Rev*. 2015;26:263-280.

192 Grom AA. Natural killer cell dysfunction: A common pathway in systemic-onset juvenile rheumatoid arthritis, macrophage activation syndrome, and hemophagocytic lymphohistiocytosis? *Arthritis Rheum*. 2004 Mar;50(3):689-698

193 Jafarzadeh A, Chauhan P, Saha B, Jafarzadeh S, Nemati M. Contribution of monocytes and macrophages to the local tissue inflammation and cytokine storm in COVID-19: Lessons from SARS and MERS, and potential therapeutic interventions. *Life Sciences*. 2020 Sep 15;257:118102.

194 Gracia-Hernandez M, Sotomayor EM, Villagra A. Targeting macrophages as a therapeutic option in coronavirus disease 2019. *Front Pharmacol*. 2020 Oct 29;11:577571.

195 Giavridis T, Van Der Stegen SJC, Eyquem J, Hamieh M, Piersigilli A and Sadelain M. CAR T cell–induced cytokine release syndrome is mediated by macrophages and abated by IL-1 blockade. *Nat Med*. 2018 Jun;24(6):731–738.

196 Norelli M, Camisa B, Barbiera G, et al. Monocyte-derived IL-1 and IL-6 are differentially required for cytokine-release syndrome and neurotoxicity due to CAR T cells. *Nat Med*. 2018 Jun;24(6):739–748.

197 Zhou J, Law HK, Cheung CY, Ng IH, Peiris JS, Lau YL. Functional tumour necrosis factor-related apoptosis-inducing ligand production by avian influenza virus-infected macrophages. *J Infect*. Dis. 2006 Apr 1;193(7):945-953.

198 Crayne CB, Albeituni S, Nichols KE, Cron RQ. The immunology of macrophage activation syndrome. *Front Immunol.* 2019 Feb 1;10:119-119.

199 Avau A, Mitera T, Put S, et al. Systemic juvenile idiopathic arthritis-like syndrome in mice following stimulation of the immune system with Freund's complete adjuvant: regulation by interferon-γ. *Arthritis Rheumatol.* 2014;66(5):1340-1351.

200 Choudhry J, Parson M, Wright J. A retrospective review of tocilizumab for the management of blinatumomab (a bispecific T cell engager)-induced cytokine release syndrome (CRS). *Blood*. 2018;132(Suppl. 1):5211.

201 Khadka RH, Sakemura R, Kenderian SS, Johnson AJ. Management of cytokine release syndrome: an update on emerging antigen-specific T cell engaging immunotherapies. *Immunotherapy*. 2019 Jul 1;11(10):851–857.

202 Jain T, Litzow MR. Management of toxicities associated with novel immunotherapy agents in acute lymphoblastic leukemia. *Ther Adv Hematol*. 2020 Jan 1;11:2040620719899897.

203 Wei Q, Lin H, Wei R-G, et al. Tocilizumab treatment for COVID-19 patients: a systematic review and meta-analysis. *Infecti Dis Poverty*. 2021 May 18;10(1):71.

204 Rubsamen R, Burkholz S, Massey C, et al. Anti-IL-6 Versus Anti-IL-6R Blocking Antibodies to Treat Acute Ebola Infection in BALB/c Mice: Potential Implications for Treating Cytokine Release Syndrome. *Front Pharmacol*. 2020 Sep 23;11:574703.

205 Somers EC, Eschenauer GA, Troost JP, et al. Tocilizumab for treatment of mechanically ventilated patients with COVID-19. *Clin Infect Dis*. 2021 Jul 15;73(2):e445-e454.

206 Kim JS, Lee JY, Yang JW, et al. Immunopathogenesis and treatment of cytokine storm in COVID-19. *Theranostics*. 2021;11(1):316–29.

207 Kenderian SS, Ruella M, Shestova O, Kim M, Klichinsky M, Chen F, *et al.* Ruxolitinib prevents cytokine release syndrome after CAR T-cell therapy without impairing the anti-tumour effect in a xenograft model. *Biology of Blood and Marrow Transplantation*. 2017 Mar 1; 23(3):S19–20.

208 Zi FM, Ye LL, Zheng JF, Cheng J, Wang QM. Using JAK inhibitor to treat cytokine release syndrome developed after chimeric antigen receptor T cell therapy for patients with refractory acute lymphoblastic leukemia: A case report. *Medicine*. 2021 May 14; 100(19):e25786.

209 Ozen S, Esenboga S. Alternative Therapies for Cytokine Storm Syndromes. In: Cron RQ, Behrens EM, editors. *Cytokine Storm Syndrome.* Springer International Publishing. 2019; 581–93

210 Pan J, Deng B, Ling Z, et al. Ruxolitinib mitigates steroid-refractory CRS during CAR T therapy. *J Cell Mol Med*. 2021 Jan;25(2):1089-1099.

211 Cao Y, Wei J, Zou L, et al. Ruxolitinib in treatment of severe coronavirus disease 2019 (COVID-19): A multicenter, single-blind, randomized controlled trial. *J Allergy Clin Immunol*. 2020;146(1):137-46.e3.

212 Richardson P, Griffin I, Tucker C, et al. Baricitinib as potential treatment for 2019-nCoV acute respiratory disease. *Lancet*. 2020;395:e30-1.

213 Vannucchi AM, Sordi B, Morettini A, et al. Compassionate use of JAK1/2 inhibitor ruxolitinib for severe COVID-19: a prospective observational study. *Leukemia*. 2021;35(4):1121–1133.

214 Sahin M, Remy MM, Merkler D, Pinschewer DD. The janus kinase inhibitor ruxolitinib prevents terminal shock in a mouse model of arenavirus haemorrhagic fever. *Microorganisms*. 2021 Mar 9;9(3):564.

215 Scheller J, Garbers C, Rose-John S. Interleukin-6: from basic biology to selective blockade of pro-inflammatory activities. *Semin Immunol.* 2014 Feb;26(1);2-12.

216 Barkhausen T, Tschernig T, Rosenstiel P, et al. Selective blockade of interleukin-6 *trans*-signalling improves survival in a murine polymicrobial sepsis model. *Crit Care Med*. 2011;39:1407-1413.

217 Jones SA, Hunter CA. Is IL-6 a key cytokine target for therapy in COVID-19? *Nat Rev Immunol*. 2021 Jun;21(6):337–339.

218 Magro G. SARS-CoV-2 and COVID-19: Is interleukin-6 (IL-6) the 'culprit lesion' of ARDS onset? What is there besides Tocilizumab? SGP130Fc. *Cytokine X*. 2020 Jun 1;2(2):100029.

219 Wunderlich CM, Delic D, Behnke K, et al. Cutting edge: Inhibition of IL-6 *trans*-signalling protects from malaria-induced lethality in mice. *J Immunol*. 2012;188:4141-4144.

220 Dinarello CA. Immunological and inflammatory functions of the interleukin-1 family. *Ann Rev Immunol*. 2009;27:519–555.

221 Adam Monteagudo L, Boothby A, Gertner E et al. Continuous intravenous anakinra infusion to calm the cytokine storm in macrophage activation syndrome. *ACR Open Rheumatol*. 2020 May;2(5):276–282.

222 Maniscalco V, Abu-Rumeileh S, Mastrolia MV, et al. The off-label use of anakinra in pediatric systemic autoinflammatory diseases. *Ther Adv Musculoskelet Dis*. 2020 Oct 16;12:1759720X20959575.

223 Sönmez HE, Demir S, Bilginer Y, Özen S. Anakinra treatment in macrophage activation syndrome: a single center experience and systemic review of literature. *Clin Rheumatol*. 2018 Dec;37(12):3329-3335.

224 Sheng CC, Sahoo D, Dugar S, et al. Canakinumab to reduce deterioration of cardiac and respiratory function in SARS-CoV-2 associated myocardial injury with heightened inflammation (canakinumab in Covid-19 cardiac injury: The three C study). *Clin Cardiol*. 2020 Oct;43(10):1055-1063.

225 Heustess AM, Allard MA, Thompson DK, Fasinu PS. Clinical management of COVID-19: a review of pharmacological treatment options. *Pharmaceuticals (Basel)*. 2021 May 28;14(6):520.

226 Tang L, Yin Z, Hu Y, Mei H. Controlling Cytokine Storm Is Vital in COVID-19. *Front Immunol*. 2020 Nov 30;11:570993.

227 Kaps L, Labenz C, Grimm D, Schwarting A, Galle PR, Schreiner O. Treatment of cytokine storm syndrome with IL-1 receptor antagonist anakinra in a patient with ARDS caused by COVID-19 infection: A case report. *Clin Case Rep*. 2020 Sep 15;8(12):2990–2994.

228 Strati P, Ahmed S, Kebriaei P, et al. Clinical efficacy of anakinra to mitigate CAR T-cell therapy–associated toxicity in large B-cell lymphoma. *Blood Adv*. 2020 Jul 9; 4(13):3123–3127.

229 Thwaites RS, Uruchurtu ASS, Siggins MK, e al. Inflammatory profiles across the spectrum of disease reveal a distinct role for GM-CSF in severe COVID-19. *Sci Immunol*. 2021 Mar 10;6(57):eabg9873.

230 Humanigen Inc. Humanigen Reports positive data with lenzilumab in the ZUMA-19 CAR-T phase 1b study in DLBCL and plans to initiate a potential registrational study. "Press Release". 2021 Apr 19. https://ir.humanigen.com/news/news-details/2021/

231 Mehta P, Porter JC, Manson JJ, et al. Therapeutic blockade of granulocyte macrophage colony-stimulating factor in COVID-19-associated hyperinflammation: challenges and opportunities. *Lancet Respir Med*. 2020 Aug;8(8):822–830.

232 Temesgen Z, Assi M, Vergidis P, e al. First Clinical Use of Lenzilumab to Neutralize GM-CSF in Patients with Severe COVID-19 Pneumonia. *medRxiv*. 2020 Jun 14;2020.06.08.20125369.

233 Paine III R, Standiford TJ, Dechert RE, et al. A randomized trial of recombinant human GM-CSF for patients with acute lung injury. *Crit Care Med.* 2012;40(1): 90–97.

234 Lang FM, Lee KM-C, Teijaro JR, Becher B, Hamilton JA. GM-CSF-based treatments in COVID-19: reconciling opposing therapeutic approaches. *Nat Rev Immunol*. 2020 Aug;20(8):507–514.

235 A Phase 2 Trial Evaluating Sargramostim in Patients With COVID-19 Associated Acute Hypoxemia. Partner Therapeutics, Inc. clinicaltrials.gov: NCT04411680; 2021 Jun.

236 Sargramostim Use in COVID-19 to Recover Patient Health (SCOPE). ClinicalTrials.gov: NCT04707664. 2021 Jan.

237 Rösler B, Herold S. Lung epithelial GM-CSF improves host defense function and epithelial repair in influenza virus pneumonia-a new therapeutic strategy? *Mol Cell Pediatr*. 2016;3:29.

238 Locatelli F, Jordan MB, Allen C, et al. Emapalumab in children with primary hemophagocytic lymphohistiocytosis. *N Engl J Med*. 2020 May 7;382(19): 1811–1822.

239 Jordan Locatelli*, et al.* Abstract LBA-6. Presented at: ASH Annual Meeting and Exposition; San Diego, 2018.

240 De Benedetti F. Anti-interferon-γ Therapy for Cytokine Storm Syndromes. In: Cron RQ, Behrens EM, editors. *Cytokine Storm Syndrome*. Springer International Publishing; 2019:569–580.

241 Benedetti FD, Brogan P, Bracaglia C, et al. Op0290 Emapalumab (anti-interferon-gamma monoclonal antibody) in patients with macrophage activation syndrome (mas) complicating systemic juvenile idiopathic arthritis (sjia). *Annals of the Rheumatic Diseases*. 2020 Jun 1;79:180.

242 Magro G. COVID-19: Review on latest available drugs and therapies against SARS-CoV-2. Coagulation and inflammation cross-talking. *Virus Res*. 2020 Sep;286:198070.

243 A Phase 2/3, Randomized, Open-label, Parallel Group, 3-arm, Multicenter Study Investigating the Efficacy and Safety of Intravenous Administrations of Emapalumab, an Anti-interferon Gamma (Anti-IFNγ) Monoclonal Antibody, and Anakinra, an Interleukin-1(IL-1) Receptor Antagonist, Versus Standard of Care, in Reducing Hyper-inflammation and Respiratory Distress in Patients With SARS-CoV-2 Infection. (Swedish Orphan Biovitrum) clinicaltrials.gov: NCT04324021. 2020 Dec.

244 Makay B, Yilmaz S, Turkyilmaz Z, Unal N, Oren H, Unsal E. Etanercept for therapy-resistant macrophage activation syndrome. *Pediatr Blood Cancer*. 2008;50(2):419-21.

245 Prahalad S, Bove KE, Dickens D, Lovell DJ, Grom AA. Etanercept in the treatment of macrophage activation syndrome. *The Journal of Rheumatology*. 2001 Sep 1;28(9):2120–4.

246 Maeshima K, Ishii K, Iwakura M, et al. Adult-onset Still's disease with macrophage activation syndrome successfully treated with a combination of methotrexate and etanercept. *Mod Rheumatol*. 2012;22(1):137-41.

247 Robinson PC, Liew DFL, Liew JW, et al. The Potential for Repurposing Anti-TNF as a Therapy for the Treatment of COVID-19. *Med*. 2020 Dec 18;1(1):90–102.

248 Abraham E, Wunderink R, Silverman H, et al. Efficacy and safety of monoclonal antibody to human tumour necrosis factor alpha in patients with sepsis syndrome. A randomized, controlled, double-blind, multicenter clinical trial. TNF-alpha MAb Sepsis Study Group. *JAMA*. 1995;273(12):934-41.

249 Clark MA, Plank LD, Connolly AB, et al. Effect of a chimeric antibody to tumour necrosis factor-alpha on cytokine and physiologic responses in patients with severe sepsis-a randomized, clinical trial. *Crit Care Med*. 1998;26(10):1650-9.

250 Zhang L, Wang S, Xu J, et al. Etanercept as a new therapeutic option for cytokine release syndrome following chimeric antigen receptor T cell therapy. *Exp Hematol Oncol*. 2021 Feb 19;10(1):16.

251 Li J, Piskol R, Ybarra R, et al. CD3 bispecific antibody-induced cytokine release is dispensable for cytotoxic T cell activity. *Sci Transl Med*. 2019 Sep 4;11(508):eaax8861.

252 Ravelli A, Grom AA, Behrens EM, Cron RQ. Macrophage activation syndrome as part of systemic juvenile idiopathic arthritis: diagnosis, genetics, pathophysiology and treatment. *Genes Immun*. 2012 Jun; 13(4):289-98.

253 Trottestam H, Horne A, Arico M, et al. Chemoimmunotherapy for hemophagocytic lymphohistiocytosis: long-term results of the HLH-94 treatment protocol. *Blood*. 2011 Oct 27;118(17):4577-4584.

254 Bergsten E, Horne A, Arico M, et al. Confirmed efficacy of etoposide and dexamethasone in HLH treatment: long-term results of the cooperative HLH-2004 study. *Blood*. 2017 Dec 21;130(25):2728–2738.

255 Lee N, Allen Chan KC, Hui DS, et al. Effects of early corticosteroid treatment on plasma SARS-associated Coronavirus RNA concentrations in adult patients. *J Clin Virol*. 2004;31(4):304–9.

256 Yang Z, Liu J, Zhou Y, Zhao X, Zhao Q, Liu J. The effect of corticosteroid treatment on patients with coronavirus infection: a systematic review and meta-analysis. *J Infect*. 2020; 81:e13–20.

257 Russell CD, Millar JE, Baillie JK. Clinical evidence does not support corticosteroid treatment for 2019-nCoV lung injury. *Lancet*. 2020;395:473–475.

258 Shashidhara KC, Murthy KAS, Gowdappa HB, Bhograj A. Effect of high dose of steroid on platelet count in acute stage of dengue fever with thrombocytopenia. *J Clin Diagn Res*. 2013;7:1397–1400.

259 Xu J, Tan D, Fu Y, Walline J, Yu X. Do corticosteroids have a role in treating Ebola virus disease? *Sci China Life Sci*. 2015;58(1):111–113.

260 Group TRC. Dexamethasone in Hospitalized Patients with Covid-19. *N Eng J Med*. 2021 Feb 25;384(8):693-704.

261 Alhazzani W, Møller MH, Arabi YM, et al. Surviving Sepsis campaign: guidelines on the management of critically ill adults with coronavirus disease 2019 (COVID-19). *Intensive Care Med.* 2020;46(5):854–87.

262 Ronco C, Brendolan A, d'Intini V, Ricci Z, Wratten ML, Bellomo R. Coupled plasma filtration adsorption: rationale, technical development and early clinical experience. *Blood Purif.* 2003;21:409–416.

263 Bellomo R, Tetta C, Ronco C: Coupled plasma filtration adsorption. *Intensive Care Med* 2003; 29:1222–1228

264 Wong JP, Viswanathan S, Wang M, Sun LQ, Clark GC, D'Elia RV. Current and future developments in the treatment of virus-induced hypercytokinemia. *Future Med Chem*. 2017 ;9(2):169-78.

265 Xiao X, He X, Li Q, et al. Plasma exchange can be an alternative therapeutic modality for severe cytokine release syndrome after chimeric antigen receptor-T cell infusion: a case report. *Clin Cancer Res*. 2019 Jan 1;25(1):29-34.

266 Bosnak M, Erdogan S, Habibe Aktekin E, Bay A. Therapeutic plasma exchange in primary hemophagocytic lymphohistiocytosis: reports of two cases and a review of the literature. *Transfus Apher Sci*. 2016 Dec;55(3):353-356.

267 Frey N, Porter D. Cytokine Release syndrome with chimeric antigen receptor t cell therapy. *Biol Blood and Marrow Transplant*. 2019 Apr;25(4):e123–7.

268 Siegler EL, Wang P. Preclinical Models in Chimeric Antigen Receptor–Engineered T-Cell Therapy. *Human Gene Therapy*. 2018 May 1;29(5):534–46.

269 Sarkar S, Heise MT. Mouse Models as Resources for Studying Infectious Diseases. *Clin Ther*. 2019 Oct; 41(10):1912–22.

270 Bouvier NM, Lowen AC. Animal Models for Influenza Virus Pathogenesis and Transmission. *Viruses*. 2010 Jul 27;2(8):1530–63.

271 Legrand N, Ploss A, Balling R, et al. Humanized mice for modeling human infectious disease: challenges, progress, and outlook. *Cell Host Microbe*. 2009 Jul 23;6(1):5–9.

272 Jiang RD, Liu MQ, Chen Y, et al. Pathogenesis of SARS-CoV-2 in transgenic mice expressing human angiotensin-converting enzyme 2. *Cell*. 2020 Jul 9;182(1):50-58.e8.

273 Muñoz-Fontela C, Dowling WE, Funnell SGP, et al. Animal models for COVID-19. *Nature*. 2020 Oct;586(7830):509–15.

274 Shultz LD, Ishikawa F, Greiner DL. Humanized mice in translational biomedical research. *Nat Rev Immunol*. 2007 Feb;7(2):118–30.

275 Zhao J, Li K, Wohlford-Lenane C, et al. Rapid generation of a mouse model for Middle East respiratory syndrome. *Proc Natl Acad Sci U S A*. 2014 Apr 1;111(13):4970–5.

276 Spengler JR, Saturday G, Kavender KJ, et al. Severity of disease in humanized mice infected with Ebola virus or Reston virus is associated with magnitude of early viral replication in liver. *J Infect Dis*. 2017;217(1):58–63.

277 Wahl A, De C, Abad Fernandez M, et al. Precision mouse models with expanded tropism for human pathogens. *Nat Biotechnol*. 2019 Oct;37(10):1163–73.

278 Spits H, Villaudy J. Modeling human lung infections in mice. *Nat Biotechnol*. 2019 Oct;37(10):1129–30

279 Bente DA, Melkus MW, Garcia JV, Rico-Hesse R. Dengue Fever in Humanized NOD/SCID Mice. *J Virol*. 2005 Nov 1;79(21):13797–9.

280 Zitvogel L, Pitt JM, Daillère R, Smyth MJ, Kroemer G. Mouse models in oncoimmunology. *Nat Rev Cancer*. 2016 Dec;16(12):759–773.

281 Lee JC, Hayman E, Pegram HJ, Santos E, Heller G, Sadelain M, and Brentjens R. *In vivo* inhibition of human CD19-targeted effector T cells by natural T regulatory cells in a xenotransplant murine model of B cell malignancy. *Cancer Res*. 2011 Apr 15;71(8):2871–2881.

282 Mardiros A, Dos Santos C, McDonald T, et al. T cells expressing CD123-specific chimeric antigen receptors exhibit specific cytolytic effector functions and antitumor effects against human acute myeloid leukemia. *Blood*. 2013 Oct31;122(18):3138–3148.

283 Lanitis E, Poussin M, Hagemann IS, et al. Redirected antitumor activity of primary human lymphocytes transduced with a fully human anti-mesothelin chimeric receptor. *Mol. Ther*. 2010 Mar;20(3):633–643.

284 Long A, Haso W, Shern J, et al. 4-1BB costimulation ameliorates T cell exhaustion induced by tonic signaling of chimeric antigen receptors. *Nat Med* 2015;21(6):581–590.

285 Dreier T, Baeuerle PA, Fichtner I, et al. T cell costimulus-independent and very efficacious inhibition of tumor growth in mice bearing subcutaneous or leukemic human B cell lymphoma xenografts by a CD19-/CD3-bispecific single-chain antibody construct. *J Immunol*. 2003 Apr 15;170(8):4397-4402.

286 Burt R, Warcel D, Fielding AK. Blinatumomab, a bispecific B-cell and T-cell engaging antibody, in the treatment of B-cell malignancies. *Hum Vaccin Immunother*. 2018 Nov 20;15(3):594–602.

287 Carpenito C, Milone M, Hassan R, et al. Control of large, established tumor xenografts with genetically retargeted human T cells containing CD28 and CD137 domains. *Proc Natl Acad Sci U S A*. 2009 Mar 3;106(9):3360–3365.

288 Bondanza A, Valtolina V, Magnani Z, et al. Suicide gene therapy of graft-versus-host disease induced by central memory human T lymphocytes. *Blood*. 2006 Mar 1;107(5):1828–1836.

289 Mastaglio S, Genovese P, Magnani Z, et al. NY-ESO-1 TCR single edited central memory and memory stem T cells to treat multiple myeloma without inducing GvHD. *Blood*. 2017 Aug 3;130(5):606–618.

290 Bouma G, Nikoloc T, Coppens JMC, et al. NOD mice have a severely impaired ability to recruit leukocytes into sites of inflammation. *Eur J Immunol*. 2005;35(1):225–235.

291 Lanitis E, Rota G, Kosti P, et al. Optimized gene engineering of murine CAR-T cells reveals the beneficial effects of IL-15 coexpression. *J Exp Med*. 2020 Feb 1;218(2):e30292203.

292 Holzapfel B, Wagner F, Thibaudeau L, et al. Concise review: humanized models of tumor immunology in the 21st century: convergence of cancer research and tissue engineering. *Stem Cells* 2015;33:1696–1704.

293 Chulpanova DS, Kitaeva KV, Rutland CS, Rizvanov AA, Solovyeva VV. Mouse Tumor Models for Advanced Cancer Immunotherapy. *Int J Mol Sci.* 2020 Jun 9;21(11):4118.

294 Morillon YM, Sabzevari A, Schlom J, Greiner JW. The Development of Next-generation PBMC Humanized Mice for Preclinical Investigation of Cancer Immunotherapeutic Agents. *Anticancer Research*. 2020 Oct 1;40(10):5329–41.

295 Nagorsen D, Kufer P, Baeuerle PA, Bargou R. Blinatumomab: A historical perspective. *Pharmacology & Therapeutics*. 2012 Dec 1;136(3):334–42.

296 Cheadle EJ, Sheard V, Rothwell DG, et al. Differential role of Th1 and Th2 cytokines in autotoxicity driven by CD19-specific second-generation chimeric antigen receptor T cells in a mouse model. *Immunol*. 2014 Apr 15;192(8):3654-3665.

297 Ferran C, Dy M, Sheehan K, et al. Inter-mouse strain differences in the *in vivo* anti-CD3 induced cytokine release. *Clin Exp Immunol*. 1991 Dec;86(3):537–43.

298 Godbersen-Palmer C, Coupet TA, Grada Z, Zhang SC, Sentman CL. Toxicity induced by a bispecific t cell–redirecting protein is mediated by both t cells and myeloid cells in immunocompetent mice. *J Immunol*. 2020 Jun 1;204(11):2973–2983.

299 Kuhn C, Weiner HL. Therapeutic anti-CD3 monoclonal antibodies: from bench to bedside. *Immunotherapy*. 2016 May 10;8(8):889–906.

300 Ferran C, Sheehan K, Dy M, et al. Cytokine-related syndrome following injection of anti-CD3 monoclonal antibody: further evidence for transient in vivo T cell activation. *Eur J Immunol*. 1990 Mar;20(3):509-515.

301 Bemelmans MH, Abramowicz D, Gouma DJ, Goldman M, Buurman WA. In vivo T cell activation by anti-CD3 monoclonal antibody induces soluble TNF receptor release in mice. Effects of pentoxifylline, methylprednisolone, anti-TNF, and anti-IFN-gamma antibodies. *J Immunology*. 1994;153:499–506.

302 Alegre ML, Vandenabeele P, Depierreux M, et al. Cytokine release syndrome induced by the 145-2C11 anti-CD3 monoclonal antibody in mice: prevention by high doses of methylprednisolone. *The Journal of Immunology*. 1991 Feb 15;146(4):1184–91.

303 Alegre ML, Gastaldello K, Abramowicz D, et al. Evidence that pentoxifylline reduces anti-cd3 monoclonal antibody-induced cytokine release syndrome. *Transplantation*. 1991 Oct;52(4):674–9.

304 Chatenoud L, Legendre C, Ferran C, Bach J-F, Kreis H. Corticosteroid inhibition of the okt3-induced cytokine-related syndrome. *Transplantation*. 1991 Feb;51(2):334–7.

305 Charpentier B, Hiesse C, Lantz O, et al. Evidence that antihuman tumor necrosis factor monoclonal antibody prevents okt3-induced acute syndrome. *Transplantation*. 1992 Dec;54(6):997–1001.

306 Ferran C, Dautry F, Mérite S, Sheehan K, Schreiber R, Grau G, et al. Anti-tumor necrosis factor modulates anti-CD3-triggered T cell cytokine gene expression in vivo. *J Clin Invest*. 1994 May 1;93(5):2189–96.

307 Chadwick E, Noll A, Jiang Y, Hause R, et al. A Syngeneic Mouse Model of CAR T-Mediated Toxicity and Neuroinflammation. Poster presented at: Society for Immunotherapy of Cancer 2017; 2017 Nov 6.

308 Li G, Boucher JC, Kotani H, et al. 4-1BB enhancement of CAR T function requires NF-κB and TRAFs. *JCI Insight*. 2018 Sep 20;3(18):e121322.

309 Xu Y, Zhang M, Ramos CA, et al. Closely related T-memory stem cells correlate with in vivo expansion of CAR.CD19-T cells and are preserved by IL-7 and IL-15. *Blood*. 2014 Jun 12;123(24):3750–9.

310 Lacroix M, Rousseau F, Guilhot F, et al. Novel insights into interleukin 6 (IL-6) cis- and *trans*-signaling pathways by differentially manipulating the assembly of the IL-6 signaling complex. *J Biol Chem*. 2015;290:26943–26953.

311 Kochenderfer JN, Yu Z, Frasheri D, Restifo NP, Rosenberg SA. Adoptive transfer of syngeneic T cells transduced with a chimeric antigen receptor that recognizes murine CD19 can eradicate lymphoma and normal B cells. *Blood*. 2010 Nov 11;116(19):3875–86.

312 Cui Y, Zhang H, Meadors J, Poon R, Guimond M, Mackall CL. Harnessing the physiology of lymphopenia to support adoptive immunotherapy in lymphoreplete hosts. *Blood*. 2009 Oct 29;114(18):3831–40.

313 Kueberuwa G, Kalaitsidou M, Cheadle E, Hawkins RE, Gilham DE. CD19 CAR T Cells Expressing IL-12 Eradicate Lymphoma in Fully Lymphoreplete Mice through Induction of Host Immunity. *Mol Ther Oncolytics*. 2017 Dec 19;8:41–51.

314 Milone MC, Fish JD, Carpenito C, et al. Chimeric Receptors Containing CD137 Signal Transduction Domains Mediate Enhanced Survival of T Cells and Increased Antileukemic Efficacy In Vivo. *Molecular Therapy*. 2009 Aug 1;17(8):1453–64.

315 Stock S, Schmitt M, Sellner L. Optimizing Manufacturing Protocols of Chimeric Antigen Receptor T Cells for Improved Anticancer Immunotherapy. *Int J Mol Sci*. 2019 Dec 10;20(24):6223.

316 Zhou J, Jin L, Wang F, Zhang Y, Liu B, Zhao T. Chimeric antigen receptor T (CAR-T) cells expanded with IL-7/IL-15 mediate superior antitumor effects. *Protein Cell*. 2019 Oct 1;10(10):764–9.

317 Xu H, Wang N, Cao W, Huang L, Zhou J, Sheng L. Influence of various medium environment to in vitro human T cell culture. *In Vitro Cell Dev Biol Anim*. 2018 Sep 1;54(8):559–566.

318 Ghassemi S, Bedoya F, Nunez-Cruz S, June C, Melenhorst J, Milone M. Shortened T Cell Culture with IL-7 and IL-15 Provides the Most Potent Chimeric Antigen Receptor (CAR)-Modified T Cells for Adoptive Immunotherapy. *J Immunol*. 2016 May 1;196:214-223.

319 Melchionda F, Fry TJ, Milliron MJ, McKirdy MA, Tagaya Y, Mackall CL. Adjuvant IL-7 or IL-15 overcomes immunodominance and improves survival of the CD8+ memory cell pool. *J Clin Invest*. 2005 May 2;115(5):1177–87.

320 Lanitis E, Rota G, Kosti P, et al. Optimized gene engineering of murine CAR-T cells reveals the beneficial effects of IL-15 coexpression. *J Exp Med*. 2020 Nov 6;218(2):e20192203.

321 Xu Y, Zhang M, Ramos CA, et al. Closely related T-memory stem cells correlate with in vivo expansion of CAR.CD19-T cells and are preserved by IL-7 and IL-15. *Blood*. 2014 Jun 12;123(24):3750–9.

322 Alizadeh D, Wong RA, Yang X, et al. IL15 enhances CAR-T-cell antitumor activity by reducing mTORC1 activity and preserving their stem cell memory phenotype. *Cancer Immunol Res*. 2019 May;7(5):759–72.

323 Mueller K, Schweier O, Pircher H. Efficacy of IL-2- versus IL-15-stimulated CD8 T cells in adoptive immunotherapy. *Eur J Immunol*. 2008 Oct;38(10):2874–85.

324 Thomsen M, Galvani S, Canivet C, Kamar N, Bohler T. Reconstitution of immunodeficient SCID/beige mice with human cells: applications in preclinical studies. *Toxicology.* 2008; 246:8-23.

325 Haynes NM, Snook MB, Trapani JA, et al. Redirecting mouse CTL against colon carcinoma: superior signaling efficacy of single-chain variable domain chimeras containing TCR-zeta vs Fc epsilon RI-gamma. *J Immunol*. 2001;166 (1):182-187.

326 Brentjens RJ, Latouche JB, Santos E, et al. Eradication of systemic B-cell tumors by genetically targeted human T lymphocytes co-stimulated by CD80 and interleukin-15 [see comment]. *Nat Med*. 2003;9(3):279-286.

327 Gattinoni L, Finkelstein SE, Klebanoff CA, et al. Removal of homeostatic cytokine sinks by lymphodepletion enhances the efficacy of adoptively transferred tumor-specific CD8+ T cells. *J Exp Med*. 2005;202:907-912.

328 Klebanoff CA, Khong HT, Antony PA, Palmer DC, Restifo NP. Sinks, suppressors and antigen presenters: how lymphodepletion enhances T cell-mediated tumor immunotherapy. *Trends Immunol*. 2005;26:111-117.

329 North RJ. Cyclophosphamide-facilitated adoptive immunotherapy of an established tumor depends on elimination of tumor-induced suppressor T cells. *J Exp Med*. 1982;155(4):1063-1074.

330 Buatois V, Chatel L, Cons L, et al. Use of a mouse model to identify a blood biomarker for IFNγ activity in pediatric secondary hemophagocytic lymphohistiocytosis. *Translational Research*. 2017 Feb 1;180:37-52.e2.

331 Deshmane SL, Kremlev S, Amini S, Sawaya BE. Monocyte Chemoattractant Protein-1 (MCP-1): An Overview. *J Interferon Cytokine Res*. 2009 Jun;29(6):313–26.

332 Klinger M, Zugmaier G, Nägele V, Goebeler M-E, Brandl C, Stelljes M, et al. Adhesion of t cells to endothelial cells facilitates blinatumomab-associated neurologic adverse events. *Cancer Res.* 2020;80:91–101.

333 Wei J, Liu Y, Wang C, et al. The model of cytokine release syndrome in CAR T-cell treatment for B-cell non-Hodgkin lymphoma. *Signal Transduct Target Ther*. 2020 Jul 29;5(1):134.

334 Jiang Z, Liao R, Lv J, et al. IL-6 *trans*-signaling promotes the expansion and anti-tumor activity of CAR T cells. *Leukemia*. 2021 May;35(5):1380–91.